Optimisation of Silicone-based Dielectric Elastomer Transducers by Means of Block Copolymers - Synthesis and Compounding

A Razak, Aliff Hisyam

Publication date:
2017

Document Version
Publisher's PDF, also known as Version of record

Optimisation of Silicone-based Dielectric Elastomer Transducers by Means of Block Copolymers – Synthesis and Compounding

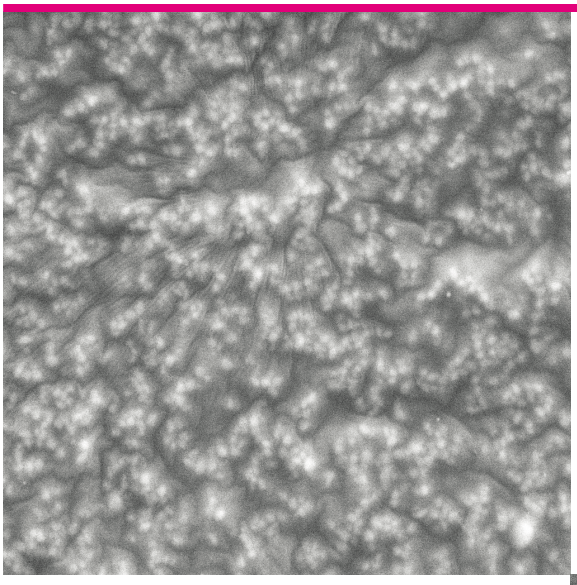

Aliff Hisyam A Razak

PhD Thesis

January 2017

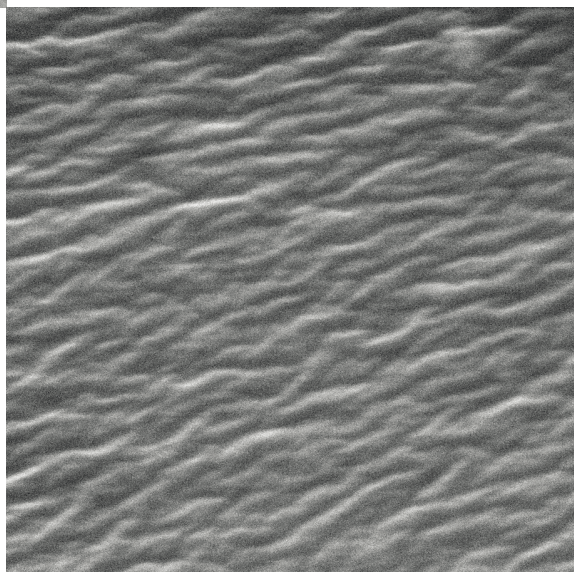

DTU Chemical Engineering
Department of Chemical and Biochemical Engineering

Optimisation of Silicone-based Dielectric Elastomer Transducers by Means of Block Copolymers – Synthesis and Compounding

Aliff Hisyam A Razak
DTU Kgs. Lyngby

Ph.D. thesis
13th January 2017

Preface

This thesis is submitted in fulfilment of the requirements of the Danish Doctor of Philosophy (Ph.D.) in chemical engineering. It contains works from December 2013 to December 2016, carried out under the main supervision of Anne Ladegaard Skov and the co-supervision of Peter Szabo. This thesis has been written based on experimental works performed on silicone dielectric elastomers and electrodes by means of block copolymers.

The aim of the thesis is to present novel work on the enhancement of relative permittivity and electrical breakdown strength by incorporating block copolymers. Herein, silicone elastomers with increased relative permittivity and high electrical breakdown strength, as well as a low Young's modulus, were successfully prepared by means of block copolymers via thorough synthesis and compounding. From the synthesised copolymers, a binary system of a copolymer blend consisting of two copolymers was prepared and cross-linked, in order to enhance electro-mechanical properties. Besides preparing silicone elastomers with increased relative permittivity and high electrical breakdown strength, a conductive composite for a stretchable DE electrode was developed from a chain-extended PDMS-based copolymer along with the incorporation of nano-sized conductive fillers.

This thesis contains eight chapters. The introduction, in Chapter 1, provides an overview of dielectric elastomer technology, including silicone elastomers and compliant electrodes. Details of block copolymers are also discussed. Chapter 2 presents the resulting silicone properties from incorporating polydimethylsiloxane-polyethyleneglycol (PDMS-PEG) copolymer in commercial silicone elastomers, and in Chapter 3, the resulting properties of the cross-linked polydimethylsiloxane-polyphenylmethylsiloxane (PDMS-PPMS) copolymer, mainly in terms of electrical breakdown strength, are presented. The synergistic effect of the electro-mechanical properties of binary system of copolymer blend consisting of PDMS-PEG and PDMS-PPMS copolymers is discussed in Chapter 4. Details on compliant electrodes, achieved by incorporating a one-dimensional (1D) conducting network containing multi-walled carbon nanotubes in a PDMS-PEG matrix are described in Chapter 5, while the main conclusion, future works and experimental methods are discussed in Chapters 6, 7 and 8, respectively.

This thesis is based on published/submitted manuscripts, which can be found in the following appendices:

1. A Razak AH, Szabo P, Skov AL (2015) 'Enhancement of dielectric permittivity by incorporating PDMS-PEG multiblock copolymers in silicone elastomers' RSC Adv. 5:53054–53062 – **Appendix I**
2. A Razak AH and Skov AL (2017) 'Silicone elastomers with covalently incorporated aromatic voltage stabilisers' RSC Adv. 7:468-477 – **Appendix II**
3. A Razak AH, Yu L, Skov AL (2017) 'Voltage-stabilised elastomers with increased relative permittivity and high electrical breakdown strength by means of phase

separating binary copolymer blends of silicone elastomers' RSC Adv. 7:17848–17856 – **Appendix III**

4. A Razak AH, Madsen FB, Skov AL (2016) 'Mechanically compliant electrodes and dielectric elastomers from PEG-PDMS copolymers' MRS Adv. 1:3497-3508 – **Appendix IV**

Acknowledgement

I would like to acknowledge gratefully the Malaysian Ministry of Education, University of Tun Hussein Onn Malaysia (UTHM) and Innovationsfonden Danmark for funding my Ph.D. project.

I express my sincere gratitude to Anne L. Skov for her full support during my research. Her continuous guidance and encouragement during these past three years have been exceptionally meaningful to me. I am blessed to have received her suggestions and ideas during the projects, as well as her thorough guidance in writing scientific articles. Also, thanks to Peter Szabo for his effort and time.

I would also like to thank the professors and my fellow colleagues at the Danish Polymer Centre (DPC), mainly Liyun Yu for a number of useful suggestions. Also, thank you to Kim Chi Szabo for running my SEC, DSC and TGA samples.

First and foremost, I would like to thank my beloved parents (A Razak and Jamalliah) and siblings (Affiz, Afifah, Afif, Aisyah and Afiqah) for their encouragement and for being good listeners. Thanks also to Jacob Eiland for the proofreading of this thesis, not forgetting to mention Marius N. Mogensen, Sandy L. Mondrup, Roselina and Karsten Mikkelsen, Effa and Steve Daines and my friends for their continuous support and lovely hospitality during my stay in Denmark.

Contents

Abstract

Emerging artificial muscle technology has developed from metal-based robotics to soft-type robotics made from soft matter. Research into artificial muscle technology based on soft matter has been conducted mainly in order to mimic soft and robust human muscle. In this regard, dielectric elastomers have been studied. Their actuation occurs when Maxwell stress exceeds elastic stress in the presence of an electrical field, resulting in contraction in thickness and planar expansion in the area. As well as an actuator, dielectric elastomers can be used as generators and sensors. As a dielectric elastomer, silicones have been used extensively in many applications, due to favourable properties such as thermal stability, non-conductivity, high gas permeability and low toxicity. However, silicones have a low dielectric constant and thereby low energy density. In order to enhance actuation performance, it is the aim of this research to develop silicone elastomers with a high dielectric constant and high electrical breakdown strength, as well as a low Young's modulus.

In this Ph.D. thesis, two methods were developed to enhance silicone properties such as the dielectric constant and electrical breakdown strength. The first method was devised to enhance the dielectric constant of silicone elastomers through the use of a polydimethylsiloxane-polyethyleneglycol (PDMS-PEG) copolymer, in order to obtain an elastomer with high electrical energy. PDMS-PEG copolymers were synthesised and blended in commercial silicone and subsequently cross-linked. The relative permittivity of cross-linked silicone with 5 wt% of PDMS-PEG copolymers increased by nearly 50%, without compromising dielectric loss and mechanical properties, compared to the commercial silicone elastomer.

The second investigated method involved enhancing the electrical breakdown strength of silicone by using an aromatic voltage stabiliser. Here, polyphenylmethylsiloxane (PPMS), which contained aromatic voltage stabilisers, was bonded covalently to PDMS through a hydrosilylation reaction obtaining PDMS-PPMS copolymers. The synthesised copolymers were subsequently cross-linked with a vinyl cross-linker. The obtained cross-linked PDMS-PPMS copolymers were inherently soft and robust with increased electrical breakdown strength (21%) compared to the reference elastomer without an aromatic voltage stabiliser.

The conducting polymer was developed through the use of a multi-walled carbon nanotube (MWCNT) in a PDMS-PEG matrix as a compliant electrode of dielectric elastomers. The conductive PDMS-PEG copolymer was incorporated with surface-treated MWCNT, in order to obtain highly conductive elastomer. The prepared sample with 4 parts per hundred rubber (phr) MWCNT was soft and the resulting conductivity of the cross-linked PDMS-PEG copolymer with the addition of MWCNT was high, at 10^{-2} S cm^{-1}, nearly equivalent to a commonly used commercial conducting polymer.

In this thesis, the elastomer and electrode system is referred to as a 'dielectric elastomer transducer.'

Resume På Dansk

I takt med at teknologien indenfor kunstige muskler udvikles, er det forventeligt, at man vil se et skift fra metalbaserede til bløde materialer baseret på elastomerer. Forskning, der har til formåe, at efterligne de bløde og robuste menneskelige muskler ved hjælp af elastomerer, forekommer i stigende omfang. I den dielektriske elastomer opnås aktuering, når et elektrisk felt medfører, at Maxwell spændingen overstiger den elastiske spænding. Dette resulterer i en sammentrækning i højderetningen og en udvidelse af overfladearealet. Ud over anvendelse som aktuatorer benyttes dielektriske elastomerer også som generatorer og sensorer. Silikone har som dielektrisk elastomer fundet udbredt anvendelse pga. attraktive egenskaber så som termisk stabilitet, elektrisk isolationsevne, høj gas permeabilitet og lav toksisitet. Silikone er dog kendetegnet ved lav dielektrisk konstant og dermed lav energitæthed. Udviklingen af silikone med høj dielektrisk konstant kombineret med høj elektrisk sammenbrudsstyrke og lavt Youngs modul er afgørende for at kunne forbedre materialets egenskaber som aktuator.

I denne PhD afhandling er der anvendt to forskellige metoder til at forbedre silikones egenskaber såsom dielektisk konstant og elektrisk sammenbrudsstyrke. Den første metode havde til hensigt at øge den dielektriske konstant for silikone elastomerer ved anvendelsen af polydimethylsiloxane-polyethyleneglycol (PDMS-PEG) copolymer. Formålet med dette var at opnå en elastomer med høj energitæthed. PDMS-PEG copolymer blev syntetiseret og iblandet kommerciel silikone og efterfølgende krydsbundet vha. krydsbindecemolekyler. Sammenlignet med den kommercielle silikone blev den resulterende relative permitivitet af krydsbundet silikone med 5 wt% PDMS-PEG øget med næsten 50%. Dette uden tab af dielektriske og mekaniske egenskaber.

Den anden metode havde til hensigt at øge den elektriske sammenbrudsstyrke af silikone ved at anvende en aromatisk spændingsstabilisator. Polyphenylmethylsiloxane (PPMS) som udgjorde den aromatiske spændingsstabilisator blev covalent bundet til PDMS via en hydrosilylation, hvorved der dannes PDMS-PPMS copolymer. Den syntetiserede copolymer blev efterfølgende krydsbundet med en vinyl krydsbinder. Den fremstillede krydsbundne PDMS-PPMS copolymer var både blød og robust samt udviste øget elektrisk sammenbrudsstyrke (21%) sammenlignet reference materialet uden den aromatiske spændingsstabilisator.

En kompatibel elektrode, i form af en ledende polymer, blev udviklet ved inkorporering af kulstof nanorør (multi-walled carbon nanotubes – MWCNT) i en PDMS-PEG matrix. Overfladebehandlet MWCNT blev inkorporeret i den ledende PDMS-PEG copolymer med henblik på at opnå en elastomer med høj ledningsevne. Det fremstillede materiale indeholdende 4 phr MWCNT var blødt, og den resulterende ledningsevne var høj, 10^{-2} S cm^{-1}, hvilket var tæt på niveauet for kommercielle polymerer.

I denne afhandling er elastomer- og elektrodesystemet refereret til som en 'dielektrisk elastomer transducer'.

1 Introduction

This thesis deals with the inclusion of copolymers into dielectric elastomers and electrodes. Therefore, three main parts are discussed in this chapter, namely elastomers, block copolymers and DE electrodes.

1.1 Dielectric elastomers

Soft elastomers such as silicones, acrylates and polyurethanes have been studied extensively for use in artificial muscle technology [1,2]. Electroactive polymers, known as EAPs, are elastomers that exhibit a change in size or shape when stimulated by an external electrical field [3]. EAPs can be divided into ionic and electronic, with the former requiring low driving voltages and an electrolyte and deforming due to the diffusion of ions in the material in the presence of an electrical field. Electronic EAPs, on the other hand, require high driving voltages and can be operated in the air. Additionally, they possess higher electrical energy than ionic EAPS and come complete with large actuation forces, rapid response times and long lifetimes [1]. Their drawback is that they require high driving voltages, between 500 V to 10 kV, to actuate [2,4]. Polymer electrets [5–7], electro-strictive graft elastomers [8], ionic polymer gels [9] and dielectric elastomers [10–12] are examples of electronic EAPs. Among all of the mentioned electronic EAPs, dielectric elastomers are the most favourable in actuation, due to high actuation speeds, large strains, high work densities and a high degree of electromechanical coupling [1].

1.1.1 Overview of DEs

Dielectric elastomers (DEs) are also known as 'compliant capacitors,' with actuation occurring when electrostatic stress exceeds elastic stress [13]. An overall ability to accumulate electrical energy through an elastomeric membrane is denoted as:

$$C = \frac{\varepsilon_0 \varepsilon_r A}{d} \tag{1.1}$$

where C is the capacitance of the material, ε_r and ε_0 correspond to the relative permittivity of the measured elastomer and vacuum permittivity ($8.854 \cdot 10^{-12}$ F m^{-1}), respectively, and A and d are film area and film thickness, respectively.

1.1.2 Modes of application

DEs have been studied extensively with respect to finding both new and better elastomer candidates for novel DE applications [14–17]. Such properties have enabled them to play

a significant role in applications such as actuators, sensors and generators, the working principles for which are described in the following subsections.

1.1.2.1 DE actuators

In general, an actuation is defined as a mechanical motion caused by external forces or applied electrical fields. The operational principle of a dielectric elastomeric actuator (DEA) is presented in Figure 1.1. For a DE film, which is sandwiched between two stretchable electrodes, electrostatic pressure is generated, due to an increase of electrical field, which subsequently induces thinning and planar expansion of the DE [18]. This electrostatic pressure, known as Maxwell pressure (p), is defined as [19]:

$$p = \varepsilon_0 \varepsilon_r E^2 \tag{1.2}$$

where E is the electrical field.

Assuming a constant Young's modulus during the actuation cycle, the strain (s) of the DE can be determined. At a given voltage (V), the actuation strain of a DE film with a Young's modulus (Y) and thickness (d) is determined from Equation 1.3:

$$s = -\frac{p}{Y} = -\frac{\varepsilon_0 \varepsilon_r E^2}{Y} = \frac{-\varepsilon_0 \varepsilon_r}{Y}\left(\frac{V}{d}\right)^2 \tag{1.3}$$

As actuators, DEs are used in various applications such as tuneable lenses [20], miniaturised actuators [21], loud speakers [22], active membrane pumps [23] and artificial muscle rotary motors [24].

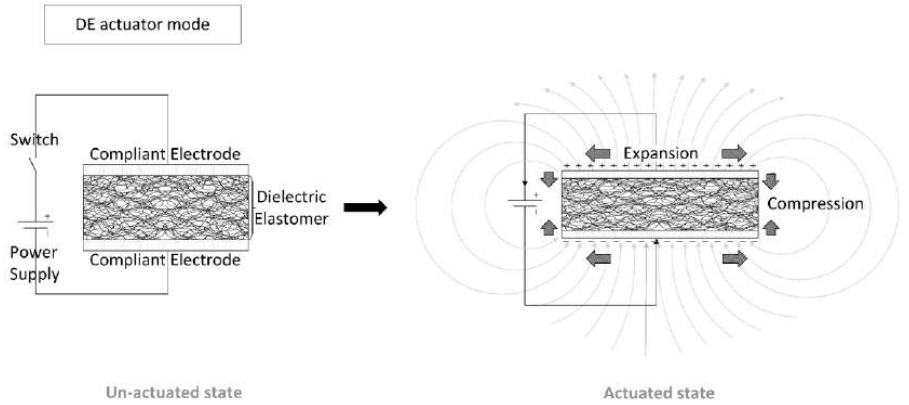

Figure 1.1 Working principle of a DE actuator (DEA).

1.1.2.2 DE generators

A generator is a device which produces electrical energy from potential or kinetic energy. In DE technology, a generator can be developed to harvest energy from ocean waves by utilising DEs, which is well-known as a wave energy harvester [25]. The operational principle of the dielectric elastomeric generator (DEG) is presented in Figure 1.2. In the

initial state, a DE film is supplied with a voltage as a pre-charged film. During oscillation of the mechanical wave, the pre-charged film is stretched, due to the force of the mechanical wave, and the film is released afterwards (relaxed mode), resulting in opposite charges on the two electrodes are pushed apart. Concurrently similar charges are brought closer as the elastomer's area decreases, thereby causing an increase in charge density and thus increasing electrical energy [26].

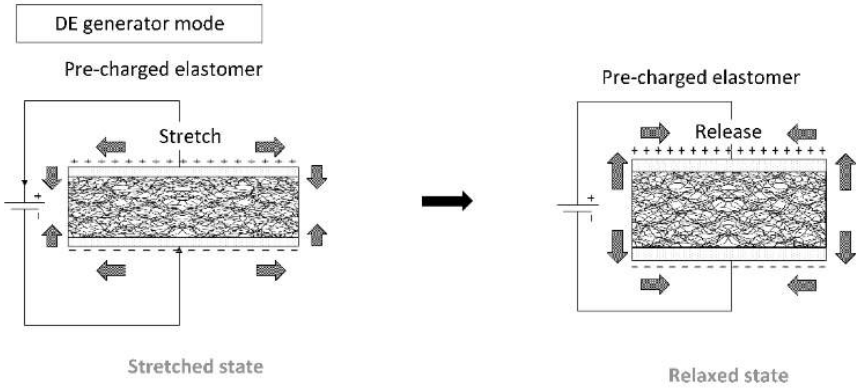

Figure 1.2 Working principle of a DE generator (DEG).

1.1.2.3 DE sensors

A sensor is a device which measures input from the physical environment, e.g. pressure and stretching, and sends the output in a form of a human-readable display for further analysis. For a pre-charged DE film, any external forces that deform the DE, such as pressing, stretching and touching, change the capacitance of the elastomer. The signal can be measured from the capacitance change, which is proportional to the square of the strain ratio between the final strain and the initial strain [27]. The operational principle of a dielectric elastomeric sensor (DES) is presented in Figure 1.3. DE-based sensors have been used for purposes of military, physiotherapeutic and haptic devices [27,28].

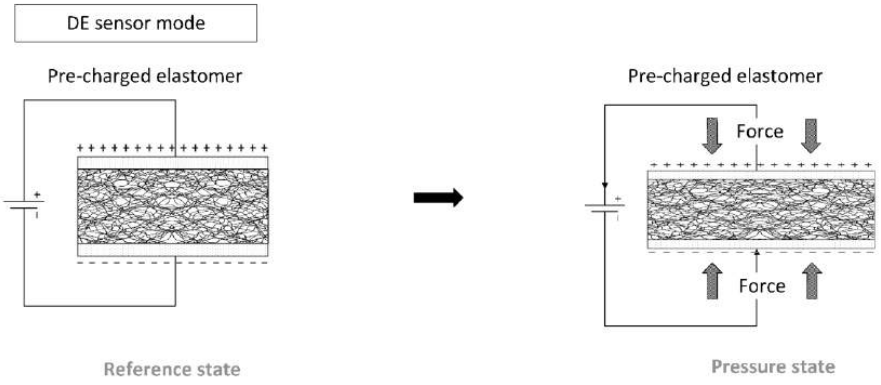

Figure 1.3 Working principle of a DE sensor (DES).

1.1.3 Performance strategies for dielectric elastomers (DEs)

1.1.3.1 Performance of a DE actuator

The actuation performance of a DE actuator at a given voltage (V) can be improved by enhancing its relative permittivity (ϵ_r) or by reducing the Young's modulus (Y). These handles are obvious from the actuation equation derived by Pelrine et al. [19], which relates actuation strain (s) to the mentioned parameters via:

$$s = \frac{-\varepsilon_0 \varepsilon_r}{Y} \left(\frac{V}{d}\right)^2 \tag{1.4}$$

where $\epsilon_0 = 8.85 \cdot 10^{-12}$ F m^{-1} is the permittivity of free space.

The largest achievable electrical field over the dielectric elastomer before electrical failure (E_{BD}) is denoted as 'electrical breakdown strength,' In this electrical field the maximum theoretical actuation strain (s_{max}) is achieved under the assumption that the elastomer is highly extensible and does not break down mechanically prior to electrical breakdown:

$$s_{max} = \frac{-\varepsilon_0 \varepsilon_r}{Y} {E_{BD}}^2 \tag{1.5}$$

1.1.3.2 Performance of a DE generator

When converting the electromechanical energy of DEs, electrostatic potential energy (U_e) occurs between maximum strain upon stretching (s_{max}) and minimum strain upon relaxing (s_{min}). The electrical field generated while harvesting wave-mechanical energy can be presented in three cycles: constant-charge, constant-voltage and constant-field, where the conversion of electromechanical energy is the most efficient in the constant-field cycle compared to the other cycles, because mechanical/electrical energy is stored temporarily in the other cycles. The electrostatic potential energy of the DE generator is constant for a constant-electrical field and is given by [29]:

$$U_e = \frac{1}{2} \varepsilon_r \varepsilon_0 V {E_{BD}}^2 \tag{1.6}$$

where V denotes total active elastomer volume.

The potential energy of the DE generator can be optimised by utilising dielectric elastomers with a high dielectric constant, high electrical breakdown strength and large sample density.

1.1.3.3 Performance of a DE sensor

A change in the capacitance of a DE is related to different modes of operation, such as pressure, stretch, touch, shear and proximity. In a sensor, the capacitance of the DE with the effect of parasitic capacitance ($C_{parasitic}$) is shown as:

$$C = \varepsilon_r \varepsilon_0 \frac{A}{d} + C_{parasitic} \tag{1.7}$$

The increased capacitance of a DE sensor depends on the mode of operation, because when one is stretched or pressurised, or applied with a shear force, capacitance increases due to an increase in the sample area to film thickness ratio. In touch mode, capacitance increases due to increased parasitic capacitance, which is defined as unavoidable capacitance occurring between parts of an electronic component. In proximity mode, the capacitance of the DE sensor increases due to the increased relative permittivity of the DE. Proximity mode occurs due to electromagnetic radiations.

1.1.3.4 Common strategies for enhancing the performance of DEs

1.1.3.4.1 Enhancement of relative permittivity

Several works have been performed on elastomers for enhancing relative permittivity by adding highly polarisable ceramic and conductive fillers from metal oxides, e.g. titanium (IV) dioxide (TiO_2) [30], barium titanate ($BaTiO_3$) [31–34] and calcium copper titanate – CCTO ($CaCu_3Ti_4O_{12}$) [35]. Besides metal oxides fillers, different alternatives to obtaining elastomers with high relative permittivity have been explored, such as chemical functionalisation through the covalent grafting of dipoles such as trifluoropropyl [36], p-nitroaniline [37] or azide groups [38] to the silicone backbone. Asides from the addition of metal oxides and chemical functionalisation, the incorporation of encapsulated high-permittivity fillers, such as polyaniline (PANI) [39], silver nanoparticles [40] and water [41], and ionic liquids, such as glycerol [42], into silicone elastomers has been reported to improve relative permittivity.

1.1.3.4.2 Strain-hardening of elastomer

Another approach to improving actuation performance for DEs is by strain-hardening the elastomer, which can be achieved by either pre-straining externally, by stretching films onto a stiff supporting structure [43], or pre-straining internally, achieved through an interpenetrating polymer network (IPN) [44,45] or by creating bimodal networks [46]. Out of all the stretching methods, stretching films using a supporting structure is the most commonly used in DE technology.

1.1.3.4.3 Enhancement of electrical breakdown strength

The effect of electrode configuration on the electrical breakdown strength of pre-stretched DEs has been studied by Tröls et al. [47] and Zakaria et al. [48]. As the electrode size increases, the sample volume also increases and the increased sample volume needs to be considered when determining electrical breakdown strength. In the work performed by Tröls et al., compliant and rigid electrodes were used for the measurement of pre-stretched elastomer electrical breakdown, and the effects of both electrodes were compared. The resulting electrical breakdown strengths depended on the electrode configuration, where the electrical breakdown strength was lower when measured using compliant electrodes than when using rigid electrodes. The drawback in the work performed by Tröls et al. is that the volume of pre-stretched samples was not conserved such that the sample volume was reduced significantly by pre-stretching. Therefore,

constant volumes of tested samples are necessary to obtain comparable data. The electrical breakdown study of a pre-stretched sample with constant volume was reported by Zakaria et al [48]. Two experimental configurations, with and without constant sample volume, were used to determine the stretch dependence of the electrical breakdown strength of PDMS elastomers. Breakdown strength was determined for samples with and without volume conservation and was found to depend strongly on the stretch ratio and the thickness of the samples.

Several film fabrication processes have been used to make DE films, including direct hot-pressing, centrifuging and drop-casting. These different types of processing method create different mechanical properties for the obtained elastomers, as reported by Kollosche et al. [49]. Among all the mentioned processing methods, films prepared via the centrifuging and drop-casting methods were softer, i.e. a decreased Young's modulus, than hot-pressed films. An elastomer with a low Young's modulus (Y) possesses decreased electrical breakdown strength compared to one with high Y [30,49,50]. Therefore, increased electrical breakdown strength can be obtained from DE films prepared by drop-casting.

A highly pre-stretched DE film results in large actuation strain. Pre-stretching enhances the actuation performance of DE film, due to the favourable realignment of material imperfections such as voids and micro-cracks. In addition, pre-stretching reduces the film thickness of the DE and lowers the driving voltage, which subsequently increases electrical breakdown strength, as reported by Zakaria et al. [51] and Huang et al. [50].

The effect of different types and amounts of filler on the electrical breakdown strength of DEs has been investigated. Several types of fillers, such as an anatase titanium(IV) oxide (TiO_2), a core–shell of titanium dioxide-silica (TiO_2-SiO_2) and a calcium copper titanate (CCTO- $CaCu_3Ti_4O_{12}$), were incorporated into liquid and room-temperature vulcanisable silicone elastomers [30]. Among these fillers, a silicone elastomer containing TiO_2-SiO_2 filler possesses very high electrical breakdown strength, as reported by Vudayagiri et al. [30]. Aside from having high electrical breakdown strength, the resulting Young's modulus of the silicone-TiO_2-SiO_2 composite was high. A DE with an increased Young's modulus delays the rapid thinning process, due to electromechanical instability (EMI), and thereby increases electrical breakdown strength [52].

1.1.4 Dielectric silicone elastomers

Polydimethylsiloxanes (PDMS) or silicones are semi-inorganic polymers that are composed of a siloxane (Si-O) backbone. Silicones possess a very low glass transition temperature (T_g), as low as -120°C, and they are usually thermally stable up to more than 300°C [53]. Other good qualities of silicones include good oxidation and UV resistance, high gas permeability, excellent electrical properties and are biocompatible. Without cross-linking, PDMS is a liquid. When making an elastomer, functional PDMS can be cross-linked with a cross-linker. For film preparation, the formulation containing PDMS, a cross-linker and a catalyst is cast on a substrate before cross-linking. Finally, the DE film is cured either at room or elevated temperatures, or in the presence of UV light.

Hydrosilylation is a commonly used reaction to produce silicone elastomers and is defined as the vinyl addition cure between a silyl hydride and a vinyl group catalysed by a platinum complex [54,55]. The formation of elastomer with a high degree of network control can be obtained through a hydrosilylation reaction. Another advantage of hydrosilylation is that no by-product is formed; however, it is sensitive to sulphur and amine moieties, which can poison the platinum catalyst and subsequently stop hydrosilylation altogether.

Silicone polymers can be cured using a room-temperature vulcanising (RTV) moisture system via a condensation reaction. At room temperature, a cross-linker which is exposed to ambient humidity is hydrolysed producing a silanol group. Subsequently, the silanol cross-linker condenses further with silanol-functionalised silicones or another silanol cross-linker, and the condensation reaction proceeds until a cured system is obtained. With the addition of a titanium 2-ethylhexoxide catalyst, the condensation reaction occurs quite quickly and thereby reduces the time taken for film formation.

Different mechanical properties of silicone elastomer can be obtained from different cross-linking densities, while non-cross-linked silicone polymers can be obtained commercially at molecular weights between 0.2 and 100 kg mol^{-1}. Silicone elastomers with low cross-linking density result in soft silicone elastomers, such that they can be actuated at a lower voltage compared to stiffer elastomers, which possess high cross-linking density; however, they suffer from poor mechanical robustness. To enhance mechanical robustness, fillers such as surface-treated silica nanoparticles are often incorporated into silicone elastomers.

Preparing a silicone elastomer film from a high-molecular weight PDMS can be difficult, due to a high viscosity mixture. Usually a film coating containing viscous PDMS reduces the quality of thin films prior to cross-linking. As a solution to reducing the viscosity of the silicone mixture, common organic solvents, such as tetrahydrofuran (THF) and toluene, or methylsiloxane fluids are used for a smooth film coating, thereby improving the quality of the film. Nevertheless, the use of solvents may trap air in the films, even for carefully prepared samples.

1.2 Block copolymers

Block copolymers are macromolecules that consist of two or more repeating polymer units. Macromolecules are obtained by combining two or more chemically immiscible polymer blocks that are thermodynamically incompatible. All block copolymers belong to soft matter and are often characterised by a fluid-like disorder on the molecular scale and a high degree of order at longer lengths [56]. In order to minimise Gibbs free energy, the blocks in a copolymer undergo self-assembly and organise themselves into well-defined and periodic nanostructures. Due to these well-defined nanostructures, block copolymers have been explored for providing many useful and desirable properties in products such as lubricant, asphalt, adhesive material and dielectric elastomer.

1.2.1 Morphologies of block copolymers

Due to the minimisation of free energy, diblock copolymers phase separately and subsequently assemble into different morphologies such as spheres (S), cylinders (C), gyroids (G) and lamellars (L), as shown in Figure 1.4 [56–60]. These architectures are achieved when two immiscible polymers, which are covalently bonded, segregate to form well-defined structures [61]. The different morphologies can be obtained by varying the volume fraction of one constituent in the diblock copolymer. The self-assembly of copolymer depends on the incompatibility degree (χN, where χ is the Flory-Huggins interaction parameter and N is the degree of polymerisation) and volume fraction of one constituent in the block copolymer (f) [56,62].

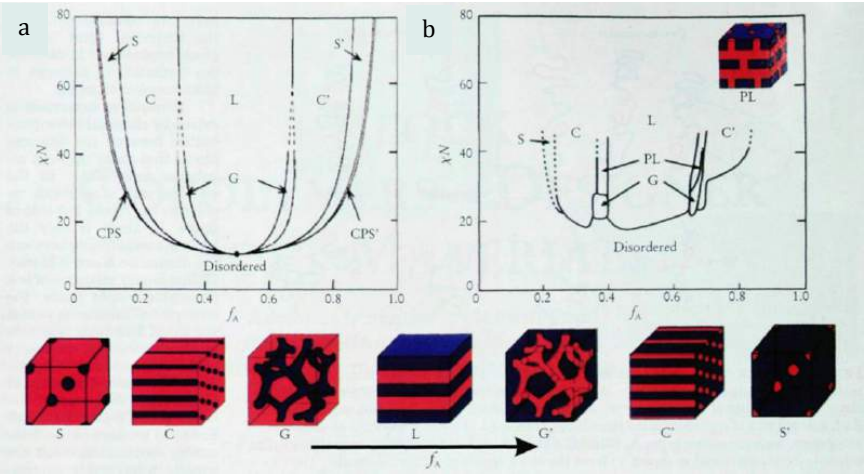

Figure 1.4 Two phase diagrams of linear AB diblock copolymers a: Prediction of four equilibrium morphologies from self-consistent mean-field theory [56], b: Phase diagram of poly(isoprene-styrene) diblock copolymers [57], reproduced from [Bates FS, Fredrickson GH (1999) Block copolymers—Designer soft materials. Phys Today 52:32–38], with the permission of the American Institute of Physics.

1.2.2 Miscibility of copolymers

Copolymer blocks are expected to phase-separate, due to the minimisation of Gibbs free energy and the miscibility of two copolymers' blocks, subsequently forming well-defined morphologies which may give the most favourable electro-mechanical properties of DEs. However, preparing an elastomer by means of a block copolymer can be rather challenging, as the phase separation may occur on the macroscale, resulting in an inhomogeneous elastomer. When utilising the block copolymer, phase separation occurring on the micro- and nanoscales is favoured, in order to obtain a homogeneous elastomer with enhanced electrical and mechanical properties.

In order to optimise a silicone dielectric elastomer, a polymer/copolymer, which is conductive or possesses a high dielectric constant, can be incorporated into the silicone elastomer by means of either a binary polymer blend or copolymerisation. In a binary

system of polymer blends consisting of a conducting polymer/copolymer and a non-conducting PDMS, an elastomer is prepared from phase separation, whereby the desired morphology of the continuous non-conducting PDMS phase and conducting polymer/copolymer discontinuous phase is created in the blends. However, the phase separation of binary polymer blends is macroscopic rather than microscopic or nanoscopic, and consequently it compromises the homogeneity of the two components in the elastomeric matrix. Preventing macroscopic phase separation when preparing the DE is significant for long DE lifetimes.

As a solution to the macroscopic phase-separated binary polymer blend, a conducting polymer, which is immiscible in PDMS, is copolymerised with PDMS as a block copolymer. The covalent-bonded copolymers' blocks, containing conducting and non-conducting polymers, phase separate and form the more favourable micro- or nanoscopic phase separation, which ascribes to the desired electro-mechanical properties of the DE. The favourable morphology of a copolymer results from phase separation between the rich domain of a non-conducting block (continuous phase) and the small domain of a conducting block (discontinuous phase). Therefore, the optimised silicone elastomer, prepared from a phase-separating system by means of copolymerisation, results in phase separation on the micro- or nanoscale, indicating that the elastomer is homogeneous.

1.2.3 Voltage-stabilised elastomer by means of a block copolymer

When optimising dielectric elastomers (DEs) a conflict exists, namely that for large, achievable actuation strains softness is required, although with increased softness electrical breakdown strength decreases. A strategy for enhanced electrical breakdown strength in DEs can be achieved by voltage stabilisation, due to electron-trapping effects, which have been investigated previously by including minute concentrations of aromatic voltage stabilisers in polymers, mainly polyethylene (PE), with the purpose of reducing power loss for high-voltage insulation cables [63–65]. Aromatic voltage stabilisers, which have delocalised π-electrons, trap energetic electrons and create radicals, as they interrupt the distribution of the π-electron cloud [66]. In high-voltage insulation cables, the electrical breakdown strength of PE increases by utilising aromatic azo-compounds, which have six different side groups with electron-acceptors (NO_2·, CN·) or electron-donors (NH_2·, CH_3·, OH·), as reported by Yamano et al. [63]. A PE composite containing an azo-compound with $(OH)_2$ and NO_2 side groups in remarkably low concentrations has the highest electrical breakdown strength, improving by 48% compared to the PE without an additive. This indicates that both electron-donating (OH·) and -accepting (NO_2·) groups efficiently increase electrical breakdown strength, due to the increased polarity in the aromatic group, and thus lower excitation energies. Yamano [64] enhanced further electrical breakdown strength in PE by employing acene compounds (naphthalene, anthracene, tetracene and pentacene) as aromatic voltage stabilisers.

The homogeneity of elastomer is affected by phase separation of the mixture. With proper sample preparation, phase separation can be achieved on the nanoscale, while the nanoscopic phase-separating system has influenced the enhanced electrical and mechanical properties of DEs.

Utilising aromatic voltage stabilisers of any kind as a silicone additive will unavoidably cause phase separation of the mixture. Preventing this on both the macro- and the microscale during preparation, as well as during actuation, is a key requirement for long DE lifetimes [65]. PPMS possesses voltage stabilisation capabilities but is immiscible in PDMS, and thus the copolymerisation of the two components is necessary for homogeneity. The effect of electron-trapping by phenyl groups, so-called 'homo-aromatics', in a silicone elastomer is illustrated in Figure 1.5. Electrons in the presence of an electrical field accumulate initially at the interfacial boundary between the film and the electrode, as shown in Figure 1.5(b). The electrons then migrate and are trapped in the phenyl groups, as seen in Figure 1.5(c). When electrons migrate and collide with the homo-aromatic group, they disturb the cloud of π-electrons in the aromatic group, and this results in the formation of electron-accepting radicals, as shown in Figure 1.5(d). The depth of the electron trap is highly influenced by the type of radical [66], where the depth of the aromatic group with the radical of an electron-accepting type is greater than that of the aromatic group without a radical [64,66]. The trapped electrons act as negative space charges in the elastomer, causing a decrease in electrical field strength on the cathode [64]. This decreased electrical field strength then reduces electron migration from the cathode. The trapped electrons remain in the film bulk and therefore delay electrical breakdown; thus, increased electrical breakdown strength is achieved.

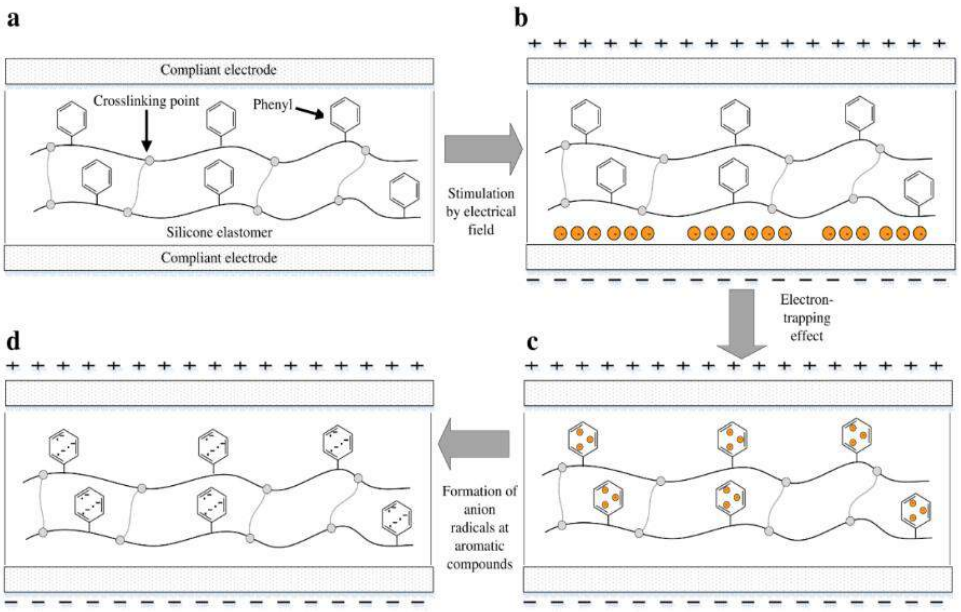

Figure 1.5 The enhancement of electrical breakdown strength, due to electron-trapping: a) A silicone elastomer with an aromatic group grafted to the silicone backbone and a coating of compliant electrodes on the top and bottom surfaces. b) The existence of electrons at the interfaces between the elastomer and the compliant electrode in the presence of an electrical field. c) The electron-trapping effect as a consequence of a collision between electrons and the phenyl group. d) The formation of anion radicals resulting from the disturbance of the cloud of phenyl group π-electrons.

1.3 Elastomer parameters

For the optimisation of elastomer, the cross-linked copolymer is further characterised for electrical and mechanical properties, and often a conflict exists between the optimised parameter and other parameters, e.g. relative permittivity versus electrical breakdown strength and mechanical properties. As a result, it is necessary to consider the compromised parameter during the optimisation of DEs.

1.3.1 Permittivity

Permittivity measures the level of electrical energy stored in the form of charge separation caused by polarisation. Relative permittivity is the ratio of the storage permittivity of an elastomer (ε') to the storage permittivity of a vacuum ($\varepsilon_0 = 8.854 \cdot 10^{-12}$ F/m). In this thesis, frequency-dependent storage permittivity (ε') is referred to as 'relative permittivity', in line with DE standards. DEs with increased relative permittivity have been studied extensively for the optimisation of DEs [38,53,67–70]. An elastomer with high relative permittivity, such as poly(vinylidene fluoride-co-hexafluoropropylene) (PVDF) with $\varepsilon_r = \sim 12$, indicates that PVDF possesses high electrical energy [69]. An elastomer with high electrical energy is important for better performance in DE applications. Tan δ is the ratio of loss permittivity (ε'') to storage permittivity (ε').

An un-actuated DE consists of dipolar molecules (Si-O, Si-CH_3) randomly aligned in an elastomeric matrix (see

Figure 1.6). When the DE is polarised, the dipolar molecules realign such that the positive charges of the dipoles orient toward the negative charges on the electrode (refer to Figure 1.7).

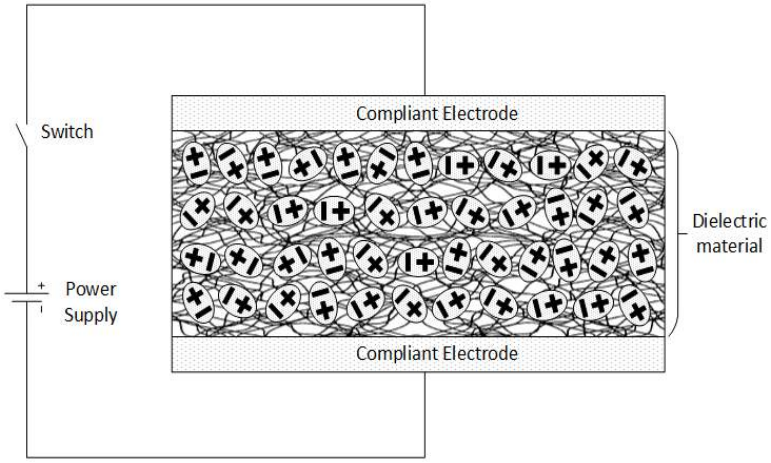

Figure 1.6 Unpolarised dipoles randomly aligned in the elastomeric matrix.

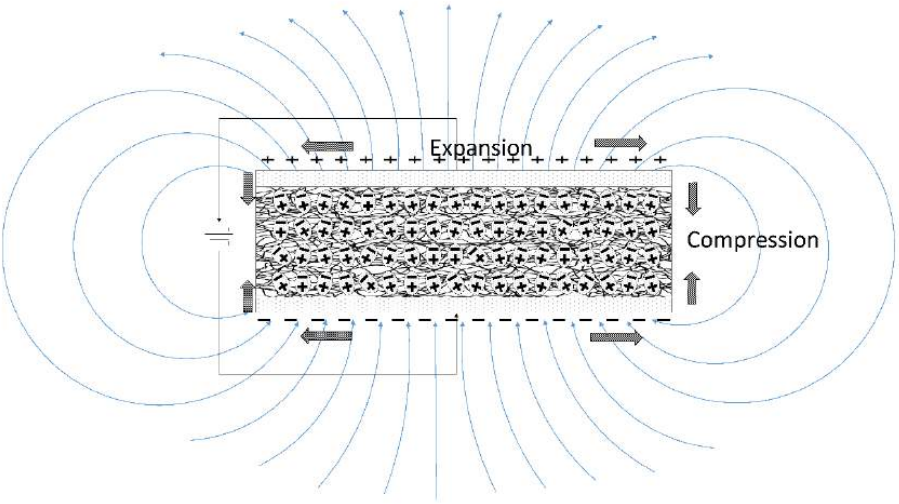

Figure 1.7 Re-orientation of polarised dipoles in the elastomeric matrix.

1.3.2 Electrical breakdown strength

The elastomer can withstand a maximum electrical field, but above the maximum electrical field the DE will short-circuit and form a pinhole, defined as the electrical breakdown strength of DEs [71]. The optimisation of electrical breakdown strength and the mechanism behind the electrical breakdown of DEs have been studied recently.

In the next subsections, several mechanisms that lead to electrical breakdown in DEs namely electromechanical breakdown, electrothermal breakdown and partial discharge, will be discussed.

1.3.2.1 Electromechanical breakdown

Another form of electrical breakdown in DEs is electromechanical breakdown, which occurs during actuation when attractive forces between the two electrodes become dominant and locally exceed a certain threshold value that cannot be balanced by the elastomer's resistance to compression [72,73]. For DEs, electromechanical breakdown is also known as 'electromechanical instability', or 'EMI'. Electrical stress in the local regions of a DE may give rise to localised thinning, known as the 'Stark and Garton' thinning process [74], which causes an increase in the electrical field, due to a decrease in film thickness, and subsequently results in an increase in electrostatic forces such as positive-feedback effect. These local regions, which are subjected to a higher electrical field, possess high shear stresses and subsequently form indentations [75], which in turn result in inhomogeneous fields where these indentations create sharp notches and caused the elastomer to push away radially by a certain degree, depending on the DE's Young's modulus. Above the critical voltage, the DE will short-circuit, due to void formation. Electromechanical breakdown can be eliminated by pre-stretching the elastomer, since

pre-stretching has a combined effect of improving the alignment of film imperfection, decreasing film thickness and increasing electrical breakdown strength [48,76].

1.3.2.2 Electrothermal breakdown

During DE electrical breakdown, heat generated inside the film, which cannot be balanced by heat lost to the surrounding area, is defined as 'electrothermal breakdown' [77]. When a voltage is applied to a DE, electrical power is dissipated, causing increased temperature, which then creates local heating and results in increased electrical power dissipation and subsequently a further increase in temperature [78]. This process is known as 'thermal runaway'. Above a critical temperature, electrothermal breakdown will occur. The electrothermal breakdown in silicone DEs has been studied by Zakaria et al. [51], who used a model based on numerical analysis with quasi-steady state approximation to estimate the thermal runaway in silicone DEs. The outcomes from the modelling were compared to experimental data on the temperature effects of silicone elastomers. Studies have proven theoretically and experimentally that electrothermal breakdown is not the main cause of the electrical breakdown of thin silicone elastomer, due to the very low electrical field required to initiate the thermal runaway.

1.3.2.3 Partial discharge

In a DE film, a partial discharge is commonly associated with voids. Whilst preparing the elastomer, the formation of small voids is unavoidable, even in the most carefully executed preparation technique. Trapped gas in the voids results in decreased relative permittivity and low electrical breakdown strength of the DE, caused by a arise in the electrical field, and subsequently these voids break down electrically before the elastomer [77,79]. In DEs, several conditions lead to partial discharges, namely gas pressure, void shape and void size [77]. For a very thin DE, partial discharge may lead rapidly to failure.

1.3.3 Young's Modulus

The Young's modulus (Y) can be estimated from a molecular theory on the viscoelastic behaviour of incompressible cross-linked polymer. In Chapter 2, Young's moduli of the prepared elastomers were calculated from this molecular theory and then used to determine the figure of merit (F_{OM}) for the DE actuator.

The elastomer is stretched uniaxially in the z-direction. Assuming the elastomer is incompressible, ${l_0}^3 = l_x l_y l_z$, where l_0 is the initial length of the cube and l_x, l_y and l_z are the dimensions after deformations in the x-, y- and z-directions, respectively. Based on Helmholtz free energy per volume and incompressibility, isotropic stress (σ_{ii}) for a chemical cross-linked elastomer is given by:

$$\sigma_{ii} = nk_B T\lambda_i^2 - P \tag{1.8}$$

where n, k_B and λ_i are the numbers of chains per volume, the Boltzmann constant and different dimensional stretch ratios, respectively, at a particular temperature (T) and pressure (P).

For uniaxial stretching, the stretch ratios in the x-, y- and z-directions are defined as $\lambda_x = \lambda_y = \lambda^{-\frac{1}{2}}$ and $\lambda_z = l_z l_0^{-1}$, respectively (see Figure 1.8). As applied stress is in the z-direction (σ_{zz}), stresses in the x- and y-directions (σ_{xx} and σ_{yy}) are zero and give:

$$\sigma_{yy} = \sigma_{xx} = nk_BT\lambda^{-1} - P = 0 \tag{1.9}$$

$$P = -nk_BT\lambda^{-1} \tag{1.10}$$

$$\sigma_{zz} = nk_BT\lambda^2 - P \tag{1.11}$$

By solving Eqns. 1.10 and 1.11, the stress (σ_{ii}) in force (F) and area (A) is expressed in Eqn. 1.11, where $\lambda_z = \lambda$:

$$\sigma_{ii} = \frac{F}{A} = nk_BT(\lambda^2 - \lambda^{-1}) \tag{1.12}$$

The stretch ratio, λ, is defined as 1+ε. Assuming that the deformation (ε) is very small, λ^2 and λ^{-1} are equal to 1+2ε and 1-ε, respectively. The expression of $\lambda^2 - \lambda^{-1}$ equals 3ε, and thereby Eqn. 1.12 can be written as $\sigma_{ii} = 3nk_BT\varepsilon$.

The shear modulus (G') is equal to nk_BT, and hence the final expression of the Young's modulus can be expressed in terms of G (see Eqn. 1.14).

$$Y = 3nk_BT \tag{1.13}$$

$$Y = 3G' \tag{1.14}$$

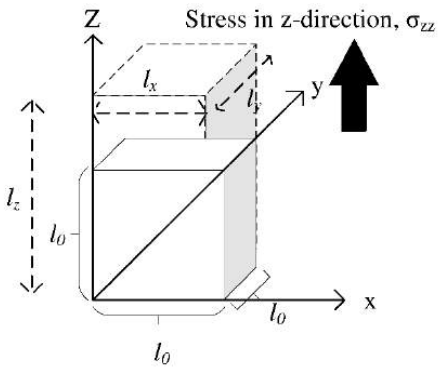

Figure 1.8 An illustration of a cube, before and after applying stress in the z-direction. Solid and dashed cubes represent the elastomer, before and after uniaxial deformation, respectively, in the z-direction.

1.3.4 Figure of merit (F_{OM}) of a dielectric elastomer actuator

The figure of merit is used to access actuation performance for DEs. A figure of merit for dielectric elastomer actuators, F_{OM} (DEA), derived by Sommer-Larsen and Larsen [80], is:

$$F_{OM}(DEA) = \frac{3\varepsilon_r\varepsilon_0 {E_{BD}}^2}{Y} \tag{1.15}$$

For a dielectric elastomer generator (DEG), the generator's performance can be evaluated from the figure of merit for DEG, F_{OM} (DEG), presented by McKay et al. [81]:

$$\mathrm{F_{OM}(DEG)} = \frac{3\varepsilon_r\varepsilon_0 {\mathrm{E_{BD}}}^2}{2\varphi} \tag{1.16}$$

where φ is the strain energy function of the elastomer.

The F_{OM} value for the investigated elastomer is normalised with the F_{OM} value for a standard silicone dielectric elastomer, e.g. RT625. The normalised F_{OM} (DEA/DEG)$_{Norm.}$ is calculated as:

$$F_{OM}(DEA/DEG)_{Norm.} = \frac{F_{OM}(DEA/DEG)_{Elastomer}}{F_{OM}(DEA/DEG)_{RT625}} \tag{1.17}$$

The strain energy function of an elastomer is defined as the strain energy per unit volume and is equal to the area under the stress-strain curve of the elastomer [30]. Stress in the elastomer can be obtained by taking the derivative of φ with respect to the strain, and for an isotropic φ relates to the energy stored in the elastomer to the three dimensional strain components.

1.4 Compliant DE electrodes

Stretchable, conductive materials have been studied extensively for many applications such as biomedical devices [82], electro-mechanical transducers [83] and solar power [84]. For dielectric elastomer (DE) technology, an inherently soft and highly conductive, compliant electrode material is required for optimum electro-mechanical transduction performance. The main function of the two compliant electrodes is to transfer in and out the electrical charges needed for actuation. The optimisation of electrodes mainly emphasises conductivity, stretchability, response speed and the lifetime of the electrodes. Ideal compliant electrodes must have large-strain actuation for DEA and efficient energy harvesting for DEG, with integrated logic or feedback based on self-sensing for DES [83].

1.4.1 Types of DE electrode

In the next subsections, carbon and metallic electrodes and ionic conductors are discussed, as well electrodes containing nano-sized particles. Presently, these electrodes are commonly used in dielectric elastomer technology.

1.4.1.1 Carbon-based electrodes

Conventional carbon-based electrodes are commonly made from carbon powders, carbon greases or carbon-elastomer composites. Aside from the low costs of carbon powders and carbon greases, they are quick to apply to an elastomer. Carbon powder has been used extensively on acrylic elastomers, and it is commonly applied using a spraying method [83]. However, handling carbon powder can be messy, whilst the conductivity of elastomer incorporating carbon powders cannot be sustained at large strains. Moreover, the lifetime of carbon powders is very limited, as they can be easily interrupted by other objects.

Carbon greases are viscous fluids containing carbon powders, and they are more practical to use compared to carbon powders and are quick to apply as well. Similar to the carbon powders, carbon greases, however, are not robust for DE applications. In fact, they diffuse into the elastomer due to high permeability, which may deteriorate the actuation performance of the DE. The viscous nature of carbon grease reduces the electrode's response speed and subsequently decreases the actuation performance of the DE.

A nanocomposite containing a silicone elastomer and conductive nanoparticles, such as carbon powders, can be utilised as a compliant electrode for DEs. The silicone-carbon nanocomposite is highly conductive, without compromising the soft nature of the silicone elastomer, and it is mechanically robust because the carbon powder acts as a filler for enhancing robustness [85]. The drawback of the silicone-carbon nanocomposite is that it may have a stiffening effect on the DE as a soft actuator, and it is difficult to achieve excellent dispersion of carbon nanoparticles in the silicone matrix. As an alternative to carbon nanoparticles, exfoliated graphite has been used as nano conductive fillers when making a conductive nanocomposite [86].

1.4.1.2 Metallic thin-film electrodes

Nano-sized metals such as silver nanowires (AgNWs) [87] are used as electrodes for DEs. Silver nanowires possess high conductivity, but they are significantly stiffer than elastomers. Furthermore, they often result in fractures at strains of only a few per cent [83]. Due to this increased stiffness, depositing AgNWs directly on a thin DE film stiffens the DE, and the film with a deposition of AgNWs breaks at 2 to 3% actuation strain. However, depositing silver nanowires on corrugated DE film does not limit the actuation strain. A corrugated electrode with a corrugation depth-to-period ratio close to 0.4-0.5 (4-5 μm depth and 10 μm period) [88] is favoured up to 33% strain in the direction of compliance, as verified by Benslimane et al. [88]. By patterning silver metallic electrodes on the corrugated DE film, an electrode with anisotropic behaviour is obtained. Benslimane et al. [88] later optimised the performance of a new configuration of the corrugated electrode by increasing the corrugation depth-to-period ratio to nearly 1 (7 μm depth and 7 μm period). This new arrangement was more compliant than electrodes with previous configurations and could achieve strains of up to 80%.

1.4.1.3 DEs electrodes with nano-sized particles

Nanowires and nanotubes are capable of maintaining a percolation network at large strains, and thus reduce the electrode thickness to avoid a stiffening effect. Conductive PANI nanofibres, poly(3-decyloxythiophene) and carbon nanotube thin films are capable of forming highly compliant electrodes [89]. PANI nanofibre films provide large actuation strain and have a negligible influence on the mechanical properties of the film, but they lose conductivity over time [90]. Similar to PANI nanofibre films, conducting films containing single-walled carbon nanotubes (SWCNTs) and multi-walled carbon nanotubes (MWCNTs) possess excellent actuation and have a negligible influence on the mechanical properties of DE film.

Both ultrathin PANI and SWCNT films are capable of 'self-clearing' [90,91]. Electrodes with self-clearing behaviour increase the lifetime of DEAs, because they are able to work, even after a certain amount of localised breakdown, by vaporising around the defect during the electrical breakdown. Obviously, PANI and SWCNT films are favourable, due to their increased lifetime, even though the films suffer from several local electrical breakdown defects.

1.4.1.4 Ionic conductors

Ionic conductors have been used in soft hydrogels as transparent and highly compliant electrodes for DEs as loudspeakers [92] and strain sensors [93]. Ionic conductors have higher resistivity than most electronic conductors, but they also have low sheet resistance when they are highly pre-stretched [92]. Another limitation when utilising ionic conductors is that their response speed from the ions is slower than the electron speed of electronic electrodes.

1.4.2 Requirements of compliant DE electrodes

When optimising compliant electrodes, they must possess high conductivity, increased softness and high robustness, even after many cycles of use.

DE electrodes must be highly conductive to transfer charges quickly on the DE. For this purpose, an electrode with conductivity above 10^{-2} S cm^{-1} is the ideal electrode to be utilised in DE technology [85]. Conductivity can be tuned using advanced synthesis methods, e.g. surface modification of MWCNT, or by advanced dispersion techniques using surfactants. An excellent electrode will remain conductive when it is stretched by more than 50%, even after millions of cycles.

In order to create an excellent soft DE actuator, electrodes must be inherently soft, such that they do not add stiffness in DEs. Upon stretching, the electrodes should possess no strain limit; furthermore, they should operate in charge mode rather than in voltage mode, in order to avoid electromechanical instabilities (EMI) inherent to DEs.

In addition, the electrodes must be robust after many cycles of use, as this indicates how well it can maintain conductivity and actuation strain after many cycles of actuation, which should be, ideally, 3 million cycles, as reported by Rosset and Shea [83].

1.5 Research motivation

At present, some works have been performed on the optimised electro-mechanical properties of silicone elastomers by means of phase separation. A strategy for increased relative permittivity has been performed by means of a phase-separating system with the incorporation of ionic or polar liquids in silicone elastomer, as verified by Mazurek et al. [42,94]. Phase separation has influenced the electro-mechanical properties of silicone elastomer, i.e. increased relative permittivity, high electrical breakdown and a low Young's modulus. In order to create a phase-separating system in silicone elastomer, the elastomer can be prepared through either copolymerisation or a binary polymer/copolymer blend of two immiscible polymers. The synthesised copolymer or the prepared blending formulation is subsequently cross-linked to obtain an elastomer. The copolymers' blocks segregate due to the minimisation of free energy, resulting in well-defined morphologies as a result of phase separation, which is favourable when the best increases in electro-mechanical properties are achieved.

In this thesis, a silicone elastomer with increased relative permittivity is prepared from a phase-separating PDMS-PEG copolymer in silicone elastomer. The PDMS-PEG copolymer, which is conductive, is incorporated into a polymer blend binary system. To enhance the electrical breakdown strength of the silicone elastomer, PPMS, which possesses voltage stabilisation, is copolymerised with PDMS and subsequently cross-linked, resulting in a voltage-stabilised silicone elastomer with increased electrical breakdown strength. Due to the increased relative permittivity and high electrical breakdown strength of the PDMS-PEG and PDMS-PPMS copolymers, respectively, a binary system of copolymer blend consisting of both copolymers is prepared and the synergistic effect of both copolymers with respect to electro-mechanical properties is investigated. All elastomers prepared from the synthesised copolymers and the interpenetrating network exhibit increased softness with a low Young's modulus. Finally, a conductive nanocomposite is prepared from PDMS-PEG copolymers by incorporating multi-walled carbon nanotubes to be utilised as a compliant electrode for DEs.

2 Enhancement of relative permittivity

By phase-separating a block copolymer, an approach to increase the relative permittivity of silicone elastomers, prepared by phase-separating PDMS-PEG copolymer, is described in this chapter. Several approaches for enhancing relative permittivity have been reported previously, with the commonest method involving blending silicone elastomers with metal oxide fillers. This blend often results in a stiff elastomer, and thereby this composite depreciates the electro-mechanical integrity of a soft dielectric elastomer actuator. In order to overcome stiff silicone elastomer, PDMS-PEG copolymers have been incorporated into commercial silicone elastomer. The miscibility of PDMS-PEG copolymer in the commercial silicone elastomer creates favourable phase separation on the microscopic scale, and hence the prepared elastomers possess increased relative permittivity without compromising their soft nature, conductivity or electrical breakdown strength. Details on preparing silicone elastomers with PDMS-PEG copolymers are presented in this chapter, as well as on electrical and mechanical properties.

The results presented in this chapter have been published in RSC Advances, volume 5, page 53054-53062 (2015) and the article is attached as Appendix I. The procedures for preparing PDMS-PEG copolymers and the composites containing synthesised PDMS-PEG copolymers are presented in Chapter 8.1.

2.1 Enhancement of dielectric permittivity by incorporating PDMS-PEG multiblock copolymers in silicone elastomers

2.1.1 Introduction

The synthesis of the PDMS-PEG multiblock copolymer utilised herein is based on hydrosilylation, as shown in Scheme 2-1.

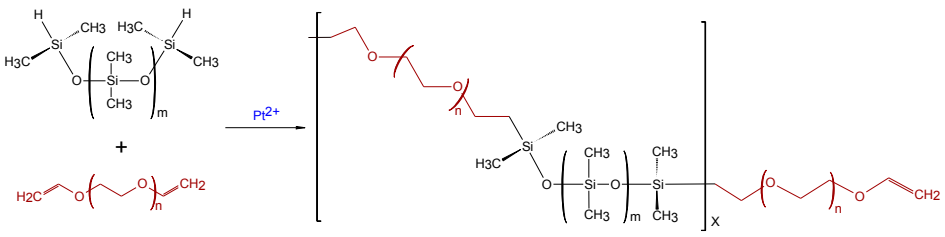

Scheme 2-1 The hydrosilylation reaction utilised when preparing a PDMS-PEG multiblock copolymer, where m is the number of repeating dimethylsiloxane units in PDMS, and n =

4 is the constant number of repeating ethyleneglycol units in PEG. X is the number of repeating PDMS-PEG units in multiblock copolymers.

Here, elastomers are prepared by means of phase separating PDMS-PEG multiblock copolymers, whereby the copolymers' blocks are expected to segregate to form well-defined structures, depending on the chain lengths of the two constituents. Subsequently the phase-separated copolymers are cross-linked via silylation into elastomers.

2.1.2 Results and discussion

2.1.2.1 PDMS-PEG multiblock copolymer

The PDMS-PEG block copolymer samples with different PDMS chain-lengths were characterised by means of size-exclusion chromatography (SEC), while the cross-linked samples were analysed by means of dielectric spectroscopy and rheology. Results for the average number of molecular weights obtained from SEC, shown in Table 2.1, indicate that synthesised PDMS-PEG multiblock copolymers possess lower M_n than targeted.

Table 2.1 Average number of multiblock copolymers molecular weights.

PDMS-PEG block copolymer	Experimental $M_{n,T}$ (10^3 g/mol)
PDMS81-PEG	13
PDMS14-PEG	2.5
PDMS7-PEG	3.6
PDMS3-PEG	1.2

The relative permittivity of the multiblock copolymers is shown in Figure 2.1. Relative permittivity for the copolymer with the least PEG (PDMS81-PEG) is constant at all frequencies, with a slight increase at low frequencies. This behaviour is similar to that of the reference elastomer (MJK), but the PDMS81-PEG multiblock copolymer has three-fold higher relative permittivity. For samples with higher PEG content, significant relaxation takes place at low frequencies, leading to increased permittivity (as seen in Figure 2.2), while dielectric loss also increases very abruptly when decreasing the frequency. This behaviour indicates conductive nature of the elastomers. In Figure 2.3 the conductivity of the copolymers is shown. It is obvious that they are all conductive, due to the display of a plateau in conductivity at low frequencies. The block copolymers have conductivities of the order of 10^2 to 10^5 higher than those of the reference elastomer (MJK).

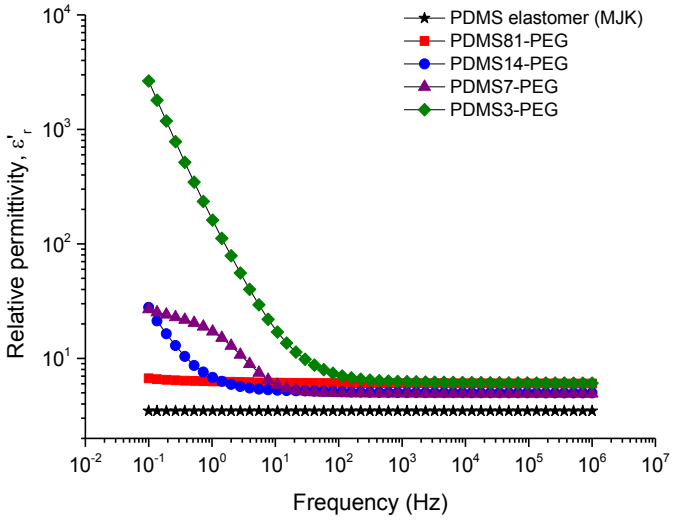

Figure 2.1 Relative permittivity of cross-linked PDMS-PEG multiblock copolymers at 23°C.

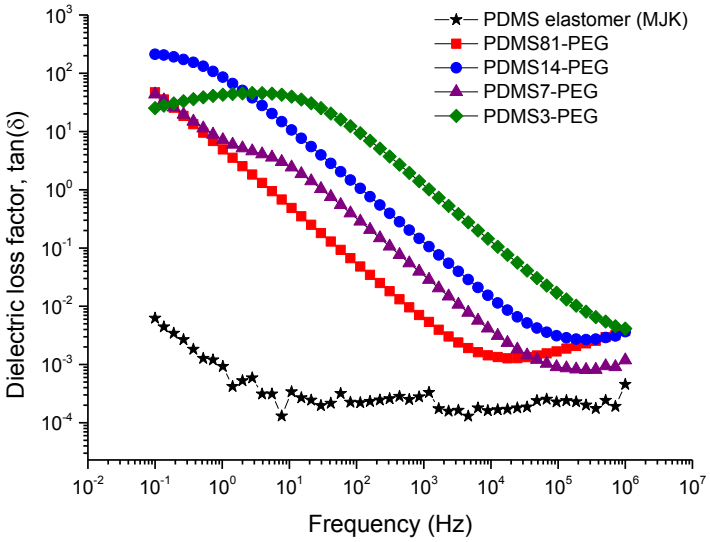

Figure 2.2 Dielectric loss factor for cross-linked PDMS-PEG multiblock copolymers at 23°C.

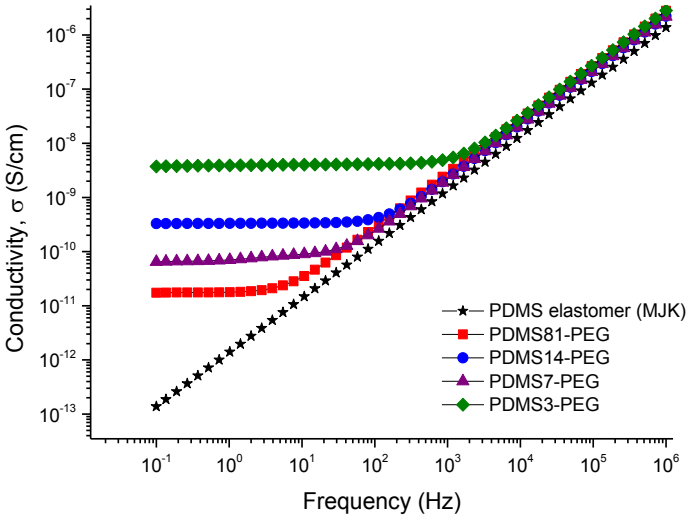

Figure 2.3 Conductivity of PDMS-PEG multiblock copolymers at 23°C.

The rheological properties of the cross-linked copolymers are shown in Figure 2.4. The PDMS14-PEG and PDMS81-PEG samples show the behaviour of very soft networks with low storage moduli compared to silicone elastomers, and they also demonstrate significant relaxation at low frequencies, which further indicates the inherent softness. In contrast, the PDMS3-PEG and PDMS7-PEG samples possess PEG-like properties with high storage moduli and low losses. Furthermore, their shear modulus is higher than that of the reinforced commercial silicone elastomer. Therefore, it is clear that an increase of PEG constituents in a PDMS-PEG multiblock copolymer reinforces the network comparable with the effect of silica fillers. It is noteworthy that PDMS81-PEG and PDMS14-PEG closely resemble each other despite PDMS81-PEG being significantly shorter than PDMS14-PEG (see Table 2.1), and thus PDMS81-PEG should provide significantly higher cross-link density and thus higher G. However, this effect cannot be seen simply because the increased content of PEG in PDMS14-PEG has an identical cross-linking effect.

2.1.2.2 Binary polymer block copolymer and silicone elastomer blends

Due to the conductivity of PDMS-PEG multiblock copolymers, they were further blended and cross-linked into a commercial PDMS elastomer (MJK). Incorporating the block copolymers into a silicone network as a binary polymer blend (BPB) can facilitate the creation of PEG spheres, as illustrated in Figure 2.5. The blends consist of PDMS-PEG multiblock copolymers at loadings of 5, 10, 15 and 20 wt% and are denoted as MJK/PDMSi, where i=81,14,7,3. When increasing PEG fractions, unfavourable and discontinuous morphologies may be formed.

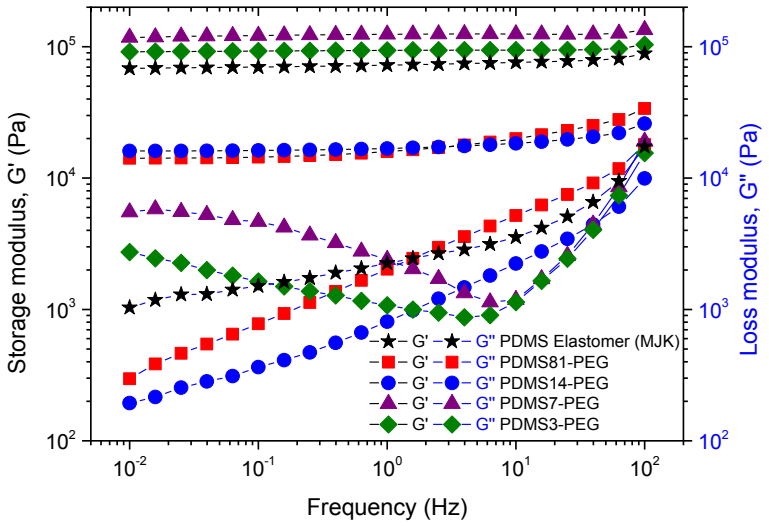

Figure 2.4 Comparison between the storage and loss modulus PDMS-PEG multiblock copolymers at 23°C.

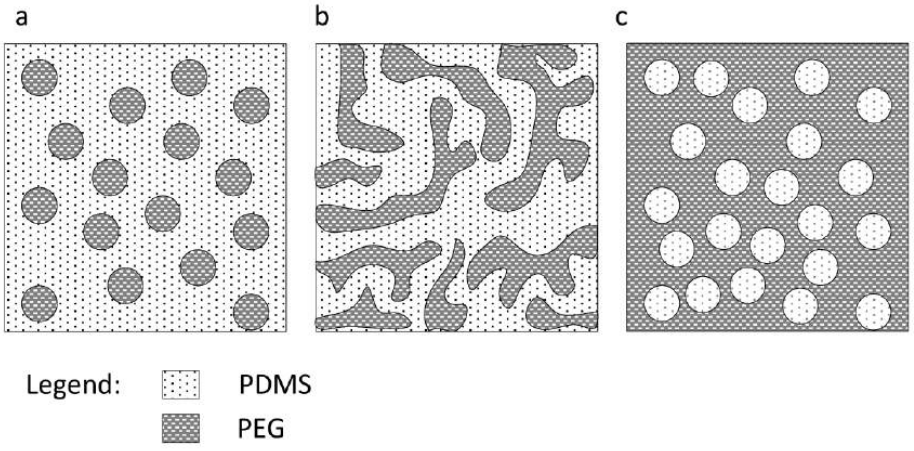

Figure 2.5 Illustration of morphologies for BPB of PDMS-PEG block copolymer and silicone elastomer: a. Continuous phase in PDMS b. Co-continuous phase in PDMS c. Discontinuous phase in PDMS.

2.1.2.3 Dielectric properties of the binary polymer blends

The relative dielectric permittivity and loss permittivity of the polymer blends are shown in Figure 2.6 and Figure 2.7, respectively. Relative permittivities are significantly improved compared to the reference elastomer (MJK), and loss

permittivities are substantially lower than those of the pure copolymers – as hypothesised. Refer to Appendix I - ESI Fig. S2-4 for data for all samples.

In general, the storage permittivity of MJK/PDMS7 increases as the wt% of the PDMS7-PEG multiblock copolymer increases in line with loadings from 5 to 20 wt%. Incorporating 20 wt% of PDMS7-PEG in a PDMS network yields the highest relative permittivity (5.2), which is an increase of 60% compared to the relative permittivity of MJK (3.5). The small increase in relative permittivity at low frequencies for MJK/PDMS7, with 5 and 10 wt%, is due to electrode polarisation effects occurring during the measurement process. However, this can be corrected by applying silicone grease between the sample and the electrode [95]. The dynamic dipole orientation of polymer molecules resulting from polarisation are observed for MJK/PDMS7 at 15 and 20 wt%, as Debye-relaxation peaks occur at frequencies of 10^0 - 10^3 Hz.

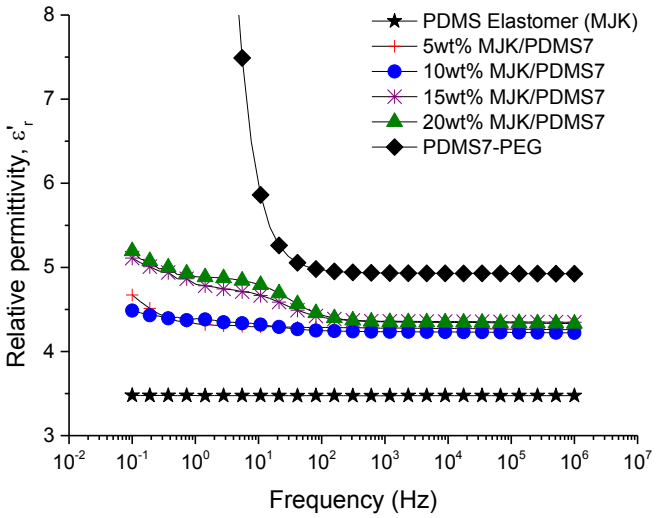

Figure 2.6 The relative permittivity of MJK/PDMS7 (5–20 wt% of PDMS7-PEG) at 23°C.

One essential finding from the dielectric characterisation is that none of the polymer blends is conductive. To further analyse the optimum polymer blend, selection based on the sample which gives the lowest dielectric loss factor is carried out. Polymer blends of MJK/PDMS3, MJK/PDMS14 and MJK/PDMS81 possess electrical loss factors in the ranges of 0.5-0.9, 0.25-0.75 and 0.06-1.25, respectively, in the investigated frequency regime. MJK/PDMS7 is the most promising blend, due to a low dielectric loss factor of 0.05- 0.125 (Figure 2.7).

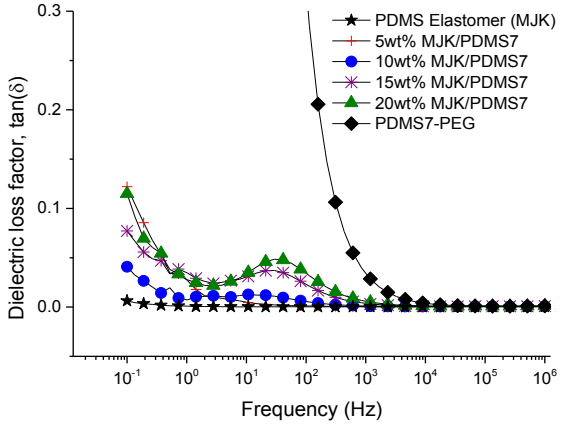

Figure 2.7 The dielectric loss factor of MJK/PDMS7 (5–20 wt% of PDMS7-PEG) at 23°C.

The behaviour of MJK/PDMS7 non-conductivity with different copolymer loadings is very promising, since no plateau regions are observed at low frequencies (Figure 2.8). This implies that a blending method applied properly causes the successful formation of a discontinuous phase for PEG that creates non-conductive behaviour of the developed polymer in the PDMS elastomer and PDMS7-PEG blends at loadings of 5, 10, 15 and 20 wt%. The conductivity of MJK/PDMS7 is consistent with respect to the MJK elastomer, which is non-conductive, as shown in Figure 2.8.

The low dielectric loss factor and non-conductivity of MJK/PDMS7 for all investigated copolymer loadings indicates that the composites consist of PEG in discontinuous phases.

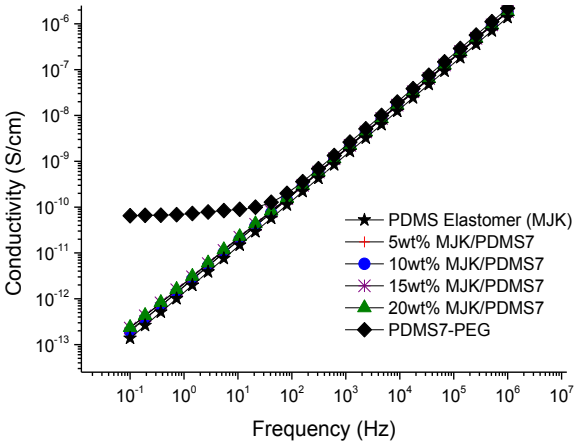

Figure 2.8 The conductivity of MJK/PDMS7 (5–20 wt% of PDMS7-PEG) at 23°C.

2.1.2.4 Rheological properties of BPB

To evaluate the effect of blending on mechanical properties, elastomers from MJK/PDMS7 with a 5–20 wt% copolymer were rheologically characterised, as shown in Figure 2.9. The storage modulus of MJK/PDMS7 with 20 wt% is relatively close to the storage modulus of silicone elastomer (MJK). In contrast, MJK/PDMS7 with 5 and 10 wt% is softer than the PDMS elastomer, with storage moduli being one-fold and three-fold lower than the storage modulus of MJK (7×10^5 Pa). The blend of MJK/PDMS7 with 15 wt% is the stiffest, with G' = 8×10^5 Pa. Another important feature observed from Figure 2.9 is the appearance of small relaxation peaks in the loss moduli for 15 and 20 wt%. This is due to the transient nature of the PEG semi-crystalline phases acting as reinforcing domains.

All elastomers, however, do show to be well cross-linked and appear very elastic, and therefore they are suitable as soft dielectric elastomers.

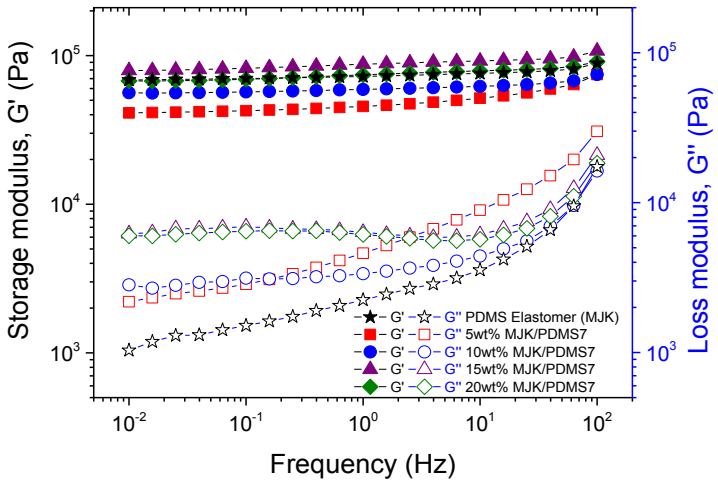

Figure 2.9 The storage and loss moduli of MJK/PDMS7 (5–20 wt% of PDMS7-PEG) at 23°C.

2.1.2.5 Dielectric breakdown (E_{BD}) strength

Electrical breakdown and the influence of different PDMS7-PEG block copolymer loadings in MJK/PDMS7 on the Weibull parameters were investigated. The Weibull fits can be seen in Figure 2.10. The Weibull β-parameter (slope of the dashed line in Figure 2.10) decreases in line with an increasing MJK/PDMS7 wt%, and it even increases at 20 wt%. The y-axis (Figure 2.10) was determined from the formula below:

$$ln[-ln(1-F)] = \beta\, ln(E_{BD}) - \beta l\, n(\eta) \qquad (2.1)$$

where F and E_{BD} were the Weibull cumulative distribution function and electrical breakdown, respectively. The value of the Weibull location parameter η was determined from $\ln[-\ln(1-F)] = 63.2\%$.

Averaged and fitted electrical breakdown data for all the samples are presented in Table 2.2. MJK/PDMS7 with 5 wt% bears the highest dielectric breakdown strength (103 V μm^{-1}) with a standard deviation of ± 4 V μm^{-1} when averaging over the 12 samples. All samples have an almost identical Weibull η parameter and respective breakdown strengths.

Table 2.2 Dielectric breakdown strength, Weibull parameters η and β, and R^2 of linear fit for the pure silicone elastomer (MJK) and MJK/PDMS7 with 5-20 wt% of the PDMS7-PEG multiblock copolymer.

MJK/ PDMS7	Dielectric breakdown E_{BD} (V μm^{-1})	Weibull η-parameter	Weibull β-parameter	R^2 of linear fit
MJK	93 ± 7	98	17	0.92
5 wt%	103 ± 4	105	31	0.84
10 wt%	92 ± 3	94	31	0.93
15 wt%	93 ± 8	96	13	0.99
20 wt%	101 ± 5	103	25	0.95

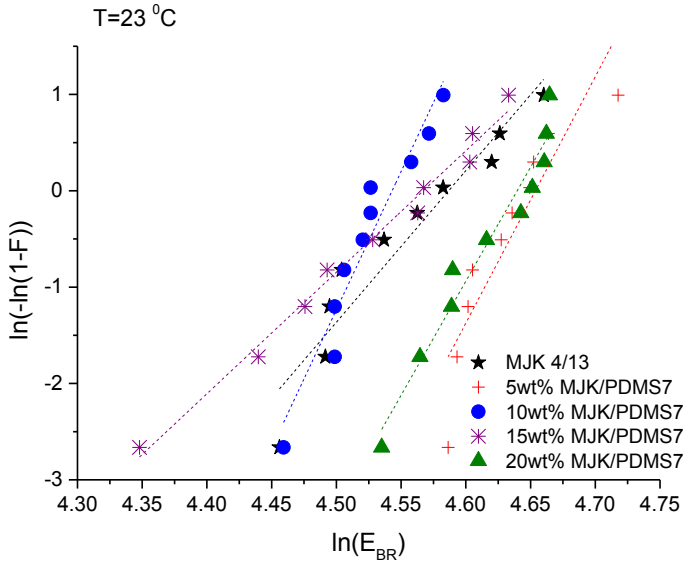

Figure 2.10 Cumulative probability of failure of the PDMS elastomer (MJK) and MJK/PDMS7 with 5–20 wt% of the PDMS7-PEG multiblock copolymer (T = 23°C). The dashed lines represent the linear fit line to the data.

Adding conductive particles usually destabilises the elastomer in respect to electrical breakdown [96], but in the composites investigated herein the conductive PEG clearly stabilises the elastomers, as the β parameters for the composites are significantly larger – and thus the materials will be more electrically stable. This may be due to the charge-trapping effects of PEG [48]. The trapping effect probably decreases in line with increased loadings, and thus there is an optimum in the composition at which the electrical stabilisation is highest. The softest sample (5wt%) is furthermore very steep, and therefore the effect cannot be attributed to increased Young's moduli, as shown in Vudayagiri et al [30].

2.1.2.6 Figure of merit (F_{OM})

One method which can be used to evaluate the actuation performance of the elastomer is by means of a figure of merit for dielectric elastomer actuators, F_{OM} (DEA). The F_{OM} (DEA) for the MJK/PDMS7 samples was determined relative to the absolute value of the F_{OM} (DEA) of Elastosil RT625 (1.86×10^{-24}), as reported by Vudayagiri et al. [30].

The calculated figures of merit are shown in Table 2.3. The composite with 5 wt% has the highest normalised F_{OM} (DEA) value of 17, i.e. 17 times greater actuation than the reference elastomer. This composition is the best-performing elastomer amongst those investigated, due to the combination of high electrical breakdown strength, a low Young's modulus and relatively high dielectric permittivity.

Table 2.3 Normalised FOM (DEA) and Young's modulus (Y) for MJK/PDMS7 with 5–20 wt% of PDMS7-PEG multiblock copolymer.

MJK/PDMS7	Young's modulus, *Y** (kPa)	Normalised F_{OM} (DEA)
0 wt% (MJK)	205	6.1
5 wt%	123	17.2
10 wt%	169	9.6
15 wt%	238	8.0
20 wt%	203	11.2

** Young's modulus calculated from Y = 3G'*

2.1.2.7 Contact angles of BPB

The wettability of MJK/PDMS7 polymer blends was evaluated by static contact angle measurements. The nature of the PDMS-PEG multiblock copolymer is known as one of the amphiphilic dynamic polymer chains. Similar to MJK/PDMS7, which consists of PDMS7-PEG block copolymers in the PDMS matrix, the trend on wettability leans toward amphiphilic behaviour. In Figure 2.11, the contact angles of MJK/PDMS7 for different wt% (5, 10, 15 and 20) decline steeply for the first 20s and are followed by a slight decrease until they are almost stable at the end of the time period. This indicates that the block copolymer in the polymer blends orients its polymer chains in order to achieve the

lowest possible surface energy, since the copolymer comprises blocks of both hydrophobic PDMS and hydrophilic PEG. When the developed elastomer is exposed to air, the surface is controlled by the hydrophobic PDMS from the block copolymer and the matrix, but upon contact with water the chains re-orient and the PDMS blocks migrate back into the bulk material and are replaced by the more hydrophilic PEG blocks at the surface [97]. This behaviour is confirmed by the contact angle measurement, where the rearrangement of the polymer chains accounts for the change in contact angle over time when a droplet of deionised water is dropped onto the top surface of the sample. Thus, classing the wettability of MJK/PDMS7 as amphiphilic is the result of incorporating the PDMS7-PEG multiblock copolymer in the network, since PEGs are well-known for their hydrophilic properties.

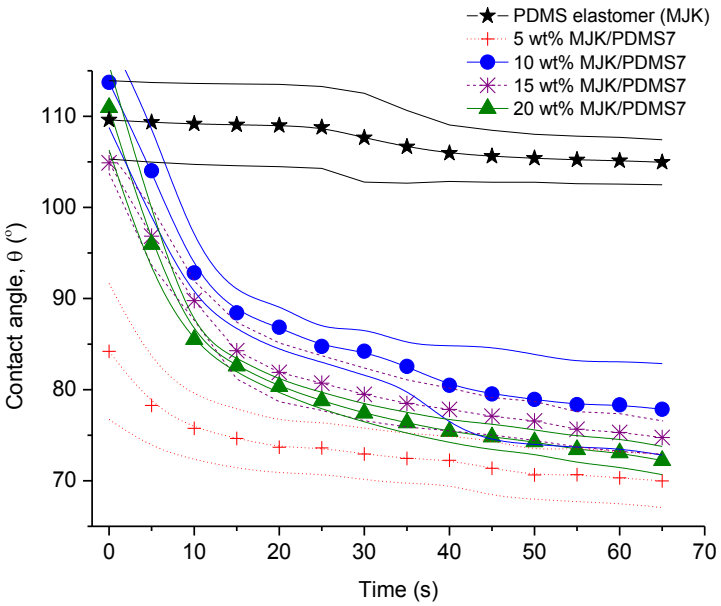

Figure 2.11 MJK/PDMS7 contact angles (5–20 wt% of PDMS7-PEG) at 23°C.

2.1.2.8 SEM analysis

In order to verify the hypothesised structure of the composites, the prepared films were investigated by SEM; the microscope pictures are shown in Figure 2.12. For MJK/PDMS7 with 5 wt% copolymer loading, a rough surface is obtained. There are no visible PEG domains observed, and the composite appears homogeneous on the microscale. When the loading of the block copolymer increases from 10 to 20 wt%, the microspherical domains become visible and the number of microspheres increases in line with an increased concentration of PEG. The domains were analysed using Image Processing and Analysis software (ImageJ). The domain sizes of visible spherical domains for MJK/PDMS7 at 10, 15 and 20 wt% are 1.3 ± 0.2 µm, 1.3 ± 0.2 µm and 1.6 ± 0.2 µm, respectively. The observation of spherical domains

is coherent with the samples from Liu et al [68], who observed pores on composite samples of PDMS and PEG etched with ethanol. The obtained morphologies indicate that the methodology of blending polymers creates the good dispersion of multiblock copolymers in a silicone network where the spherical domain size seems independent on concentration, as the chain length of the PEG was not a variable in this study. Since the composite with the lowest concentration of PEG possesses different morphology, and at the same time possesses the best overall properties for actuation and lifetime, it may be argued that the introduction of additional surfaces into the system is unfavourable, especially as these surfaces may increase permittivity but they also destabilise the elastomer.

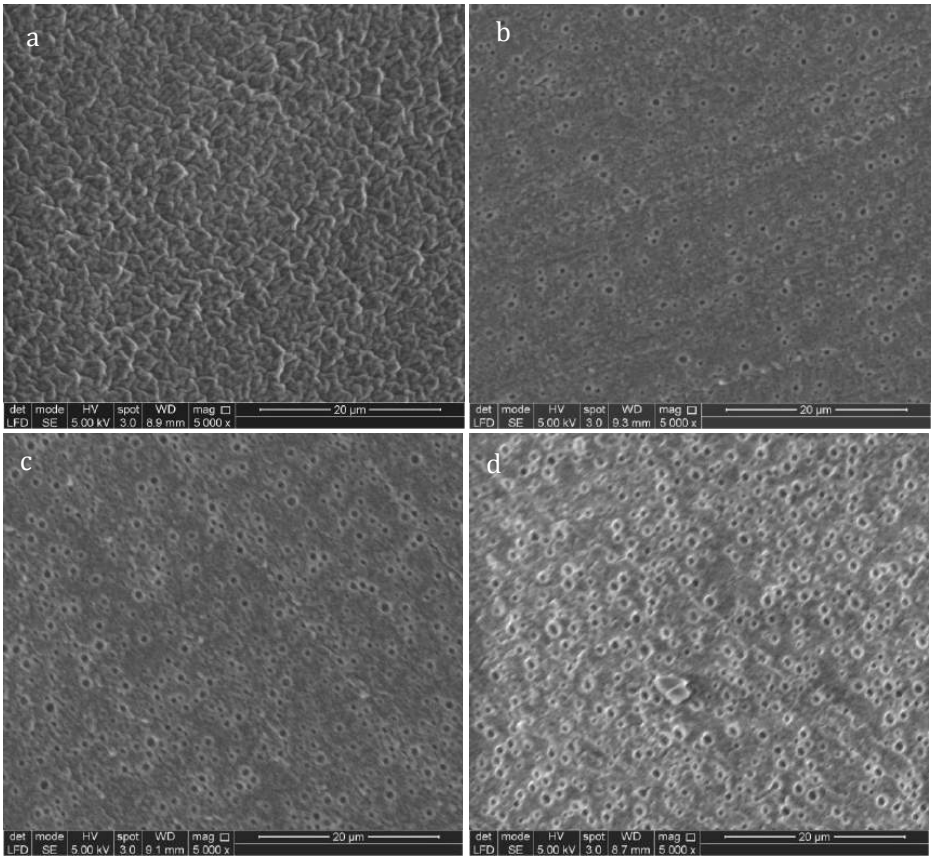

Figure 2.12 SEM images of MJK/PDMS7 at: a. 5 wt% b. 10 wt% c. 15 wt% d. 20 wt%.

2.1.3 Part conclusion

A new composite elastomer, which has high relative and low loss permittivity, was successfully created from a binary system of polymer blends consisting of conducting PDMS7-PEG multiblock copolymer and non-conducting PDMS

elastomer (MJK). The desired morphology (discontinuous phase of the block copolymer and continuous phase of PDMS) was successfully created in the blends, thereby indicating the development of non-conductive behaviour in the elastomer. Low copolymer loading is favourable, since it creates a homogeneous elastomer on the micro-scale which in turn facilitates a more electrically stable elastomer. Even though the PDMS7-PEG multiblock copolymer is conductive and has high loss permittivity, a good composite elastomer can be developed by incorporating the block copolymer into a silicone network at different wt% and by employing a proper mixing technique. The dielectric breakdown strengths for cross-linked MJK/PDMS7 polymer blends were relatively high, with values in the order of 100 V/µm. Finally, by integrating all the characterised parameters, i.e. Young's modulus, breakdown strength and relative permittivity, figures of merit for the dielectric elastomer actuation of the various MJK/PDMS7s were determined, and it was concluded that by incorporating low concentrations of PEG, actuation could be improved 17-fold along with the extension to the lifetime of the dielectric elastomer.

3 Enhancement of electrical breakdown strength

A strategy for increasing the electrical breakdown strength of silicone dielectric elastomers via a voltage-stabilising effect is described in this chapter. The idea behind this work came from literature studies of the enhancement of electrical breakdown strength in polyethylene as a high-voltage insulation cable. From the literature studies, aromatic-based additives were incorporated into polyethylene (PE), and these additives acted as a voltage stabiliser to improve the electrical breakdown strength of PE via electron-trapping effects. Increased electrical breakdown strength is achieved through voltage stabilisation. When synthesising PDMS-PPMS, the optimised condition of the hydrosilylation reaction occurs in a very convenient environment, namely speed-mixing for a few minutes at room temperature. The cross-linked PDMS-PPMS copolymers are soft and highly elastic. Details on preparing cross-linked PDMS-PPMS copolymers, and their electrical and mechanical properties, are explained thoroughly in this chapter.

The results presented herein have been published in RSC Advances, volume 7, page 468-477 (2017) and the article is attached as Appendix II. The procedures for preparing cross-linked PDMS-PPMS copolymers with different concentrations of phenyl groups are presented in Chapter 8.2.

3.1 Silicone elastomers with covalently incorporated aromatic voltage stabilisers

3.1.1 Introduction

Increasing the electrical breakdown strength of DEs allows for greater actuation, due to the possibility of utilising larger electrical fields without failure [19,98]. For DEs, several mechanisms lead to electrical breakdown, namely partial discharge [79] and electromechanical [74] and electrothermal breakdown [51,99]. Multiple studies on pre-strained DE electrical breakdown have been conducted, with the main emphasis on reliability and the effect of electrical breakdown strength on external properties such as effective electrode configurations [47,48], elastomer processing techniques [49] and pre-stretching methods [19,47,98]. As an alternative approach to enhancing electrical breakdown strength, blending in additives with a voltage-stabilising effect or via polymer structure modifications remains unexplored for dielectric elastomers.

In this work, the voltage stabilisation effect of PPMS in cross-linked PDMS-PPMS copolymers is investigated, while cross-linked materials are characterised mechanically and dielectrically. Herein, soft dielectric silicone elastomers with increased electrical

breakdown strength, due to the incorporation of an aromatic voltage stabiliser, were prepared by cross-linking synthesised polydimethylsiloxane-polyphenylmethylsiloxane (PDMS-PPMS) copolymers. Concentrations of the voltage stabiliser were varied by changing the molecular weights of the PPMS in the copolymer.

3.1.2 Results and discussion

PDMS-PPMS block copolymers were prepared from the hydrosilylation of hydride-terminated PPMS and vinyl-terminated PDMS at room temperature in the presence of a platinum (Pt) catalyst, as shown in Scheme 3-1. The synthesised block copolymer has *X*+1 blocks of phenylmethylsiloxane and *X* blocks of dimethylsiloxane.

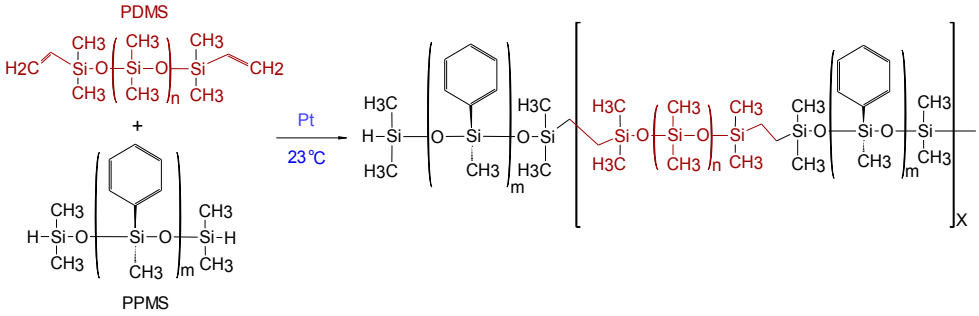

Scheme 3-1 The hydrosilylation reaction utilised when preparing the PDMS-PPMS block copolymer with a stoichiometric ratio of r = (X + 1) / X, where m is the number of repeating phenylmethylsiloxane units in PPMS (m = 2 and 6) and n is the number of repeating dimethylsiloxane units in PDMS (n = 377, 231, 126 and 80).

The targeted elastomers with covalently grafted voltage stabilisers are shown in Figure 3.1. In order to realise these elastomers, copolymers were first synthesised and characterised before being cross-linked into elastomers.

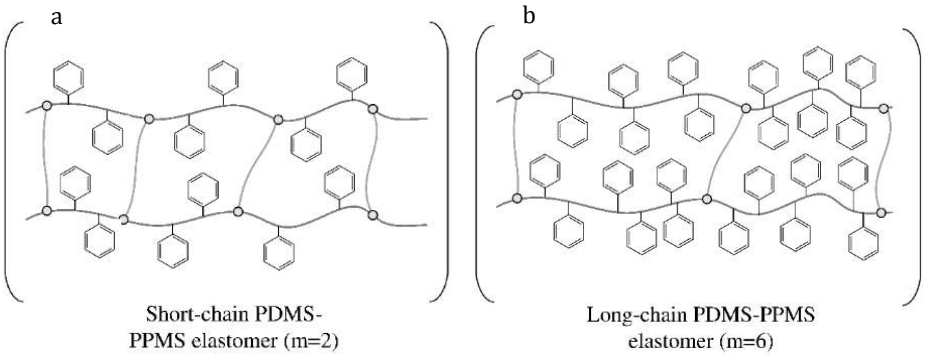

Figure 3.1 Illustration of a cross-linked copolymer with a) short- and b) long-chain.

3.1.2.1 Synthesised PDMS-PPMS copolymers

Determined molecular weights of synthesised PDMS-PPMS copolymers are shown in Table 3.1. All copolymers have low polydispersity indexes (PDI ≤ 2.1). The disappearance of the Si-CH_2=CH_2 bond signal at 5.8 - 6.2 ppm was confirmed by ^{1}H-NMR, to ensure that all vinyl groups in the PDMS had been consumed fully during the hydrosilylation of vinyl-terminated PDMS and hydride-terminated PPMS; refer to Appendix II - ESI 5 for NMR spectra in Figures S2-9. ^{1}H-NMR spectra confirmed that the synthesised PDMS-PPMS copolymers were hydride functional, and all vinyl groups in the PDMS were fully reacted.

3.1.2.2 Linear viscoelasticity

To evaluate the effect of the increased concentration of the phenyl group on viscoelastic properties, the prepared elastomers were characterised rheologically, as shown in Figure 3.2. This is an important investigation to perform for these systems, since aromatics are well-known to inhibit utilised silylation chemistry. The PDMS-PPMS elastomers show to be well cross-linked and behave elastically, i.e. the inhibiting nature of the phenyl groups did not affect the final properties of the elastomers. The resulting storage moduli (G') for all elastomers and the reference are between 10^4 and 10^5 Pa, and they all behave in a similar manner with close-to-identical relaxations. From these results it is obvious that the elastomers maintain network integrity. Relative losses [tan (δ)] are comparable to these of commercial silicone elastomers such as Elastosil RT625 from Wacker Chemie [100].

Table 3.1 Average number of molecular weights and actual concentrations of the phenyl group of synthesised PDMS-PPMS copolymers.

Cross-linked PDMS-PPMS copolymer	Actual $M_{n,T}$ (kg mol^{-1})	Polydispersity index, PDI (M_w / M_n)
377DMS_2PMS	32	2.1
231DMS_2PMS	36	1.9
126DMS_2PMS	73	1.5
80DMS_2PMS	39	1.8
377DMS_6PMS	42	1.7
231DMS_6PMS	37	1.8
126DMS_6PMS	82	1.6
80DMS_6PMS	32	2.0

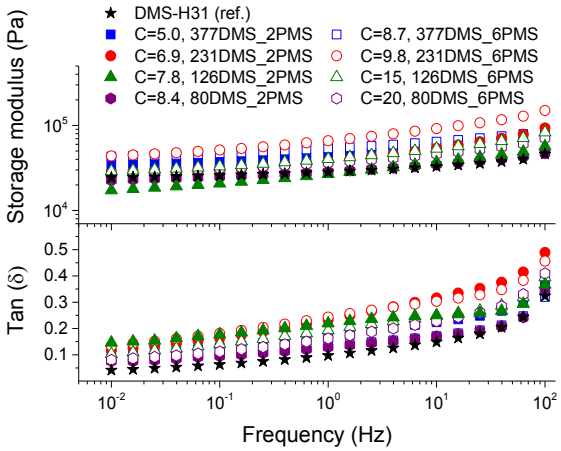

Figure 3.2 The storage and tan (δ) of cross-linked PDMS-PPMS copolymers at 23°C; C is in 10^{-4} mol g^{-1}.

3.1.2.3 Stress-strain relationship

Stress-strain curves and Young's moduli of the cross-linked copolymers are shown in Figure 3.3and Figure 3.4, respectively. All cross-linked copolymers show increased strain at breaking, compared to the reference (DMS-H31), due to an evident 'plasticising' effect (see Figure 3.3). All elastomers are still strain-hardening despite being plasticised. The resulting Young's moduli at 5% strains of the cross-linked copolymers are shown in Figure 3.4, and the soft nature of all the elastomers is obvious. Common Young's moduli of silicone elastomers are around 1 MPa [100]. Another finding is that the cross-linked copolymer 80DMS_2PMS is slightly stronger than the reference elastomer (DMS-H31), not only with respect to the initial Young's modulus, but also with respect to ultimate strength.

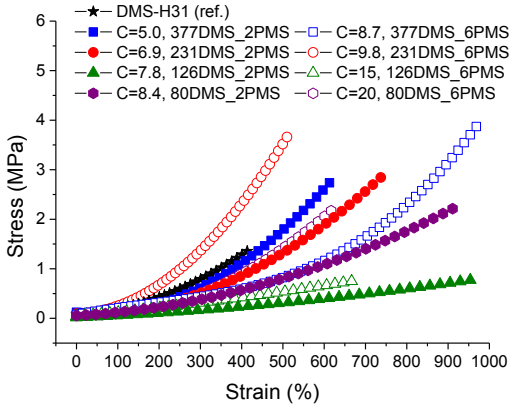

Figure 3.3 Stress-strain curves for PDMS-PPMS elastomers with different phenyl group concentrations at 23°C (typical standard deviations in tensile measurements were of the order ± 5%).

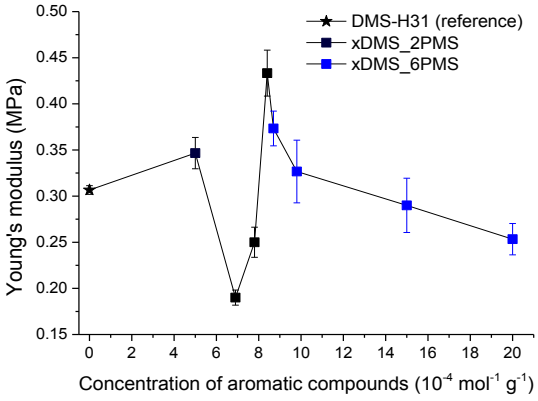

Figure 3.4 Young's moduli for the PDMS-PPMS and reference elastomers.

With respect to actuation, elastomers C=7.8 and 15·10^{-4} mol g^{-1} show the most softness. On the other hand, both elastomers do not possess any significant strain-hardening behaviour. The slightly stronger elastomers C=8.4 and 8.7·10^{-4} mol g^{-1} show ideal properties for actuation with good, ultimately strain-hardening, behaviour.

Obviously, from the mechanical data, there is no clear trend in mechanical behaviours except that a concentration of around 8.5·10^{-4} mol g^{-1} seems to be the most favourable. This is most likely due to local phase separation, which serves both to stabilise and to plasticise the elastomer, i.e. some regions will be rich in PPMS (rigid zones) and other regions poor (plasticised zones). This can be seen to some extent from SEM imaging of the resulting films with two examples shown in Figure 3.5. As investigated by Luo et al. [101], PDMS shows a distinct triangular pattern whereas PMMS shows a pattern with bent rectangles. This is illustrated below by the elastomers 377DMS_2PMS and 80DMS_2PMS, wherein sample 377DMS_2PMS shows a distinct PDMS structure while elastomer 80DMS_2PMS has areas with both signatures. SEM pictures of all elastomers can be seen in Appendix II - ESI 6, Figure S10.

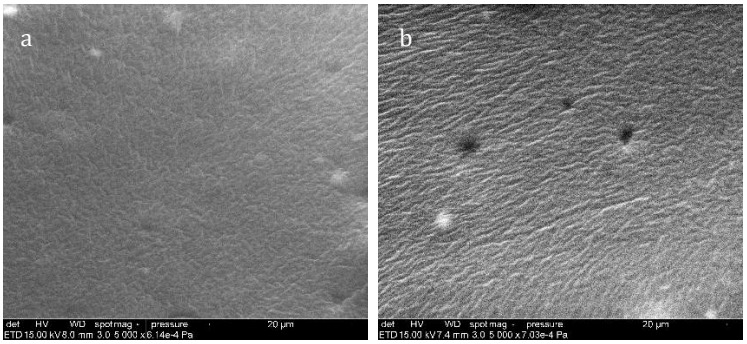

Figure 3.5 SEM pictures of two representative samples, namely a) 377DMS_2PMS and b) 80DMS_2PMS.

3.1.2.4 Dielectric properties

The conductivity and dielectric properties of the cross-linked PDMS-PPMS copolymers and the reference elastomer are shown in Figure 3.6 and Figure 3.7, respectively. The resulting conductivities indicate that none of the cross-linked copolymers is conductive, as illustrated in Figure 3.6. Low conductivity is a key element in the actuation performance of the DE. The relative permittivity of prepared elastomers with short-chain PPMS initially increases and reaches a maximum phenyl group concentration of $6.9 \cdot 10^{-4}$ mol g^{-1}, albeit it decreases thereafter. On the other hand, the relative permittivity of cross-linked copolymers with long-chain PPMS decreases in line with an increase in phenyl concentration. The flat curves furthermore indicate that phase separation is not macroscopic but rather limited to the lower microscale or nanoscale. These observations again indicate that micro- or nanoscale phase separation takes place and that the morphology of the elastomers depends strongly on the concentration of phenyl groups. Dielectric losses, which are represented by tan (δ), are relatively low for all cross-linked copolymers, as shown in Figure 3.7. The reference elastomer (DMS-H31) shows low tan (δ) as well.

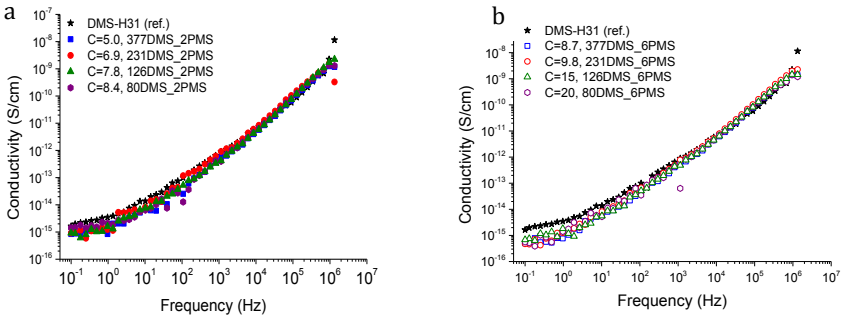

Figure 3.6 The conductivity of PDMS-PPMS elastomers with different phenyl concentrations of at 23 °C: a) short-chain and b) long-chain PPMS; C is in 10^{-4} mol g^{-1}.

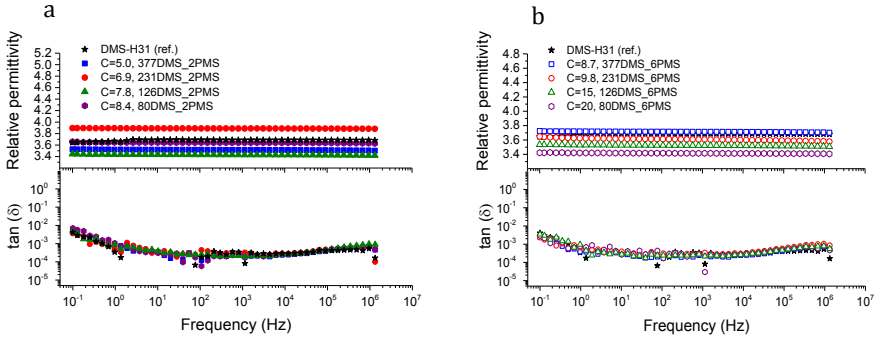

Figure 3.7 The dielectric properties of PDMS-PPMS elastomers with different phenyl concentrations at 23°C: a) short-chain and b) long-chain PPMS; C is in 10^{-4} mol g^{-1}.

3.1.2.5 Electrical breakdown and Weibull analysis

The influence of the concentration of the phenyl group in cross-linked PDMS-PPMS copolymer on electrical breakdown strength was investigated. The resulting electrical breakdown strength of the cross-linked copolymers with different phenyl group concentrations is shown in Figure 3.8, namely an optimum electrical breakdown strength (72 ± 3 V μm^{-1}) occurring at a phenyl concentration of $8.4 \cdot 10^{-4}$ mol g^{-1}. In other words, electrical breakdown strength has increased 36% compared to the reference elastomer. The optimum is most likely due to the combination of favourable phase separation and a relatively high concentration of phenyl groups. Stiffness may also affect electrical breakdown strength strongly [102], i.e. the electrical breakdown strength of the reference elastomer is low due to the inherently soft nature of silicone elastomers cross-linked from high molecular weight PDMS polymers [103], and there is a broad amount of variation in the Young's moduli of the prepared elastomers. To evaluate whether the voltage stabilisation effect is rather an effect of increased stiffness, the influence of Y on electrical breakdown strength was investigated. There is no correlation, as seen from Appendix II - ESI 7 in Figure S11, which means that the effect is due to the voltage stabilisation effect.

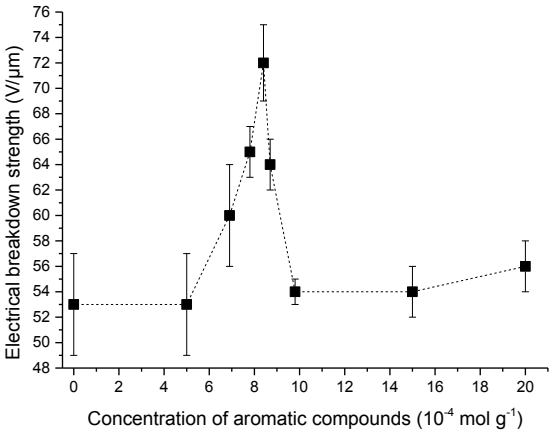

Figure 3.8 Electrical breakdown strength of PDMS elastomer and PDMS-PPMS copolymers with different phenyl group concentrations.

Weibull analysis was used to obtain a further understanding of the electrical reliability of the prepared elastomers. The Weibull probability distribution of failure for all films is shown in Figure 3.9. The η-parameter, which is the Weibull scale parameter, was determined from the Weibull plot as the value at which failure probability, ln[-ln(1 - F)], was 63.2% [10]. The β-parameter is the Weibull shape parameter, representing the broadness of distribution. The η-parameter is closely correlated to the mean breakdown voltage [104]. A small value of the Weibull shape parameter indicates that electrical breakdown occurrences are broadly dispersed [104].

Due to different prepared PDMS-PPMS elastomer film thicknesses, the determined electrical breakdown strengths were normalised based on a reference thickness for better comparison. Normalised dielectric breakdown strength can be determined by [48]:

$$E_n = n^{-\frac{1}{\beta}} E_0 \tag{3.1}$$

where E_0 is the electrical breakdown strength of a 100 µm film, β is the Weibull shape parameter and n is relative sample thickness compared to the chosen reference thickness of (t_0 = 100 µm).

The results for the normalised electrical breakdown strength (E_n), Weibull η- and β-parameters and R^2 of the linear fits for cross-linked copolymers, including the reference, are summarised in Table 3.2. Cross-linked PDMS-PPMS copolymers with long-chain PPMS possess lower electrical breakdown strength standard deviation than the copolymers with short-chain PPMS, as illustrated in Table 3.2. The coefficient of determination (R^2) of all investigated elastomers is above 0.85, indicating that the measured electrical breakdown strengths correlate well with the fitted regression lines.

Table 3.2 Electrical breakdown strength at 23°C, Weibull parameters η and β and R^2 of the linear fit for all prepared cross-linked copolymers and the reference.

Cross-linked PDMS-PPMS copolymer	Thick-ness (µm)	Electrical breakdown strength (V µm^{-1})	Weibull β-parameter	Weibull η-parameter	R^2	Normalised electrical breakdown (V µm^{-1})
DMS-H31 (ref.)	105	53 ± 4	17	55	0.85	52.9 ± 3.6
377DMS_2PMS	81	53 ± 4	17	55	0.85	53.7 ± 3.7
231DMS_2PMS	91	60 ± 4	20	61	0.91	60.1 ± 3.4
126DMS_2PMS	80	65 ± 2	32	66	0.94	65.5 ± 2.5
80DMS_2PMS	90	72 ± 3	26	73	0.92	71.9 ± 3.1
377DMS_6PMS	81	64 ± 2	47	65	0.89	64.1 ± 1.6
231DMS_6PMS	95	54 ± 1	60	54	0.94	54.0 ± 1.6
126DMS_6PMS	95	54 ± 2	39	55	0.88	54.0 ± 1.8
80DMS_6PMS	95	56 ± 2	28	57	0.94	56.1 ± 2.2

The Weibull plots for all samples are shown in Figure 3.9. The plotted data in the Weibull probability distribution of failure of elastomers with short-chain PPMS clearly show two domains (refer to Figure 3.9a). This is an indication of the inhomogeneity of the phenyl group in the PDMS-PPMS matrix containing short-chain PPMS. On the other hand, the Weibull distribution data for the elastomers with long-chain PPMS show one domain with only a small discrepancy at high voltages, thereby indicating better homogeneity of the phenyl group in the PDMS-PPMS matrix.

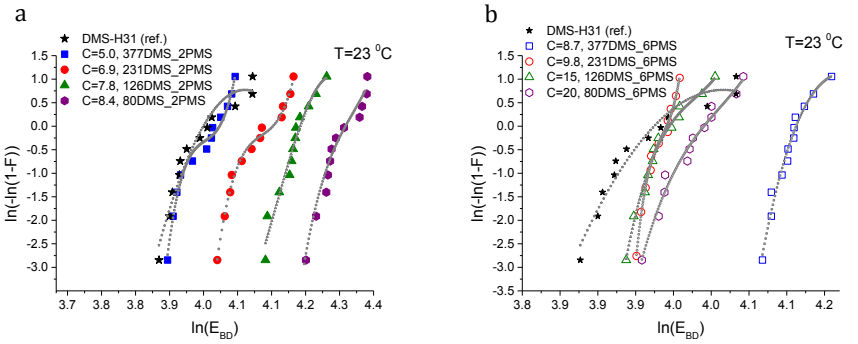

Figure 3.9 Weibull plots of PDMS elastomer and PDMS-PPMS copolymers with different phenyl group concentrations: copolymers from a) short-chain and b) long-chain PPMS. The dashed lines serve solely as guidelines for the eyes to differentiate between data slopes; C is in units of 10^{-4} mol g^{-1}.

Weibull parameters η and β at different phenyl group concentrations are compared and summarised in Figure 3.10. One important finding from the values of the Weibull β-parameter is that the PDMS-PPMS elastomers with long-chain PPMS have larger β-parameter values compared to the elastomers with short-chain PPMS except at very high phenyl group loadings, where β drops. For both types of cross-linked copolymers an optimum η parameter value of around $8 \cdot 10^{-4}$ is found. Furthermore no links between the Weibull parameters and the Young's moduli of the elastomers could be identified, as shown in Appendix II - ESI 8, Figure S12.

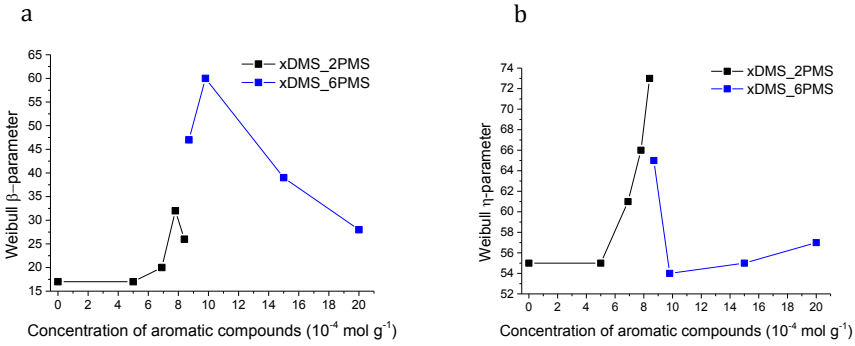

Figure 3.10 Weibull parameters for prepared PDMS-PPMS copolymer and reference (DMS-H31) samples: a) β-parameter and b) η-parameter.

3.1.3 Part conclusion

Inherently soft elastomers based on cross-linked PDMS-PPMS copolymers were synthesised successfully and proven to possess increased electrical breakdown strength, due to voltage stabilisation arising from aromatic groups of PPMS. Cross-linked copolymers with varying concentrations of aromatic groups were prepared from

copolymers synthesised by varying the chain length of PDMS while maintaining the chain length of PPMS. The cross-linked copolymers possessed higher electrical breakdown strength than the pure PDMS-based reference elastomer, due to π-electrons of the aromatic group being capable of trapping charges. Aside from having high electrical breakdown strength, the cross-linked copolymers showed an increased storage modulus and low viscous loss, hence maintaining the network integrity of the dielectric elastomer. All cross-linked copolymers demonstrated strain-hardening behaviours. From the electrical breakdown strength, optimal phenyl group concentration was determined at approximately $8.4 \cdot 10^{-4}$ mol g^{-1}. As a result of these properties, voltage-stabilised elastomers were synthesised. Further studies will hopefully uncover better voltage stabilisers, which would subsequently be a giant step toward producing reliable dielectric elastomers.

4 Optimisation of electro-mechanical properties

An approach for enhancing electro-mechanical properties of silicone elastomers by means of phase separating binary copolymer blends is presented in this chapter. Phase separation on the nanoscopic to microscopic scale may create favourable, well-defined morphologies in silicone dielectric elastomers for enhanced electro-mechanical properties. To achieve the ultimate goal with respect to actuation, namely a soft dielectric actuator with high permittivity and electromechanical stability, so-called voltage-stabilised silicone elastomers prepared from PDMS-PPMS copolymers are chosen as the basis for a cross-linked binary copolymer mixture. The relative permittivity of the voltage-stabilised elastomers, however, is not higher than that of a commercial silicone elastomer. As a solution to voltage-stabilised elastomers with enhanced relative permittivity, high-permittivity PDMS-PEG copolymers are covalently incorporated into silicone elastomers from a voltage-stabilised silicone copolymer. The resulting electrical and mechanical properties of the cross-linked binary copolymer blends consisting PDMS-PPMS and PDMS-PEG copolymers are described in this chapter.

The results presented in this chapter have been submitted to RSC Advances and the article is attached as Appendix III. The procedures for preparing voltage-stabilised silicone elastomers with incorporation of the PDMS-PEG copolymers by means of binary system of copolymer blends are presented in Chapter 8.3.

4.1 Voltage-stabilised elastomers with increased relative permittivity and high electrical breakdown strength by means of phase separating binary copolymer blends of silicone elastomers

4.1.1 Introduction

Phase separation is commonly known to occur in polymer blends and block copolymers. Polymer blends phase separate due to the immiscibility of the polymers as a result of minimising free energy when the polymers separate [105,106]. Thermoplastic polymer blends possess different types of well-defined structures, such as bi-continuous structures [106–108], islands [106] and holes [106], and these phase-separated structures depend strongly on the volume fraction of the constituents in the polymer blends. A silicone elastomer prepared from a binary polymer blend consisting of a conducting PDMS-PEG copolymer and non-conducting PDMS results in the creation of a continuous phase of PDMS and a discontinuous

phase of PEG [10]. Favourable phase separation in cross-linked blends can be achieved via proper blending and preparation methods. Silicone elastomers prepared from polymer blends have been shown to optimise elastomer as a soft actuator with a large strain.

In this work, phase separation as means of optimising silicone elastomers is explored further by combining two recently synthesised copolymers (PDMS-PEG and PDMS-PPMS copolymers), which have been shown to enhance relative permittivity and electrical breakdown strength, respectively. A synergistic effect of the cross-linked binary system of copolymer blends consisting of a PDMS-PEG and a PDMS-PPMS copolymer is also explored further.

4.1.2 Results and discussion

A cross-linked binary copolymer blend consisting of PDMS-PPMS and PDMS-PEG copolymers with a possible morphology is illustrated in Figure 4.1. The targeted morphology of the binary system of copolymer blends containing PDMS-PEG and PDMS-PPMS copolymers is a well-defined structure forming a continuous PDMS-rich phase and discontinuous phases of PEG and PPMS, as illustrated in Figure 4.1.

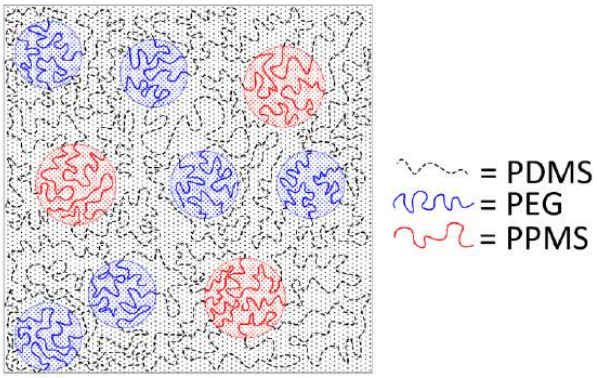

Figure 4.1 Illustration of a silicone copolymers, prepared by phase-separating a PDMS-PEG copolymer in a PDMS-PPMS matrix by means of a binary system of copolymer blends.

4.1.2.1 Synthesised PDMS-PPMS copolymer (80DMS_2PMS)

It has been shown previously that PDMS-PPMS copolymers possess excellent mechanical properties when they are cross-linked with a vinyl-functional cross-linker [109]. All vinyl groups of PDMS were consumed during the hydrosilylation of vinyl-terminated PDMS and hydride-terminated PPMS, which was confirmed by the disappearance of the Si-CH=CH_2 bond signal at 5.8 - 6.2 ppm in the ^{1}H-NMR spectra (refer to Appendix III, ESI 2 for NMR spectra in Figure S1). The synthesised PDMS-PPMS copolymer was telechelic hydride-functional. The determined molecular weight of 80DMS_2PMS was 32 kg mol^{-1}, while the molar concentration of phenyl

groups of 80DMS_2PMS was $8.8 \cdot 10^{-4}$ g mol^{-1}, determined from NMR integration areas [109]. A PDMS-PPMS copolymer containing a PDMS chain length of m_1= 80 and a PPMS chain length of n_1= 2 (80DMS_2PMS) was used in all cross-linked binary copolymer blends (BCBs), due to the highest electrical breakdown strength (E_{BD} = 72 V μm^{-1}) occurring at a phenyl concentration of $8.8 \cdot 10^{-4}$ g mol^{-1}, resulting from a synergistic effect of favourable phase separation and a relatively high concentration of phenyl groups.

4.1.2.2 Synthesised PDMS-PEG copolymers

The disappearance of the Si-H bond signal at 4.70 ppm was checked by ^{1}H-NMR for a complete conversion of hydride PDMS groups in the hydrosilylation of hydride-terminated PDMS and vinyl-terminated PEG; refer to Appendix III, ESI 2 for NMR spectra in Figures S2-5. Determined molecular weights from the SEC of PDMS-PEG copolymers PDMS81-PEG, PDMS14-PEG, PDMS7-PEG and PDMS3-PEG were 49, 29, 3 and 5 kg mol^{-1}, respectively.

4.1.2.3 Linear viscoelasticity

To evaluate the effect of loading different types of PDMS-PEG copolymers on viscoelastic properties, the prepared elastomers were characterised rheologically, as shown in Figure 4.2. They are well cross-linked and behave elastically, i.e. the incorporation of PDMS-PEG copolymer into the BCB does not destabilise the PDMS-PPMS elastomers. The resulting storage moduli (G') for all prepared cross-linked BCBs and the reference are between 10^4 and 10^6 Pa. The cross-linked BCBs with 10 and 20 phr of PDMS81-PEG are the most rigid elastomers compared to other prepared elastomers and the reference elastomer, revealing that the elastomers have PEG-like properties, due to the semi-crystalline PEG acting as a reinforcing domain in the matrix. All prepared cross-linked BCBs and the reference elastomer possess close-to-identical relaxations. Relative losses [tan (δ)] for all elastomers are low and are comparable to that of Elastosil RT625 (a commercial silicone elastomer from Wacker Chemie) [100], as well as that of the reference elastomer. It is obvious from Figure 4.2 that all of the prepared elastomers maintain their network integrity in the small deformation regime.

4.1.2.4 Stress-strain relationship

Stress-strain curves and the Young's moduli of prepared samples are shown in Figure 4.3 and Table 4.1, respectively. It is evident from Figure 4.3 that all prepared samples and the reference elastomer show strain-hardening behaviour. The cross-linked BCBs with 10 and 20 phr of PDMS81-PEG show the most increased ultimate strain compared to other cross-linked BCBs and the reference elastomer, indicating that PDMS81-PEG plasticises the elastomer without compromising network integrity and thereby results in increased softness with high extensibility (refer to Figure 4.3). Obviously, the increased ultimate strain of cross-linked BCBs with loadings of PDMS81-PEG indicates that the incorporation of PDMS81-PEG softens the elastomer

whilst strain-hardening it, which results in an elastomer with increased softness with respect to extensibility. Furthermore, the elastomers mentioned herein possess higher ultimate strain than the strain of the VHB 4910 elastomer from 3M, where VHB 4910 possesses an ultimate strain of 800%, as reported by Tugui et al. [110]. On the other hand, the cross-linked BCB with 20 phr of PDMS14-PEG shows very low ultimate strain, indicating that the high loading of the PDMS14-PEG copolymer deteriorates network integrity, due to the macroscopic phase separation of PEG domains in the copolymer blend matrix.

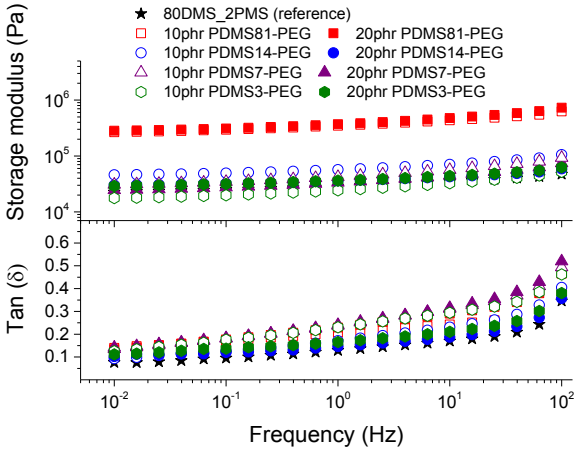

Figure 4.2 The storage modulus and tan (δ) of prepared voltage-stabilised elastomers with different types and concentrations of PDMS-PEG copolymers at 23°C.

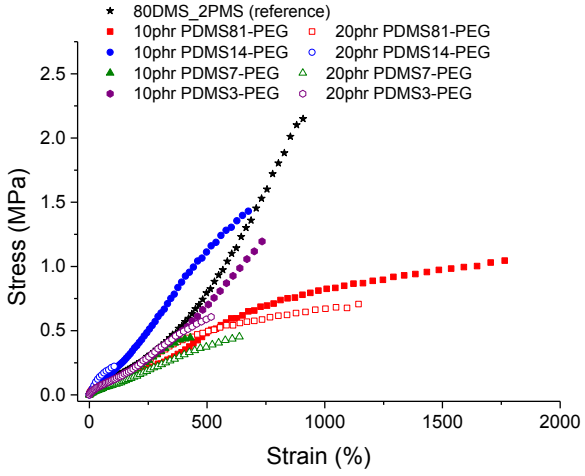

Figure 4.3 Stress-strain curves for prepared cross-linked BCBs and the reference elastomer at 23°C (standard deviations of ultimate strains and ultimate strengths were of order ± 1 – 19% and ± 3 – 16 %, respectively).

All cross-linked BCBs show decreased ultimate strength compared to the reference elastomer. Cross-linking with 10 phr of PDMS14-PEG results in the most increased ultimate stress compared to other cross-linked BCBs, due to semi-crystalline PEGs acting as reinforcing domains.

Obviously, the resulting Young's moduli of all cross-linked BCBs are low, as well as that of the reference elastomer, as shown in Table 4.1. In comparison to the commercial silicone elastomer (RT625 from Wacker Chemie), all cross-linked BCBs and the reference elastomer are softer than RT625, which possesses Y = 1 MPa[100].

Table 4.1 Young's moduli for cross-linked BCBs and reference elastomer

Sample	Young's modulus, *Y* (MPa)
0 phr PDMS-PEG (reference)	0.41 ± 0.05
10phr PDMS81-PEG BCB	0.45 ± 0.08
20phr PDMS81-PEG BCB	0.25 ± 0.05
10phr PDMS14-PEG BCB	0.43 ± 0.05
20phr PDMS14-PEG BCB	0.58 ± 0.13
10phr PDMS7-PEG BCB	0.30 ± 0.10
20phr PDMS7-PEG BCB	0.21 ± 0.03
10phr PDMS3-PEG BCB	0.34 ± 0.06
20phr PDMS3-PEG BCB	0.36 ± 0.05

4.1.2.5 Dielectric properties

The conductivity and dielectric properties of the prepared elastomers are shown in Figure 4.4 and Figure 4.5, respectively. The resulting conductivities indicate that none of elastomers is conductive. The resulting conductivity of the cross-linked BCB with 20 phr of PDMS3-PEG indicates increased relaxation occurring at the frequencies 10^0 to 10^2 Hz, compared to other cross-linked BCBs and the reference elastomer, which may indicate a local phase separation of PEG-rich domains.

The resulting relative permittivity for the prepared elastomers with a low loading (10 phr) of PDMS-PEG copolymers is lower than the reference elastomer, except the cross-linked BCBs with 10 phr of PDMS7-PEG, which shows increased relative permittivity, improving by 27%. For the prepared elastomers with a high loading (20 phr) of PDMS-PEG copolymers, the relative permittivities are almost higher than the reference elastomer, whereby the cross-linked copolymer with 20 phr of PDMS7-PEG has the highest relative permittivity. Figure 4.5 clearly shows that the cross-linked copolymers with low and high loadings of PDMS7-PEG possess increased relative permittivity, compared to the other elastomers and the reference. The phase separation of PDMS-PEG copolymers in the PDMS-PPMS matrix seems to occur on the

micro- or nanoscopic scale, since the elastomers are macroscopically homogenous, as observed from light microscopy.

Dielectric losses, here represented by tan (δ), are relatively low for all cross-linked copolymers as well as the reference elastomer (see Figure 4.5). Similar to the relaxation in Figure 4.4, the cross-linked BCB with 20 phr of PDMS3-PEG shows increased relaxation occurring at the same frequency.

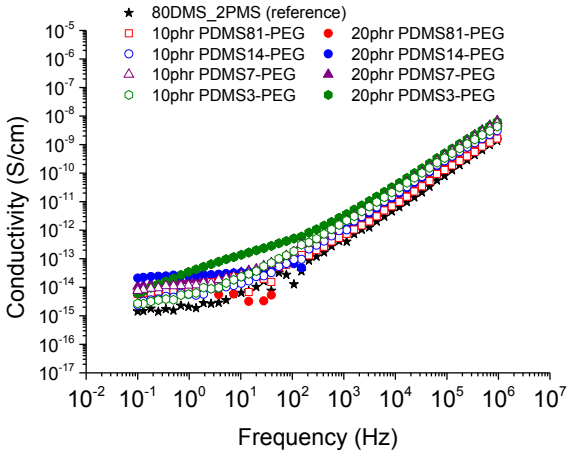

Figure 4.4 The conductivity of 80DMS_2PMS elastomers with different concentrations of PDMS-PEG copolymers at 23°C.

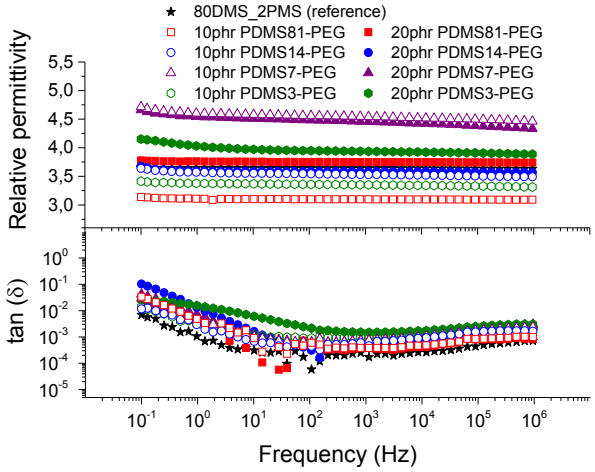

Figure 4.5 The dielectric properties of 80DMS_2PMS elastomers with different concentrations of PDMS-PEG copolymers at 23°C.

SEM imaging shows obviously different morphologies for prepared elastomers, as illustrated in Figure 4.6. The SEM image of the cross-linked BCB with 20 phr of

PDMS7-PEG shows clearly distinct PEG domains (white circles), which are well-distributed in the PDMS matrix, thereby indicating that a homogeneous elastomer on the macroscopic scale has been obtained (see Figure 4.6b). On the other hand, SEM imaging of the reference elastomer shows the presence of PDMS and PPMS domains in the matrix (see Figure 4.6a). Furthermore, the reference elastomer has a triangular pattern (PDMS domain) and that of a bent rectangle (PPMS domain), which is agrees with the SEM image of the cross-linked PDMS-PPMS copolymer [109] (see Figure 4.6a). Other SEM images of prepared elastomers, which show different morphologies, can be seen in Appendix III, ESI 3, Figure 6.

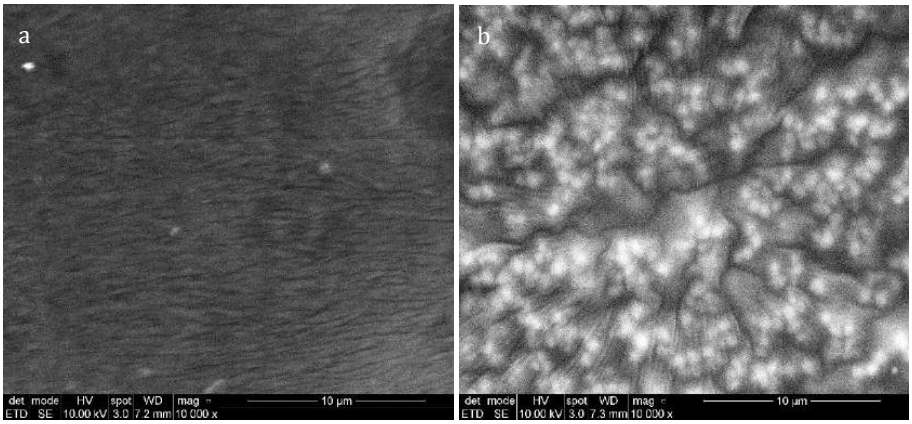

Figure 4.6 SEM pictures of two representative samples, namely a) 80DMS_2PMS (reference elastomer) and b) binary copolymer blends with 20 phr of PDMS7-PEG.

For the reference elastomer, the PDMS-rich domains, which act as plasticisers by increasing free volume, enhance elastomer softness, whilst PPMS domains which act as rigid zones reinforce the network, thus resulting in an elastomer with increased ultimate stress and increased ultimate strain, as shown in Table 4.2.

Previous work has shown elastomers with an increased Young's modulus possess increased electrical breakdown strength [30,111]. In order to investigate the influence of increased relative permittivity, relative permittivity is evaluated based on the effects of increased stiffness and increased stretchability. The influences of the Young's modulus (Y) and ultimate strain (ϵ) on relative permittivity are shown in Figure 4.7 and Figure 4.8, respectively. No direct correlation of increased relative permittivity as an effect of stiffness can be seen in Figure 4.7. Furthermore, no clear trend can be seen from increased relative permittivity as a result of increased ultimate strain, as shown in Figure 4.8.

Table 4.2 Relative permittivity and mechanical properties of prepared cross-linked BCBs and the reference elastomer

Sample	Young's modulus (MPa)	Relative permittivity	Ultimate stress (MPa)	Ultimate strain (%)
80DMS_2PMS (reference)	0.41 ± 0.05	3.71	1.86 ± 0.31	967 ± 33
10 phr PDMS81-PEG BCB	0.45 ± 0.08	3.14	1.10 ± 0.10	1748 ± 40
20 phr PDMS81-PEG BCB	0.25 ± 0.05	3.78	0.74 ± 0.02	1164 ± 17
10 phr PDMS14-PEG BCB	0.43 ± 0.05	3.64	1.57 ± 0.12	635 ± 52
20 phr PDMS14-PEG BCB	0.58 ± 0.13	3.67	0.25 ± 0.03	104 ± 1
10 phr PDMS7-PEG BCB	0.30 ± 0.10	4.71	0.40 ± 0.03	431 ± 19
20 phr PDMS7-PEG BCB	0.21 ± 0.03	4.66	0.42 ± 0.04	552 ± 103
10 phr PDMS3-PEG BCB	0.34 ± 0.06	3.41	1.14 ± 0.10	724 ± 40
20 phr PDMS3-PEG BCB	0.36 ± 0.05	4.15	0.56 ± 0.03	491 ± 43

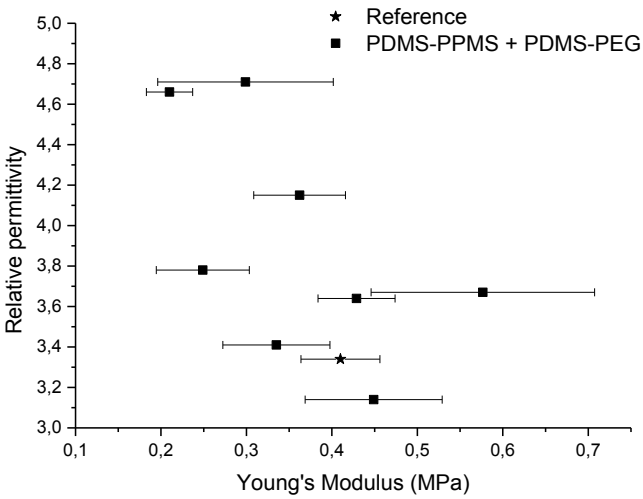

Figure 4.7 Relative permittivity versus Young's modulus.

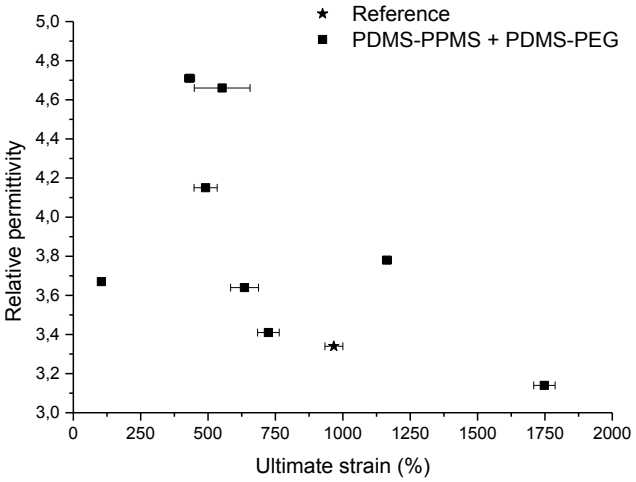

Figure 4.8 Relative permittivity versus ultimate strain.

4.1.2.6 Electrical breakdown and Weibull analysis

The influence of the different PDMS-PEG copolymer molecular weights and their concentrations in cross-linked BCBs on electrical breakdown strength was investigated. The thicknesses of the prepared samples were in the range of 81 to 135 µm. The resulting electrical breakdown strengths of prepared elastomers incorporating PDMS-PEG copolymers are shown in Table 4.3. The cross-linked BCBs with 10 and 20 phr of PDMS14-PEG possess the highest electrical breakdown strength, namely 80 ± 5 and 81 ± 18 V μm^{-1}, respectively, improving by approximately 10% compared to the reference elastomer. Increased electrical breakdown is most likely due to the synergistic effect of the favourable phase separation of PEG and voltage stabilisation. Moreover, the cross-linked BCBs with PDMS7-PEG and PDMS3-PEG with a loading of 20 phr possess increased electrical breakdown strength compared to the reference elastomer. Clearly, the incorporation of PDMS81-PEG in the BCB decreases electrical breakdown strength (see Table 4.3), which indicates that PDMS81-PEG may destabilise voltage stabilisation and hence deteriorate the charge trapping effect caused by the π-electrons of phenyl groups.

The electrical reliability of the prepared elastomers was investigated via Weibull analysis. The β-parameter, the Weibull shape parameter, was determined from the slope of the Weibull plot of failure probability versus electrical breakdown strength. The η-parameter, the Weibull scale parameter, was determined at a point at which failure probability, ln[-ln(1 - F)], was 63.2% [10]. Due to different film thicknesses, the determined electrical breakdown strengths were normalised, based on a reference thickness for better comparison. Normalised dielectric breakdown strengths were calculated using the equation of normalised electrical breakdown strength verified by Zakaria et al. [48]. The reference thickness for normalisation was

100 µm. The results for the Weibull η- and β-parameters, R^2 of the linear fits for cross-linked copolymers and normalised electrical breakdown strength are presented in Table 4.3. The values of the coefficient of determination (R^2) for all investigated elastomers are above 0.80, excluding elastomers with 10 phr of PDMS7-PEG and 20 phr of PDMS3-PEG. A coefficient of determination above 0.85 indicates that the measured electrical breakdown strength correlates well with the fitted regression lines [109]. Cross-linked BCBs with 20 phr of PDMS81-PEG, 10 and 20 phr of PDMS7-PEG, 20 phr of PDMS3-PEG and the reference elastomer possess a high β-parameter, thereby indicating that electrical breakdown occurrences are narrowly dispersed and hence homogenous elastomers are obtained. The β-parameters of elastomers with the most increased electrical breakdown strength (10 and 20 phr of PDMS14-PEG BCBs) are lower than the β-parameter of the reference elastomer. Combining the results for relative permittivity, electrical breakdown strength and ultimate strain (ϵ), the cross-linked BCB with 20 phr of PDMS7-PEG possesses the most enhanced electrical properties (ε_r = 4.66, E_{BD} = 76 ± 3 V µm^{-1}) as well as good ultimate strain (ϵ = 552 ± 103 %).

Table 4.3 Electrical breakdown strength at 23°C, Weibull parameters η and β and R^2 of the linear fit for all prepared cross-linked copolymers and the reference.

Cross-linked PDMS-PPMS copolymer (80DMS_2PMS)	Electrical breakdown strength (V µm^{-1})	Weibull β-parameter	Weibull η-parameter	R^2	Normalised electrical breakdown strength
0 phr PDMS-PEG (reference)	72 ± 3	26	73	0.93	71.9 ± 3.1
10phr PDMS81-PEG	61 ± 8	9	64	0.89	61.1 ± 7.8
20phr PDMS81-PEG	54 ± 2	36	55	0.96	54.3 ± 1.7
10phr PDMS14-PEG	80 ± 5	19	82	0.84	80.5 ± 5.2
20phr PDMS14-PEG	81 ± 18	5	88	0.93	82.9 ± 18.8
10phr PDMS7-PEG	64 ± 2	38	65	0.70	64.3 ± 2.3
20phr PDMS7-PEG	76 ± 3	34	77	0.89	76.4 ± 2.6
10phr PDMS3-PEG	63 ± 9	7	67	0.94	60.6 ± 8.7
20phr PDMS3-PEG	74 ± 3	30	75	0.76	73.7 ± 3.0

Increased electrical breakdown strength has been established as the result of either an increased Young's modulus [30] or voltage stabilisation [109]. Further investigation into electrical breakdown was performed to evaluate whether increased electrical breakdown strength is the effect of other elements, i.e. increased stiffness, increased relative permittivity or increased stretchability. The influences of the Young's modulus, relative permittivity and ultimate strain on electrical breakdown strength are shown in Figure 4.9, Figure 4.10 and Figure 4.11. No obvious

trend can been seen in Figure 4.9 for increased electrical breakdown strength as a function of stiffness, showing that the increased electrical breakdown strength of all prepared elastomers is due to the synergistic effect of voltage stabilisation and the favourable phase separation of PEGs. No clear trend can be observed for electrical breakdown strength versus relative permittivity, indicating that the increased electrical breakdown strength is not due to increased relative permittivity (see Figure 4.10). An obvious trend can be observed that the resulting electrical breakdown strengths of prepared elastomers are minimal, occurring at an ultimate stress of around 1.1 MPa, thereby indicating that decreased electrical breakdown strength occurs close to an ultimate stress of 1.1 MPa (refer to Figure 4.11).

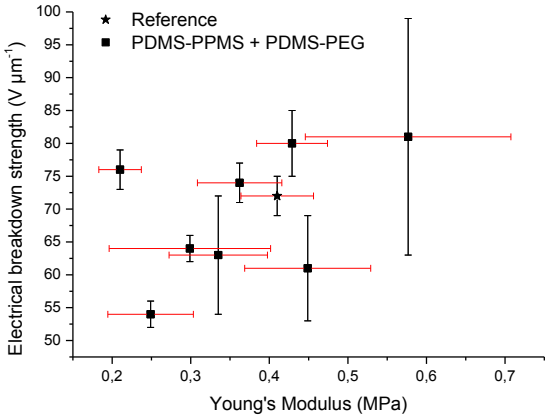

Figure 4.9 Electrical breakdown strength versus Young's modulus.

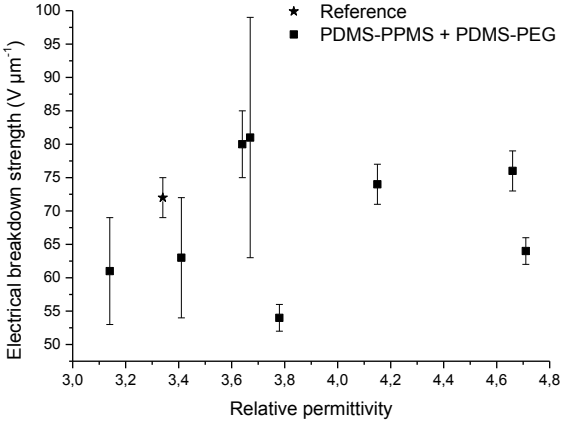

Figure 4.10 Electrical breakdown strength versus relative permittivity.

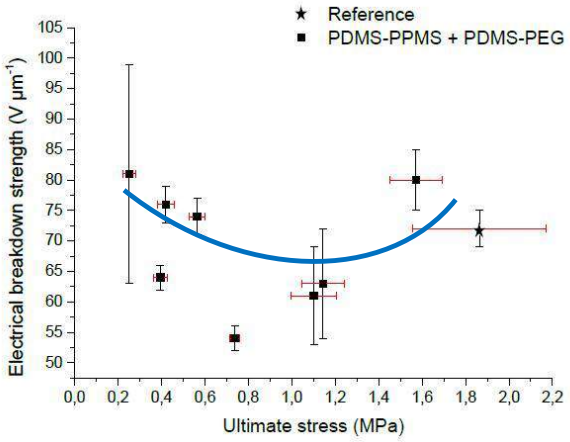

Figure 4.11 Electrical breakdown strength versus ultimate stress. Blue line is a visual guideline.

The theoretical actuation strains were calculated from the actuation equation [19], by assuming the maximum applicable electrical field, i.e. electrical breakdown strength can be achieved when the elastomer possesses softness with high extensibility and does not breakdown mechanically before electrically [109]. Theoretical actuation strains and measured ultimate strains are shown in Table 4.4. The elastomer with 10 phr of PDMS81-PEG, which is highly extensible, shows the lowest theoretical actuation strain compared to the other elastomers. No correlation can be seen from an increased theoretical actuation strain as an effect of increased ultimate strain. A large actuation strain is influenced by increased electrical breakdown strength and increased relative permittivity. Obviously, elastomers with decreased ultimate strain, such as the example with 20 phr of PDMS14-PEG, may break down mechanically before they break down electrically (see Table 4.4).

Table 4.4 Theoretical actuation strain and measured ultimate strain for prepared elastomers.

Sample	Theoretical actuation strain (%)	Ultimate strain (%)
80DMS_2PMS (reference)	600	967 ± 33
10 phr PDMS81-PEG BCB	366	1748 ± 40
20 phr PDMS81-PEG BCB	629	1164 ± 17
10 phr PDMS14-PEG BCB	769	635 ± 52
20 phr PDMS14-PEG BCB	590	104 ± 1
10 phr PDMS7-PEG BCB	928	431 ± 19

20 phr PDMS7-PEG BCB	1821	552	±	103
10 phr PDMS3-PEG BCB	578	724	±	40
20 phr PDMS3-PEG BCB	881	491	±	43

4.1.2.7 Part conclusion

A soft elastomer with respect to high extensibility was prepared from phase-separating a PDMS-PEG copolymer in a binary copolymer blend consisting of a PDMS-PPMS copolymer as a primary copolymer, and it possessed increased relative permittivity and increased electrical breakdown. The synergistic effect of the cross-linked binary copolymer blend consisting of PDMS-PPMS and PDMS-PEG copolymers shows that the elastomer, namely a cross-linked binary copolymer blend with 20 phr of PDMS7-PEG, has the most enhanced electrical properties, i.e. increased relative permittivity and high electrical breakdown strength, without compromising highly extensible softness. This increased electrical breakdown strength is due to voltage stabilisation arising from the phenyl groups of PPMS, while increased relative permittivity is due to the most favourable phase separation of the PDMS7-PEG copolymer in the binary copolymer blend matrix. Furthermore, the cross-linked binary copolymer blend with 20 phr of PDMS7-PEG possesses a substantially high theoretical actuation strain, which could be utilised as a soft actuator.

5 Compliant dielectric elastomer electrodes

Due to their conductive nature, excellent softness and great adhesion to a silicone elastomer, cross-linked PDMS-PEG copolymers can be utilised as electrodes for dielectric elastomers. However, the network of cross-linked PDMS-PEG copolymers is weak and the cross-linked copolymer does not possess enough conductivity to be utilised as an electrode. Due to this weak network, a PDMS-PEG oligomer was chain-extended with long-chain PDMS through a hydrosilylation reaction, in order to obtain a soft elastomer. To increase the conductivity of chain-extended PDMS-PEG copolymers, a conductive nano-sized filler, i.e. a multi-walled carbon nanotube (MWCNT), was incorporated into the chain-extended PDMS-PEG matrix. In this chapter, details in this regard, as well as the dispersion method used for MWCNT prior to blending, are discussed.

The results presented in this chapter have been published in MRS Advances, volume 1, page 3497-3508 (2016), and the article is attached as Appendix IV. The procedures for preparing chain-extended PDMS-PEG copolymer/MWCNT nanocomposites are presented in Chapter 8.4.

5.1 Mechanically-compliant electrodes and dielectric elastomers from PEG-PDMS copolymers

5.1.1 Introduction

Conventional compliant electrodes, such as carbon black in the form of powder and carbon grease, can be applied easily on surfaces, but they lack adhesion to the elastomer. Other investigated electrode materials for DEs include silver nanowires, ionic hydrogels, single-walled carbon nanotubes (SWCNTs) and polymer-carbon conductive composites [83]. These materials, however, suffer from poor stretchability, which renders them unattractive as flexible electrodes [83]. On the other hand, commercial conductive elastomers, such as LR3162 from Wacker Chemie, have high conductivity, but they contribute a stiffening effect, due to their high Young's modulus.

As an alternative to the abovementioned materials, polydimethylsiloxane-polyethyleneglycol (PDMS-PEG) copolymers, which are somewhat conductive with conductivities around 10^{-8} S cm^{-1} [10], adhere very well to silicone surfaces and exhibit great flexibility and compliance, due to their partly silicone nature. Furthermore, their moderate conductivity can be enhanced easily by incorporating highly conductive nano-fillers such as multi-walled carbon nanotubes (MWCNTs). The high interaction energies of MWCNTs, due to strong van der Waals forces, however, often result in poor dispersibility and weak interfacial interactions with the matrix [112]. Well-dispersed

MWCNTs are important when seeking to avoid agglomeration, which would otherwise result in uneven conductive and mechanical properties throughout the matrix.

High levels of dispersion of MWCNTs in polymer matrices can be obtained by using probe sonicators and ball milling prior to mixing with the matrix [113,114]. Chemical modification of MWCNTs can also lead to a higher degree of dispersion, due to higher compatibilities with the matrix. Methods such as oxidation by nitric acid [115] and solutions of hydrogen peroxide/ammonium hydroxide [116], however, worsen the intrinsic properties of MWCNTs through, for instance, decreases in tube length and conductivity. On the other hand, treatment of MWCNT surfaces, using non-ionic surfactants such as Triton X-100 and sodium dodecyl sulphate (SDS), does not change the intrinsic properties of MWCNTs significantly, since each one is coated with surfactant molecules through their hydrophilic head and hydrophobic tails, thus leading to surfactant-stabilised MWCNTs [117].

In this paper we demonstrate how synthesised PDMS-PEG copolymer matrices with different concentrations of surface-modified MWCNT nano-fillers show promising properties for high-conductivity, stretchable electrodes. The conductivities and mechanical properties of prepared PDMS-PEG copolymer samples with different concentrations of MWCNTs were investigated, as well as the dispersion of MWCNT in the polymer matrix, by SEM and TEM analysis.

5.1.2 Results and discussion

Stretchable and high-conductivity electrode materials for dielectric elastomers were prepared by synthesising PDMS-PEG copolymers according to Scheme 8-3. The copolymers were prepared by the chain extension of a previously synthesised PDMS-PEG co-oligomer [10] with commercially available telechelic hydride-functional PDMS of M_n = 17,200 g mol^{-1}, resulting in a telechelic hydride-functional CE-(PDMS-PEG) copolymer of M_n = 24 kg mol^{-1}. Well-dispersed surface-modified MWCNTs were prepared by ultra-sonication, using 1 wt% of non-ionic surfactant (Triton X-100) in an organic solvent (NMP). The CE-(PDMS-PEG) copolymer was then cross-linked, using a vinyl-functional cross-linker containing on average 15 vinyl groups in the presence of a Pt catalyst and surface-modified MWCNTs in various concentrations (one, two and three parts per hundred rubber (phr)).

5.1.2.1 Dispersion MWCNTs in CE-(PEG-PDMS)

It has been shown previously that the conductivity of conductive materials depends greatly on how well MWCNTs (or other nano-fillers) are dispersed in the polymer matrix [114,117]. Therefore, in order to obtain high-conductivity elastomer electrodes, a high level of MWVNT dispersion is required. As mentioned previously, strong van der Waals forces exist between single MWCNT strands, which are therefore agglomerated and intertwined in their natural and pure state, as shown in Figure 5.1. This behaviour makes the direct dispersion of pure MWCNTs in polymer matrices extremely difficult. Pre-

dispersal in solvent and surface modifications to the MWCNTs, using surfactants, however, can result in well-dispersed fillers [7], [10].

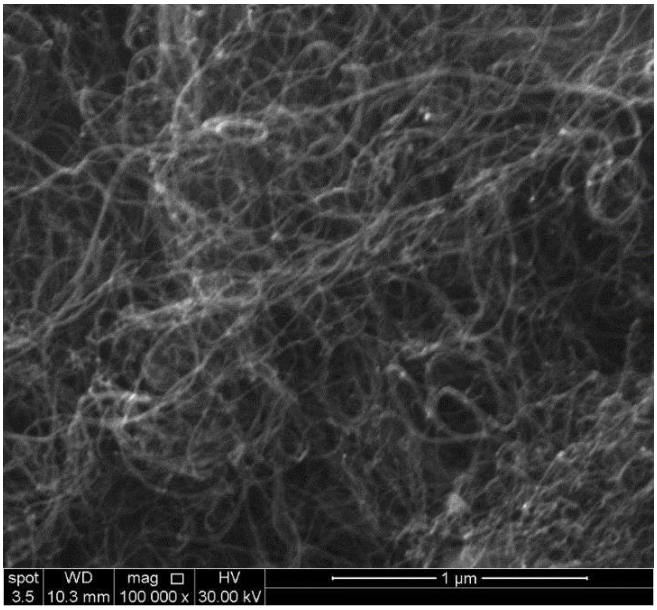

Figure 5.1 SEM image of pure MWCNTs, showing their agglomerated and intertwined nature.

Based on the studies undertaken by Geng et al. [7] and Rastogi et al. [10], who tested the dispersion of MWCNT in organic solvents by using different surfactants, a polyoxyethylene octyl phenyl ether-type surfactant (Triton X-100) was chosen as the ideal surfactant for well-dispersed MWCNTs. It was also found to have a high degree of tolerance to various organic solvents in which the MWCNTs were dispersed. The optimal solvent for a high level of dispersion was chosen based on the study carried out by Goswami et al. [11], who used *N*-methyl pyrrolidinone (NMP) as a compatible organic solvent to disperse low concentrations of MWCNTs in a PDMS matrix. The system chosen in our study was therefore based on a solution containing MWCNTs in 1 wt% Triton X-100 in NMP solvent, which was ultra-sonicated for several hours before the resulting dispersed MWCNTs were mixed into the CE-(PDMS-PEG) matrix.

In order to investigate the effectiveness of MWCNT-treated dispersion by Triton X-100, the settling of MWCNTs in the organic solution after sonication was monitored over time. The dispersion method used in this work was compared to a reference method, using the same surface treatment method of 1 wt% Triton X-100 and NMP, albeit with a mechanical shaker instead of ultra-sonication. Theoretically, no MWCNT settlement in the Triton X-100 and NMP solution should be observed when the surface of the MWCNT is treated well by Triton X-100.

In Figure 5.2 (top) the settlement of MWCNTs dispersed by means of the reference method (mechanical shaking) is seen. It is evident that over time, the MWCNTs have settled on the bottom of the white-capped flask. This indicates that each MWCNT strand is not well-covered by surfactant when mechanical shaking has been used as the mixing method. The MWCNTs are therefore able to agglomerate and the dispersion will not be stable over time.

On the other hand, the same system of MWCNTs in 1 wt% of Triton X-100 in NMP, which were mixed via ultra-sonication for 6 hours at 23°C, creates a stable dispersion of MWCNTs over time. This is shown in Figure 5.2 (bottom). No settling/agglomeration of MWCNTs was observed over the investigated time frame, which indicates that ultra-sonication provides MWCNTs that are well-covered in Triton X-100 surfactant.

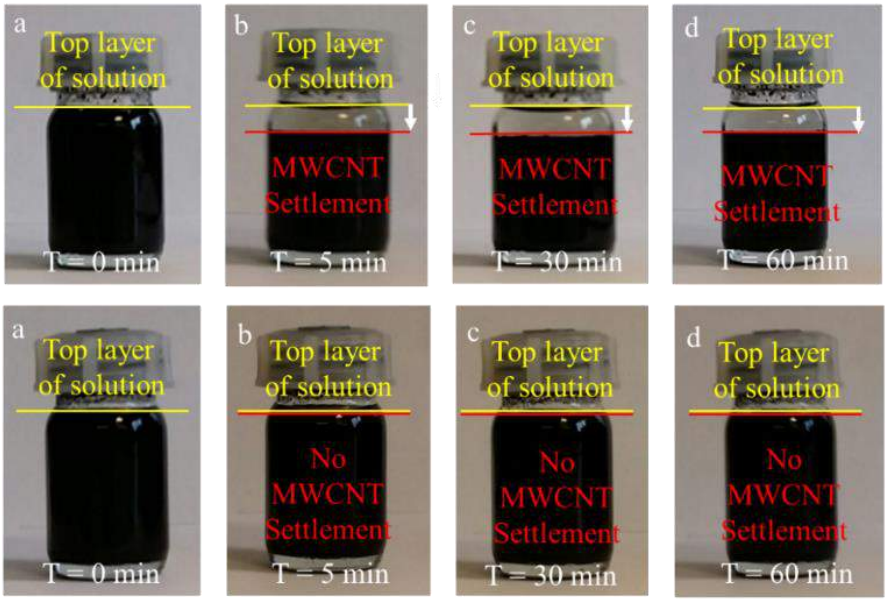

Figure 5.2 Top: Settlement of MWCNTs over time for the reference method (MWCNT/NMP/Triton X-100) dispersed by a mechanical shaker at 23°C after standing for: a) 0 min; b) 5 min; c) 30 min; d) 60 min. **Bottom**: MWCNT/NMP/Triton X-100 mixed by ultra-sonication at 23°C

After the initial successful dispersion of MWCNTs in NMP solvent, the obtained MWCNT mixture was blended with CE-(PDMS-PEG) copolymer, cross-linker and a catalyst, following which the NMP solvent was allowed to evaporate slowly during the elastomer cross-linking process, thus creating MWCNT/CE-(PDMS-PEG) nanocomposites. In order to verify the effectiveness of the dispersion of MWCNTs in the CE-(PDMS-PEG) elastomer matrix, microscale and nanoscale images were obtained by SEM and TEM, respectively. SEM images revealed details on overall dispersion of

MWCNTs in the copolymer matrix, whereas TEM images revealed details on the morphology of MWCNTs in the CE-(PDMS-PEG) matrix.

In Figure 5.3 (top), SEM images are shown, displaying random micro-structures of MWCNTs in the CE-(PDMS-PEG) matrix. The attained images are similar to those observed in the literature for well-dispersed MWCNTs in polymer matrices [118]. Figure 5.3 (bottom) shows a single strand of MWCNT, illustrating that the MWCNTs are well-dispersed as single strands in the matrix. The dimension of the single strand of MWCNT observed in TEM matches data specifications provided by the supplier, in that diameter and length are 6–9 nm and 1.5 µm, respectively. SEM and TEM thus corroborate that the used dispersion method creates nanocomposites with well-dispersed MWCNTs.

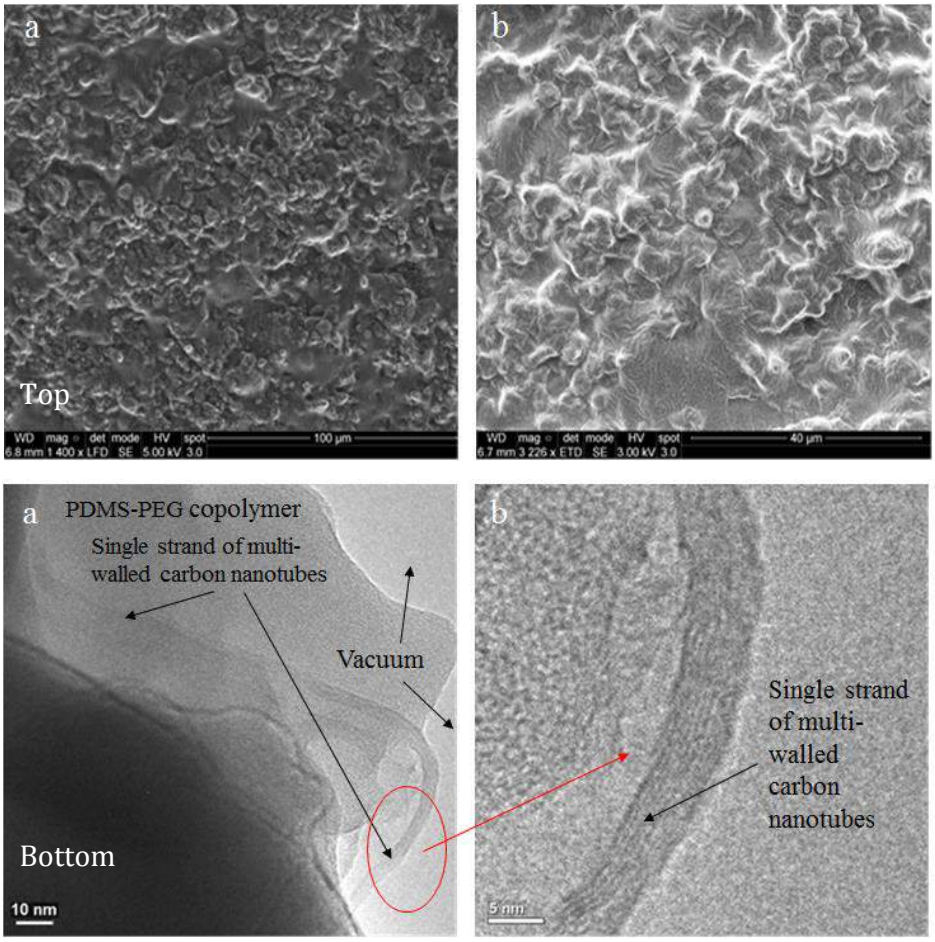

Figure 5.3 Top: An SEM image of CE-(PDMS-PEG) nanocomposites with 3 phr MWCNTs: a) 1400 magnification at 100 µm scale b) 3226 magnification at 40 µm scale. **Bottom**: TEM images of CE-(PDMS-PEG) nanocomposites with 3 phr MWCNTs: a) Low magnification at scale of 10 nm b) High magnification at scale of 5 nm.

5.1.2.2 Mechanical properties of CE-(PDMS-PEG)/MWCNTs nanocomposites

Mechanical properties of the obtained CE-(PDMS-PEG)/MWCNTs nanocomposites were tested by shear rheology. Rheological properties of the cross-linked CE-(PDMS-PEG) copolymers with 0 – 3 phr of MWCNT were compared to a commercial conductive elastomer reference material, LR3162, as shown in Figure 5.4, and then furthermore compared to a CE-PDMS-PEG elastomer prepared without MWCNTs. The reference elastomer (CE-PDMS-PEG copolymer with 0 wt% MWCNTs) is seen to be stiffer than CE-(PDMS-PEG)/MWCNT nanocomposites with 1 to 3 phr of MWCNT. Compared to LR3162, CE-(PDMS-PEG)/MWCNTs nanocomposites are also softer, which implies that incorporating MWCNT in a CE-(PDMS-PEG) copolymer matrix results in soft, stretchable elastomers which therefore hold great promise as stretchable electrode materials for dielectric elastomers. Modulus loss factors (tan (δ)) for CE-(PDMS-PEG)/MWCNT nanocomposites with 1 – 3 phr MWCNTs are low (< 0.5) at various frequencies.

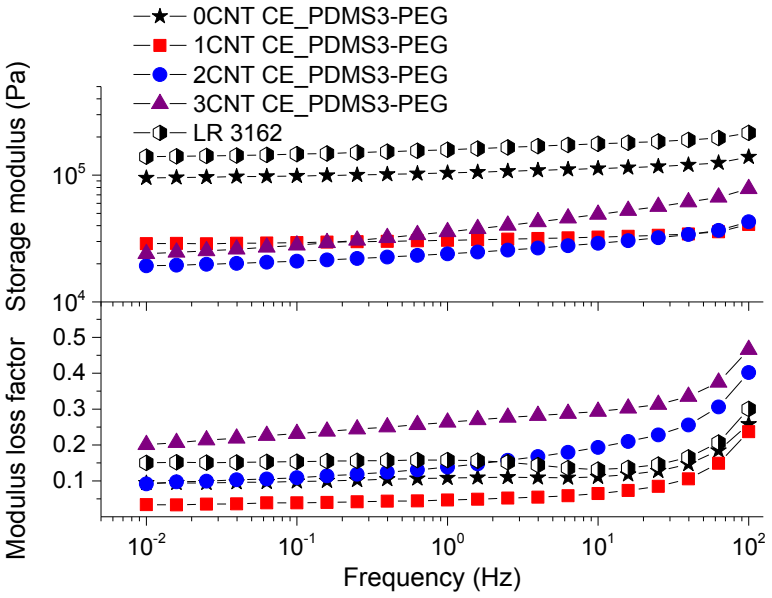

Figure 5.4 The storage modulus and modulus loss factor for CE-(PDMS-PEG)/MWCNT nanocomposites, as well as a CE-(PDMS-PEG) reference elastomer and a commercial elastomer LR3162.

Table 5.1 shows the maximum elongation and stress at break of the commercial conductive elastomer and CE-(PDMS-PEG) elastomers with different concentrations of MWCNTs. The benchmark conductive elastomer, LR3162, has higher elongation at break (168) than CE-(PDMS-PEG) elastomer nanocomposites with 1-3 phr MWCNTs. LR3162, however, shows strain-hardening behaviour with high stress at break. The strain-hardening behaviour of LR3162 is coherent with a high Young's modulus at 5% strain (Y = 4.11 MPa). On the other hand, CE-(PDMS-PEG) elastomers, with and without MWCNTs, demonstrate increased strain-softening behaviour as the concentration of MWCNT

increases, thus demonstrating that CE-(PDMS-PEG) elastomers with MWCNTs become softer under strain compared to LR3162. Another significant finding from Table 5.1 is that CE-(PDMS-PEG) elastomers with 0 – 3 phr of MWCNT show more than 100% strain, meaning that the addition of MWCNT does not destroy the properties of the elastomers at the micro-scale. This could also be a further indication of the well-dispersed nature of MWCNTs.

Table 5.1 Elongation and stress at break of PDMS-PEG/MWCNTs elastomers and LR3162

Sample	Elongation at break (%)	Stress at break (MPa)	Young's modulus (MPa)
LR3162	168	1.8	4.11
CE_PDMS-PEG + 0CNT	120	0.67	0.92
CE_PDMS-PEG + 1CNT	116	0.58	1.28
CE_PDMS-PEG + 2CNT	112	0.19	0.32
CE_PDMS-PEG + 3CNT	118	0.19	0.31

5.1.2.3 Conductivity of CE-(PDMS-PEG)/MWCNTs nanocomposites

The measured conductivities as functions CE-(PDMS-PEG)/MWCNT nanocomposite frequency, as well as the CE-(PDMS-PEG) reference elastomer and commercial elastomer LR162, are shown in Figure 5.5. The CE-(PDMS-PEG) copolymer shows increased conductivities as the concentration of MWCNT in the polymer matrix increases. CE PDMS-PEG) elastomer without the addition of MWCNT is non-conductive, ($\sim 10^{-13}$ S cm^{-1} at low frequencies). For CE-(PDMS-PEG) with 1 phr of MWCNT, conductivity increases substantially to 10^{-7}. The addition of 2 and 3 phr of MWCNT in the PDMS-PEG copolymer causes conductivities of 10^{-4} and 10^{-3} S cm^{-1}, respectively, comparable to that of the commercial conductive elastomer supplied by Wacker Chemie (LR3162). Another interesting finding from the conductivity test is that plateau regions are observed in Figure 5.5 for samples with 2 and 3 phr of MWCNT, indicating that the materials are highly conductive.

High observed conductivities, together with their soft and stretchable nature, makes the prepared CE-(PDMS-PEG)/MWCNTs nanocomposites ideal candidates for flexible dielectric elastomer electrodes.

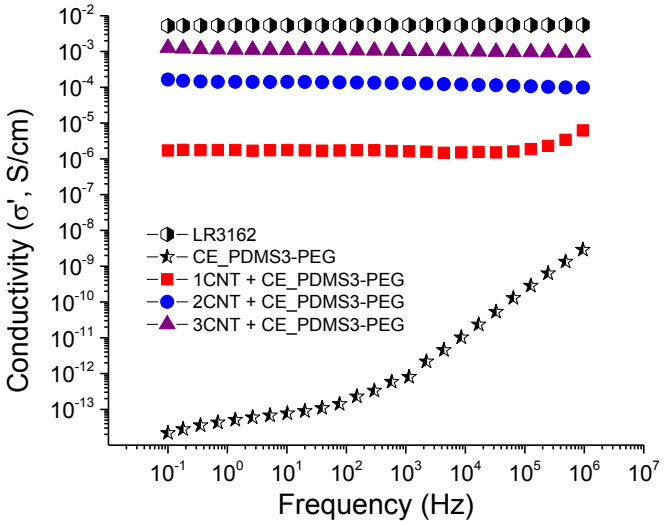

Figure 5.5 Conductivity of PDMS-PEG/MWCNTs elastomers at room temperature compared to the conductivity of a commercial benchmark elastomer (LR3162).

5.1.2.4 Interpenetrating network of PDMS-PEG copolymer and ionic network

In an attempt to increase the conductivities of the prepared CE-(PDMS-PEG)/MWCNTs nanocomposite elastomers even further, ionic silicone-based networks were included as an extra way of creating interpenetrating networks. The ionic network was prepared by mixing stoichiometric amounts (r = 1) of amine-functional PDMS (four amine groups on average, AMS-162) and telechelic carboxylic acid-functional PDMS (DMS-B12). Upon mixing the two components, a network was formed due to protonation of the functional groups. The preparation procedure for the ionic networks was amended from Yu et al.[119]. The interpenetrating networks consisted of the CE-(PDMS-PEG) copolymer and the silicone-based ionic network. Preliminary studies on the interpenetrating network from the ionic network and the CE-(PDMS-PEG) copolymer were carried out to determine optimum conditions for the conductivity and morphology of the system, before incorporating MWCNTs. Interpenetrating network samples without MWCNT were prepared at 10, 20, 30, 40 and 50 wt% of the ionic network. The dielectric and conductive properties of the interpenetrating networks with a 10–50 wt% ionic network were investigated and are shown in Figure 5.6. Interpenetrating network sample conductivities increase gradually in line with increased concentration in the ionic network. Interpenetrating networks with a 10–50 wt% ionic network have conductivities in the order of 10 to 10^3 higher than pure CE-(PDMS-PEG) copolymer, as seen in Figure 5.6a. Relative permittivities and dielectric losses (tan (δ)) of the interpenetrating networks also increase in line with increasing concentration in the ionic network, as illustrated in Figure 5.6b. The dynamic dipole orientation of polymer molecules resulting from

polarisation are observed for an interpenetrating network with a 30 and 40 wt% ionic network, as Debye-relaxation peaks occur at frequencies of 10^0 to 10^2 Hz.

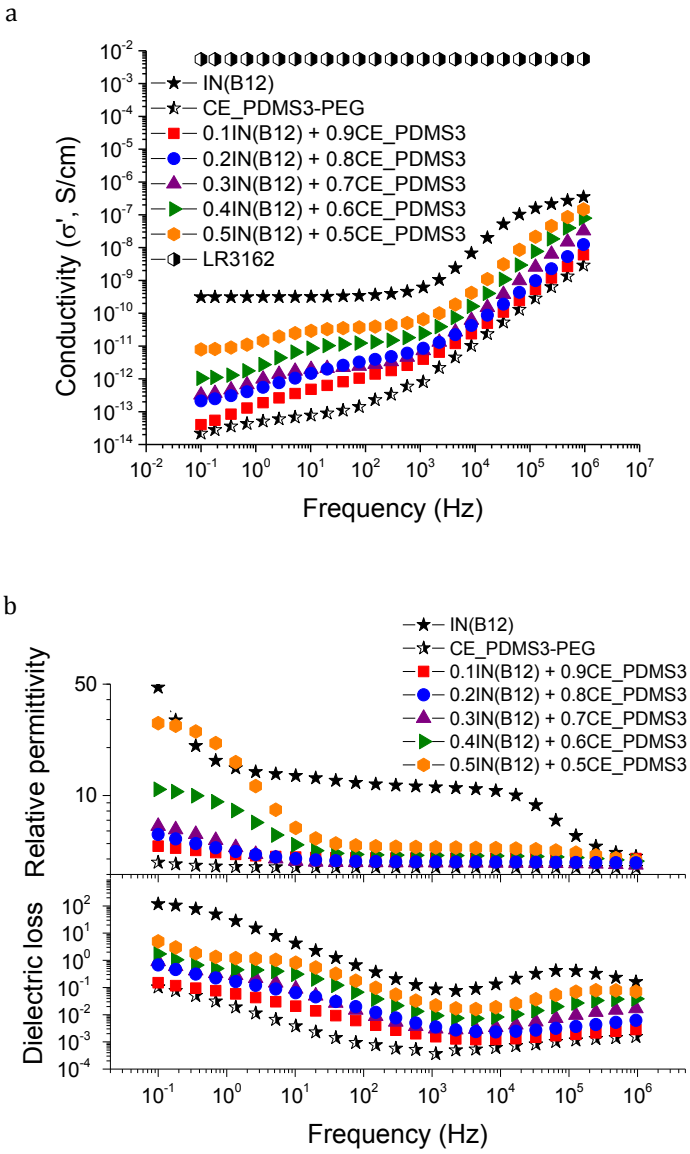

Figure 5.6 Dielectric properties of the interpenetrating network of PDMS-PEG copolymer and an ionic network: a) conductivities and b) relative permittivity and dielectric loss factor.

SEM analysis shows the presence of visible spheres in the interpenetrating network with a 30–50 wt% ionic network, as seen in Figure 5.7. These spheres are ionic networks formed by phase separation in the CE-(PDMS-PEG) copolymer matrix. The size of the

spheres increases as the volume of the ionic network increases from 30 to 50 wt%. Interpenetrating networks with a 40 and 50 wt% ionic network contain large spheres (>50 μm) which may destabilise the elastomers (see Figure 5.7b and c). Therefore, further work is required where MWCNT is incorporated into the interpenetrating network using a 30 wt% ionic network, due to the resulting smaller spheres (10 – 20 μm), as shown in Figure 5.7a.

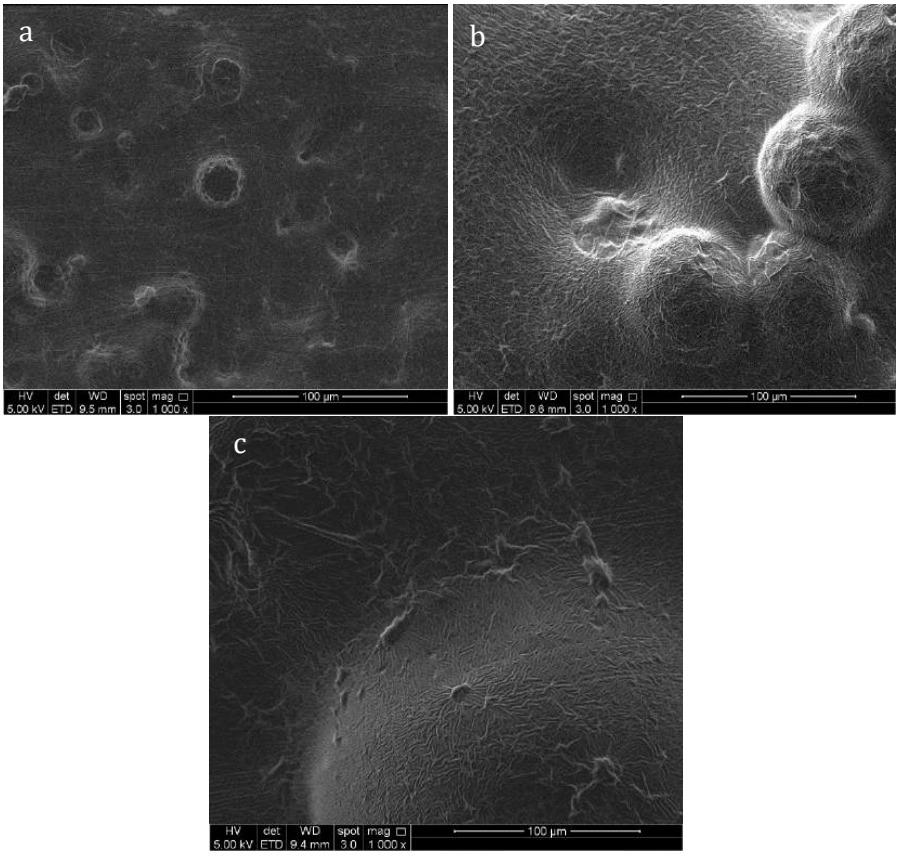

Figure 5.7 SEM images of interpenetrating networks of CE-(PDMS-PEG) copolymer and ionic network: a) 30 wt% b) 40 wt % c) 50 wt% ionic networks.

Samples from interpenetrating networks with a 30 wt% ionic network had 1–3 phr of MWCNTs added. Conductivities of the interpenetrating networks (30 wt% ionic network) with MWCNTs were compared with reference elastomers based on a pure ionic network, pure CE-(PDMS-PEG) copolymer and LR3162, as shown in Figure 5.8. Conductivities of the interpenetrating networks with 1–3 phr of MWCNTs are lower than CE-PDMS-PEG copolymer with the same amount of MWCNTs, and the addition of MWCNT to an interpenetrating network may destabilise the resulting elastomers, thereby causing less conductivity than the CE-(PDMS-PEG) copolymer with MWCNTs. One major advantage of

elastomers with ionic networks, however, may be that they exhibit self-healing properties [119,120].

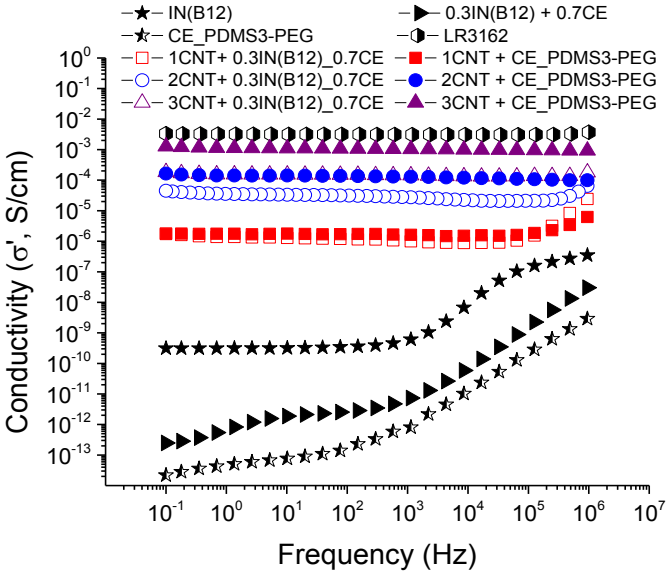

Figure 5.8 Conductivities of interpenetrating networks of CE-(PDMS-PEG) copolymers and ionic networks with MWCNTs compared to LR3162.

5.1.3 Part conclusion

A new, stretchable elastomer with high conductivity was successfully created from PDMS-PEG copolymers and MWCNT. PDMS-PEG copolymer-based elastomers with 3 phr of MWCNT are not only soft, but they also have conductivity levels close to those of a commercial conducting polymer benchmark, which possesses limited softness. A high level of MWCNT dispersion within the PDMS-PEG matrix was obtained by using a combination of surfactant and ultra-sonication. Higher loadings of MWCNT (> 3phr) in PDMS-PEG copolymer may increase conductivity further, but excessive amounts of MWCNT may, on the other hand, weaken the elastomer, thus resulting in poor mechanical properties. Furthermore, the elongation strain of the PDMS-PEG/3 phr MWCNT nanocomposite elastomer is more than 100%. Interpenetrating networks of PDMS-PEG copolymer and a silicone-based ionic network with MWCNTs may have self-healing properties, but conductivity is lower than PDMS-PEG copolymer with MWCNTs.

6 Main conclusion

The optimisation of silicone elastomer electro-mechanical properties has been proven by means of the phase separation of a block copolymer. In this thesis, two approaches were utilised, in order to obtain a phase-separating system in a silicone matrix. First, the phase-separating system was obtained by copolymerising two immiscible polymers, whereby one block was PDMS and the other was a polymer with optimised properties, i.e. a high dielectric constant and a voltage-stabilised effect. Second, phase separation was facilitated by compounding, whereby the phase-separating region was created by blending an immiscible polymer or copolymer in PDMS, and then it was immediately cross-linked again, to obtain free-standing elastomeric films. By employing the proper blending method and sample preparation, phase separation in the elastomer was minimised from the macro- and microscale to the nanoscale, which was very important for the homogeneity of the elastomer and for a long lifetime.

To enhance the relative permittivity of silicone elastomer, its phase-separating system was acquired by incorporating a conducting copolymer, namely a PDMS-PEG copolymer, which was immiscible in PDMS and created phase separation in the silicone matrix, resulting in a PDMS-rich phase (non-conducting region) and a PEG-poor phase (conducting region). The PEG-poor phase was caused by low loadings of PDMS-PEG copolymer. The PEG domain segregated to form a well-defined discontinuous phase, while the PDMS created the continuous region. By phase separating PDMS-PEG copolymer in the silicone matrix, the best phase separation was achieved, which resulted in an increase in relative permittivity. Furthermore, phase separation in the PDMS-PEG elastomer did not deteriorate the network integrity of the elastomer, due to the reinforcing effect of the semi-crystalline PEG, thereby maintaining the soft natured elastomer while retaining low viscous loss.

Voltage stabilisation has been proven to improve the electrical breakdown strength of insulating polymers such as polyethylene. Utilising voltage stabilisation in silicone elastomer is another method of enhancing electrical breakdown strength, and previous studies on electrical breakdown have been conducted by utilising reinforcing fillers in the silicone matrix, as the effect of an increased Young's modulus. Herein polyphenylmethylsiloxane (PPMS), which contained voltage-stabilised phenyl groups, was copolymerised with PDMS as a high M_n PDMS-PPMS copolymer and was further cross-linked to obtain the voltage-stabilised PDMS-PPMS elastomer. The cross-linked PDMS-PPMS showed phase-separating behaviour due to the immiscibility of PPMS in PDMS. Voltage stabilisation was shown to enhance the electrical breakdown strength of cross-linked PDMS-PPMS copolymer, due to the charge-trapping effect of π-delocalised electrons. To ensure that increased electrical breakdown strength resulted from voltage

stabilisation, the influence of the Young's modulus on electrical breakdown strength was investigated. The correlation in this regard was not obvious, indicating that the increased electrical breakdown of cross-linked PDMS-PPMS copolymers was not due to an increase in the Young's modulus.

Thus far, phase separation has been shown to be another strategy for optimising silicone elastomer. A soft silicone elastomer with increased relative permittivity and high electrical breakdown strength was prepared by means of phase separating two copolymers, namely PDMS-PEG and PDMS-PPMS. A binary system of copolymer blends, consisting of PDMS-PEG and PDMS-PPMS copolymers, was prepared, and subsequently both copolymers were cross-linked, which resulted in an interpenetrating network consisting of PDMS-PEG and PDMS-PPMS copolymers. The synergistic effects of a binary system of copolymer blend consisting of PDMS-PEG and PDMS-PPMS copolymers showed enhanced electro-mechanical properties. The morphology containing the PDMS-rich phase and PEG-discontinuous phase was the most favourable, which resulted in increased relative permittivity. The phase separation of PDMS-PEG copolymers in the PDMS-PPMS matrix seems to occur on the micro- or nanoscopic scale, since the elastomers are macroscopically homogenous, as observed from light microscopy. Furthermore, the PDMS-rich domains enhance elastomer softness, whilst PPMS domains which act as rigid zones reinforce the network. The voltage-stabilised phenyl groups in PPMS trapped electrons through delocalised aromatic π-electrons, and the trapped electrons remained in the film bulk and hence delayed electrical breakdown, subsequently resulting in increased electrical breakdown strength. Moreover, the elastomer did not compromise the soft nature of the silicone elastomer and showed remarkable increased ultimate strain. These excellent mechanical properties indicated that the network consisted of an inherent soft PDMS-rich phase rather than PPMS- and PEG-rich phases, which were achieved following the favourable phase separation. In this work, the interpenetrating network, consisting of a binary phase-separating system of PDMS-PEG and PDMS-PPMS copolymers, was created successfully.

An excellent soft electrode with high conductivity is often sought for utilisation with soft silicone dielectric elastomer. PDMS-based electrodes are highly compatible with silicone elastomer, due to their great adhesion properties and inherent softness. By means of phase separation, PDMS-PEG copolymer can be prepared in a conductive manner, such that the continuous morphology of conducting PEG is formed by increasing appropriate loadings of PEG, without destroying the soft nature and the network integrity of the elastomer. In this thesis, the conductive PDMS-PPMS copolymer was used as an elastomeric conducting network, albeit conductivity was very poor. By incorporating conductive nanofillers, i.e. MWCNT in the PDMS-PEG copolymer, the conducting composite showed increased conductivity and increased softness.

In conclusion, this thesis has successfully summarised the work involved in optimising silicone electro-mechanical properties and compliant electrodes by means of phase separating block copolymers. Further studies utilising block copolymers will hopefully result in silicone elastomers with enhanced electro-mechanical properties and hence will be the next step in producing reliable elastomers for dielectric elastomer technology

needs. Furthermore, the optimisation of electrodes utilised from conductive block copolymers could be explored from different perspectives, such as expanding from the conducting network from one or two dimensions to three dimensions, and employing silica aerogel as a medium for dispersing conductive fillers or conducting networks.

7 Future works

7.1 Optimisation of electro-mechanical properties of DEs

Further studies looking at enhancing silicone electro-mechanical properties by means of block copolymers could be performed by utilising different types of PDMS-based copolymers. Previously, utilising PDMS-PEG and PDMS-PPMS copolymers has shown increased relative permittivity and increased electrical breakdown strength, respectively. However, utilising other block copolymers such as polydimethylsiloxane-polyetheretherketone (PDMS-PEEK) and polydimethylsiloxane-polyvinylidenefluoride (PDMS-PVDF) may result in silicone elastomers with enhanced electro-mechanical properties, due to a combination effect of a high dielectric constant and the semi-crystalline nature of PVDF and PEEK as a reinforcing domain. Enhanced electro-mechanical properties indicate that the most favourable phase separation may be achieved where it occurs on the nanoscale rather than the macro- or microscale. Consequently, the optimisation of silicone elastomers by phase separating other block copolymers would be the next step towards producing reliable silicone dielectric elastomers.

7.2 Optimisation of conductivity and mechanical properties of electrodes

Stretchable electrodes have received increasing attention due to their attractive applications, mainly in dielectric elastomer technology. Previous studies on stretchable electrodes have been conducted by utilising active conductive nanoparticles such as one-dimensional (1D) multi-walled carbon nanotubes (MWCNTs) [85] and two-dimensional (2D) multilayer graphite [121] in the elastomeric matrix. Recently, studies of three-dimensional (3D) conducting networks consisting of MWCNTs and graphene or graphite oxide (GO) have been carried out to enhance the conductivities and mechanical properties of stretchable conductive electrodes [122,123].

Conducting elastomer incorporating a 3D MWCNT/GO conducting network may possess high conductivity, but incorporating the conducting network into the elastomeric matrix is not possible via the direct blending method, due to strong van der Waals forces in MWCNTs and GO sheets, which results in overlapping and aggregating them [122]. As an alternative to enhancing the dispersion of the MWCNT/GO 3D network in the matrix, a strategy of constructing 3D carbon architectures consisting of GO and MWCNTs can be achieved by means of aerogel, which results in a 3D conducting network with high porosity. In other words, a well-defined 3D MWCNT/GO conducting aerogel-network keeps the structure of the 3D MWCNT/GO network through the aerogel, thereby avoiding the possibility of overlapping GO sheets and MWCNTs. Subsequently, the 3D MWCNT/GO

conducting aerogel network, which is highly porous, is backfilled with a silicone mixture using a vacuum-suction method, resulting in a nanocomposite-containing silicone elastomer and a 3D MWCNT/GO conducting aerogel-network.

Utilising an aerogel, however, results in a silicone elastomer with increased stiffness, due to the stiff nature of aerogel, which limits the strain for soft actuation [122]. Hence, silica aerogel is the most favourable aerogel, due to its flexibility and increased softness, which is introduced by incorporating organic parts into inorganic networks [124]. In order to synthesise silica aerogel, a reactive functional group is introduced onto silica surfaces by reacting functionalised trialkoxysilanes with conventional silane precursors such as tetraethoxysilane (TEOS) [125,126] or methyltriethoxysilane (MTES) [127].

For future work, a conducting elastomer could be prepared from a soft conducting nanocomposite consisting of a 3D conducting MWCNT/GO silica aerogel network and PDMS-PEG copolymer. Prior to cross-linking, the liquid mixture of the PDMS-PEG copolymer can be incorporated into the nano-porous 3D conducting MWCNT/GO silica aerogel network by using a vacuum-backfilled method. Herein, a modified silica aerogel containing PDMS, which is softer than other aerogel, is utilised in order to have a conducting elastomer with increased strain. In order to achieve a soft and well-defined PDMS-based silica aerogel, during the condensation step PDMS and hydrolysed MTES must be well dispersed, which can be achieved by increasing appropriately the mixing time and mixing rate. While adding PDMS to the MTES solution, it must be added at an appropriately slow rate to avoid flocculation. Besides that, temperature during the transformation of alcosols to alcogels is important for obtaining a well-defined aerogel.

8 Experimental methods

In this chapter, experimental methods of Chapter 2, 3, 4 and 5 are described, as well as the characterisations of prepared samples.

8.1 Chapter 2: Enhancement of relative permittivity

8.1.1 Materials and reagents

Hydride-terminated polydimethylsiloxanes (H-PDMS) used in the synthesis of the PDMS-PEG multiblock copolymer were DMS-H21, DMS-H11, DMS-H03 and SIH6117.0, each with an average molecular weight (M_n) of 6000, 1050, 550 and 208 g mol^{-1}, respectively. They were purchased from Gelest Inc., while polyethyleneglycol divinyl ether (PEG-DE) was acquired from Sigma Aldrich. A commercial PDMS elastomer [MJK 4/13] was obtained from Wacker Chemie AG, and platinum-divinyl-tetramethyl disiloxane complex [SIP6830.3] was purchased from Gelest Inc. and contained 3.25% of platinum in xylene. A hydride-terminated methyl-hydrosiloxane-dimethylsiloxane copolymer [HMS-501] (M_n of 1050 g mol^{-1}, 9-functional) cross-linker, along with tetravinyltetramethyl-cyclotetrasiloxane [SIT-7900] as an inhibitor, was purchased from Gelest Inc. Both methanol and toluene were purchased from Sigma Aldrich.

8.1.2 Synthesis of the PDMS-PEG prepolymer

The procedure used to synthesise PDMS-PEG multiblock copolymer was amended from that employed by Klasner et al. [97] and Jukarainen et al. [128]. All apparatus was thoroughly cleaned and dried at a temperature of 200°C. The characterisations on M_n of DMS-H21, DMS-H11, DMS-H03, SIH6117.0 and PEG-DE were performed using ^{1}H-NMR to obtain precise M_n for the stoichiometry calculations.

The theoretical PDMS-PEG repeating units in the multiblock copolymer were calculated from a target molecular weight of 30 kg mol^{-1}, whereby the number of blocks for PDMS and PEG were X and (X+1), respectively:

$$X = \frac{30000 - M_{n,PEG}}{M_{n,PDMS} + M_{n,PEG}} \tag{8.1}$$

where $M_{n,PDMS}$ and $M_{n,PEG}$ are the molecular weight of PDMS and PEG, respectively.

The stoichiometric ratio for preparing multiblock copolymers (r_1) was calculated as:

$$r_1 = \frac{[vinyl]}{[hydride]} = \frac{(X+1)f_{PEG-DE}}{Xf_{H-PDMS}} = \frac{X+1}{X} \quad (8.2)$$

where $f_{PEG\text{-}DE}$ and $f_{H\text{-}PDMS}$ are the functionality of PEG-DE and H-PDMS, respectively [129]. Both polymers in this case were di-functional (f=2), and the telechelic vinyl groups of the resulting copolymer were targeted.

Dry toluene (prepared by molecular sieving) was added into the flask at 30 wt% of the total mass of H-PDMS and PEG-DE. The initial concentration of the platinum catalyst was 3120 parts per million (ppm). From this solution, the amount of catalyst solution was determined, in order to obtain a final concentration of 30 ppm in the reaction mixture, by assuming the density of the mixture was 1 g cm^{-3}. The reaction occurred at 60°C with mild stirring and in the presence of nitrogen gas to eliminate air inside the flask. The duration of the hydrosilylation reaction depended on the chain length of H-PDMS and ranged from 2 to 6 hours. The disappearance of a Si-H bond signal at 4.70 ppm was checked by H-NMR, to ensure that all hydrides in the PDMS had been fully consumed during the reaction; refer to Appendix I - ESI 1, Figs. S1.a, S1.b, S1.c and S1.d for NMR spectra. The final solution was viscous and appeared light bronze in colour. Any remaining solvent (toluene) was removed with a rotary evaporator for a couple of hours. The product was purified by cold methanol precipitation, in order to remove excess PEG-DE, and washing was repeated at least five times. Methanol from the precipitation process was excluded by using a rotary evaporator for a few hours and then placing the mixture in a vacuum for a day.

8.1.3 Experimental setup for the PDMS-PEG block copolymer

To distinguish the PDMS-PEG multiblock copolymer samples from different PDMS volume fractions, they were named based on four different repeating unit numbers in the constituent polymer, as listed in Table 8.1. Asymmetrical morphologies in the PDMS-PEG multiblock copolymer were obtained by varying PDMS chain lengths (m=3,7,14,81) while sustaining the equivalent PEG chain length (n=4), which in turn produced PDMS3-PEG, PDMS7-PEG, PDMS14-PEG and PDMS81-PEG, respectively. Hence PDMS81-PEG constituted the highest volume fraction of PDMS in the block copolymer (0.94), whereas the lowest volume fraction produced in this study was 0.45 (belonging to PDMS3-PEG).

8.1.4 Binary polymer blends (BPBs)

PDMS-PEG multiblock copolymers were incorporated into PDMS elastomer (MJK) at 5, 10, 15 and 20 wt%. All mixtures were speedmixed at 3500 rpm for 2 minutes. After that, the blends were immediately cross-linked. The blends produced 16 samples in total.

Table 8.1 Sample details for PDMS-PEG multiblock copolymers

PDMS-PEG block copolymer	Number average molecular weight of H-PDMS ($M_{n,PDMS}$) [g mol^{-1}]	Number of repeating units in PDMS (m)	Theoretical number of repeating units in (PDMS-PEG)$_X$ (X)	Stoichio-metric ratio (r_1)	Volume fraction of PDMS (f_A)
PDMS81-PEG	6000.00	81	5	1.21	0.94
PDMS14-PEG	1050.00	14	23	1.04	0.75
PDMS7-PEG	550.00	7	37	1.03	0.62
PDMS3-PEG	208.00	3	56	1.02	0.45

Note: M_n of PEG in PDMS-PEG block copolymer is 250 g mol^{-1}

8.1.5 Cross-linking

Four samples of PDMS-PEG multiblock copolymers and 16 samples of BPB were prepared. The stoichiometric ratio for the cross-linking (r_2) was calculated as:

$$r_2 = \frac{[hydride]}{[vinyl]} = \frac{f_{HMS}[HMS]}{f_{BCP}[BCP]} \tag{8.3}$$

where f_{HMS} and f_{BCP} were the numbers of the HMS-501 (9-functional) functional group and the PDMS-PEG block copolymer (2-functional), respectively, while [...] indicates the initial concentration [130,131].

The values of r_2 were calculated based on the mass of PDMS-PEG prepolymers added into the blends. The inhibitor (SIT7900) and the platinum catalyst were added to the blends at 1 wt% and 30 ppm, respectively. Those blends which consisted of PDMS-PEG prepolymer, namely MJK4/13, SIT7900 and 30 ppm platinum catalyst, were speed-mixed rigorously at 3,000 rpm for 2 minutes. Cross-linker (HMS-501) was added, and the resulting mixture was additionally speed-mixed at 1,500 rpm for 2 minutes. The cross-linked films were cured at a temperature of 60°C overnight and then subsequently post-cured at 110°C for 2 hours.

8.2 Chapter 3: Enhancement of electrical breakdown strength

8.2.1 Materials

Telechelic vinyl-terminated polydimethylsiloxanes (V-PDMS) were DMS-V31, DMS-V25, DMS-V22 and DMS-V21, with a number average molecular weight (M_n) of 28, 17.2, 9.4 and 6 kg mol^{-1}, respectively. Telechelic hydride-terminated polyphenylmethyl-siloxanes (H-PPMS) were PMS-H03 (M_n = 0.4 kg mol^{-1}) and PMS-H11 (M_n = 1 kg mol^{-1}). The catalyst was a platinum-divinyl-tetramethyl disiloxane complex [SIP6830.3] containing 3.25% of platinum in xylene. The vinyl-functional cross-linker was methyl-

hydrosiloxane-dimethylsiloxane copolymer [VDT-431] (M_n = 28 kg mol^{-1}, 15-functional). All polymers, cross-linkers and catalysts were purchased from Gelest Inc. Fumed silica (SIS6962.0) was purchased from Fluorochem.

8.2.2 Synthesis of PDMS-PPMS block copolymers

The procedure to synthesise PDMS-PPMS block copolymers was taken from A Razak et al. [10]. The required amount of hydride-terminated PPMS was added based on a targeted molecular weight ($M_{n,T}$) of 30 kg mol^{-1} of the copolymer (refer to Appendix II - ESI 1, equation 1). The mixture containing V-PDMS, H-PPMS and 30 ppm of the Pt catalyst was speed-mixed at 3000 rpm for 5 min. The stoichiometric ratio was calculated based on the number of PDMS-PPMS repeating units, *X* (see Appendix II - ESI 1, equation 2).

8.2.3 Cross-linking and sample preparation

All PDMS-PPMS block copolymer samples were cross-linked with the vinyl-functional 15-functional cross-linker. The stoichiometric ratio for cross-linking (r_2) was 1.5, with an excess of cross-linker (see Appendix II - ESI 2, equation 3). Blends containing copolymer, cross-linker, 30 ppm of Pt catalyst and 25 parts per hundred rubber (phr) of silica were speed-mixed at 2500 rpm for 4 minutes.

The final mixtures were casted on Teflon plates for easy release. The cross-linked copolymer films were prepared in thicknesses of approximately 1 mm (thick film) and 100 ± 20 µm (thin film). Thick films were used to measure linear viscoelasticity (LVE), the stress-strain relationship and dielectric properties. All films were placed in a vacuum oven at 23°C for 4 to 8 hours, due to trapped air during fabrication, and were thereafter cured at 40°C for 12 hours to ensure proper film formation. The curing process was continued at 150°C for 8 to 12 hours. Subsequently, all films were post-cured at 200°C for 2 hours to remove all volatiles [132,133].

The cross-linked PDMS-PPMS copolymer is referred as a PDMS-PPMS elastomer. Samples were named based on repeating numbers of PDMS and PPMS as *n*DMS_*m*PMS. The realised molar concentrations of the phenyl group ($C_{C_6H_5}$) were calculated from the ratio of the mole number of the phenyl group to the total mass of PDMS and PPMS. The mole number of the phenyl group was determined based on integration areas and H's numbers of CH_3-Si-C_5H_5 and Si-$(CH_3)_2$ in ^{1}H-NMR (refer to Appendix II - ESI 3, equations 4-7). Details of the PDMS-PPMS copolymers are presented in Table 8.2.

Table 8.2 Sample details and realised molar concentrations of the phenyl group of cross-linked PDMS-PPMS copolymers.

Vinyl-functional PDMS	Hydride-functional PPMS	PDMS-PPMS copolymer (*n*DMS_*m*PMS)	Realised molar concentration of phenyl group $C_{C_6H_5}$ [10^{-4} mol g^{-1}]
DMS-V31	PMS-H03	377DMS_2PMS	5.0
DMS-V25		231DMS_2PMS	6.9
DMS-V22		126DMS_2PMS	7.8
DMS-V21		80DMS_2PMS	8.4
DMS-V31	PMS-H11	377DMS_6PMS	8.7
DMS-V25		231DMS_6PMS	9.8
DMS-V22		126DMS_6PMS	15
DMS-V21		80DMS_6PMS	20

8.3 Chapter 4: Optimisation of electro-mechanical properties

8.3.1 Materials

Telechelic vinyl-terminated polydimethylsiloxanes and telechelic hydride-terminated polyphenylmethylsiloxanes, which were used in the synthesis of a PDMS-PPMS copolymer, were DMS-V21 and PMS-H03, with an average molecular weight (M_n) of 6000 and 400 g mol^{-1}, respectively. In the synthesis of the PDMS-PEG copolymer, telechelic hydride-terminated polydimethylsiloxanes (H-PDMS) were DMS-H21, DMS-H11, DMS-H03 and SIH6117.0, with M_n of 6000, 1050, 550 and 208 g mol^{-1}, respectively. All of the abovementioned PDMS copolymers were purchased from Gelest Inc. The catalyst was platinum-divinyl-tetramethyl disiloxane complex [SIP6830.3], containing 3.25% of platinum in xylene, and the cross-linkers were vinyl-functional (4-5% vinylmethylsiloxane)-dimethylsiloxane copolymers [VDT-431] (M_n = 28 kg mol^{-1}, 15-functional) and hydride-functional (45-55% methylhydrosiloxane)-dimethylsiloxane copolymers [HMS-501] (M_n = 1050 g/mol, 9-functional). Both the catalyst and the cross-linkers were purchased from Gelest Inc. Telechelic vinyl-terminated polyethyleneglycol (V-PEG) was acquired from Sigma Aldrich. Fumed silica (SIS6962.0) and volatile methylsiloxane (VMS) [OS-20] were purchased from Fluorochem and Dow Corning, respectively.

8.3.2 PDMS-PPMS copolymer synthesis

The procedure used to synthesise the PDMS-PPMS copolymer was taken from A Razak and Skov [109]. PDMS-PPMS copolymers were prepared through the hydrosilylation of hydride-terminated PPMS and vinyl-terminated PDMS, as illustrated in Scheme 8-1. The

synthesised copolymer was telechelic hydride-functional. The theoretical number of PDMS-PPMS repeating units in the copolymer (X_1) was calculated from the targeted M_n of 30 kg/mol. The mixture containing DMS-V21, PMS-H03 and a 30 ppm Pt catalyst was speed-mixed at 3000 rpm for 5 min. The stoichiometric ratio for preparing the PDMS-PPMS copolymer (r_1) was calculated from the ratio (X_1 +1) to X_1 [109].

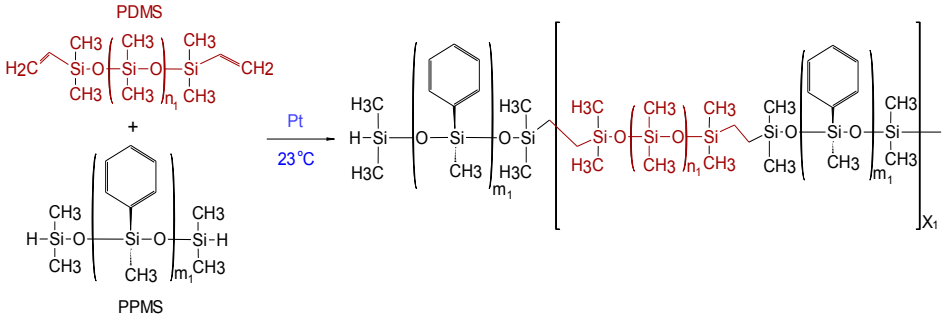

Scheme 8-1 The hydrosilylation reaction of a PDMS-PPMS copolymer, where m_1 is the number of repeating phenylmethylsiloxane (PMS) units in PPMS (m_1= 2), and n_1 is the number of repeating dimethylsiloxane (DMS) units in PDMS (n_1 = 80).

8.3.3 Synthesis of PDMS-PEG copolymers

PDMS-PEG copolymers were synthesised as described by A Razak et al. [10] The theoretical number of PDMS-PEG repeating units in the copolymer (X_2) was calculated from M_n of 30 kg mol^{-1}. The stoichiometric ratio for preparing the PDMS-PEG copolymers (r_2) was calculated from the ratio (X_2+1) to X_2 [10]. The synthesis of the PDMS-PEG copolymer was based on the hydrosilylation of hydride-terminated PDMS and vinyl-terminated PEG, as shown in Scheme 8-2. The synthesised PDMS-PEG copolymers were telechelic vinyl-functional.

Various volume fractions of PDMS in the PDMS-PEG copolymer were obtained by varying PDMS chain lengths, i.e. repeating PDMS units (m_2) were varied such that m_2 = 3,7,14,81, while the number of repeating PEG units remained constant (n_2 = 4). The synthesised copolymers were named PDMS3-PEG, PDMS7-PEG, PDMS14-PEG and PDMS81-PEG, respectively.

8.3.4 Binary copolymer blends and sample preparations

PDMS-PEG copolymers were incorporated into a PDMS-PPMS copolymer in concentrations of 10 and 20 phr before being speed-mixed at 3500 rpm for 2 minutes. The loadings of 10 and 20 phr are considered low and high loadings, respectively. One possible network is illustrated in Figure 8.1, such that hydride-functional PDMS-PPMS copolymers may bond covalently to vinyl-functional PDMS-PEG copolymers to form double copolymers, while some of them may cross-link with vinyl-functional cross-linkers (VDT-431) and vinyl-functional PDMS-PEG copolymers cross-link with hydride-functional cross-linkers (HMS-501). The stoichiometric ratios between PDMS-PPMS and

PDMS-PEG copolymers were 1.5, with an excess of VDT-431 and HMS-501, respectively [10,109]. Blends containing copolymers, cross-linkers, 30 ppm of Pt catalyst, 25 phr of silica and 25 phr of VMS solvent (OS-20 from Dow Corning) were speed-mixed at 3000 rpm for 4 minutes.

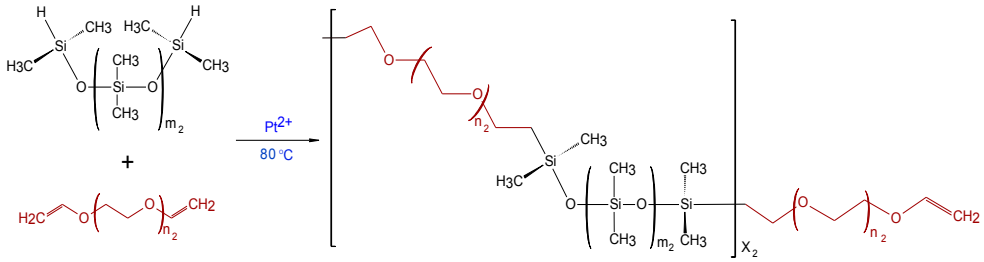

Scheme 8-2 Hydrosilylation reaction when synthesising a PDMS-PEG copolymer, where m_2 is the number of repeating DMS units in PDMS, n_2 = 4 is the constant number of repeating ethyleneglycol (EG) units in PEG.

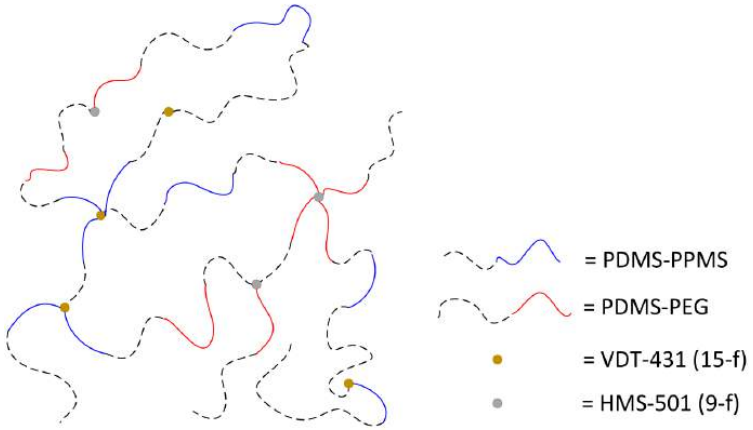

Figure 8.1 Illustration of the random network structure of PDMS-PPMS and PDMS-PEG copolymers, hydride-functional 9-functional and vinyl-functional 15-functional cross-linkers (HMS-501 and VDT-431, respectively). The cross-linkers are illustrated with fewer cross-linking sites than in the true network.

The final mixtures were cast on Teflon substrates for easy release, and the films were prepared at thicknesses of approximately 1±0.5 mm and 100±35 μm, as thick and thin films, respectively. Thin films were used for the measurement of electrical breakdown strength and thick films were used for measurements of linear viscoelasticity (LVE), the stress-strain relationship and dielectric properties. All films were placed in a vacuum oven at 23°C for 2 hours and were subsequently cured at 40°C for 12 hours for proper

film formation. The samples were placed in the oven at 150°C for 5-8 hours and subsequently post-cured at 200°C for 2 hours.

The cross-linked PDMS-PPMS copolymer containing 80 repeating DMS units and two repeating PMS units, referred to as 80DMS_2PMS. 80DMS_2PMS, was used as the reference elastomer and was prepared without incorporating the PDMS-PEG copolymer. Due to its proven versatility as a voltage-stabilised silicone elastomer, 80DMS-2PMS was utilised in all prepared binary copolymer blends (BCBs). Furthermore, 80DMS-2PMS has been proven to possess the most increased electrical breakdown strength compared to other PDMS-PPMS elastomers[109]. Details of the cross-linked BCBs containing 802DMS_2PMS and PDMS-PEG copolymers, and the reference elastomer, are shown in Table 8.3.

Table 8.3 Sample details of cross-linked BCBs containing PDMS-PPMS and PDMS-PEG copolymers.

No.	PDMS-PEG copolymer		Samples
	Concentration (phr)	PDMS*xx*-PEG	
1	-	-	80DMS_2PMS (reference)
2	10	PDMS81-PEG	10 phr PDMS81-PEG BCB
3	20		20 phr PDMS81-PEG BCB
4	10	PDMS14-PEG	10 phr PDMS14-PEG BCB
5	20		20 phr PDMS14-PEG BCB
6	10	PDMS7-PEG	10 phr PDMS7-PEG BCB
7	20		20 phr PDMS7-PEG BCB
8	10	PDMS3-PEG	10 phr PDMS3-PEG BCB
9	20		20 phr PDMS3-PEG BCB

Note: *xx* is the PDMS chain length.

8.4 Chapter 5: Compliant DE electrodes

8.4.1 Materials

Vinyl-terminated polydimethylsiloxane-polyethyleneglycol block co-oligomers (PDMS-PEG) were synthesised according to a previously published procedure [10]. The number average molecular weight (M_n) of the resulting PDMS-PEG copolymer was M_n = 3900 g mol^{-1}. Vinyl-functional PDMS cross-linker (15-functional, VDT-431), telechelic hydride-functional PDMS (DMS-H25, M_n = 17.2 kg mol^{-1}) and platinum-divinyltetramethyl disiloxane complex with 3.25% of platinum in xylene (SIP6830.3) were purchased from Gelest Inc. Pristine, multi-walled carbon nanotubes (MWCNTs) (NANOCYL™ NC7000)

with an average diameter, length and surface area of 9.5 nm, 1.5 µm and 250-300 m^2/g, respectively, were obtained from Nanocyl S.A., Belgium. N-methyl pyrrolidinone (NMP) and polyoxyethylene octyl phenyl ether (Triton X-100) were obtained from Sigma-Aldrich.

8.4.2 Synthesis of PDMS-PEG copolymers

The previously synthesised PDMS-PEG co-oligomer (M_n = 3900 g mol^{-1}) was chain-extended by hydrosilylation with telechelic hydride-functional PDMS, PDMS232 (M_n = 17,200 g mol^{-1}) in the presence of a Pt catalyst according to Scheme 8-3. PDMS-PEG co-oligomer, PDMS232 and the Pt catalyst were speed-mixed at 3000 rpm for 4 min. The transparent reaction mixture turned a milky yellow. The resulting CE-(PDMS-PEG) copolymer was characterised and verified by size-exclusive chromatography (SEC) to observe the shift in molecular weight from the low molecular weight of the PDMS-PEG copolymer to the high molecular weight of the CE-(PDMS-PEG) copolymer (M_n = 24 kg mol^{-1} / M_w = 52 kg mol^{-1}). ^{1}H-NMR spectroscopy was used to confirm the completion of the reaction through the absence of vinyl protons from the PDMS-PEG co-oligomer between δ_{H} = 5.8 and 6.2 ppm.

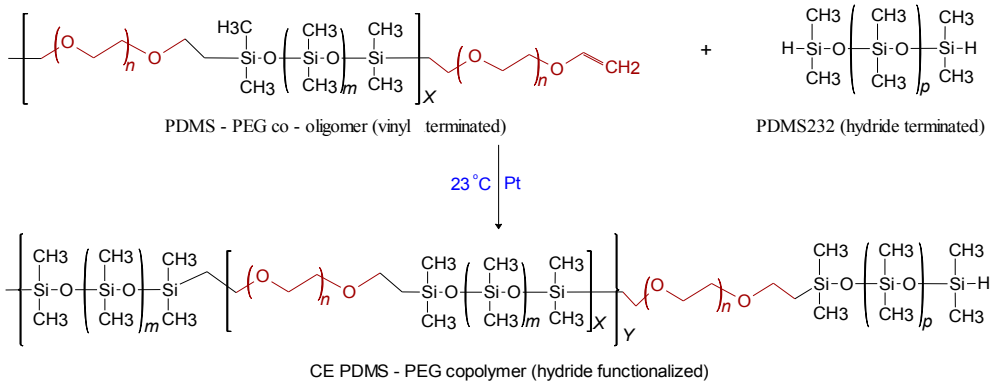

Scheme 8-3 The hydrosilylation reaction utilised for chain-extended CE-(PDMS-PEG) copolymer in the presence of a 30 ppm Pt catalyst at 23°C, where m = 3 and p = 232, respectively, are the numbers of repeating dimethylsiloxane units in the two PDMS parts. n = 4 is the constant number of repeating ethyleneglycol units, and X and Y are the number of repeating PDMS-PEG units and the number of CE-(PDMS-PEG) blocks, respectively.

8.4.3 Dispersion of MWCNTs

Dispersion of MWCNTs in 96 wt% NMP and 1 wt% Triton X-100 was achieved by ultrasonication in a water bath (1510E-DTH, BRANSONIC–Ultrasound Cleaner, USA, Input: 155 W & 50-60 kHz, Output: 70 W & 42 kHz).

8.4.4 Preparation of CE-(PDMS-PEG) elastomers with surface-modified MWCNT

CE-(PDMS-PEG) copolymer was cross-linked using a 15-functional vinyl cross-linker (VDT-431) with the addition of surface-treated MWCNTs in NMP and Triton X-100 (1, 2 and 3 phr MWCNT) by speed-mixing using SpeedMixer™ (DAC 150 FVZ, Flack Tek. Inc.) at 3000 rpm for 3 - 6 min. The final mixtures were cast on hollow metal plates placed on Teflon substrates. Films ~ 1 mm in thickness were cured initially at a temperature of 70°C, which was gradually increased to 150°C over a period of 7 days to ensure the gradual removal of NMP solvent and proper film formation.

8.5 Characterisations

8.5.1 Degree of conversion of vinyl or hydride groups in synthesis of copolymer

The synthesised copolymers were a telechelic vinyl functional PDMS-PEG copolymer and a telechelic hydride functional PDMS-PPMS copolymer, respectively. The degree of conversion of vinyl or hydride group of PDMS from the hydrosilylation reaction was determined from proton nuclear magnetic resonance spectroscopy (^{1}H-NMR) by observing the disappearance of vinyl peaks in the NMR spectra. The NMR equipment utilised for ^{1}H was a Bruker 300 MHz NMR. The number of scannings per sample was 128. The samples were prepared with a concentration of 100 mg mL^{-1} in deuterated chloroform ($CDCl_3$).

8.5.2 Number average molecular weight

The number average molecular weights (M_n) of the copolymers were determined from size-exclusive chromatography (SEC). SEC was performed on a Viscotek GPCmax VE-2001 instrument equipped with a Viscotek TriSEC Model 302 triple detector using two PLgel mixed-D columns from Polymer Laboratories. The copolymer concentrations were between 2 – 3 mg mL^{-1} in toluene, and solutions were run at 35°C at an elution rate of 1 mL min^{-1}. Molecular weight distributions were calculated using WinGPC Unity 7.4.0 software and linear PDMS standards acquired from Polymer Standards Service GmbH.

8.5.3 Linear viscoelasticity (LVE) properties

Prepared films were characterised at 23°C using an advanced rotational rheometer from TA Instruments (ARES-G2). The utilised parallel plates have diameter of 25 mm. The axial force ranged from 5 to 12 N depending on samples to ensure a sufficient contact between the plate and the sample (diameter of 25 mm). The strain and frequency in the linear regime were 2% and 10^{-2} – 10^2 Hz, respectively.

8.5.4 Stress–strain relationship

In Chapter 2, the Young's moduli were determined as Y = 2(1 + ν)G = 3G, since Poisson's ratio (ν) was close to 0.5, due to the incompressibility of silicones.

In Chapter 3 and 4, tensile strengths and elongations at break as well as Young's moduli at 5 % strain were measured in extensional rheological tests. The rheological test was performed on ARES-G2 rheometer from TA Instruments by means of a SER2 universal testing platform. The SER2 universal testing platform consists of two rotating drums with diameter of 10.3 mm and the lateral offset of the centre axis of the two drums is 12.7 mm. The sample, which was a rectangular strip of 6 mm (width), 30 mm (length) and 1 mm (thickness), elongated within a confined length (L = 12.7 mm) by winding up the strip with two rotary drums. The ends of the strip were secured by means of a strong glue to the surfaces of drums. For incompressible samples, the ends of the strip move at a speed [v_{end} = (L/2)dε_H/dt]. Integrating the mentioned speed from initial length (L_o) to the final length (L_f), lead to an exponential increase of the sample length over time L(t) = $L_o$exp[(dε_H/dt)t] and final Hencky strain (ε_H) thus can be expressed as follows: ε_H = ln[L_f/L_o]. Here engineering stress and strain were used for stress-strain relationship. The engineering strain was calculated from the measured Hencky strains and the engineering stress was calculated from the measured torque over cross-sectional area of sample.

From stress-strain curves, tensile strengths and elongations at breaking of the samples can be determined, as well as the Young's moduli. Stress-strain curves are measured in extensional rheological tests, performed using an advanced rheometer with a geometry consisting two rotating drums. For each sample, the strip was stretched from s = 0 % until it ruptures.

Stress and strain at breakthrough points are determined from engineering stress and strain. The engineering stress (σ_E) can be calculated from the force (F) and the cross-sectional area of the strip (A):

$$\sigma_E = \frac{F}{A} = \frac{F}{t \cdot w} = \frac{\tau \cdot d}{t \cdot w} \tag{8.4}$$

where t and w are a sample thickness and a constant width equal to 6 mm, respectively. The force is calculated from the torque (τ) and constant drum diameter (d = 10.3 mm).

The engineering strain (ϵ_E) was calculated as a ratio of the strain difference before and after stretching ($L - L_0$) to an initial strain (L_0) as:

$$\epsilon_E = \frac{L - L_0}{L_0} \tag{8.5}$$

where the final strain after stretching (L) can be determined from Hencky strain (ϵ_H):

$$\epsilon_H = ln\frac{L}{L_0} \tag{8.6}$$

$$L = L_0 e^{\epsilon_H} = L_0 e^{r_H \cdot t_s} \tag{8.7}$$

where r_H and t_s are the constant Hencky rate at 0.001 rotation/s and the step time, respectively.

By inserting Eqn. 8.7 in 8.5 the final expression of engineering strain was obtained as:

$$\epsilon_E = e^{r_H \cdot t_s} - 1 \tag{8.8}$$

Young's moduli were determined from the tangent line of linear regime of stress-strain curves at 5 % strain.

8.5.5 Dielectric properties

Dielectric properties were measured by dielectric spectroscopy. The dielectric spectroscopy was performed on a Novocontrol Alpha-A high-performance frequency analyser (Novo-control Technologies GmbH & Co. KG, Germany) operating in the frequency range 10^{-1} – 10^{6} Hz at 23°C. The electrode diameter was 20 mm. The sample was sandwiched between two gold-coated plates prior to the measurement.

8.5.6 Electrical breakdown strength

The measurement of electrical breakdown strength was performed on an in-house-built device based on international standards (IEC 60243-1 (1998) and IEC 60243-2 (2001)). Samples were prepared with thickness of less than 110 µm. The film was slid between the two spherical metal electrodes (diameter of 20 mm). The electrical breakdown measurement was measured at the point of contact with a stepwise increasing voltage applied (50 – 100 V per step) at a rate of 0.5 – 1 steps s^{-1}. The electrical breakdown measurement was repeated 12 times for each sample, and the average of these values was then stated as the electrical breakdown strength.

8.5.7 Scanning electron microscope (SEM) image

8.5.7.1 SEM image (Chapters 2, 3, and 5)

The morphologies of the cross-linked copolymers and the reference elastomer were examined by scanning electron microscopy (SEM) (FEI Inspect S, USA). The samples were cross-sectional films and were firstly immersed into liquid nitrogen for a few minutes, then broken and deposited on a sample holder. All samples were coated with gold under vacuum before test. Energy dispersive x-ray (EDX) spectroscopy (Oxford INCAWave 500, UK) was applied to detect the element distribution profile on the surface of the samples.

8.5.7.2 SEM image (Chapter 4)

The morphologies of prepared elastomers and the reference elastomer were inspected via scanning electron microscopy (SEM) images which were performed on FEI Quanta 200 ESEM FEG. Cross-sectional SEM samples were coated with 2 nm thickness of gold by means of sputter coater (Cressington, model 208HR) under vacuum conditions and the current of 10 mA. Field emission gun with accelerating voltage between 500 V- 30 kV was applied to detect the element distribution profile on the surface of the samples.

8.5.8 Transmission electron microscopy (TEM) image

The TEM model, FEI Tecnai T20 G2 was used to characterize micro and nano-scale images using transmitted electrons from the electron source of Thermionic LaB6/CeB6. TEM samples were prepared using grinding tool and were placed on a grid coated by Copper Naphthenate (Coppernate).

8.5.9 Static contact angle

Static contact angles, created by using the "sessile drop-needle in" method, were taken at a room temperature of 23°C using Dataphysics OCA20. The contact angle was measured by dropping 6 µL of deionised water onto the PDMS-PEG multiblock copolymer and BPB films. Measurements for each contact angle were taken for 65 seconds, and the contact angles were analysed every 5 seconds, in order to obtain contact angle versus time profiles.

8.5.10 UV/Vis absorbance

The presence of phenyl groups in the cross-linked copolymers was detected from the absorbance energy of ultraviolet (UV) or visible light (Vis). The energy absorbance from UV/Vis light was measured by an UV/Vis spectrometer from BMG Labtech (SPECTROstar Omega). The wavelength range of UV/Vis spectrometer was in a range of 220 to 1000 nm. The range of optical density (OD) was between 0 to 4 OD with the accuracy of < 1% at 2 OD. The energy absorbance was measured within wavelengths of 220 to 350 nm. The measurements were performed on 8 wells of a module plate of Nunc 96-Well LockWellTM PolySorp from Thermo Scientific for thin films with approximate thickness of 100 µm.

Bibliography

1. Madsen FB, Daugaard AE, Hvilsted S, Skov AL. “The current state of silicone-based dielectric elastomer transducers.” Macromolecular Rapid Communications. 37 : 378–413 (2016).

2. Brochu P, Pei Q. “Advances in dielectric elastomers for actuators and artificial muscles.” Macromolecular Rapid Communications. 31 : 10–36 (2010).

3. Carpi F, Bauer S, De Rossi D. “Stretching dielectric elastomer performance.” Science. 330 : 1759–61 (2010).

4. Bar-cohen Y. “Artificial muscles using electroactive polymers (EAP): Capabilities , challenges and potential.” Jet Propulsion Laboratory, National Aeronautics and Space Administration. : Pasedena, CA (2005).

5. Graz I, Kaltenbrunner M, Keplinger C, Schwödiauer R, Bauer S, Lacour SP, et al. “Flexible ferroelectret field-effect transistor for large-area sensor skins and microphones.” Applied Physics Letters. 89 : 73501-1–3 (2006).

6. Krause M, Graz I, Bauer-Gogonea S, Bauer S, Ploss B, Zirkl M, et al. “PbTiO3-P(VDF-TrFE) – Nanocomposites for pressure and temperature sensitive skin.” Ferroelectrics. 419 : 23–7 (2011).

7. Ploss B, Ploss B, Shin FG, Chan HLW, Choy CL. “Pyroelectric or piezoelectric compensated ferroelectric composites.” Applied Physics Letters. 76 : 2776–8 (2000).

8. Wang Y, Sun C, Zhou E, Su J. “Deformation mechanisms of electrostrictive graft elastomer.” Smart Materials and Structures. 13 : 1407–13 (2004).

9. Osada Y, Okuzaki H, Hori H. “A polymer gel with electrically driven motility.” Nature. 355 : 242–4 (1992).

10. A Razak AH, Szabo P, Skov AL. “Enhancement of dielectric permittivity by incorporating PDMS-PEG multiblock copolymers in silicone elastomers.” RSC Adv. 5 : 53054–62 (2015).

11. Madsen FB, Yu L, Daugaard AE, Hvilsted S, Skov AL. “A new soft dielectric silicone elastomer matrix with high mechanical integrity and low losses.” RSC Adv. 5 : 10254–9 (2015).

12. Fukuda T, Luo ZW, Ito A. “Development of dielectric elastomer actuators - Part I: Performance of polyurethane film actuators with dangling chains and network structures.” Advanced Materials Research. 557–559 : 1852–6 (2012).

13. Pelrine R, Kornbluh R, Joseph J, Heydt R, Pei Q, Chiba S. “High-field deformation of elastomeric dielectrics for actuators.” Materials Science and Engineering: C. 11 : 89–100 (2000).

14. Bauer S, Bauer-Gogonea S, Graz I, Kaltenbrunner M, Keplinger C, Schwödiauer R. “25th anniversary article: A soft future: From robots and sensor skin to energy harvesters.” Advanced Materials. 26 : 149–62 (2014).

15. Araromi OA, Gavrilovich I, Shintake J, Rosset S, Richard M, Gass V, et al. “Rollable multisegment dielectric elastomer minimum energy structures for a deployable microsatellite gripper.” IEEE/ASME Transactions on Mechatronics. 20 : 438–46 (2014).

16. Anderson IA, Ieropoulos IA, McKay T, O’Brien B, Melhuish C. “Power for robotic artificial muscles.” IEEE/ASME Transactions on Mechatronics. 16 : 107–11 (2011).

17. McKay TG, O’Brien BM, Calius EP, Anderson IA. “Soft generators using dielectric elastomers.” Applied Physics Letters. 98 : 142903 (2011).

18. Zhao X, Suo Z. “Theory of dielectric elastomers capable of giant deformation of actuation.” Physical Review Letters. 104 : 178302-1–4 (2010).

19. Pelrine R, Kornbluh R, Pei Q, Joseph J. “High-speed electrically actuated elastomers with

strain greater than 100%." Science. 287 : 836–9 (2000).

20. Carpi F, Frediani G, Turco S, De RD. "Bioinspired tunable lens with muscle-like electroactive elastomers." Advanced Functional Materials. 21 : 4152–8 (2011).

21. Rosset S, Dubois P, Niklaus M, Shea H. "Large stroke miniaturized dielectric elastomer actuators." Transducers 2009 - 15th International Conference on Solid-state Sensors, Actuators and Microsystems. : 2401–4 (2009).

22. Hosoya N, Baba S, Maeda S. "Hemispherical breathing mode speaker using a dielectric elastomer actuator." The Journal of the Acoustical Society of America. 138 : EL424-EL428 (2015).

23. Pope K, Tews A, Frecker MI, Mockensturm E, Goulbourne N, Snyder AJ. "Dielectric elastomer laminates for active membrane pump applications." Proc. of SPIE. 5385 : 60–7 (2004).

24. Anderson IA, Hale T, Gisby T, Inamura T, McKay T, O'Brien B, et al. "A thin membrane artificial muscle rotary motor." Applied Physics A: Materials Science and Processing. 98 : 75–83 (2010).

25. Pelrine R, Kornbluh R, Eckerle J, Jeuck P, Oh S, Pei Q, et al. "Dielectric elastomers - Generator mode fundamentals & applications." Proc. of SPIE of SPIE. 4329 : 148–56 (2001).

26. Koh SJA, Keplinger C, Li T, Bauer S, Suo Z. "Dielectric elastomer generators: How much energy can be converted?" IEEE/ASME Transactions on Mechatronics. 16 : 33–41 (2011).

27. O'Brien BM, Calius EP, Inamura T, Xie SQ, Anderson IA. "Dielectric elastomer switches for smart artificial muscles." Applied Physics A: Materials Science and Processing. 100 : 385–9 (2010).

28. Araromi O, Poulin A, Rosset S, Favre M, Giazzon M, Martin-Olmos C, et al. "Thin-film dielectric elastomer sensors to measure the contraction force of smooth muscle cells." Proc. of SPIE. 9430 : 94300Z–1–8 (2015).

29. Kessel R Van, Wattez A, Bauer P. "The effect of converter efficiency on DEAP-based energy conversion : an overview and optimization method." Proc. of SPIE. 9056 : 90561D–1–12 (2014).

30. Vudayagiri S, Zakaria S, Yu L, Hassouneh SS, Benslimane M, Skov AL. "High breakdown-strength composites from liquid silicone rubbers." Smart Materials and Structures. 23 : 105017 (2014).

31. Zhang Z, Liu L, Fan J, Yu K, Liu Y, Shi L, et al. "New silicone dielectric elastomer with a high dielectric constant." Proceedings of SPIE. 6926 : 692610-1–8 (2008).

32. Lotz P, Matysek M, Lechner P, Hamann M, Schlaak HF. "Dielectric elastomer actuators using improved thin film processing and nanosized particles." Proc. of SPIE. 6927 : 692723 (2008).

33. Carpi F, De Rossi D. "Improvement of electromechanical actuating performances of a silicone dielectric elastomer by dispersion of titanium dioxide powder." IEEE Transactions on Dielectrics and Electrical Insulation. 12 : 835–43 (2005).

34. Szabo JP, Hiltz JA, Cameron CG, Underhill RS, Massey J, White B, et al. "Elastomeric composites with high dielectric constant for use in Maxwell stress actuators." Proceedings of SPIE. 5051 : 180–90 (2003).

35. Romasanta LJ, Leret P, Casaban L, Hernández M, de la Rubia MA, Fernández JF, et al. "Towards materials with enhanced electro-mechanical response: CaCu3Ti4O12–polydimethylsiloxane composites." Journal of Materials Chemistry. 22 : 24705–12 (2012).

36. Böse H, Uhl D, Rabindranath R. "Novel DEA with organically modified silicone elastomer for permittivity enhancement." Proc. of SPIE. 8340 : 83402E–1–10 (2012).

37. Kussmaul B, Risse S, Kofod G, Waché R, Wegener M, McCarthy DN, et al. "Enhancement of dielectric permittivity and electromechanical response in silicone elastomers: Molecular

grafting of organic dipoles to the macromolecular network." Advanced Functional Materials. 21 : 4589–94 (2011).

38. Madsen FB, Daugaard AE, Hvilsted S, Benslimane MY, Skov AL. "Dipolar cross-linkers for PDMS networks with enhanced dielectric permittivity and low dielectric loss." Smart Materials and Structures. 22 : 1–11 (2013).

39. Molberg M, Crespy D, Rupper P, Nüesch F, Manson JAE, Löwe C, et al. "High breakdown field dielectric elastomer actuators using encapsulated polyaniline as high dielectric constant filler." Advanced Functional Materials. 20 : 3280–91 (2010).

40. Quinsaat JEQ, Nüesch FA, Hofmann H, Opris DM. "Dielectric properties of silver nanoparticles coated with silica shells of different thicknesses." RSC Advances. 3 : 6964–71 (2013).

41. Mazurek P, Daugaard AE, Skolimowski M, Hvilsted S, Skov AL. "Preparing mono-dispersed liquid core PDMS microcapsules from thiol-ene-epoxy-tailored flow-focusing microfluidic devices." RSC Adv. Royal Society of Chemistry; 5 : 15379–86 (2015).

42. Mazurek P, Hvilsted S, Skov AL. "Green silicone elastomer obtained from a counterintuitively stable mixture of glycerol and PDMS." Polymer. 87 : 1–7 (2016).

43. Muffoletto DP, Burke KM, Zirnhel JL. "Partial discharge analysis of prestretched and unstretched acrylic elastomers for dielectric elastomer actuators (DEA)." Proc. of SPIE. 8340 : 834021-1–8 (2012).

44. Ha SM, Yuan W, Pei Q, Pelrine R, Stanford S. "Interpenetrating polymer networks for high-performance electroelastomer artificial muscles." Advanced Materials. 18 : 887–91 (2006).

45. Brochu P, Stoyanov H, Niu X, Pei Q. "All-silicone prestrain-locked interpenetrating polymer network elastomers: free-standing silicone artificial muscles with improved performance and robustness." Smart Materials and Structures. 22 : 55022 (2013).

46. Madsen FB, Daugaard AE, Fleury C, Hvilsted S, Skov AL. "Visualisation and characterisation of heterogeneous bimodal PDMS networks." RSC Advances. 4 : 6939–45 (2014).

47. Trols A, Kogler A, Baumgartner R, Kaltseis R, Keplinger C, Schwodiauer R, et al. "Stretch dependence of the electrical breakdown strength and dielectric constant of dielectric elastomers." Smart Materials and Structures. 22 : 104012 (2013).

48. Zakaria S, Morshuis PHF, Benslimane MY, Yu L, Skov AL. "The electrical breakdown strength of pre-stretched elastomers, with and without sample volume conservation." Smart Materials and Structures. 24 : 55009-1–10 (2015).

49. Kollosche M, Melzer M, Becker A, Stoyanov H, McCarthy DN, Ragusch H, et al. "The influence of mechanical properties in the electrical breakdown in poly-styrene-ethylene-butadiene-styrene thermoplastic elastomer." Proc. of SPIE. 7287 : 728729-1–9 (2009).

50. Huang J, Shian S, Diebold RM, Suo Z, Clarke DR. "The thickness and stretch dependence of the electrical breakdown strength of an acrylic dielectric elastomer." Applied Physics Letters. 101 : 122905 (2012).

51. Zakaria S, Morshuis PHF, Benslimane MY, Gernaey K V., Skov AL. "The electrical breakdown of thin dielectric elastomers: thermal effects." Proc. of SPIE. 9056 : 90562V (2014).

52. Fothergill JC. "Filamentary electromechanical breakdown." IEEE transactions on electrical insulation. 26 : 1124–9 (1991).

53. Madsen FB, Dimitrov I, Daugaard AE, Hvilsted S, Skov AL. "Novel cross-linkers for PDMS networks for controlled and well distributed grafting of functionalities by click chemistry." Polymer Chemistry. 4 : 1700–7 (2013).

54. Stoyanov H, Brochu P, Niu X, Lai C, Yun S, Pei Q. "Long lifetime, fault-tolerant freestanding actuators based on a silicone dielectric elastomer and self-clearing carbon

nanotube compliant electrodes." RSC Advances. 3 : 2272–8 (2013).

55. Bejenariu AG, Yu L, Skov AL. "Low moduli elastomers with low viscous dissipation." Soft Matter. 8 : 3917–23 (2012).

56. Bates FS, Fredrickson GH. "Block copolymers—Designer soft materials." Physics Today. 52 : 32–8 (1999).

57. Khandpurj AK, Farster S, Bates FS, Hamley IW, Ryan AJ. "Diblock Copolymer Phase Diagram near the Order-Disorder Transition." Macromolecules. 28 : 8796–806 (1995).

58. Alegria A, Lund R, Barroso-Bujans F, Arbe A, Colmenero J. "Component dynamics in nanostructured PI-PDMS diblock copolymers with PI segregated in lamellas, cylinders, and spheres." Colloid and Polymer Science. 292 : 1863–76 (2014).

59. Mai Y, Eisenberg A. "Self-assembly of block copolymers." Chemical Society reviews. 41 : 5969–85 (2012).

60. Zheng W, Wang ZG. "Morphology of ABC triblock copolymers." Macromolecules. 28 : 7215–23 (1995).

61. Gazit O, Khalfin R, Cohen Y, Tannenbaum R. "Self-Assembled Diblock Copolymer 'Nanoreactors' as 'Catalysts' for Metal Nanoparticle Synthesis." The Journal of Physical Chemistry C. 113 : 576–83 (2009).

62. Hamley IW. "The physics of block copolymers." Oxford, New York; (1998).

63. Yamano Y, Endoh H. "Increase in breakdown strength of PE film by additives of azocompounds." IEEE Transactions on Dielectrics and Electrical Insulation. 5 : 270–5 (1998).

64. Yamano Y. "Roles of polycyclic compounds in increasing breakdown Strength of LDPE film." IEEE Transactions on Dielectrics and Electrical Insulation. 13 : 773–81 (2006).

65. Englund V, Huuva R, Gubanski SM, Hjertberg T. "High efficiency voltage stabilizers for XLPE cable insulation." Polymer Degradation and Stability. 94 : 823–33 (2009).

66. J. McMurry. "Organic Chemistry 8th edition." California: Brooks/Cole; (2011).

67. Benslimane MY, Kiil H-E, Tryson MJ. "Dielectric electro-active polymer push actuators: performance and challenges." Polymer International. 59 : 415–21 (2010).

68. Liu H, Zhang L, Yang D, Ning N, Yu Y, Yao L, et al. "A new kind of electro-active polymer composite composed of silicone elastomer and polyethylene glycol." Journal of Physics D: Applied Physics; 45 : 485303 (2012).

69. Barber P, Balasubramanian S, Anguchamy Y, Gong S, Wibowo A, Gao H, et al. "Polymer composite and nanocomposite dielectric materials for pulse power energy storage." Materials. 2 : 1697–733 (2009).

70. Goswami K, Galantini F, Mazurek P, Daugaard AE, Gallone G, Skov AL. "Reinforced poly(propylene oxide): a very soft and extensible dielectric electroactive polymer." Smart Materials and Structures. 22 : 1–7 (2013).

71. Bigue JL, Chouinard P, Proulx S, Miron G, Plante JS. "Preliminary assessment of manufacturing impacts on dielectric elastomer actuators reliability." Cansmart Workshop. : 303–14 (2014).

72. Zhao X, Suo Z. "Method to analyze electromechanical stability of dielectric elastomers." Applied Physics Letters. 91 : 61921 (2007).

73. Plante J, Dubowsky S. "On the nature of dielectric elastomer actuators and its implications for their design." Proceeding of SPIE. 6168 : 61681J (2006).

74. Stark KH, Garton CG. "Electric strength of irradiated polythene." Nature. 176 : 1225–6 (1955).

75. Blok J, Legrand DG. "Dielectric breakdown of polymer films." Journal of Applied Physics. 40 : 288–93 (1969).

76. Kornbluh RD, Pelrine R, Joseph J, Heydt R, Pei Q, Chiba S. "High-field electrostriction of

elastomeric polymer dielectrics for actuation." Proceeding of SPIE. 3669 : 149–61 (1999).

77. Dissado LA, Fothergill JC. "Electrical degradation and breakdown in polymers." IET, UK; (1992).

78. Qi X, Zheng Z, Boggs S. "Computation of electro-thermal breakdown of polymer films." Conference on Electrical Insulation and Dielectric Phenomena IEEE. : 337–40 (2003).

79. Morshuis PHF, Smit JJ. "Partial discharges at dc voltage: Their mechanism, detection and analysis." IEEE Transactions on Dielectrics and Electrical Insulation. 12 : 328–40 (2005).

80. Sommer-Larsen P., Larsen AL. "Materials for dielectric actuators." Proceeding of SPIE. 5385 : 68–77 (2004).

81. McKay TG, Calius E, Anderson I a. "The dielectric constant of 3M VHB: a parameter in dispute." Proc. of SPIE. 7287 : 72870P–1–10 (2009).

82. Kim D, Lu N, Ma R, Kim Y-S, Kim R-H, Wang S, et al. "Epidermal electronics." Science [Internet]. 333 : 838–43 (2011).

83. Rosset S, Shea HR. "Flexible and stretchable electrodes for dielectric elastomer actuators." Applied Physics A: Materials Science and Processing. 110 : 281–307 (2013).

84. Lipomi DJ, Bao Z. "Stretchable, elastic materials and devices for solar energy conversion." Energy & Environmental Science. 4 : 3314–28 (2011).

85. A Razak AH, Madsen FB, Skov AL. "Mechanically compliant electrodes and dielectric elastomers from PEG-PDMS copolymers." MRS Advances. 1 : 3497–508 (2016).

86. Kujawski M, Pearse JD, Smela E. "Elastomers filled with exfoliated graphite as compliant electrodes." Carbon. 48 : 2409–17 (2010).

87. Li J, Liang J, Li L, Ren F, Hu W, Li J, et al. "Healable Capacitive Touch Screen Sensors Based on Transparent Composite Electrodes Comprising Silver Nanowires and a Furan/Maleimide Diels-Alder Cycloaddition Polymer." ACS nano. 8 : 12874–82 (2014).

88. Benslimane MY, Kiil H-E, Tryson MJ. "Electromechanical properties of novel large strain polypower film and laminate com- ponents for deap actuator and sensor applications." Proc. of SPIE. 7642 (2010).

89. Yuan W, Lam T, Biggs J, Hu L, Yu Z, Ha S, et al. "New electrode materials for dielectric elastomer actuators." Proceeding of SPIE. 6524 : 65240N (2007).

90. Lam T, Tran H, Yuan W, Yu Z, Ha S, Kaner R, et al. "Polyaniline nanofibers as a novel electrode material for fault- tolerant dielectric elastomer actuators." Proceeding of SPIE. 6927 : 692700 (2008).

91. Yuan W, Hu L, Yu Z, Lam T, Biggs J, Ha SM, et al. "Fault-tolerant dielectric elastomer actuators using single-walled carbon nanotube electrodes." Advanced Materials. 20 : 621–5 (2008).

92. Keplinger C, Sun J, Foo CC, Rothemund P, Whitesides GM, Suo Z. "Stretchable, transparent, ionic conductors." Science. 341 : 984–7 (2013).

93. Chen B, Lu JJ, Yang CH, Yang JH, Zhou J, Chen YM, et al. "Highly stretchable and transparent ionogels as nonvolatile conductors for dielectric elastomer transducers." ACS Applied Materials and Interfaces. 6 : 7840–5 (2014).

94. Mazurek P, Yu L, Gerhard R, Wirges W, Skov AL. "Glycerol as high-permittivity liquid filler in dielectric silicone elastomers." Journal of Applied Polymer Science. 133 : 1–8 (2016).

95. Ishai P Ben, Talary MS, Caduff A, Levy E, Feldman Y. "Electrode polarization in dielectric measurements: a review." Measurement Science and Technology. 24 : 102001 (2013).

96. Goswami K, Daugaard AE, Skov AL. "Dielectric properties of ultraviolet cured poly(dimethyl siloxane) sub-percolative composites containing percolative amounts of multi-walled carbon nanotubes." RSC Adv. Royal Society of Chemistry; 5 : 12792–9 (2015).

97. Klasner SA, Metto EC, Roman GT, Culbertson CT. "Synthesis and characterization of a poly(dimethylsiloxane)-poly(ethylene oxide) block copolymer for fabrication of amphiphilic

surfaces on microfluidic devices." Langmuir : the ACS journal of surfaces and colloids. 25 : 10390–6 (2009).

98. Zakaria S, Yu L, Kofod G, Skov AL. "Influence of static pre-stretching on mechanical ageing of filled silicone rubbers for dielectric elastomer applications." Materials Today Communications. 4 : 204–13 (2015).

99. Kochetov R, Korobko A V, Andritsch T, Morshuis PHF, Picken SJ, Smit JJ. "Modelling of the thermal conductivity in polymer nanocomposites and the impact of the interface between filler and matrix." Journal of Physics D: Applied Physics. 44 : 395401-1–12 (2011).

100. Skov AL, Bejenariu AG, Bøgelund J, Benslimane MY. "Influence of micro- and nanofillers on electro-mechanical performance of silicone EAPs." Proc. of SPIE. 8340 : 83400M–1–10 (2012).

101. Luo Y, Tan S, Wang H, Wu F, Liu X, Li L, et al. "PPMS composite membranes for the concentration of organics from aqueous solutions by pervaporation." Chemical Engineering Journal. 137 : 496–502 (2008).

102. Yu L, Skov AL. "Silicone rubbers for dielectric elastomers with improved dielectric and mechanical properties as a result of substituting silica with titanium dioxide." International Journal of Smart and Nano Materials. 6 : 268–89 (2015).

103. Larsen AL, Hansen K, Sommer-Larsen P, Hassager O, Bach A, Ndoni S, et al. "Elastic properties of nonstoichiometric reacted PDMS networks." Macromolecules. 36 : 10063–70 (2003).

104. Nandi SK, Liu X, Venkatachalam DK, Elliman RG. "Effect of electrode roughness on electroforming in HfO2 and defect-induced moderation of electric-field enhancement." Physical Review Applied. 4 : 64010-1–11 (2015).

105. Li Y, Hu K, Han X, Yang Q, Xiong Y, Bai Y, et al. "Phase separation of silicon-containing polymer/polystyrene blends in spin-coated films." Langmuir. 32 : 3670–8 (2016).

106. Raczkowska J, Bernasik A, Budkowski A, Sajewicz K, Penc B, Lekki J, et al. "Structures formed in spin-cast films of polystyrene blends with poly(butyl methacrylate) isomers." Macromolecules. 37 : 7308–15 (2004).

107. Jinnai H, Nishikawa Y, Koga T, Hashimoto T. "Direct observation of three-dimensional bicontinuous structure developed via spinodal decomposition." Macromolecules. 28 : 4782–4 (1995).

108. Walheim S, Ramstein M, Steiner U. "Morphologies in ternary polymer blends after spin-coating." Langmuir. 15 : 4828–36 (1999).

109. A Razak AH, Skov AL. "Silicone elastomers with covalently incorporated aromatic voltage stabilisers." RSC Adv. 7 : 468–77 (2017).

110. Tugui C, Vlad S, Iacob M, Varganici CD, Pricop L, Cazacu M. "Interpenetrating poly(urethane-urea)–polydimethylsiloxane networks designed as active elements in electromechanical transducers." Polym. Chem. Royal Society of Chemistry; 7 : 2709–19 (2016).

111. Hikita M, Tajima S, Kanno I, Ishinoj I, Sawa G, Ieda M. "High-field conduction and electrical breakdown of polyethylene at high temperatures." Japanese Journal of Applied Physics. 24 : 988–96 (1985).

112. Thess A, Lee R, Nikolaev P, Dai H, Petit P, Xu C, et al. "All use subject to JSTOR Terms and Conditions Crystalline Ropes of Metallic Carbon Nanotubes." Science. 273 : 483–7 (2014).

113. Ma PC, Wang SQ, Kim J-K, Tang BZ. "In-Situ amino functionalization of carbon nanotubes using ball milling." Journal of Nanoscience and Nanotechnology. 9 : 749–53 (2009).

114. Geng Y, Liu MY, Li J, Shi XM, Kim JK. "Effects of surfactant treatment on mechanical and electrical properties of CNT/epoxy nanocomposites." Composites Part A: Applied Science and Manufacturing. 39 : 1876–83 (2008).

115. Park KC, Hayashi T, Tomiyasu H, Endo M, Dresselhaus MS. “Progressive and invasive functionalization of carbon nanotube sidewalls by diluted nitric acid under supercritical conditions.” Journal of Materials Chemistry. 15 : 407–11 (2005).

116. Kim YJ, Shin TS, Choi H Do, Kwon JH, Chung Y-C, Yoon HG. “Electrical conductivity of chemically modified multiwalled carbon nanotube/epoxy composites.” Carbon. 43 : 23–30 (2005).

117. Rastogi R, Kaushal R, Tripathi SK, Sharma AL, Kaur I, Bharadwaj LM. “Comparative study of carbon nanotube dispersion using surfactants.” Journal of Colloid and Interface Science. 328 : 421–8 (2008).

118. Vladár AE. “Strategies for scanning electron microscopy sample preparation and characterization of multiwall carbon nanotube polymer composites.” NIST Special Publication 1200-17. 1 : 1–16 (2015).

119. Yu L, Madsen FB, Hvilsted S, Skov AL. “High energy density interpenetrating networks from ionic networks and silicone.” Proceedings of SPIE. 9430 : 94300T–1–94300T–11 (2015).

120. Wu DY, Meure S, Solomon D. “Self-healing polymeric materials: A review of recent developments.” Progress in Polymer Science. 33 : 479–522 (2008).

121. Hassouneh SS, Daugaard AE, Skov AL. “Design of elastomer structure to facilitate incorporation of expanded graphite in silicones without compromising electromechanical integrity.” Macromolecular Materials and Engineering. 300 : 542–50 (2015).

122. Chen M, Tao T, Zhang L, Gao W, Li C. “Highly conductive and stretchable polymer composites based on graphene/MWCNT network.” Chemical Communications. 49 : 1612–4 (2013).

123. Zhang L, Fan W, Liu T. “A flexible free-standing defect-rich MoS2 /graphene/carbon nanotube hybrid paper as a binder-free anode for high-performance lithium ion batteries.” RSC Adv. Royal Society of Chemistry; 5 : 43130–40 (2015).

124. Wen J, Wilkes GL. “Organic/inorganic hybrid network materials by the sol–gel approach.” Chem. Mater. 8 : 1667–81 (1996).

125. Duan Y, Jana SC, Reinsel AM, Lama B, Espe MP. “Surface modification and reinforcement of silica aerogels using polyhedral oligomeric silsesquioxanes.” Langmuir. 28 : 15362–71 (2012).

126. Barczak M, Borowski P, Dabrowski A. “Structure-adsorption properties of ethylene-bridged polysilsesquioxanes and polysiloxanes functionalized with different groups.” Colloids and Surfaces A: Physicochemical and Engineering Aspects. 347 : 114–20 (2009).

127. Zhong L, Chen X, Song H, Guo K, Hu Z. “Highly flexible silica aerogels derived from methyltriethoxysilane and polydimethylsiloxane.” New J. Chem. Royal Society of Chemistry; 39 : 7832–8 (2015).

128. Jukarainen H, Clarson S, Seppala J, Oy L. “Surface and phase studies of multi block PDMS.B-PEO copolymers.” American Chemical Society. Ohio, USA, Turku, Finland & TKK, Finland: Univ. of Cincinnati & Helsinki Uni of Technical; 729 : 353–7 (2000).

129. Stevens MP. “Polymer Chemistry (An Introduction).” 3rd ed. New York: Oxford University Press; (1999).

130. Larsen AL, Hansen K, Sommer-Larsen P, Hassager O, Bach A, Ndoni S, et al. “Elastic Properties of Nonstoichiometric Reacted PDMS Networks.” Macromolecules. 36 : 10063–70 (2003).

131. Frankær SMG, Jensen MK, Bejenariu AG, Skov AL. “Investigation of the properties of fully reacted unstoichiometric polydimethylsiloxane networks and their extracted network fractions.” Rheologica Acta. 51 : 559–67 (2012).

132. Brook MA, Saier HU, Schnabel J, Town K, Maloney M. “Pretreatment of liquid silicone rubbers to remove volatile siloxanes.” Industrial and Engineering Chemistry Research. 46 : 8796–805 (2007).

133. Zakaria S, Madsen FB, Skov AL. “Post-curing as an effective means of ensuring the long-term reliability of PDMS thin films for dielectric elastomer applications.” Polymer-plastics Technology and Engineering. : DOI: 10.1080/03602559.2016.1211689 (2016).

Abbreviations and symbols

A	cross-sectional area of a strip
β	Weibull shape parameter
BPB	binary polymer blend
BCB	binary copolymer blend
d	thickness of elastomer
CE-(PDMS-PEG)	chain-extended PDMS-PEG copolymer
DE	dielectric elastomer
DEA	dielectric elastomer actuator
ε'	storage permittivity/dielectric permittivity
ε''	dielectric loss/loss permittivity
ε_r	relative permittivity
ε_0	vacuum permittivity
ϵ_H	Hencky strain
ϵ_E	engineering strain
ϵ_U	ultimate strain
EMI	electromechanical instability
E_{BD}	electrical breakdown strength
E_n	normalised electrical breakdown strength
f	functionality
F	Weibull cumulative distribution function
F_{OM}	figure of merit
G'	storage modulus
G''	loss modulus
IN	ionic network
LVE	linear viscoelasticity
l_0	initial length before deformation
l_i ; i=x,y,z	length after deformation in x-, y-, and z-direction
λ_i	stretch ratio in particular direction
MWCNT	multi-walled carbon nanotube
NMP	*N*-methyl-2-pyrrolidone

NMR	nuclear magnetic resonance
ν	Poisson's ratio
M_n	number average molecular weight
M_w	weight average molecular weight
μ	dipole moment
η	Weibull scale parameter
PDI	polydispersity index
PDMS	polydimethylsiloxane
PEG	polyethyleneglycol
phr	part per hundred rubber
PPMS	polyphenylmethylsiloxane
Pt	platinum
R^2	coefficient of determination
r	stoichiometric ratio
r_H	Hencky rate
σ_E	engineering stress
σ_U	ultimate stress
s	actuation strain
SEC	size exclusion chromatography
SEM	scanning electron microscope
T	temperature
tan δ	loss tangent
TEM	transmission electron microscopy
τ	torque
t_s	step time
w	width
wt%	weight percent
X	theoretical number of repeating units in copolymer
Y	Young's modulus

List of figures

List of schemes

List of tables

Appendix I

A Razak AH, Szabo P, Skov AL (2015) 'Enhancement of dielectric permittivity by incorporating PDMS-PEG multiblock copolymers in silicone elastomers' RSC Adv. 5:53054–53062

RSC Advances

PAPER

Cite this: *RSC Adv.*, 2015, **5**, 53054

Enhancement of dielectric permittivity by incorporating PDMS-PEG multiblock copolymers in silicone elastomers†

Aliff Hisyam A. Razak,[ab] Peter Szabo[a] and Anne Ladegaard Skov*[a]

Received 23rd May 2015
Accepted 10th June 2015

DOI: 10.1039/c5ra09708h

www.rsc.org/advances

A silicone elastomer from PDMS-PEG multiblock copolymer has been prepared by use of silylation reactions for both copolymer preparation and crosslinking. The dielectric and mechanical properties of the silicone elastomers were carefully investigated, as well as the morphology of the elastomers was investigated by SEM. The developed silicone elastomers were too conductive to be utilized as dielectric elastomers but it was shown that when the above silicone elastomers were mixed with a commercial silicone elastomer, the resulting elastomer had very favourable properties for dielectric elastomers due to a significantly increased dielectric permittivity. The conductivity also remained low due to the resulting discontinuity in PEG within the silicone matrix.

Introduction

Dielectric elastomers (DEs) have been studied extensively with respect to finding both new and better elastomer candidates and novel applications.[1–4] DEs are elastomers which exhibit a change in size or shape when stimulated by an external electric field. They are also known as "compliant capacitors", with actuation occurring when electrostatic stress exceeds elastic stress.[5] Such properties have enabled DEs to play a significant role in applications as actuators, sensors and generators.

Dielectric elastomers with high relative permittivity possess high electrical energy in the form of charge separation, due to polarisation. In an unactuated state, the elastomer can withstand a given electrical field, the so-called electrical "breakdown strength",[6] but above this electrical field the DE will short-circuit. Another common failure associated with DEs is electromechanical instability (EMI), which arises during actuation when attractive forces between the two electrodes become dominant and locally exceed a certain threshold value that cannot be balanced by the material's resistance to compression.[7,8] This phenomenon, which is also known as "electromechanical breakdown", can usually be eliminated by prestretching the elastomer, since prestretching has a combined effect of hardening the silicone elastomer, decreasing film thickness and increasing electrical breakdown strength.[9,10]

Polydimethylsiloxanes (PDMS), as one promising type of dielectric elastomer, exhibit large ultimate extension.[11–14] Despite its significant deformation, the drawback of PDMS is that it has low permittivity, in relation to the net dipole moment (μ), of 0.6–0.9 D.[15] On the positive side, PDMS is known to have very low conductivity.[16] In contrast, polyethyleneglycols (PEG) show high permittivity as a result of a dipole moment of 3.91 D,[17] yet they are incapable of actuating, as they are highly conductive.[18] Combining PDMS and PEG as a block copolymer presents the possibility of substantially improving properties such as high permittivity and non-conductivity, whereby PEG enhances permittivity and PDMS facilitates actuation through its non-conductive nature and inherent softness. The synthesis of the PDMS-PEG multiblock copolymer utilised herein is based on hydrosilylation, as shown in Fig. 1.

An astonishing feature of block copolymers is the variety of morphologies due to self-assembly in bulk or in solution.[19,20] In principle, a diblock copolymer, which is the simplest block copolymer, assembles into different morphologies, such as sphere (S), cylinder (C), gyroid (G) and lamellar (L).[19,21] These morphologies can be achieved when two immiscible, covalently-bonded polymers microphase separately.[22] These morphologies can be changed by varying the volume fraction of one constituent in the diblock copolymer. For triblock copolymers, the morphologies are more complex, mainly due to the sequence order of three distinct polymers, *e.g.* ABC, ACB, BAC and BCA, which introduces further degrees of freedom and thus allows for the assembly of nearly 30 different morphologies.[19] The

[a]*Danish Polymer Center, Department of Chemical and Biochemical Engineering, Technical University of Denmark, Building 229, 2800 Kgs. Lyngby, Denmark. E-mail: al@kt.dtu.dk*

[b]*Department of Chemical Engineering Technology, Faculty of Engineering Technology, University of Tun Hussein Onn Malaysia, 86400 Parit Raja, Batu Pahat, Johor, Malaysia*

† Electronic supplementary information (ESI) available: ^{1}H-NMR spectra and contact angles of the synthesised PDMS-PEG multiblock copolymers (PDMS81-PEG, PDMS14-PEG, PDMS7-PEG and PDMS3-PEG). Results of dielectric and rheology for binary polymer blends by incorporating PDMS-PEG multiblock copolymers at different wt% (5, 10, 15 and 20) into a PDMS network (MJK). See DOI: 10.1039/c5ra09708h

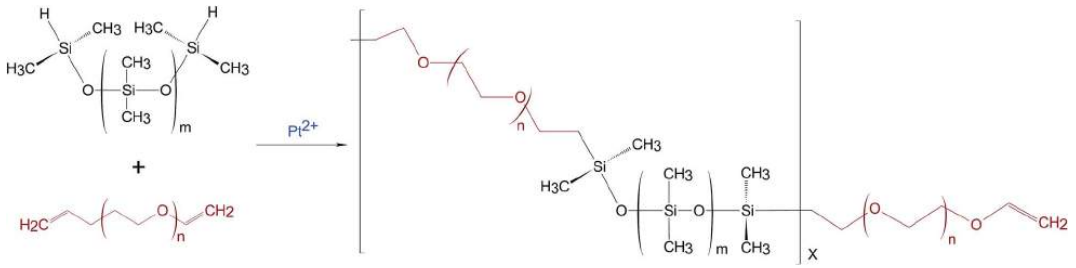

Fig. 1 The hydrosilylation reaction utilized when preparing a PDMS-PEG multiblock copolymer, where m is the number of repeating dimethylsiloxane units in PDMS, and $n = 4$ is the constant number of repeating ethyleneglycol units in PEG. X is the number of repeating PDMS-PEG units in multiblock copolymers.

similarity shared by the block copolymers is that they have four common equilibrium morphologies (S, C, G and L).[21]

Here, elastomers are prepared by means of phase separating PDMS-PEG multiblock copolymers, whereby the copolymers' blocks are expected to segregate to form well-defined structures, depending on the chain lengths of the two constituents. Subsequently the phase-separated copolymers are cross-linked *via* silylation into elastomers.

Experimental

Materials and reagents

Hydride-terminated polydimethylsiloxanes (H-PDMS) used in the synthesis of the PDMS-PEG multiblock copolymer were DMS-H21, DMS-H11, DMS-H03 and SIH6117.0, each with an average molecular weight (M_n) of 6000, 1050, 550 and 208 g mol^{-1}, respectively. They were purchased from Gelest Inc., while polyethyleneglycol divinyl ether (PEG-DE) was acquired from Sigma Aldrich. A commercial PDMS elastomer [MJK 4/13] was obtained from Wacker Chemie AG, and platinum-divinyltetramethyl disiloxane complex [SIP6830.3] was purchased from Gelest Inc. and contained 3.25% of platinum in xylene. A hydride-terminated methyl-hydrosiloxane-dimethylsiloxane copolymer [HMS-501] (M_n of 1050 g mol^{-1}, 9-functional) cross-linker, along with tetravinyltetramethyl-cyclotetrasiloxane [SIT-7900] as an inhibitor, was purchased from Gelest Inc. Both methanol and toluene were purchased from Sigma Aldrich.

Synthesis of the PDMS-PEG prepolymer

The procedure used to synthesise PDMS-PEG multiblock copolymer was amended from that employed by Klasner *et al.*[23] and Jukarainen *et al.*[24] All glassware was thoroughly cleaned and dried at a temperature of 200 °C. The characterisations on M_n of DMS-H21, DMS-H11, DMS-H03, SIH6117.0 and PEG-DE were performed using ^{1}H-NMR to obtain precise M_n for the stoichiometry calculations.

The theoretical PDMS-PEG repeating units in the multiblock copolymer were calculated from a target molecular weight of 30 kg mol^{-1}, whereby the number of blocks for PDMS and PEG were X and $(X + 1)$, respectively:

$$X = \frac{30\,000 - M_{n,PEG}}{M_{n,PDMS} + M_{n,PEG}} \quad (1)$$

where $M_{n,PDMS}$ and $M_{n,PEG}$ are the molecular weight of PDMS and PEG, respectively.

The stoichiometric ratio for preparing multiblock copolymers (r_1) was calculated as:

$$r_1 = \frac{[\text{vinyl}]}{[\text{hydride}]} = \frac{(X+1)f_{PEG\text{-}DE}}{Xf_{H\text{-}PDMS}} = \frac{X+1}{X} \quad (2)$$

where $f_{PEG\text{-}DE}$ and $f_{H\text{-}PDMS}$ are the functionality of PEG-DE and H-PDMS, respectively.[25] Both polymers in this case were difunctional ($f = 2$), and the telechelic vinyl groups of the resulting copolymer were targeted.

Dry toluene (prepared by molecular sieving) was added into the flask at 30 wt% of the total mass of H-PDMS and PEG-DE. The initial concentration of the platinum catalyst was 3120 parts per million (ppm). From this solution, the amount of catalyst solution was determined, in order to obtain a final concentration of 30 ppm in the reaction mixture, by assuming the density of the mixture was 1 g cm^{-3}. The reaction occurred at 60 °C with mild stirring and in the presence of nitrogen gas to eliminate air inside the flask. The duration of the hydrosilylation reaction depended on the chain length of H-PDMS and ranged from 2 to 6 hours. The disappearance of a Si–H bond signal at 4.70 ppm was checked by H-NMR, to ensure that all hydrides in the PDMS had been fully consumed during the reaction; refer to ESI for NMR spectra in Fig. S1a–d.† The final solution was viscous and appeared light bronze in colour. Any remaining solvent (toluene) was removed with a rotary evaporator for a couple of hours. The product was purified by cold methanol precipitation, in order to remove excess PEG-DE, and washing was repeated at least five times. Methanol from the precipitation process was excluded by using a rotary evaporator for a few hours and then placing the mixture in a vacuum for a day.

Experimental setup for the PDMS-PEG block copolymer

To distinguish the PDMS-PEG multiblock copolymer samples from different PDMS volume fractions, they were named based on four different repeating unit numbers in the constituent

Table 1 Sample details for PDMS-PEG multiblock copolymers[a]

PDMS-PEG block copolymer	Number average molecular weight of H-PDMS ($M_{n,PDMS}$) [g mol^{-1}]	Number of repeating units in PDMS (m)	Theoretical number of repeating units in (PDMS-PEG)$_X$ (X)	Stoichiometric ratio (r_1)	Volume fraction of PDMS (f_A)
PDMS81-PEG	6000.00	81	5	1.21	0.94
PDMS14-PEG	1050.00	14	23	1.04	0.75
PDMS7-PEG	550.00	7	37	1.03	0.62
PDMS3-PEG	208.00	3	56	1.02	0.45

[a] Note: M_n of PEG in PDMS-PEG block copolymer is 250 g mol^{-1}.

polymer, as listed in Table 1. Asymmetrical morphologies in the PDMS-PEG multiblock copolymer were obtained by varying PDMS chain lengths (m = 3, 7, 14, 81) while sustaining the equivalent PEG chain length (n = 4), which in turn produced PDMS3-PEG, PDMS7-PEG, PDMS14-PEG and PDMS81-PEG, respectively. Hence PDMS81-PEG constituted the highest volume fraction of PDMS in the block copolymer (0.94), whereas the lowest volume fraction produced in this study was 0.45 (belonging to PDMS3-PEG).

Binary polymer blends (BPBs)

PDMS-PEG multiblock copolymers were incorporated into PDMS elastomer (MJK) at 5, 10, 15 and 20 wt%. All mixtures were speedmixed at 3500 rpm for 2 minutes. After that, the blends were immediately cross-linked. The blends produced 16 samples in total.

Cross-linking

Four samples of PDMS-PEG multiblock copolymers and 16 samples of BPB were prepared. The stoichiometric ratio for the cross-linking (r_2) was calculated as:

$$r_2 = \frac{[\text{hydride}]}{[\text{vinyl}]} = \frac{f_{\text{HMS}}[\text{HMS}]}{f_{\text{BCP}}[\text{BCP}]} \quad (3)$$

where f_{HMS} and f_{BCP} were the numbers of the HMS-501 (9-functional) functional group and the PDMS-PEG block copolymer (2-functional), respectively, while […] indicates the initial concentration.[26,27]

The values of r_2 were calculated based on the mass of PDMS-PEG prepolymers added into the blends. The inhibitor (SIT7900) and the platinum catalyst were added to the blends at 1 wt% and 30 ppm, respectively. Those blends which consisted of PDMS-PEG prepolymer, namely MJK4/13, SIT7900 and 30 ppm platinum catalyst, were speed-mixed rigorously at 3000 rpm for 2 minutes. Cross-linker (HMS-501) was added, and the resulting mixture was additionally speed-mixed at 1500 rpm for 2 minutes. The cross-linked films were cured at a temperature of 60 °C overnight and then subsequently post-cured at 110 °C for 2 hours.

Characterisations

The NMR equipment utilised in this instance was the Bruker 300 MHz NMR. The number of scannings per sample was 128. The sample was prepared by diluting 50 mg of the sample in 0.5 mL of deuterated chloroform ($CDCl_3$).

Static contact angles, created by using the "sessile drop-needle in" method, were taken at a room temperature of 23 °C using Dataphysics OCA20. The contact angle was measured by dropping 6 μL of deionised water onto the PDMS-PEG multiblock copolymer and BPB films. Measurements for each contact angle were taken for 65 seconds, and the contact angles were analysed every 5 seconds, in order to obtain contact angle *versus* time profiles.

Linear viscoelasticity (LVE) properties, *i.e.* storage and loss moduli, were characterised at room temperature using TA Instruments' ARES-G2. The geometry of the parallel plate was 25 mm. The axial force, strain and frequency ranges were 5 N, 2% and 100–0.01 Hz, respectively. The Young's modulus can be determined as $Y = 2(1 + \nu)G = 3G$, since Poisson's ratio (ν) is close to 0.5, due to the incompressibility of silicones.

Dielectric permittivity, loss permittivity and conductivity were measured at a frequency of 10^6 to 10^{-1} using a broadband dielectric spectrometer from Novocontrol Technologies GmbH & Co. KG, Germany. The electrode diameter was 20 mm.

The breakdown tests were carried out on an in-house-built device based on international standards (IEC 60243-1 (1998) and IEC 60243-2 (2001)).[28] Samples with a film thickness less than 100 μm were used, as breakdown strength depends greatly on sample thickness.[10] The film was slid between the two spherical electrodes (radius of 20 mm), and breakdown was measured at the point of contact, with a stepwise increasing voltage applied (50 to 100 V per step) at a rate of 0.5–1 steps per s.[29] Each sample was measured up to 12 times, and the average of these values was then taken as the breakdown strength.

The SEM model, FEI Inspect S, used to characterise nanoscale images, performed energy-dispersive X-ray and wavelength dispersive measurements. The accelerating voltage and resolution were 200 V to 30 kV and 50 nm at 30 kV, respectively, while the imaging modes used high and low vacuums.

The number average molecular weight (M_n) determinations for PDMS-PEG multiblock copolymers were performed on an SEC instrument consisting of a Viscotek GPCmax VE-2001 instrument equipped with a Viscotek TriSEC Model 302 triple detector using two PLgel mixed-D columns from Polymer Laboratories. Samples were run in tetrahydrofuran (THF) at 30 °C and at a rate of 1 mL min^{-1}. Molar mass characteristics were calculated using polydimethylsiloxane standards.

Results and discussion

PDMS-PEG multiblock copolymer

The PDMS-PEG block copolymer samples with different PDMS chain-lengths were characterised by means of size-exclusion chromatography (SEC), while the cross-linked samples were analysed by means of dielectric spectroscopy and rheology. Results for the average number of molecular weights obtained from SEC, shown in Table 2, indicate that synthesised PDMS-PEG multiblock copolymers possess lower M_n than targeted.

The relative permittivity of the multiblock copolymers is shown in Fig. 2. Relative permittivity for the copolymer with the least PEG (PDMS81-PEG) is constant at all frequencies, with a slight increase at low frequencies. This behaviour is similar to that of the reference elastomer (MJK), but the PDMS81-PEG multiblock copolymer has three-fold higher relative permittivity. For samples with higher PEG content, significant relaxation takes place at low frequencies, leading to increased permittivity (as seen in Fig. 3), while dielectric loss also increases very abruptly when decreasing the frequency. This behaviour indicates conductive nature of the elastomers. In Fig. 4 the conductivity of the copolymers is shown. It is obvious that they are all conductive, due to the display of a plateau in conductivity at low frequencies. The block copolymers have conductivities of the order of 10^2 to 10^5 higher than those of the reference elastomer (MJK).

Table 2 Average number of multiblock copolymers molecular weights

PDMS-PEG block copolymer	Experimental $M_{n,T}$ (10^3 g mol^{-1})
PDMS81-PEG	13
PDMS14-PEG	2.5
PDMS7-PEG	3.6
PDMS3-PEG	1.2

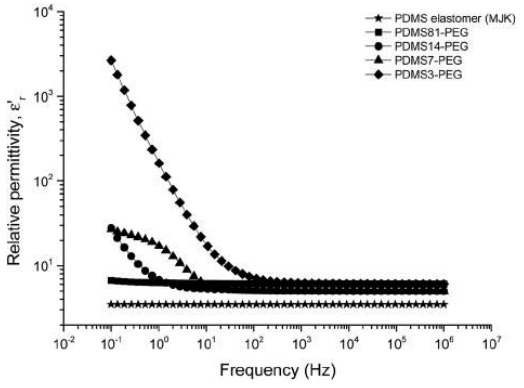

Fig. 2 Relative permittivity of cross-linked PDMS-PEG multiblock copolymers at 23 °C.

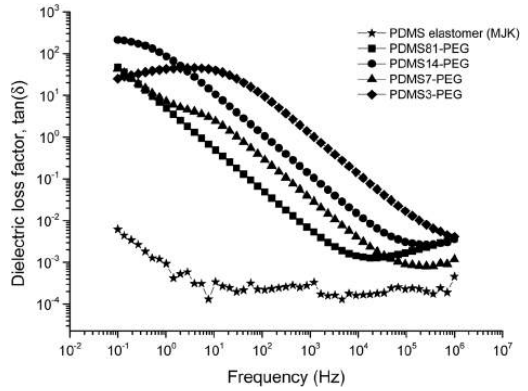

Fig. 3 Dielectric loss factor for cross-linked PDMS-PEG multiblock copolymers at 23 °C.

The rheological properties of the cross-linked copolymers are shown in Fig. 5. The PDMS14-PEG and PDMS81-PEG samples show the behaviour of very soft networks with low storage moduli compared to silicone elastomers, and they also demonstrate significant relaxation at low frequencies, which further indicates the inherent softness. In contrast, the PDMS3-PEG and PDMS7-PEG samples possess PEG-like properties with high storage moduli and low losses. Furthermore, their shear modulus is higher than that of the reinforced commercial silicone elastomer. Therefore, it is clear that an increase of PEG constituents in a PDMS-PEG multiblock copolymer reinforces the network comparable with the effect of silica fillers. It is noteworthy that PDMS81-PEG and PDMS14-PEG closely resemble each other despite PDMS81-PEG being significantly shorter than PDMS14-PEG (see Table 2), and thus PDMS81-PEG should provide significantly higher cross-link density and thus higher G. However, this effect cannot be seen simply because the increased content of PEG in PDMS14-PEG has an identical cross-linking effect.

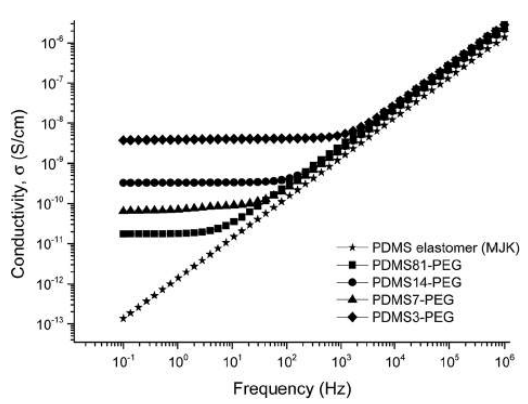

Fig. 4 Conductivity of PDMS-PEG multiblock copolymers at 23 °C.

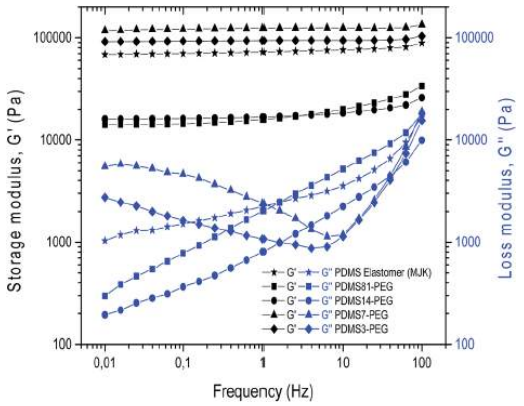

Fig. 5 Comparison between the storage and loss modulus PDMS-PEG multiblock copolymers at 23 °C.

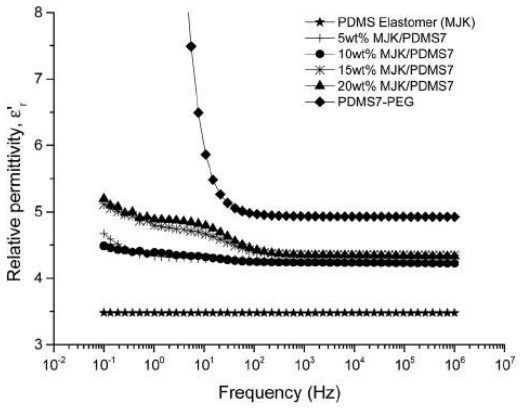

Fig. 7 The relative permittivity of MJK/PDMS7 (5–20 wt% of PDMS7-PEG) at 23 °C.

Binary polymer block copolymer and silicone elastomer blends

Due to the conductivity of PDMS-PEG multiblock copolymers, they were further blended and cross-linked into a commercial PDMS elastomer (MJK). Incorporating the block copolymers into a silicone network as a binary polymer blend (BPB) can facilitate the creation of PEG spheres, as illustrated in Fig. 6. The blends consist of PDMS-PEG multiblock copolymers at loadings of 5, 10, 15 and 20 wt% and are denoted as MJK/PDMS*i*, where $i = 81$, 14, 7, 3. When increasing PEG fractions, unfavourable and discontinuous morphologies may be formed.

Dielectric properties of the binary polymer blends

The relative dielectric permittivity and loss permittivity of the polymer blends are shown in Fig. 7 and 8. Relative permittivities are significantly improved compared to the reference elastomer (MJK), and loss permittivities are substantially lower than those of the pure copolymers – as hypothesised. Refer to ESI Fig. S2–4† for data for all samples.

In general, the storage permittivity of MJK/PDMS7 increases as the wt% of the PDMS7-PEG multiblock copolymer increases in line with loadings from 5 to 20 wt%. Incorporating 20 wt% of PDMS7-PEG in a PDMS network yields the highest relative permittivity (5.2), which is an increase of 60% compared to the relative permittivity of MJK (3.5). The small increase in relative permittivity at low frequencies for MJK/PDMS7, with 5 and 10 wt%, is due to electrode polarisation effects occurring during the measurement process. However, this can be corrected by applying silicone grease between the sample and the electrode.[30] The dynamic dipole orientation of polymer molecules resulting from polarisation are observed for MJK/PDMS7 at 15 and 20 wt%, as Debye-relaxation peaks occur at frequencies of 10^0 to 10^3 Hz.

One essential finding from the dielectric characterisation is that none of the polymer blends is conductive. To further analyse the optimum polymer blend, selection based on the sample which gives the lowest dielectric loss factor is carried out. Polymer blends of MJK/PDMS3, MJK/PDMS14 and

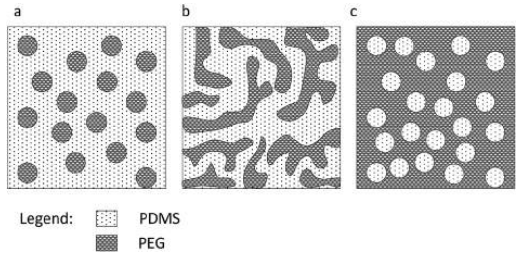

Fig. 6 Illustration of morphologies for BPB of PDMS-PEG block copolymer and silicone elastomer: (a) continuous phase in PDMS (b). Co-continuous phase in PDMS (c). Discontinuous phase in PDMS.

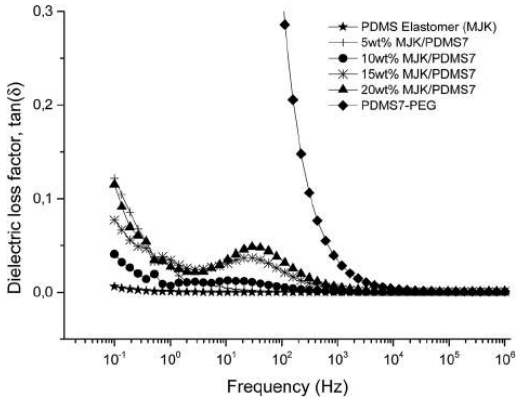

Fig. 8 The dielectric loss factor of MJK/PDMS7 (5–20 wt% of PDMS7-PEG) at 23 °C.

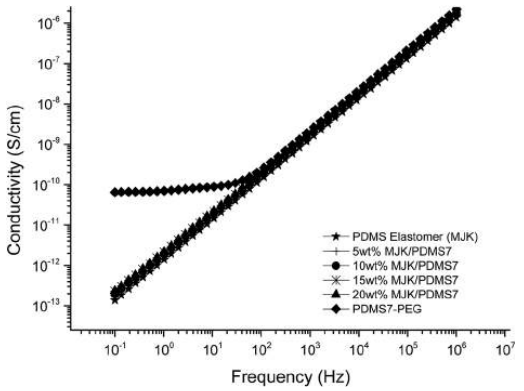

Fig. 9 The conductivity of MJK/PDMS7 (5–20 wt% of PDMS7-PEG) at 23 °C.

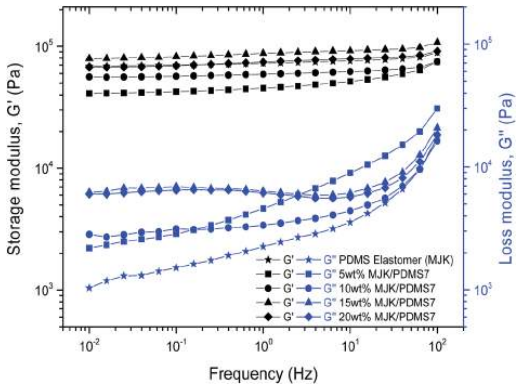

Fig. 10 The storage and loss moduli of MJK/PDMS7 (5–20 wt% of PDMS7-PEG) at 23 °C.

MJK/PDMS81 possess electrical loss factors in the ranges of 0.5–0.9, 0.25–0.75 and 0.06–1.25, respectively, in the investigated frequency regime. MJK/PDMS7 is the most promising blend, due to a low dielectric loss factor of 0.05–0.125 (Fig. 8).

The behaviour of MJK/PDMS7 non-conductivity with different copolymer loadings is very promising, since no plateau regions are observed at low frequencies (Fig. 9). This implies that a blending method applied properly causes the successful formation of a discontinuous phase for PEG that creates non-conductive behaviour of the developed polymer in the PDMS elastomer and PDMS7-PEG blends at loadings of 5, 10, 15 and 20 wt%. The conductivity of MJK/PDMS7 is consistent with respect to the MJK elastomer, which is non-conductive, as shown in Fig. 9.

The low dielectric loss factor and non-conductivity of MJK/PDMS7 for all investigated copolymer loadings indicates that the composites consist of PEG in discontinuous phases.

Rheological properties of BPB

To evaluate the effect of blending on mechanical properties, elastomers from MJK/PDMS7 with a 5–20 wt% copolymer were rheologically characterised, as shown in Fig. 10. The storage modulus of MJK/PDMS7 with 20 wt% is relatively close to the storage modulus of silicone elastomer (MJK). In contrast, MJK/PDMS7 with 5 and 10 wt% is softer than the PDMS elastomer, with storage moduli being one-fold and three-fold lower than the storage modulus of MJK (7×10^5 Pa). The blend of MJK/PDMS7 with 15 wt% is the stiffest, with $G' = 8 \times 10^5$ Pa. Another important feature observed from Fig. 10 is the appearance of small relaxation peaks in the loss moduli for 15 and 20 wt%. This is due to the transient nature of the PEG semi-crystalline phases acting as reinforcing domains.

All elastomers, however, do show to be well cross-linked and appear very elastic, and therefore they are suitable as soft dielectric elastomers.

Dielectric breakdown (E_{BD}) strength

Electrical breakdown and the influence of different PDMS7-PEG block copolymer loadings in MJK/PDMS7 on the Weibull parameters were investigated. The Weibull fits can be seen in Fig. 11. The Weibull β-parameter (slope of the dashed line in Fig. 11) decreases in line with an increasing MJK/PDMS7 wt%, and it even increases at 20 wt%. The y-axis (Fig. 11) was determined from the formula below:

$$\ln[-\ln(1 - F)] = \beta \ln(E_{BD}) - \beta \ln(\eta) \quad (4)$$

where F and E_{BD} were the Weibull cumulative distribution function and electrical breakdown, respectively. The value of the Weibull location parameter η was determined from $\ln[-\ln(1 - F)] = 63.2$.

Averaged and fitted electrical breakdown data for all the samples are presented in Table 3. MJK/PDMS7 with 5 wt% bears

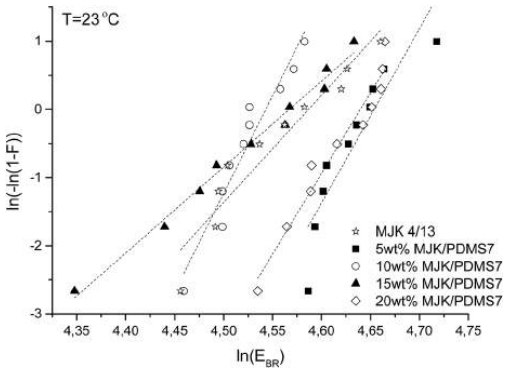

Fig. 11 Cumulative probability of failure of the PDMS elastomer (MJK) and MJK/PDMS7 with 5–20 wt% of the PDMS7-PEG multiblock copolymer ($T = 23$ °C). The dashed lines represent the linear fit line to the data.

Table 3 Dielectric breakdown strength, Weibull parameters η and β, and R^2 *of linear fit* for the pure silicone elastomer (MJK) and MJK/PDMS7 with 5–20 wt% of the PDMS7-PEG multiblock copolymer

MJK/PDMS7	Dielectric breakdown E_{BD} (V μm^{-1})	Weibull η-parameter	Weibull β-parameter	R^2 *of linear fit*
MJK	93 ± 7	98	17	0.92
5 wt%	103 ± 4	105	31	0.84
10 wt%	92 ± 3	94	31	0.93
15 wt%	93 ± 8	96	13	0.99
20 wt%	101 ± 5	103	25	0.95

the highest dielectric breakdown strength (103 V μm^{-1}) with a standard deviation of ±4 V μm^{-1} when averaging over the 12 samples. All samples have an almost identical Weibull η parameter and respective breakdown strengths.

Adding conductive particles usually destabilises the elastomer in respect to electrical breakdown,[31] but in the composites investigated herein the conductive PEG clearly stabilises the elastomers, as the β parameters for the composites are significantly larger – and thus the materials will be more electrically stable. This may be due to the charge-trapping effects of PEG.[10] The trapping effect probably decreases in line with increased loadings, and thus there is an optimum in the composition at which the electrical stabilisation is highest. The softest sample (5 wt%) is furthermore very steep, and therefore the effect cannot be attributed to increased Young's moduli, as shown in Vudayagiri *et al.*[28]

Figure of merit (F_{OM})

One method which can be used to evaluate the actuation performance of the elastomer is by means of a figure of merit for dielectric elastomer actuators, F_{OM}(DEA), derived by Sommer-Larsen and Larsen:[32]

$$F_{OM}(\mathrm{DEA}) = \frac{3\varepsilon_r\varepsilon_0 {E_{BD}}^2}{Y} \quad (5)$$

where E_{BD} is electrical breakdown, ε_0 is vacuum permittivity (8.85×10^{-12} F m^{-1}), ε_r is relative permittivity and Y is the Young's modulus.

The F_{OM}(DEA) for the MJK/PDMS7 samples was determined relative to the absolute value of the F_{OM}(DEA) of Elastosil RT625 (1.86×10^{-24}%), as reported by Vudayagiri *et al.*[28] The normalised F_{OM}(DEA) was calculated as:

$$F_{OM}(\mathrm{DEA})_{\mathrm{Norm.}} = \frac{F_{OM}(\mathrm{DEA})_{\mathrm{Elastomer}}}{F_{OM}(\mathrm{DEA})_{\mathrm{RT625}}} \quad (6)$$

The calculated figures of merit are shown in Table 4. The composite with 5 wt% has the highest normalised F_{OM}(DEA) value at 17, *i.e.* 17 times greater actuation than the reference elastomer. This composition is the best-performing elastomer amongst those investigated, due to the combination of high electrical breakdown strength, a low Young's modulus and relatively high dielectric permittivity.

Contact angles of BPB

The wettability of MJK/PDMS7 polymer blends was evaluated by static contact angle measurements. The nature of the PDMS-PEG multiblock copolymer is known as one of the amphiphilic dynamic polymer chains. Similar to MJK/PDMS7, which consists of PDMS7-PEG block copolymers in the PDMS matrix, the trend on wettability leans toward amphiphilic behaviour. In Fig. 12, the contact angles of MJK/PDMS7 for different wt% (5, 10, 15 and 20) decline steeply for the first 20 s and are followed by a slight decrease until they are almost stable at the end of the time period. This indicates that the block copolymer in the polymer blends orients its polymer chains in order to achieve the lowest possible surface energy, since the copolymer comprises blocks of both hydrophobic PDMS and hydrophilic PEG. When the developed elastomer is exposed to air, the surface is controlled by the hydrophobic PDMS from the block copolymer and the matrix, but upon contact with water the chains re-orient and the PDMS blocks migrate back into the

Table 4 Normalised F_{OM}(DEA) and Young's modulus (Y) for MJK/PDMS7 with 5–20 wt% of PDMS7-PEG multiblock copolymer

MJK/PDMS7	Young's modulus, Y^a (kPa)	Normalised F_{OM}(DEA)
0 wt% (MJK)	205	6.1
5 wt%	123	17.2
10 wt%	169	9.6
15 wt%	238	8.0
20 wt%	203	11.2

[a] Young's modulus calculated from $Y = 3G'$.

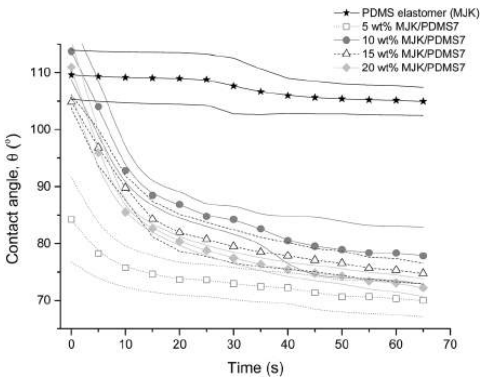

Fig. 12 MJK/PDMS7 contact angles (5–20 wt% of PDMS7-PEG) at 23 °C.

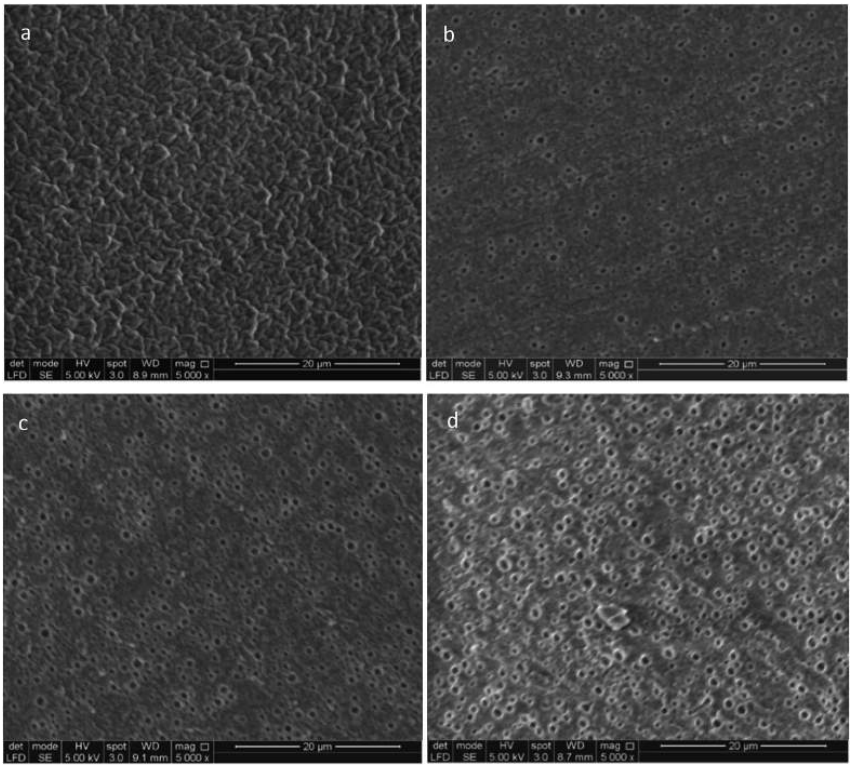

Fig. 13 SEM images of MJK/PDMS7 at: (a) 5 wt% (b). 10 wt% (c). 15 wt% (d). 20 wt%.

bulk material and are replaced by the more hydrophilic PEG blocks at the surface.[23] This behaviour is confirmed by the contact angle measurement, where the rearrangement of the polymer chains accounts for the change in contact angle over time when a droplet of deionised water is dropped onto the top surface of the sample. Thus, classing the wettability of MJK/PDMS7 as amphiphilic is the result of incorporating the PDMS7-PEG multiblock copolymer in the network, since PEGs are well-known for their hydrophilic properties.

SEM analysis

In order to verify the hypothesised structure of the composites, the prepared films were investigated by SEM; the microscope pictures are shown in Fig. 13. For MJK/PDMS7 with 5 wt% copolymer loading, a rough surface is obtained. There are no visible PEG domains observed, and the composite appears homogeneous on the microscale. When the loading of the block copolymer increases from 10 to 20 wt%, the microspherical domains become visible and the number of microspheres increases in line with an increased concentration of PEG. The domains were analysed using Image Processing and Analysis software (ImageJ). The domain sizes of visible spherical domains for MJK/PDMS7 at 10, 15 and 20 wt% are 1.3 ± 0.2 μm, 1.3 ± 0.2 μm and 1.6 ± 0.2 μm, respectively. The observation of spherical domains is coherent with the samples from Liu *et al.*,[33] who observed pores on composite samples of PDMS and PEG etched with ethanol.[33] The obtained morphologies indicate that the methodology of blending polymers creates the good dispersion of multiblock copolymers in a silicone network where the spherical domain size seems independent on concentration, as the chain length of the PEG was not a variable in this study. Since the composite with the lowest concentration of PEG possesses different morphology, and at the same time possesses the best overall properties for actuation and lifetime, it may be argued that the introduction of additional surfaces into the system is unfavourable, especially as these surfaces may increase permittivity but they also destabilise the elastomer.

Conclusion

A new composite elastomer, which has high relative and low permittivity, was successfully created from a binary system of polymer blends consisting of conducting PDMS7-PEG multiblock copolymer and non-conducting PDMS elastomer (MJK). The desired morphology (discontinuous phase of the block copolymer and continuous phase of PDMS) was successfully

created in the blends, thereby indicating the development of non-conductive behaviour in the elastomer. Low copolymer loading is favourable, since it creates a homogeneous elastomer on the micro-scale which in turn facilitates a more electrically stable elastomer. Even though the PDMS7-PEG multiblock copolymer is conductive and has high loss permittivity, a good composite elastomer can be developed by incorporating the block copolymer into a silicone network at different wt% and by employing a proper mixing technique. The dielectric breakdown strengths for cross-linked MJK/PDMS7 polymer blends were relatively high, with values in the order of 100 V μm^{-1}. Finally, by integrating all the characterised parameters, *i.e.* Young's modulus, breakdown strength and relative permittivity, figures of merit for the dielectric elastomer actuation of the various MJK/PDMS7s were determined, and it was concluded that by incorporating low concentrations of PEG, actuation could be improved 17-fold along with the extension to the lifetime of the dielectric elastomer.

Acknowledgements

The Malaysian Ministry of Education (MoE) and Universiti Tun Hussein Onn Malaysia (UTHM), as well as Innovationsfonden Danmark, are gratefully acknowledged for their funding.

Notes and references

1 S. Bauer, S. Bauer-Gogonea, I. Graz, M. Kaltenbrunner, C. Keplinger and R. Schwödiauer, *Adv. Mater.*, 2014, **26**, 149–162.
2 O. A. Araromi, I. Gavrilovich, J. Shintake, S. Rosset, M. Richard, V. Gass and H. R. Shea, *IEEE ASME Trans. Mechatron.*, 2014, **20**, 438–446.
3 I. A. Anderson, I. A. Ieropoulos, T. McKay, B. O'Brien and C. Melhuish, *IEEE ASME Trans. Mechatron.*, 2011, **16**, 107–111.
4 T. G. McKay, B. M. O'Brien, E. P. Calius and I. A. Anderson, *Appl. Phys. Lett.*, 2011, **98**, 1–3.
5 R. Pelrine, R. Kornbluh, J. Joseph, R. Heydt, Q. Pei and S. Chiba, *Mater. Sci. Eng., C*, 2000, **11**, 89–100.
6 J. L. Bigue, P. Chouinard, S. Proulx, G. Miron and J. S. Plante, *Cansmart Work*, 2014, 303–314.
7 X. Zhao and Z. Suo, *Appl. Phys. Lett.*, 2007, **91**, 24–27.
8 J. Plante and S. Dubowsky, *Proc. SPIE*, 2006, **6168**, 61681J.
9 R. Kornbluh, R. Pelrine, Q. Pei, R. Heydt, S. Stanford, S. Oh and J. Eckerle, *Proc. SPIE*, 2002, **4698**, 254–270.
10 S. Zakaria, P. H. F. Morshuis, M. Y. Benslimane, L. Yu and A. L. Skov, *Smart Mater. Struct.*, 2015, **24**, 1–10.
11 F. B. Madsen, A. E. Daugaard, C. Fleury, S. Hvilsted and A. L. Skov, *RSC Adv.*, 2014, **4**, 6939–6945.
12 P. Brochu and Q. Pei, *Macromol. Rapid Commun.*, 2010, **31**, 10–36.
13 F. B. Madsen, L. Yu, A. E. Daugaard, S. Hvilsted and A. L. Skov, *RSC Adv.*, 2015, **5**, 10254–10259.
14 B. Kussmaul, S. Risse, M. Wegener, M. Bluemke, J. Krause, J. Wagner, T. Feller, K. Clauberg, J. Hitzbleck, R. Gerhard and H. Krueger, *Proc. SPIE*, 2013, **8687**, 86872S.
15 J. N. Lee, C. Park and G. M. Whitesides, *Anal. Chem.*, 2003, **75**, 6544–6554.
16 Y. Poojari and S. J. Clarson, *J. Inorg. Organomet. Polym. Mater.*, 2009, **20**, 46–52.
17 R. J. Sengwa, K. Kaur and R. Chaudhary, *Polym. Int.*, 2000, **608**, 599–608.
18 W. Tiejun, Q. I. Yingqun, X. U. Jingkun, H. U. Xiujie and C. Ping, *Chin. Sci. Bull.*, 2003, **48**, 2444–2445.
19 Y. Mai and A. Eisenberg, *Chem. Soc. Rev.*, 2012, **41**, 5969–5985.
20 A. L. Larsen and E. M. Terentjev, *Macromolecules*, 2006, **39**, 9497–9507.
21 F. S. Bates and G. H. Fredrickson, *Phys. Today*, 1999, **52**, 32–38.
22 O. Gazit, R. Khalfin, Y. Cohen and R. Tannenbaum, *J. Phys. Chem. C*, 2009, **113**, 576–583.
23 S. A. Klasner, E. C. Metto, G. T. Roman and C. T. Culbertson, *Langmuir*, 2009, **25**, 10390–10396.
24 H. Jukarainen, S. Clarson, J. Seppala and L. Oy, *Am. Chem. Soc.*, 2000, **729**, 353–357.
25 M. P. Stevens, *Polymer Chemistry (An Introduction)*, Oxford University Press, New York, 3rd edn, 1999.
26 A. L. Larsen, K. Hansen, P. Sommer-Larsen, O. Hassager, A. Bach, S. Ndoni and M. Jørgensen, *Macromolecules*, 2003, **36**, 10063–10070.
27 S. M. G. Frankær, M. K. Jensen, A. G. Bejenariu and A. L. Skov, *Rheol. Acta*, 2012, **51**, 559–567.
28 S. Vudayagiri, S. Zakaria, L. Yu, S. S. Hassouneh, M. Benslimane and A. L. Skov, *Smart Mater. Struct.*, 2014, **23**, 1–15.
29 M. Y. Benslimane, H. Kiil and M. J. Tryson, *Polym. Int.*, 2010, **59**, 415–421.
30 P. Ben Ishai, M. S. Talary, A. Caduff, E. Levy and Y. Feldman, *Meas. Sci. Technol.*, 2013, **24**, 1–21.
31 K. Goswami, A. E. Daugaard and A. L. Skov, *RSC Adv.*, 2015, **5**, 12792–12799.
32 P. Sommer-Larsen and A. L. Larsen, *Proc. SPIE*, 2004, **5385**, 68–77.
33 H. Liu, L. Zhang, D. Yang, N. Ning, Y. Yu, L. Yao, B. Yan and M. Tian, *J. Phys. D: Appl. Phys.*, 2012, **45**, 1–9.

† Electronic Supplementary Information (ESI)

Enhancing relative permittivity by incorporating PDMS-PEG multi block copolymers in binary polymer blends

Aliff Hisyam A Razak,[a,b] Peter Szabo[a] and Anne Ladegaard Skov[a*]

[a] *Danish Polymer Center, Department of Chemical and Biochemical Engineering, Technical University of Denmark, Building 229, 2800 Kgs. Lyngby, Denmark. Email:al@kt.dtu.dk*
[b] *Department of Chemical Engineering Technology, Faculty of Engineering Technology, University of Tun Hussein Onn Malaysia, 86400 Parit Raja, Batu Pahat, Johor, Malaysia.*

Results

1. NMR spectra of multiblock copolymers

The NMR spectra for PDMS-PEG multiblock copolymers with different chain-length of PDMS are shown in figures (S1.a), (S1.b), (S1.c) and (S1.d).

a. PDMS81-PEG multiblock copolymer

^{1}H-NMR ($CDCl_3$, 300 MHz): δ 0.05 - δ 0.09 (m, 6 H's, -Si(C**H**$_3$)$_2$O-), δ 3.50 - δ 3.70 (m, 4 H's, -C$_2$**H**$_4$O-), δ 0.98 - δ 1.03 (t, 2 H's, -SiC**H**$_2$-), δ 3.53 - δ 3.57 (m, 2 H's, -CC**H**$_2$O-).

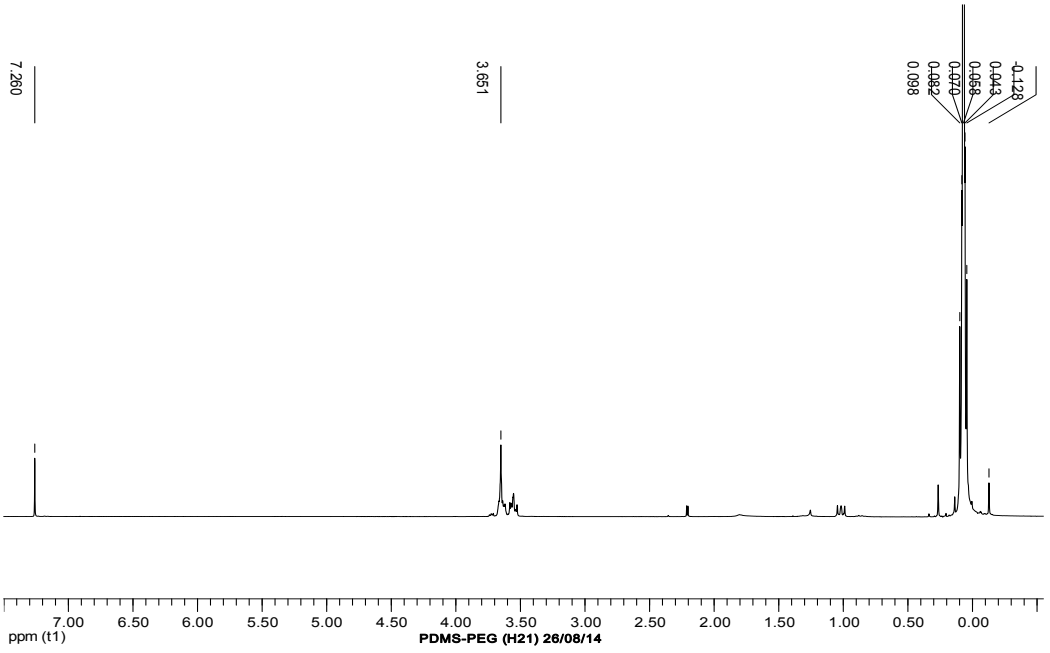

Fig. S1.a The NMR for PDMS81-PEG multiblock copolymer.

b. PDMS14-PEG multiblock copolymer

^{1}H-NMR ($CDCl_3$, 300 MHz): δ 0.05 - δ 0.09 (m, 6 H's, -Si(C**H$_3$**)$_2$O-), δ 3.50 - δ 3.70 (m, 4 H's, -C$_2$**H$_4$**O-), δ 0.98 - δ 1.03 (t, 2 H's, -SiC**H$_2$**-), δ 3.53 - δ 3.57 (m, 2 H's, -CC**H$_2$**O-)

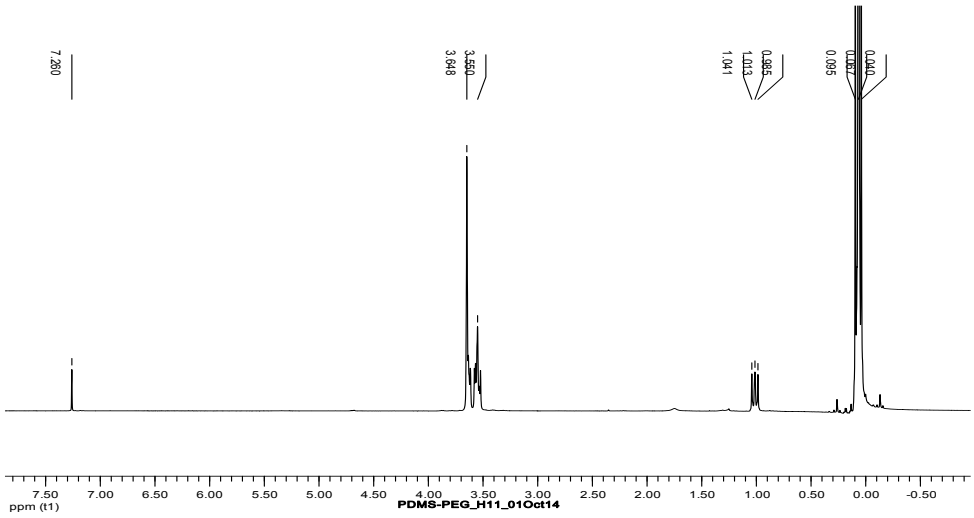

Fig. S1.b The NMR for PDMS14-PEG multiblock copolymer.

c. PDMS7-PEG multiblock copolymer

^{1}H-NMR ($CDCl_3$, 300 MHz): δ 0.05 - δ 0.09 (m, 6 H's, -Si(C**H$_3$**)$_2$O-), δ 3.50 - δ 3.70 (m, 4 H's, -C$_2$**H$_4$**O-), δ 0.98 - δ 1.03 (t, 2 H's, -SiC**H$_2$**-), δ 3.53 - δ 3.57 (m, 2 H's, -CC**H$_2$**O-).

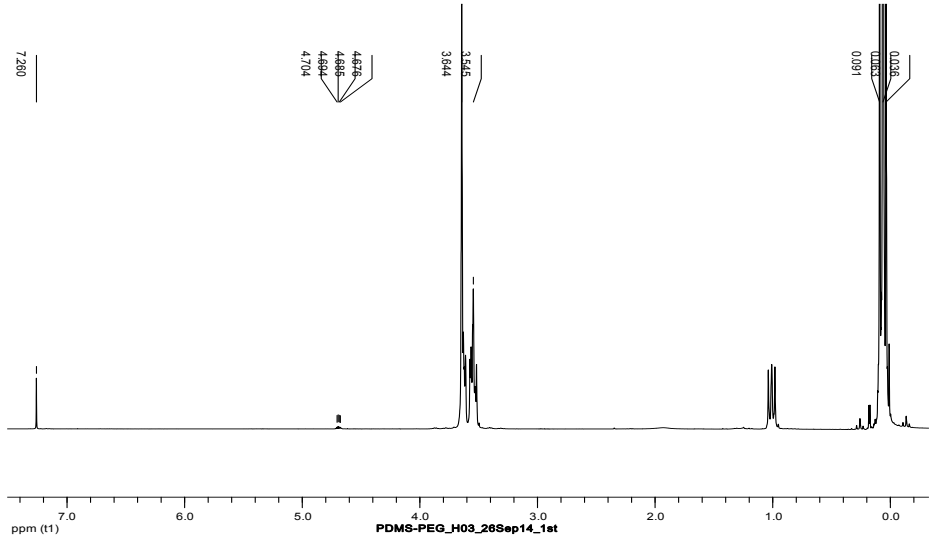

Fig. S1.c The NMR for PDMS7-PEG multiblock copolymer.

d. PDMS3-PEG multiblock copolymer

^{1}H-NMR ($CDCl_3$, 300 MHz): δ 0.05 - δ 0.09 (m, 6 H's, -Si(C**H$_3$**)$_2$O-), δ 3.50 - δ 3.70 (m, 4 H's, -C$_2$**H$_4$**O-), δ 0.98 - δ 1.03 (t, 2 H's, -SiC**H$_2$**-), δ 3.53 - δ 3.57 (m, 2 H's, -CC**H$_2$**O-)

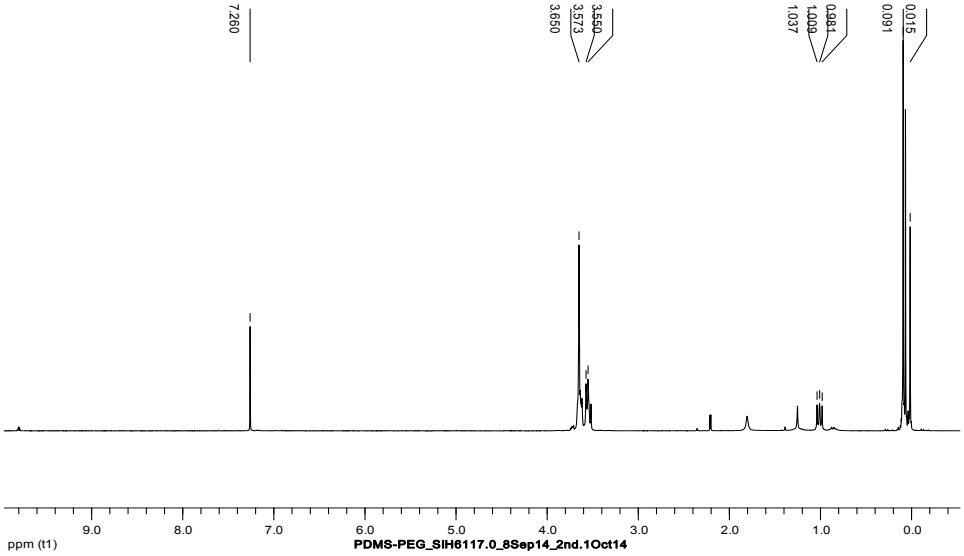

Fig. S1.d The NMR for PDMS3-PEG multiblock copolymer.

2. Data for binary blends (MJK/PDMS81)

The results of dielectric and mechanical properties are presented in figures (S2.a), (S2.b) & (S2.c) and (S2.d), respectively, for blends of MJK/PDMS81:

a. Dielectric permittivity of MJK/PDMS81

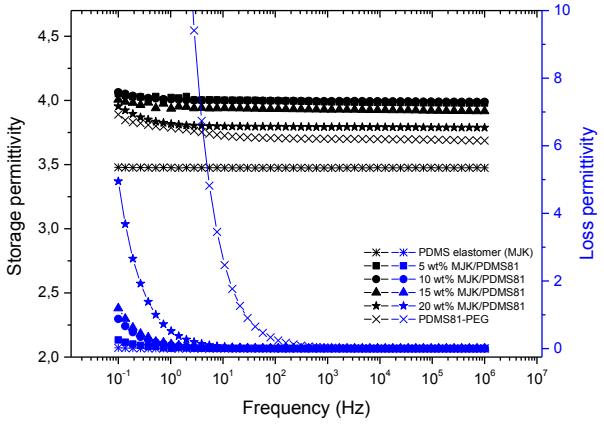

Fig. S2.a The relative storage and loss permittivity for MJK/PDMS81 (5 – 20 wt% of PDMS81-PEG) at 23 °C.

b. Conductivity of MJK/PDMS81

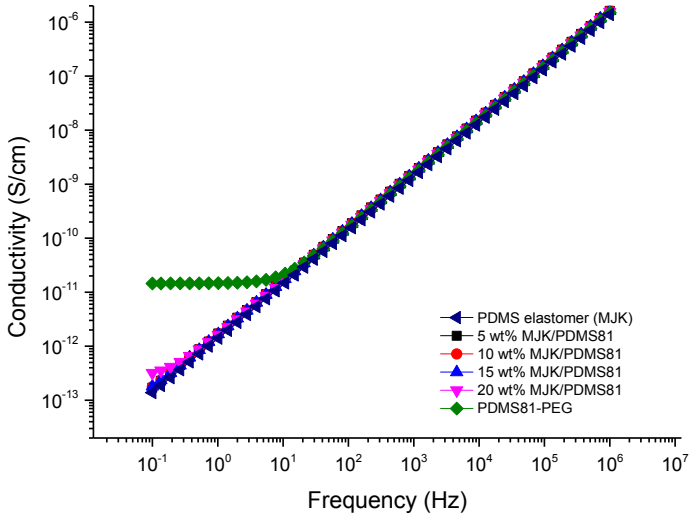

Fig. S2.b The conductivity of samples from MJK/PDMS81 (5 – 20 wt% of PDMS81-PEG) at 23 °C.

c. Dielectric loss factor of MJK/PDMS81

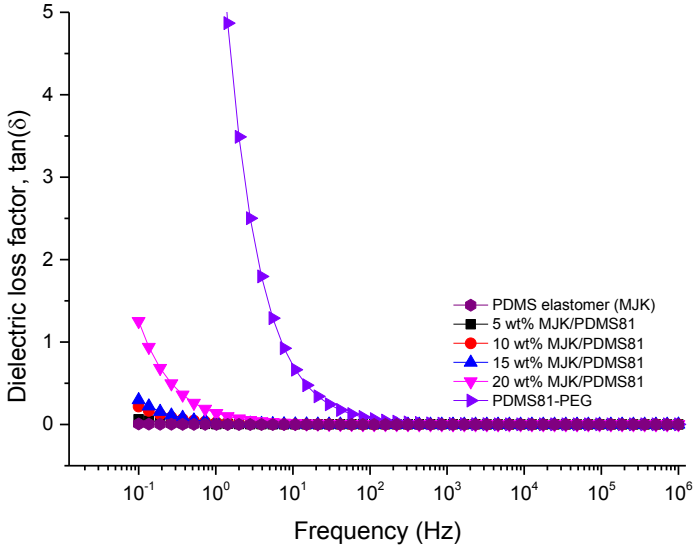

Fig. S2.c The dielectric loss factor for MJK/PDMS81 (5 – 20 wt% of PDMS81-PEG) at 23 °C.

d. Linear viscoelastic data of MJK/PDMS81

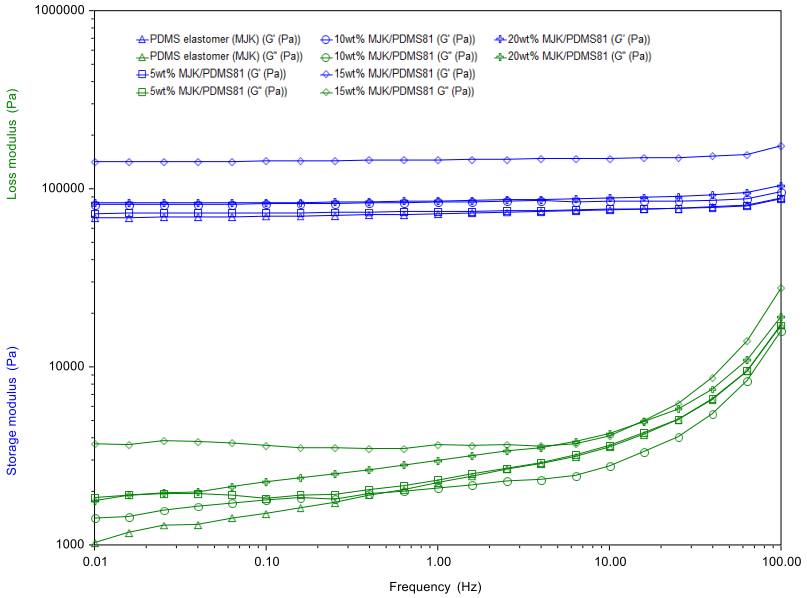

Fig. S2.d The storage and loss modulus for MJK/PDMS81 (5 – 20 wt% of PDMS81-PEG) at 23 °C.

3. Binary blends - MJK/PDMS14

The results of dielectric and mechanical properties are presented in figures (S3.a), (S3.b) & (S3.c) and (S3.d), respectively, for blends of MJK/PDMS14:

a. Dielectric permittivity of MJK/PDMS14

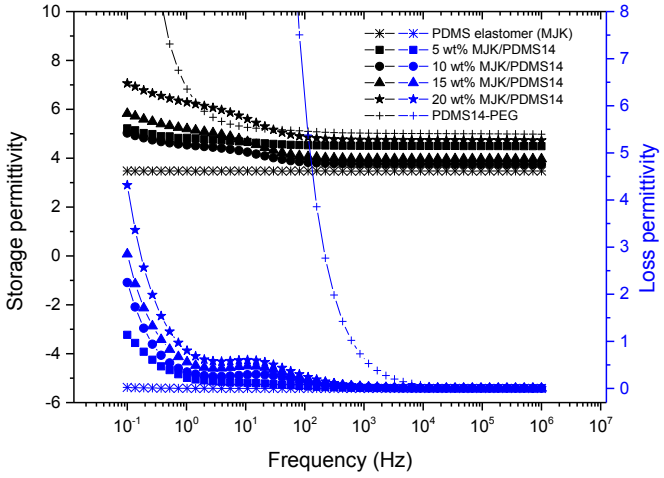

Fig. S3.a The relative storage and loss permittivity for MJK/PDMS14 (5 – 20 wt% of PDMS14-PEG) at 23 °C.

b. Conductivity of MJK/PDMS14

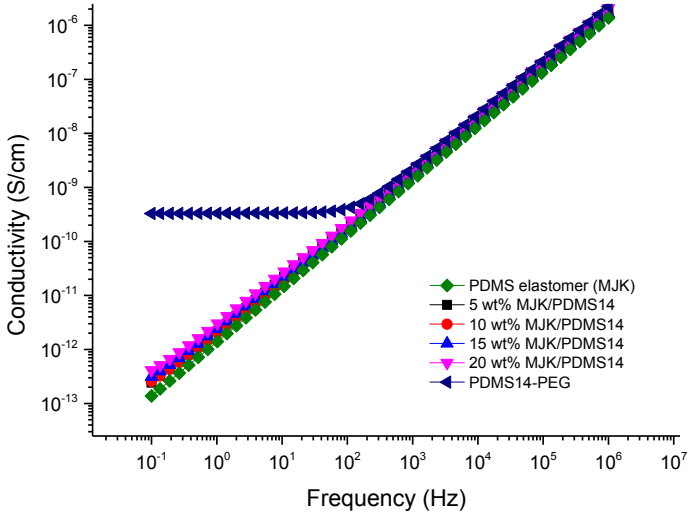

Fig. S3.b The conductivity for MJK/PDMS14 (5 – 20 wt% of PDMS14-PEG) at 23 °C.

c. Dielectric loss factor of MJK/PDMS14

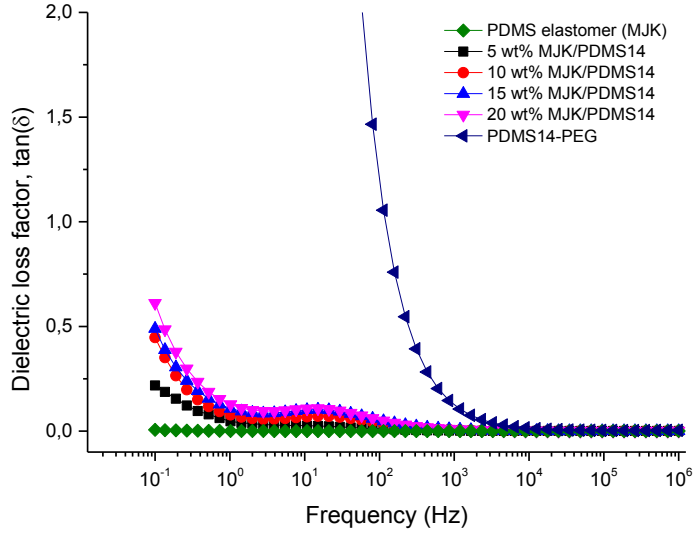

Fig. S3.c The dielectric loss factor for MJK/PDMS14 (5 – 20 wt% of PDMS14-PEG) at 23 °C.

d. Linear viscoelastic data of MJK/PDMS14

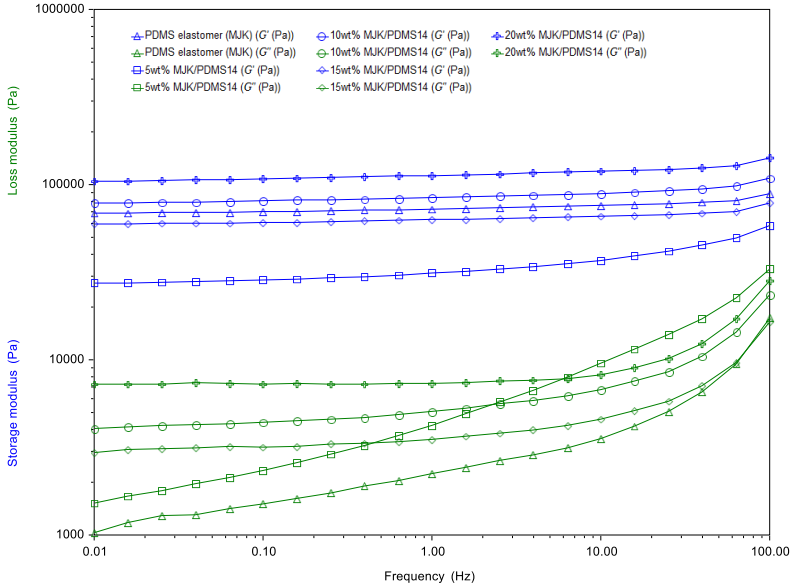

Fig. S3.d The storage and loss modulus for MJK/PDMS14 (5 – 20 wt% of PDMS14-PEG) at 23 °C.

4. Binary polymer blends - MJK/PDMS3

The dielectric and mechanical properties are presented in figures (S4.a), (S4.b) & (S4.c) and (S4.d), respectively, for blends of MJK/PDMS3:

a. Permittivity of MJK/PDMS3

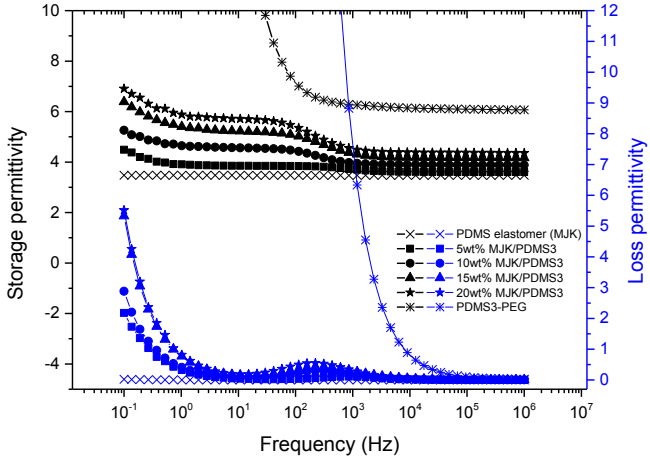

Fig. S4.a The relative storage and loss permittivity for MJK/PDMS3 (5 – 20 wt% of PDMS3-PEG) at 23 °C.

b. Conductivity of MJK/PDMS3

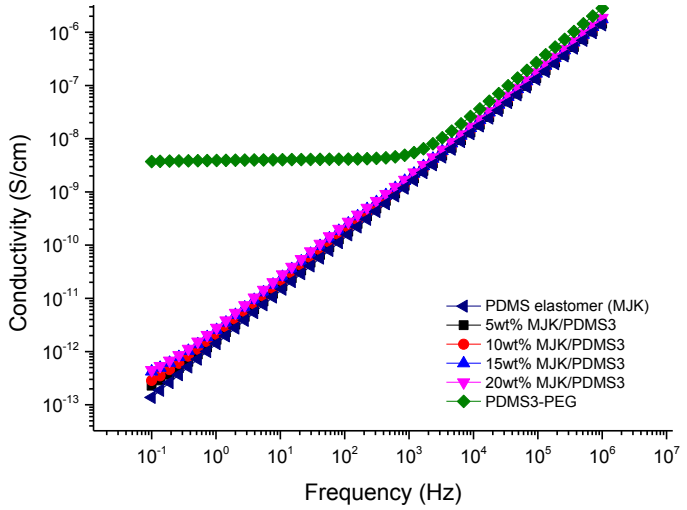

Fig. S4.b The conductivity for MJK/PDMS3 (5 – 20 wt% of PDMS3-PEG) at 23 °C.

c. Dielectric loss factor of MJK/PDMS3

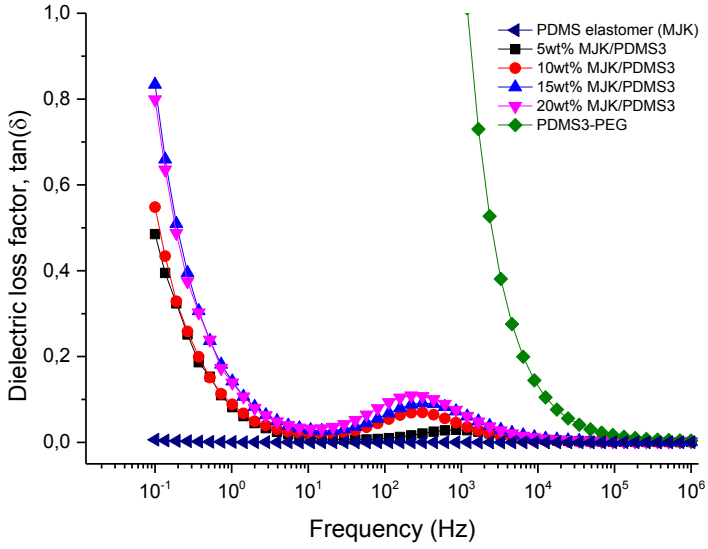

Fig. S4.c The dielectric loss factor for MJK/PDMS3 (5 – 20 wt% of PDMS3-PEG) at 23 °C.

d. Linear viscoelastic data of MJK/PDMS3

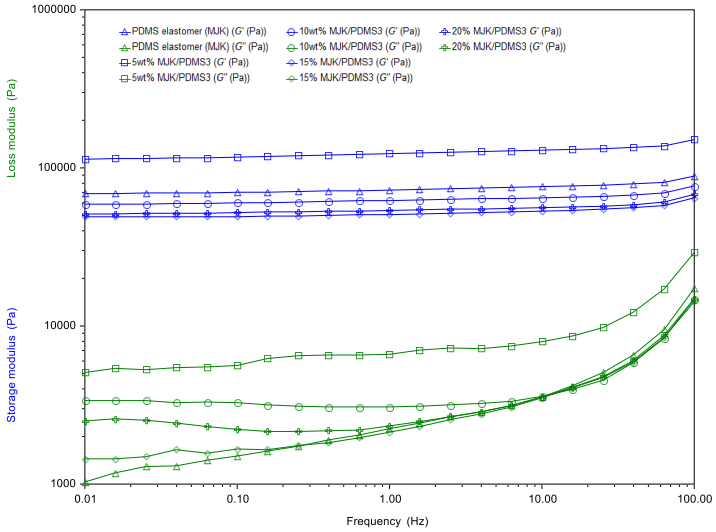

Fig. S4.d The storage and loss modulus for MJK/PDMS3 (5 – 20 wt% of PDMS3-PEG) at 23 °C.

5. Contact angles of PDMS-PEG multiblock copolymers

The coherence of hydrophobic behaviour between PDMS-PEG multi block copolymers and PDMS elastomer (MJK) with previously published data was investigated from the contact angle measurements. The block copolymer which comprises blocks of both hydrophobic PDMS and hydrophilic PEG, orients its polymer chains in such a fashion as to obtain the lowest possible surface energy.[1] The contact angle of MJK is coherent with the contact angle of e.g. another commercial PDMS (Sylgard 184)[1,2] and hence MJK act hydrophobically with a consistent contact angle of 105° throughout the period of measurement. On the other hand, the synthesized PDMS-PEG multiblock copolymers behave amphiphilic since the rearrangement of the polymer chains accounts for the change in contact angle over time. There is an obvious trend of decrement of contact angles from ~ 105° to below 95° with time for all the block copolymers and they behave similarly to previously published data[1,3]. The affinity towards hydrophobicity depends on the numbers of PEG in the PDMS-PEG block copolymer where greater numbers of PEG increase the tendency towards hydrophilic nature as expected. For instance, PDMS81-PEG is the most hydrophobic with a contact angle of 92° compared to the other block copolymers. The other multiblock copolymers have lower contact angle than PDMS81-PEG due to more PEGs in the block copolymers. PDMS3-PEG with 228 number of PEG chains possesses the lowest wettability (contact angle of nearly 65°).

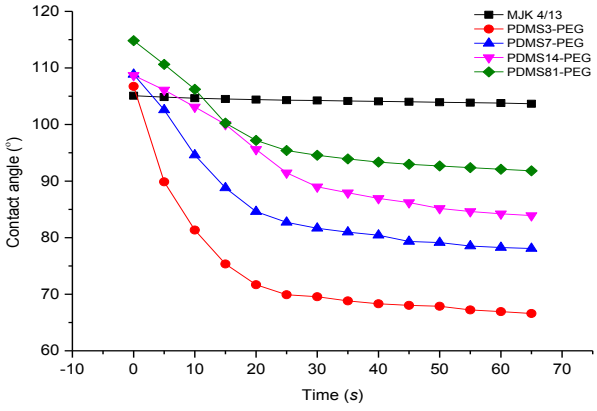

Fig. S5 The contact angles of PDMS-PEG multiblock copolymers and silicone elastomer (MJK 4/13) at 23 °C.

Appendix I

Reference

1. S. A. Klasner, E. C. Metto, G. T. Roman and C. T. Culbertson, *Langmuir*, 2009, **25**, 10390–10396.
2. J. A. Vickers, M. M. Caulum and C. S. Henry, *Anal. Chem.*, 2006, **78**, 7446–52.
3. H. Jukarainen, S. Clarson, J. Seppala and L. Oy, *Am. Chem. Soc.*, 2000, **729**, 353–357.

Appendix II

A Razak AH and Skov AL (2017) 'Silicone elastomers with covalentlty incorporated aromatic voltage stabilizers' RSC Adv. 7:468-477

RSC Advances

PAPER

Cite this: *RSC Adv.*, 2017, **7**, 468

Silicone elastomers with covalently incorporated aromatic voltage stabilisers†

A. H. A. Razak[ab] and A. L. Skov*[a]

Received 26th October 2016
Accepted 13th November 2016

DOI: 10.1039/c6ra25878f

www.rsc.org/advances

When optimising dielectric elastomers (DEs) a conflict exists, namely that for large achievable actuation strains softness is required, but with increased softness electrical breakdown strength decreases. Herein, soft dielectric silicone elastomers with increased electrical breakdown strength, due to the incorporation of an aromatic voltage stabiliser, were prepared by cross-linking synthesised polydimethylsiloxane–polyphenylmethylsiloxane (PDMS–PPMS) copolymers. PPMS possesses voltage stabilisation capabilities but is immiscible in PDMS, and thus the copolymerisation of the two components was necessary for homogeneity. Concentrations of the voltage stabiliser were varied by changing the molecular weights of the PPMS in the copolymer. The developed elastomers were inherently soft with enhanced electrical breakdown strengths, due to delocalised π-electrons of the aromatic constituent. An optimum concentration was found for the voltage stabilisation effect. The relative permittivities of the PDMS–PPMS elastomers varied from 3.4 to 3.9 and therefore were also improved from pure PDMS elastomers. The elastomers were furthermore non-conductive and possessed low dielectric losses. These properties are evaluated as favourable for soft actuation.

Introduction

Numerous studies on formulating elastomers, with the ultimate goal of achieving better dielectric elastomer (DE) actuation performance, have been performed, mainly by utilising silicone elastomers[1] or other elastomers such as acrylics, polyurethanes and natural rubber.[2] The actuation performance of a DE at a given voltage (V) can be improved by enhancing the relative permittivity (ε_r) or by reducing the Young's modulus (Y). These handles are obvious from the actuation equation derived by Pelrine *et al.*,[3] which relates the actuation strain (s) to the mentioned parameters *via*:

$$s = \frac{-\varepsilon_r \varepsilon_0}{Y}\left(\frac{V}{d}\right)^2 \quad (1)$$

where $\varepsilon_0 = 8.85 \times 10^{-12}$ F m^{-1} is the permittivity of free space. The largest achievable electrical field over the dielectric elastomer before electrical failure (E_{BD}) is denoted the electrical breakdown strength. In this electrical field the maximum theoretical actuation strain is achieved under the assumption that the elastomer is highly extensible and does not break down mechanically prior to electrical breakdown:

$$s_{max} = \frac{-\varepsilon_r \varepsilon_0}{Y} {E_{BD}}^2 \quad (2)$$

However, this strain is not always possible to achieve, since the elastomer may undergo electro-mechanical instability (EMI) which results in premature breakdown.[4–7] The EMI effect is most common for elastomers with strain-softening behaviour. In the following this effect is ignored, since all investigated elastomers have strain-hardening behaviour. Thus, the maximum achievable strain will be described by eqn (2). Furthermore, it also requires that the electrodes do not contribute to the elastic modulus, whilst they should also be stretchable to the same extent as the elastomer.[8]

As solutions to enhanced relative permittivity, several works have been performed on elastomers by adding titanium(IV) oxide (TiO_2),[9,10] barium titanate ($BaTiO_3$)[11] and calcium copper titanate ($CaCu_3Ti_4O_{12}$).[12] Silicone elastomer composites are usually relatively stiff and lead to significant losses,[1] and as alternatives to elastomers with improved permittivity, chemical functionalisation, *via* the covalent grafting of dipoles such as trifluoropropyl,[13] *p*-nitroaniline[14] or azide groups[15,16] to the silicone backbone, has been investigated. Recently, a novel method for introducing high-permittivity liquids into silicone elastomers was developed, and these elastomers were shown to possess high dielectric permittivity.[17,18]

[a]*Danish Polymer Centre, Department of Chemical and Biochemical Engineering, Technical University of Denmark, Building 227, 2800 Kgs. Lyngby, Denmark. E-mail: al@kt.dtu.dk*

[b]*Faculty of Engineering Technology, University of Tun Hussein Onn Malaysia, 86400 Parit Raja, Batu Pahat, Johor, Malaysia*

† Electronic supplementary information (ESI) available: Number of PDMS–PPMS repeating units, stoichiometric ratios of synthesised copolymer and cross-linking, theoretical and realised molar concentrations of phenyl groups, ^{1}H-NMR spectra of copolymers, SEM images, electrical breakdown strength and Weibull parameters as function of Young's moduli, and UV/Vis spectra. See DOI: 10.1039/c6ra25878f

As mentioned previously, another approach to improving actuation performance is reducing the Young's modulus. This can be achieved by either pre-straining externally, using a stiff supporting structure, or pre-straining internally, *via* an interpenetrating polymer network (IPN)[19,20] or by creating bimodal networks with reduced cross-linking density in the elastomer matrix.[21,22] The mentioned elastomers with high relative permittivity and a low Young's modulus improve actuation performance at a given voltage, but these optimised elastomers often possess relatively low electrical breakdown strength. For a given elastomer system (*i.e.* elastomer matrix and filler) the electrical breakdown strength decreases when the Young's modulus is decreased.[9]

Increasing the electrical breakdown strength of DEs allows for greater actuation, due to the possibility of utilising larger electrical fields without failure.[3,23] For DEs, several mechanisms lead to electrical breakdown, namely partial discharge[24] and electromechanical[25] and electrothermal breakdown.[26,27] Multiple studies on pre-strained DE electrical breakdown have been conducted, with the main emphasis on reliability and the effect of electrical breakdown strength on external properties such as effective electrode configurations,[28,29] elastomer processing techniques[30] and pre-stretching methods.[3,23,29] As an alternative approach to enhancing electrical breakdown strength, blending in additives with a voltage-stabilising effect or *via* polymer structure modifications remains unexplored for dielectric elastomers.

Electron-trapping effects have been investigated previously by including aromatic voltage stabilisers in minute concentrations in polymers, mainly polyethylene (PE), with the purpose of reducing power loss for high-voltage insulation cables.[31–33] Aromatic voltage stabilisers, which have delocalised π-electrons, trap energetic electrons and create radicals, as they interrupt the distribution of the π-electron cloud.[34] For high-voltage insulation cables, Yamano *et al.*[31] increased the electrical breakdown strength in PE by using aromatic azo-compounds which had six different side groups with electron-acceptors ($NO_2^{\bullet}$, $CN^{\bullet}$) or electron-donors ($NH_2^{\bullet}$, $CH_3^{\bullet}$, $OH^{\bullet}$). The PE composite containing the azo-compound with $(OH)_2$ and NO_2 side groups with a remarkably low concentration of 1×10^{-5} mol g^{-1} had the highest electrical breakdown strength, improving by 48% compared to the PE without an additive. This indicates that both electron donating ($OH^{\bullet}$) and accepting ($NO_2^{\bullet}$) groups efficiently increase electrical breakdown strength, due to the increased polarity in the aromatic group and thus lower excitation energies. Yamano[32] enhanced further electrical breakdown strength in PE with acene compounds (naphthalene, anthracene, tetracene and pentacene) as aromatic voltage stabilisers.

However, utilising aromatic voltage stabilisers of any kind as a silicone additive will unavoidably cause phase separation of the resulting mixture. Preventing this on both the macro and the micro scale during preparation, as well as during actuation, is a key requirement for long DE lifetimes.[33] The effect of electron-trapping by phenyl groups, so-called 'homo-aromatics', in a silicone elastomer is illustrated in Fig. 1. Electrons in the presence of an electrical field accumulate initially at the interfacial boundary between the film and the electrode, as shown in Fig. 1(b). The electrons then migrate and are trapped in the

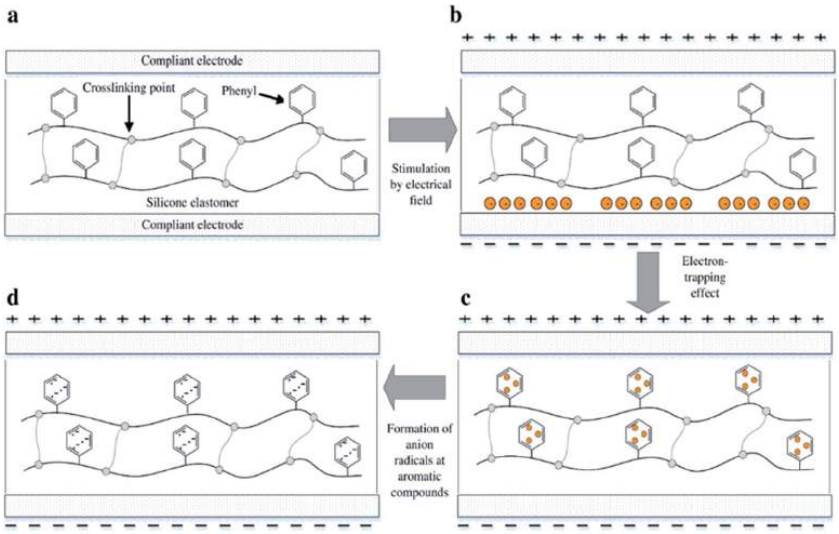

Fig. 1 The enhancement of electrical breakdown strength due to electron-trapping: (a) a silicone elastomer with an aromatic group grafted to the silicone backbone and a coating of compliant electrodes on the top and bottom surfaces. (b) The existence of electrons at the interfaces between the elastomer and the compliant electrode in the presence of an electrical field. (c) The electron-trapping effect as a consequence of a collision between electrons and the phenyl group. (d) The formation of anion radicals resulting from the disturbance of the cloud of π-electrons of the phenyl group.

phenyl group, as seen in Fig. 1(c). When electrons migrate and collide with the homo-aromatic group, they disturb the cloud of pi-electrons in the aromatic group, and this results in the formation of electron-accepting radicals, as shown in Fig. 1(d). The depth of the electron trap is highly influenced by the type of radical,[34] where the depth for the aromatic group with the radical of an electron-accepting type is larger than that of the aromatic group without a radical.[32,34] The trapped electrons act as negative space charges in the elastomer, causing a decrease in electrical field strength on the cathode.[32] This decreased electrical field strength then reduces electron migration from the cathode. The trapped electrons remain in the film bulk and therefore delay electrical breakdown; thus, increased electrical breakdown strength is achieved.

In this work, the voltage stabilisation effect of PPMS in cross-linked PDMS–PPMS copolymers is investigated, while cross-linked materials are characterised mechanically and dielectrically.

Experimental

Materials

Telechelic vinyl-terminated polydimethylsiloxanes (V-PDMS) were DMS-V31, DMS-V25, DMS-V22 and DMS-V21, with a number average molecular weight (M_n) of 28, 17.2, 9.4 and 6 kg mol^{-1}, respectively. Telechelic hydride-terminated polyphenylmethylsiloxanes (H-PPMS) were PMS-H03 (M_n = 0.4 kg mol^{-1}) and PMS-H11 (M_n = 1 kg mol^{-1}). The catalyst was a platinum-divinyl-tetramethyl disiloxane complex [SIP6830.3] containing 3.25% of platinum in xylene. The vinyl-functional cross-linker was methyl-hydrosiloxane-dimethylsiloxane copolymer [VDT-431] (M_n = 28 kg mol^{-1}, 15-functional). All polymers, cross-linkers and catalysts were purchased from Gelest Inc. Fumed silica (SIS6962.0) was purchased from Fluorochem.

Synthesis of PDMS–PPMS block copolymers

PDMS–PPMS block copolymers were prepared from the hydrosilylation of hydride-terminated PPMS and vinyl-terminated PDMS at room temperature in the presence of a platinum (Pt) catalyst, as shown in Scheme 1. The synthesised block copolymer has $X + 1$ blocks of phenylmethylsiloxane and X blocks of dimethylsiloxane.

The procedure to synthesise PDMS–PPMS block copolymers was taken from A. Razak *et al.*[35] The required amount of hydride-terminated PPMS was added based on a targeted molecular weight ($M_{n,T}$) of 30 kg mol^{-1} of the copolymer (refer to ESI 1, eqn (1)†). The mixture containing V-PDMS, H-PPMS and 30 ppm of the Pt catalyst was speed-mixed at 3000 rpm for 5 min. The stoichiometric ratio was calculated based on the number of PDMS–PPMS repeating units, X (see ESI 1, eqn (2)†).

Cross-linking and sample preparation

All PDMS–PPMS block copolymer samples were cross-linked with the vinyl-functional 15-functional cross-linker. The stoichiometric ratio for cross-linking (r_2) was 1.5, with an excess of cross-linker (see ESI 2, eqn (3)†). Blends containing copolymer, cross-linker, 30 ppm of Pt catalyst and 25 parts per hundred rubber (phr) of silica were speed-mixed at 2500 rpm for 4 minutes.

The final mixtures were casted on Teflon plates for easy release. The cross-linked copolymer films were prepared in thicknesses of approximately 1 mm (thick film) and 100 ± 20 μm (thin film). Thick films were used to measure linear viscoelasticity (LVE), the stress–strain relationship and dielectric properties. All films were placed in a vacuum oven at 23 °C for 4 to 8 hours, due to trapped air during fabrication, and were thereafter cured at 40 °C for 12 hours to ensure proper film formation. The curing process was continued at 150 °C for 8 to 12 hours. Subsequently, all films were post-cured at 200 °C for 2 hours to remove all volatiles.[36,37]

The cross-linked PDMS–PPMS copolymer is referred as a PDMS–PPMS elastomer. Samples were named based on repeating numbers of PDMS and PPMS as *n*DMS_*m*PMS. The realised molar concentrations of the phenyl group ($C_{C_6H_5}$) were calculated from the ratio of the mole number of the phenyl group to the total mass of PDMS and PPMS. The mole number of the phenyl group was determined based on integration areas and H's numbers of CH_3–Si–C_5H_5 and Si–$(CH_3)_2$ in ^{1}H-NMR

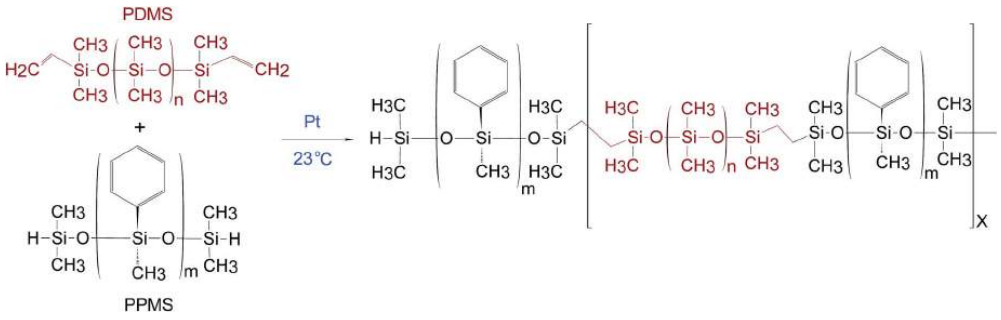

Scheme 1 The hydrosilylation reaction utilised when preparing the PDMS–PPMS block copolymer with a stoichiometric ratio of $r = (X + 1)/X$, where m is the number of repeating phenylmethylsiloxane units in PPMS (m = 2 and 6) and n is the number of repeating dimethylsiloxane units in PDMS (n = 377, 231, 126 and 80).

(refer to ESI 3, eqn (4–7)†). Details of the PDMS–PPMS copolymers are presented in Table 1.

Instrumentation

Degree of conversion of vinyl groups in the synthesis of PDMS–PPMS copolymer. The synthesised copolymer was a telechelic hydride-functional PDMS–PPMS copolymer. The degree of conversion of the PDMS vinyl group from the hydrosilylation of hydride-terminated PPMS and vinyl-terminated PDMS was determined *via* proton nuclear magnetic resonance spectroscopy (^{1}H-NMR) by observing the disappearance of vinyl peaks in the NMR spectra. The NMR equipment utilised for ^{1}H was a Bruker 300 MHz NMR. The number of scannings per sample was 128. The samples were prepared at a concentration of 100 mg mL^{-1} in deuterated chloroform ($CDCl_3$).

Number average molecular weight. The number average molecular weights (M_n) of the copolymers were determined from size-exclusive chromatography (SEC). SEC was performed on a Viscotek GPCmax VE-2001 instrument equipped with a Viscotek TriSEC Model 302 triple detector using two PLgel mixed-D columns from Polymer Laboratories. The copolymer concentrations were between 2 and 3 mg mL^{-1} in toluene, and solutions were run at 35 °C at an elution rate of 1 mL min^{-1}. Molecular weight distributions were calculated using WinGPC Unity 7.4.0 software and linear PDMS standards acquired from Polymer Standards Service GmbH.

Electrical breakdown strength. The measurement of electrical breakdown strength was performed on an in-house-built device based on international standards (IEC 60243-1 (1998) and IEC 60243-2 (2001)). Samples were prepared with a thickness of less than 110 μm. The film was slid between two spherical metal electrodes (diameter of 20 mm). The electrical breakdown measurement was taken at the point of contact with a stepwise increasing voltage applied (50–100 V per step) at a rate of 0.5–1 steps per s. The electrical breakdown measurement was repeated 12 times for each sample, and the average of these values was then stated as electrical breakdown strength.

Dielectric properties. Dielectric properties were measured by dielectric spectroscopy performed on a Novocontrol Alpha-A high-performance frequency analyser (Novo-control Technologies GmbH & Co. KG, Germany) operating in the frequency range 10^{-1} to 10^6 Hz at 23 °C. The electrode diameter was 20 mm. The sample was sandwiched between two gold-coated plates prior to the measurement.

Linear viscoelastic (LVE) properties. Prepared films were characterised at 23 °C using an advanced rotational rheometer from TA Instruments (ARES-G2). The utilised parallel plates had a diameter of 25 mm. The axial force ranged from 5 to 12 N, depending on the samples, to ensure sufficient contact between the plate and the sample (diameter of 25 mm). The strain and frequency in the linear regime were 2% and 10^{-2} to 10^2 Hz, respectively.

Stress–strain relationship. Tensile strengths and elongations at breaking, as well as the Young's moduli at a 5% strain, were measured in extensional rheological tests. The rheological test was performed on an ARES-G2 rheometer from TA Instruments by means of an SER2 universal testing platform consisting of two rotating drums with a diameter of 10.3 mm, with the lateral offset of the centre axis of these two drums at 12.7 mm. The sample, which was a rectangular strip of 6 mm (width), 30 mm (length) and 1 mm (thickness), elongated within a confined length ($L = 12.7$ mm) by winding up the strip with the two rotary drums. The ends of the strip were secured by means of strong glue to the surfaces of the drums. For incompressible samples, the ends of the strip moved at speed $[v_{end} = (L/2)\mathrm{d}\varepsilon_H/\mathrm{d}t]$. Integrating this speed from an initial length (L_o) to the final length (L_f) led to an exponential increase in sample length over time $L(t) = L_o \exp[(\mathrm{d}\varepsilon_H/\mathrm{d}t)t]$, and so the final Hencky strain (ε_H) can thus be expressed as follows: $\varepsilon_H = \ln[L_f/L_o]$. Here, engineering stress and strain were used for the stress–strain relationship. Engineering strain was calculated from the measured Hencky strains, and engineering stress was calculated from the measured torque over a cross-sectional area of the sample (refer to eqn (8–12)† in ESI 4 for engineering stress and strain, respectively).

Scanning electron microscopy (SEM) images. The morphologies of the cross-linked copolymers and the reference elastomer were examined *via* scanning electron microscopy (SEM) (FEI Inspect S, USA). The samples were cross-sectional films and were firstly immersed in liquid nitrogen for a few minutes, then broken and deposited on a sample holder. All samples were coated with gold under vacuum conditions before testing. Energy-dispersive X-ray (EDX) spectroscopy (Oxford INCAWave 500, UK) was applied to detect the element distribution profile on the surface of the samples.

UV/Vis absorbance. The presence of phenyl groups in the cross-linked copolymers was detected from the absorbance energy of ultraviolet (UV) or visible light (Vis). Energy absorbance from UV/Vis light was measured by an UV/Vis spectrometer from BMG Labtech (SPECTROstar Omega). The wavelength range of the UV/Vis spectrometer was from 220 to 1000 nm, while optical density (OD) range was between 0 and 4 OD with an accuracy of <1% at 2 OD. Energy absorbance was measured within wavelengths of 220 to 350 nm. These measurements were performed on eight wells of a Nunc 96-Well LockWell™ PolySorp module plate from Thermo Scientific for thin films with an approximate thickness of 100 μm.

Table 1 Sample details and realised molar concentrations of the phenyl group of cross-linked PDMS–PPMS copolymers

Vinyl-functional PDMS	Hydride-functional PPMS	PDMS–PPMS copolymer (*n*DMS_*m*PMS)	Realised concentration of phenyl groups [10^{-4} mol g^{-1}]
DMS-V31	PMS-H03	377DMS_2PMS	5.0
DMS-V25		231DMS_2PMS	6.9
DMS-V22		126DMS_2PMS	7.8
DMS-V21		80DMS_2PMS	8.4
DMS-V31	PMS-H11	377DMS_6PMS	8.7
DMS-V25		231DMS_6PMS	9.8
DMS-V22		126DMS_6PMS	15
DMS-V21		80DMS_6PMS	20

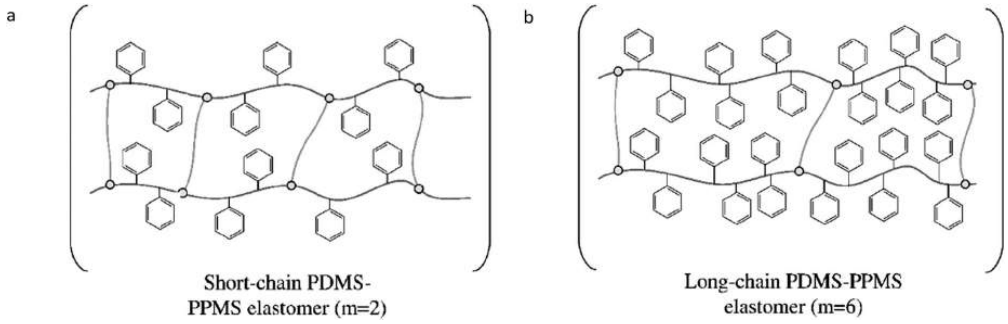

Fig. 2 Illustration of a cross-linked PDMS–PPMS copolymer with (a) short chain and (b) long chain.

Results and discussion

The targeted elastomers with covalently grafted voltage stabilisers are shown in Fig. 2. In order to realise these elastomers, copolymers were first synthesised and characterised before being cross-linked into elastomers.

Synthesised PDMS–PPMS copolymers

Determined molecular weights of synthesised PDMS–PPMS copolymers are shown in Table 2. All copolymers have low polydispersity indexes (PDI $\leq$ 2.1). The disappearance of the Si–CH_2=CH_2 bond signal at 5.8–6.2 ppm was confirmed by ^{1}H-NMR, to ensure that all vinyl groups in the PDMS had been consumed fully during the hydrosilylation of vinyl-terminated PDMS and hydride-terminated PPMS; refer to ESI 5 for NMR spectra in Fig. S2–9.† ^{1}H-NMR spectra confirmed that the synthesised PDMS–PPMS copolymers were hydride functional, and all vinyl groups in the PDMS were fully reacted.

Linear viscoelasticity

To evaluate the effect of the increased concentration of the phenyl group on viscoelastic properties, the prepared elastomers were characterised rheologically, as shown in Fig. 3. This is an important investigation to perform for these systems, since aromatics are well-known to inhibit utilised silylation chemistry. The PDMS–PPMS elastomers show to be well cross-linked and behave elastically, *i.e.* the inhibiting nature of the phenyl groups did not affect the final properties of the elastomers. The resulting storage moduli (G') for all elastomers and the reference are between 10^4 and 10^5 Pa, and they all behave in a similar manner with close-to-identical relaxations. From these results it is obvious that the elastomers maintain network integrity. Relative losses [tan(δ)] are comparable to these of commercial silicone elastomers such as Elastosil RT625 from Wacker Chemie.[38]

Table 2 Average number of molecular weights and actual concentrations of the phenyl group of synthesised PDMS–PPMS copolymers

Cross-linked PDMS–PPMS copolymer	Actual $M_{n,T}$ (kg mol^{-1})	Polydispersity index, PDI (M_w/M_n)
377DMS_2PMS	32	2.1
231DMS_2PMS	36	1.9
126DMS_2PMS	73	1.5
80DMS_2PMS	39	1.8
377DMS_6PMS	42	1.7
231DMS_6PMS	37	1.8
126DMS_6PMS	82	1.6
80DMS_6PMS	32	2.0

Stress–strain relationship

Stress–strain curves and Young's moduli of the cross-linked copolymers are shown in Fig. 4 and 5, respectively. All cross-linked copolymers show increased strain at breaking, compared to the reference (DMS-H31), due to an evident 'plasticising' effect (see Fig. 4). All elastomers are still strain-hardening despite being plasticised. The resulting Young's moduli at 5% strains of the cross-linked copolymers are shown in Fig. 5, and the soft nature of all the elastomers is obvious. Common Young's moduli of silicone elastomers are around

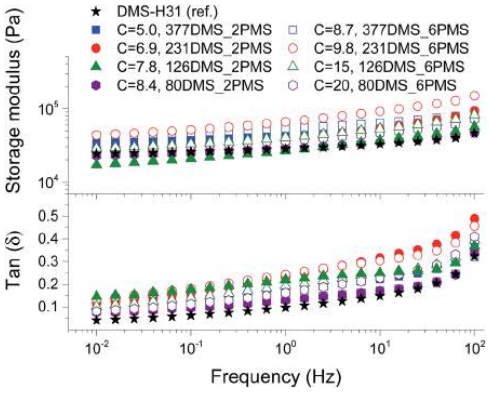

Fig. 3 The storage and tan(δ) of cross-linked PDMS–PPMS copolymers at 23 °C; C is in 10^{-4} mol g^{-1}.

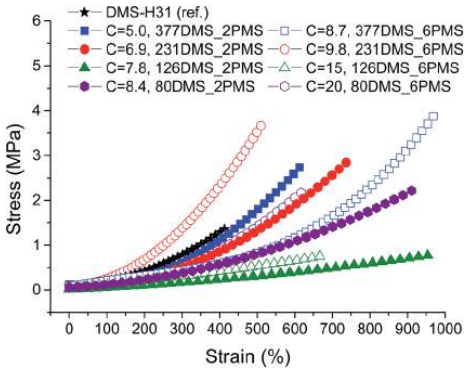

Fig. 4 Stress–strain curves for PDMS–PPMS elastomers with different phenyl group concentrations at 23 °C (typical standard deviations in tensile measurements were of the order ±5%).

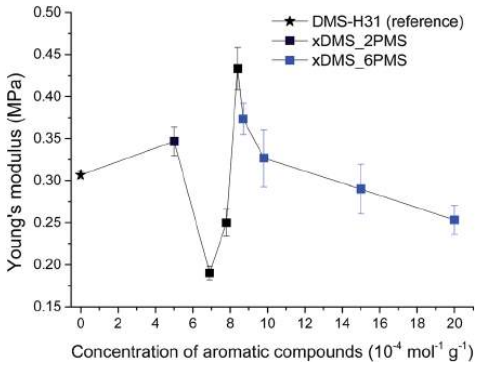

Fig. 5 Young's moduli for the PDMS–PPMS and reference elastomers.

1 MPa.[38] Another finding is that the cross-linked copolymer 80DMS_2PMS is slightly stronger than the reference elastomer (DMS-H31), not only with respect to the initial Young's modulus, but also with respect to ultimate strength.

With respect to actuation, elastomers $C = 7.8$ and 15×10^{-4} mol g^{-1} show the most softness. On the other hand, both elastomers do not possess any significant strain-hardening behaviour. The slightly stronger elastomers $C = 8.4$ and 8.7×10^{-4} mol g^{-1} show ideal properties for actuation with good, ultimately strain-hardening, behaviour.

Obviously, from the mechanical data, there is no clear trend in mechanical behaviours except that a concentration of around 8.5×10^{-4} mol g^{-1} seems to be the most favourable. This is most likely due to local phase separation, which serves both to stabilise and to plasticise the elastomer, *i.e.* some regions will be rich in PPMS (rigid zones) and other regions poor (plasticised zones). This can be seen to some extent from SEM imaging of the resulting films with two examples shown in Fig. 6. As investigated by Luo *et al.*,[39] PDMS shows a distinct triangular pattern whereas PMMS shows a pattern with bent rectangles.

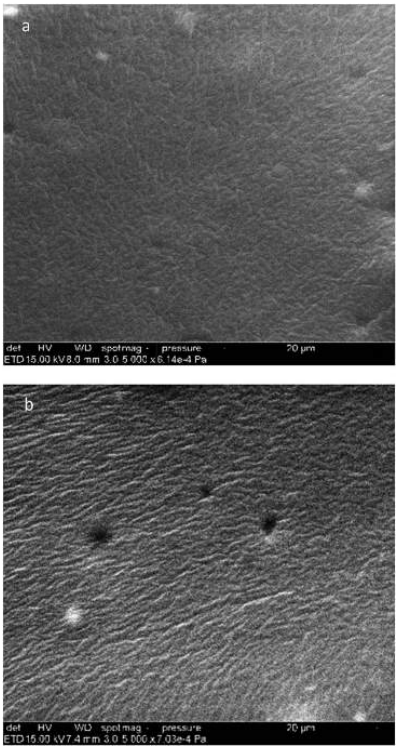

Fig. 6 SEM pictures of two representative samples, namely (a) 377DMS_2PMS and (b) 80DMS_2PMS.

This is illustrated below by the elastomers 377DMS_2PMS and 80DMS_2PMS, wherein sample 377DMS_2PMS shows a distinct PDMS structure while elastomer 80DMS_2PMS has areas with both signatures. SEM pictures of all elastomers can be seen in ESI 6, Fig. S10.†

Dielectric properties

The conductivity and dielectric properties of the cross-linked PDMS–PPMS copolymers and the reference elastomer are shown in Fig. 7 and 8, respectively. The resulting conductivities indicate that none of the cross-linked copolymers is conductive, as illustrated in Fig. 7. Low conductivity is a key element in the actuation performance of the DE. The relative permittivity of prepared elastomers with short-chain PPMS initially increases and reaches a maximum phenyl group concentration of 6.9×10^{-4} mol g^{-1}, albeit it decreases thereafter. On the other hand, the relative permittivity of cross-linked copolymers with long-chain PPMS decreases in line with an increase in phenyl concentration. The flat curves furthermore indicate that phase separation is not macroscopic but rather limited to the lower microscale or nanoscale. These observations again indicate that micro- or nanoscale phase separation takes place and that the morphology of the elastomers depends strongly on the

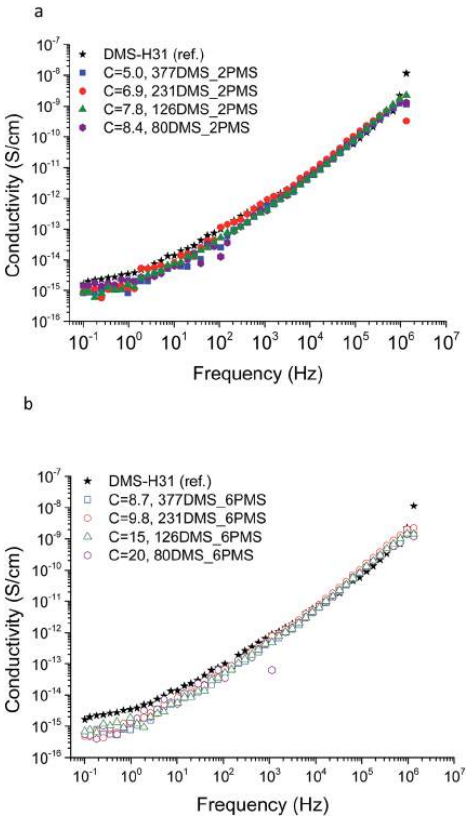

Fig. 7 The conductivity of PDMS–PPMS elastomers with different phenyl concentrations of at 23 °C: (a) short-chain and (b) long-chain PPMS; C is in 10^{-4} mol g^{-1}.

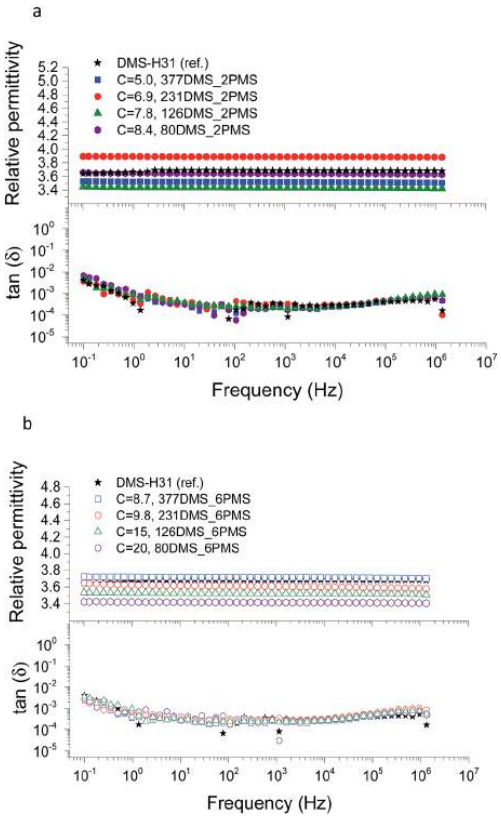

Fig. 8 The dielectric properties of PDMS–PPMS elastomers with different phenyl concentrations at 23 °C: (a) short-chain and (b) long-chain PPMS; C is in 10^{-4} mol g^{-1}.

concentration of phenyl groups. Dielectric losses, which are represented by tan(δ), are relatively low for all cross-linked copolymers, as shown in Fig. 8. The reference elastomer (DMS-H31) shows low tan(δ) as well.

Electrical breakdown and Weibull analysis

The influence of the concentration of the phenyl group in cross-linked PDMS–PPMS copolymer on electrical breakdown strength was investigated. The resulting electrical breakdown strength of the cross-linked copolymers with different phenyl group concentrations is shown in Fig. 9, namely an optimum electrical breakdown strength (72 ± 3 V μm^{-1}) occurring at a phenyl concentration of 8.4×10^{-4} mol g^{-1}. In other words, electrical breakdown strength has increased 36% compared to the reference elastomer. The optimum is most likely due to the combination of favourable phase separation and a relatively high concentration of phenyl groups. Stiffness may also affect electrical breakdown strength strongly,[9] *i.e.* the electrical breakdown strength of the reference elastomer is low due to the inherently soft nature of silicone elastomers cross-linked from high molecular weight PDMS polymers,[40] and there is a broad amount of variation in the Young's moduli of the prepared elastomers. To evaluate whether the voltage stabilisation effect is

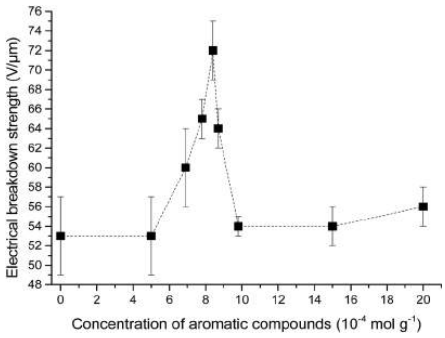

Fig. 9 Electrical breakdown strength of PDMS elastomer and PDMS–PPMS copolymers with different phenyl group concentrations.

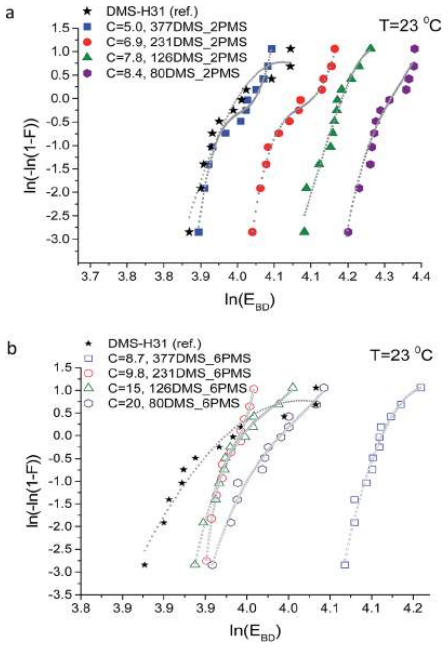

Fig. 10 Weibull plots of PDMS elastomer and PDMS–PPMS copolymers with different phenyl group concentrations: copolymers from (a) short-chain and (b) long-chain PPMS. The dashed lines serve solely as guidelines for the eyes to differentiate between data slopes; C is in units of 10^{-4} mol g^{-1}.

rather an effect of increased stiffness, the influence of Y on electrical breakdown strength was investigated. There is no correlation, as seen from ESI 7 in Fig. S11,† which means that the effect is due to the voltage stabilisation effect.

Weibull analysis was used to obtain a further understanding of the electrical reliability of the prepared elastomers. The Weibull probability distribution of failure for all films is shown in Fig. 10. The η-parameter, which is the Weibull scale parameter, was determined from the Weibull plot as the value at which failure probability, $\ln[-\ln(1 - F)]$, was 63.2%.[35] The β-parameter is the Weibull shape parameter, representing the broadness of distribution. The η-parameter is closely correlated to the mean breakdown voltage.[41] A small value of the Weibull shape parameter indicates that electrical breakdown occurrences are broadly dispersed.[41]

Due to different prepared PDMS–PPMS elastomer film thicknesses, the determined electrical breakdown strengths were normalised based on a reference thickness for better comparison. Normalised dielectric breakdown strength can be determined by:[28]

$$E_n = n^{-\frac{1}{\beta}} E_0 \quad (3)$$

where E_0 is the electrical breakdown strength of a 100 μm film, β is the Weibull shape parameter and n is relative sample thickness compared to the chosen reference thickness of (t_0 = 100 μm).

The results for the normalised electrical breakdown strength (E_n), Weibull η- and β-parameters and R^2 of the linear fits for cross-linked copolymers, including the reference, are summarised in Table 3. Cross-linked PDMS–PPMS copolymers with long-chain PPMS possess lower electrical breakdown strength standard deviation than the copolymers with short-chain PPMS, as illustrated in Table 3. The coefficient of determination (R^2) of all investigated elastomers is above 0.85, indicating that the measured electrical breakdown strengths correlate well with the fitted regression lines.

The Weibull plots for all samples are shown in Fig. 10. The plotted data in the Weibull probability distribution of failure of elastomers with short-chain PPMS clearly show two domains (refer to Fig. 10(a)). This is an indication of the inhomogeneity of the phenyl group in the PDMS–PPMS matrix containing short-chain PPMS. On the other hand, the Weibull distribution data for the elastomers with long-chain PPMS show one domain with only a small discrepancy at high voltages, thereby indicating better homogeneity of the phenyl group in the PDMS–PPMS matrix.

Weibull parameters η and β at different phenyl group concentrations are compared and summarised in Fig. 11. One important finding from the values of the Weibull β-parameter is that the PDMS–PPMS elastomers with long-chain PPMS have larger β-parameter values compared to the elastomers with short-chain PPMS except at very high phenyl group loadings, where β drops. For both types of cross-linked copolymers an optimum η parameter value of around 8×10^{-4} is found.

Table 3 Electrical breakdown strength at 23 °C, Weibull parameters η and β and R^2 of the linear fit for all prepared cross-linked copolymers and the reference

Cross-linked PDMS–PPMS copolymer	Thickness (μm)	Electrical breakdown strength (V μm^{-1})	Weibull β-parameter	Weibull η-parameter	R^2	Normalised electrical breakdown (V μm^{-1})
DMS-H31 (ref.)	105	53 ± 4	17	55	0.85	52.9 ± 3.6
377DMS_2PMS	81	53 ± 4	17	55	0.85	53.7 ± 3.7
231DMS_2PMS	91	60 ± 4	20	61	0.91	60.1 ± 3.4
126DMS_2PMS	80	65 ± 2	32	66	0.94	65.5 ± 2.5
80DMS_2PMS	90	72 ± 3	26	73	0.92	71.9 ± 3.1
377DMS_6PMS	81	64 ± 2	47	65	0.89	64.1 ± 1.6
231DMS_6PMS	95	54 ± 1	60	54	0.94	54.0 ± 1.6
126DMS_6PMS	95	54 ± 2	39	55	0.88	54.0 ± 1.8
80DMS_6PMS	95	56 ± 2	28	57	0.94	56.1 ± 2.2

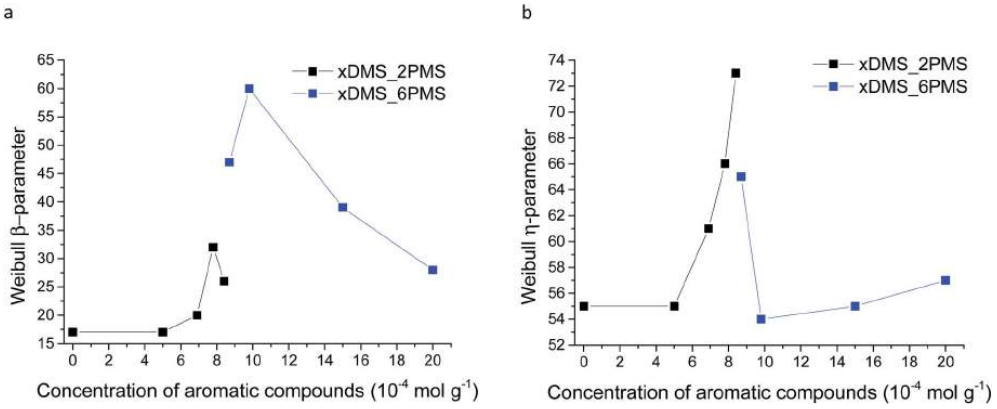

Fig. 11 Weibull parameters for prepared PDMS–PPMS copolymer and reference (DMS-H31) samples: (a) β-parameter and (b) η-parameter.

Furthermore no links between the Weibull parameters and the Young's moduli of the elastomers could be identified, as shown in ESI 8, Fig. S12.†

Conclusion

Inherently soft elastomers based on cross-linked PDMS–PPMS copolymers were synthesised successfully and proven to possess increased electrical breakdown strength, due to voltage stabilisation arising from aromatic groups of PPMS. Cross-linked copolymers with varying concentrations of aromatic groups were prepared from copolymers synthesised by varying the chain length of PDMS while maintaining the chain length of PPMS. The cross-linked copolymers possessed higher electrical breakdown strength than the pure PDMS-based reference elastomer, due to π-electrons of the aromatic group being capable of trapping charges. Aside from having high electrical breakdown strength, the cross-linked copolymers showed an increased storage modulus and low viscous loss, hence maintaining the network integrity of the dielectric elastomer. All cross-linked copolymers demonstrated strain-hardening behaviours. From the electrical breakdown strength, optimal phenyl group concentration was determined at approximately 8.4×10^{-4} mol g^{-1}. As a result of these properties, voltage-stabilised elastomers were synthesised. Further studies will hopefully uncover better voltage stabilisers, which would subsequently be a giant step toward producing reliable dielectric elastomer-based products.

Acknowledgements

The Malaysian Ministry of Education (MoE), Universiti Tun Hussein Onn Malaysia (UTHM) and Innovationsfonden Danmark are gratefully acknowledged for their funding.

Notes and references

1 F. B. Madsen, A. E. Daugaard, S. Hvilsted and A. L. Skov, *Macromol. Rapid Commun.*, 2016, **37**, 378–413.
2 P. Brochu and Q. Pei, *Macromol. Rapid Commun.*, 2010, **31**, 10–36.
3 R. Pelrine, R. Kornbluh, Q. Pei and J. Joseph, *Science*, 2000, **287**, 836–839.
4 Z. Suo, *Acta Mech. Solida Sin.*, 2010, **23**, 549–577.
5 X. Zhao, W. Hong and Z. Suo, *Phys. Rev. B: Condens. Matter Mater. Phys.*, 2007, **76**, 134113.
6 Y. Liu, L. Liu, K. Yu, S. Sun and J. Leng, *Smart Mater. Struct.*, 2009, **18**, 95040.
7 L. Liu, Y. Liu, J. Leng and K. Lau, *Smart Mater. Struct.*, 2011, **20**, 115015.
8 S. Rosset and H. R. Shea, *Appl. Phys. A: Mater. Sci. Process.*, 2013, **110**, 281–307.
9 L. Yu and A. L. Skov, *Int. J. Smart Nano Mater.*, 2015, **6**, 268–289.
10 S. Vudayagiri, S. Zakaria, L. Yu, S. S. Hassouneh, M. Benslimane and A. L. Skov, *Smart Mater. Struct.*, 2014, **23**, 105017.
11 Z. Zhang, L. Liu, J. Fan, K. Yu, Y. Liu, L. Shi and J. Leng, *Proc. SPIE*, 2008, **6926**, 692610.
12 L. J. Romasanta, P. Leret, L. Casaban, M. Hernández, M. A. de la Rubia, J. F. Fernández, J. M. Kenny, M. A. Lopez-Manchado and R. Verdejo, *J. Mater. Chem.*, 2012, **22**, 24705–24712.
13 H. Böse, D. Uhl and R. Rabindranath, *Proc. SPIE*, 2012, **8340**, 83402E.
14 B. Kussmaul, S. Risse, G. Kofod, R. Waché, M. Wegener, D. N. McCarthy, H. Krüger and R. Gerhard, *Adv. Funct. Mater.*, 2011, **21**, 4589–4594.
15 F. B. Madsen, A. E. Daugaard, S. Hvilsted, M. Y. Benslimane and A. L. Skov, *Smart Mater. Struct.*, 2013, **22**, 1–11.
16 F. B. Madsen, I. Javakhishvili, R. E. Jensen, A. E. Daugaard, S. Hvilsted and A. L. Skov, *Polym. Chem.*, 2014, **5**, 7054–7061.
17 P. Mazurek, S. Hvilsted and A. L. Skov, *Polymer*, 2016, **87**, 1–7.
18 P. Mazurek, L. Yu, R. Gerhard, W. Wirges and A. L. Skov, *J. Appl. Polym. Sci.*, 2016, **133**, 44153.

19 S. M. Ha, W. Yuan, Q. Pei, R. Pelrine and S. Stanford, *Adv. Mater.*, 2006, **18**, 887–891.
20 P. Brochu, H. Stoyanov, X. Niu and Q. Pei, *Smart Mater. Struct.*, 2013, **22**, 55022.
21 F. B. Madsen, A. E. Daugaard, C. Fleury, S. Hvilsted and A. L. Skov, *RSC Adv.*, 2014, **4**, 6939–6945.
22 C. Tugui, G. Stiubianu, M. Iacob, C. Ursu, A. Bele, S. Vlad and M. Cazacu, *J. Mater. Chem. C*, 2015, **3**, 8963–8969.
23 S. Zakaria, L. Yu, G. Kofod and A. L. Skov, *Mater. Today Commun.*, 2015, **4**, 204–213.
24 P. H. F. Morshuis and J. J. Smit, *IEEE Trans. Dielectr. Electr. Insul.*, 2005, **12**, 328–340.
25 K. H. Stark and C. G. Garton, *Nature*, 1955, **176**, 1225–1226.
26 S. Zakaria, P. H. F. Morshuis, M. Y. Benslimane, K. V. Gernaey and A. L. Skov, *Proc. SPIE*, 2014, **9056**, 90562V.
27 R. Kochetov, A. V. Korobko, T. Andritsch, P. H. F. Morshuis, S. J. Picken and J. J. Smit, *J. Phys. D: Appl. Phys.*, 2011, **44**, 395401.
28 S. Zakaria, P. H. F. Morshuis, M. Y. Benslimane, L. Yu and A. L. Skov, *Smart Mater. Struct.*, 2015, **24**, 55009.
29 A. Trols, A. Kogler, R. Baumgartner, R. Kaltseis, C. Keplinger, R. Schwodiauer, I. Graz and S. Bauer, *Smart Mater. Struct.*, 2013, **22**, 104012.
30 M. Kollosche, M. Melzer, A. Becker, H. Stoyanov, D. N. McCarthy, H. Ragusch and G. Kofod, *Proc. SPIE*, 2009, **7287**, 728729.
31 Y. Yamano and H. Endoh, *IEEE Trans. Dielectr. Electr. Insul.*, 1998, **5**, 270–275.
32 Y. Yamano, *IEEE Trans. Dielectr. Electr. Insul.*, 2006, **13**, 773–781.
33 V. Englund, R. Huuva, S. M. Gubanski and T. Hjertberg, *Polym. Degrad. Stab.*, 2009, **94**, 823–833.
34 J. McMurry, *Organic Chemistry*, Brooks/Cole, California, 8th edn, 2011.
35 A. H. A. Razak, P. Szabo and A. L. Skov, *RSC Adv.*, 2015, **5**, 53054–53062.
36 M. A. Brook, H. U. Saier, J. Schnabel, K. Town and M. Maloney, *Ind. Eng. Chem. Res.*, 2007, **46**, 8796–8805.
37 S. Zakaria, F. B. Madsen and A. L. Skov, *Polym.-Plast. Technol. Eng.*, 2016, DOI: 10.1080/03602559.2016.1211689.
38 A. L. Skov, A. G. Bejenariu, J. Bøgelund and M. Y. Benslimane, *Proc. SPIE*, 2012, **8340**, 83400M.
39 Y. Luo, S. Tan, H. Wang, F. Wu, X. Liu, L. Li and Z. Zhang, *Chem. Eng. J.*, 2008, **137**, 496–502.
40 A. L. Larsen, K. Hansen, P. Sommer-Larsen, O. Hassager, A. Bach, S. Ndoni and M. Jørgensen, *Macromolecules*, 2003, **36**, 10063–10070.
41 S. K. Nandi, X. Liu, D. K. Venkatachalam and R. G. Elliman, *Phys. Rev. Appl.*, 2015, **4**, 64010.

Electronic Supplementary information

Silicone elastomers with covalently incorporated aromatic voltage stabilizers

Aliff Hisyam A Razak[a,b] and Anne Ladegaard Skov[a]

[a] *Danish Polymer Center, Department of Chemical and Biochemical Engineering, Technical University of Denmark, Building 227, 2800 Kgs. Lyngby, Denmark.*
[b] *Faculty of Engineering Technology, University of Tun Hussein Onn Malaysia, 86400 Parit Raja, Batu Pahat, Johor, Malaysia.*

1) Number of PDMS-PPMS repeating units and stoichiometric ratio of cross-linked PDMS-PPMS copolymers

The targeted number of PDMS-PPMS repeating units in the copolymer (X) was calculated such that the targeted $M_{n,T}$ results in a telechelic hydride terminated PDMS-PPMS copolymer as shown below:

$$X = \frac{M_{n,T} - M_{n,PPMS}}{M_{n,PDMS} + M_{n,PPMS}}$$

Equation 1

where $M_{n,PDMS}$ and $M_{n,PPMS}$ are the molecular weight of PDMS and PPMS, respectively.

The stoichiometric ratio for preparing telechelic hydride-functional PDMS-PPMS copolymers (r_1) was calculated as:

$$r_1 = \frac{[hydride]}{[vinyl]} = \frac{(X+1)f_{PPMS}}{Xf_{PDMS}} = \frac{X+1}{X}$$

Equation 2

where f_{PDMS} and f_{PPMS} are the functionality of PDMS (f_{PDMS} = 2) and PPMS (f_{PPMS} = 2), respectively.

2) Stoichiometric ratio of crosslinking

The stoichiometric ratio for the cross-linking (r_2) was 1.5 and was calculated below:

$$r_2 = \frac{[vinyl]}{[hydride]} = \frac{F_{CL}[CL]_0}{F_{CP}[CP]_0} = \frac{F_{CL}}{F_{CP}} \cdot \frac{m_{CL}/M_{CL}}{m_{CP}/M_{CP}}$$

Equation 3

where F_{CL} and F_{CP} are average numbers of functional group on the crosslinker (15-functional) and the PDMS-PPMS copolymer (2-functional), respectively, while $[\ldots]_0$, m_x, and M_x are the initial concentration, the mass and the molecular weight, respectively, (x = *CL*, *CP*).

3) Calculation of molar concentration of phenyl groups in PDMS-PPMS elastomers from ^{1}H-NMR

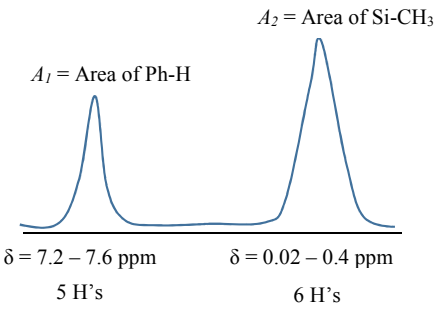

Figure S1 The illustration of NMR spectrum with peaks of phenyl and methyl of PDMS-PPMS elastomer.

a) Relative number of moles of phenylmethylsiloxane (X_1):
Note: The proton signal at δ = 7.2 – 7.6 ppm representing the phenyl (C_6H_5) protons (5H's).

$$X_1 = \frac{A_1}{H_1}$$

Equation 4

where A_1 and H_1 are the area of integration and the number of protons for phenyl group, respectively.

b) Relative number of moles of dimethylsiloxane (X_2):
Note: The proton signal at δ = 0.02 – 0.4 ppm representing the dimethyl [$(CH_3)_2$] protons (6H's).

$$X_2 = \frac{A_2 - Me(end) - Me(PMS)}{H_2} = \frac{A_2 - 12X_1 - 3m \cdot X_1}{H_2}$$

Equation 5

where A_2 and H_2 are the area of integration and the number of protons for methyl, respectively, while $Me(end)$ and $Me(PMS)$ are methyl groups for telechelic hydride end-groups and phenylmethylsiloxane unit (m), respectively.

c) Actual mole percentage of phenyl groups of PDMS-PPMS elastomer ($n_{C_6H_6}$ in mol):

$$n_{C_6H_6} = \frac{X_1}{X_1 + X_2}$$

Equation 6

d) True molar concentration of phenyl groups of PDMS-PPMS elastomer ($C_{C_6H_6}$ in mol/g):

$$C_{C_6H_6} = \frac{n_{C_6H_6}}{m_{PPMS} + m_{PDMS}}$$

Equation 7

where m_{PPMS} and m_{PDMS} are masses of PPMS and PDMS, respectively.

4) Calculation of engineering stress and strain

The engineering stress (σ_E) was calculated from the force (*F*) and the cross-sectional area of the strip (*A*):

$$\sigma_E = \frac{F}{A} = \frac{F}{t \times w} = \frac{\tau \cdot d}{t \cdot w}$$

Equation 8

where *A* = film thickness (t) · constant width (w = 6 mm) and *F* = torque (τ) · drum diameter (d = 10.3 mm).

The engineering strain (ϵ_E) was calculated as a ratio of a stretched strain ($L - L_0$) to an initial strain (L_0) as:

$$\epsilon_E = \frac{L - L_0}{L_0}$$

Equation 9

where a final strain after stretching (L) was determined from Hencky strain (ϵ_H) as follows:

$$\epsilon_H = ln\frac{L}{L_0}$$

Equation 10

$$L = L_0 e^{\epsilon_H} = L_0 e^{(r_H)t_s}$$

Equation 11

where ϵ_H is a product of Hencky rate ($r_H = 1\times10^{-3}$ rotation/s) and step time (t_s).

By putting equation (11) in (9), the final expression of engineering strain (ϵ_E) was obtained as below:

$$\epsilon_E = e^{\epsilon_H} - 1$$

Equation 12

Young's moduli were determined from slopes in the linear regime of stress-strain plots at 5 % strain.

5) NMR spectra of PDMS-PPMS copolymers

The NMR spectra for PDMS-PPMS copolymers with different true molar concentrations of phenyl groups ($C_{C_6H_6}$) are shown in Figures S2– S9.

a) PDMS-PPMS copolymer (**377DMS_2PMS**, $C_{C_6H_6}$ = 5.0 × 10^{-4} mol g^{-1})

^{1}H-NMR ($CDCl_3$, 300 MHz): δ -0.02 - δ 0.6 (m, 6 H's, -SiO(C**H$_3$**)$_2$-), δ 4.70 (m, 1 H, -Si**H**-), δ 7.10 - δ 7.60 (m, 5 H's, -SiC$_6$**H$_5$**-).

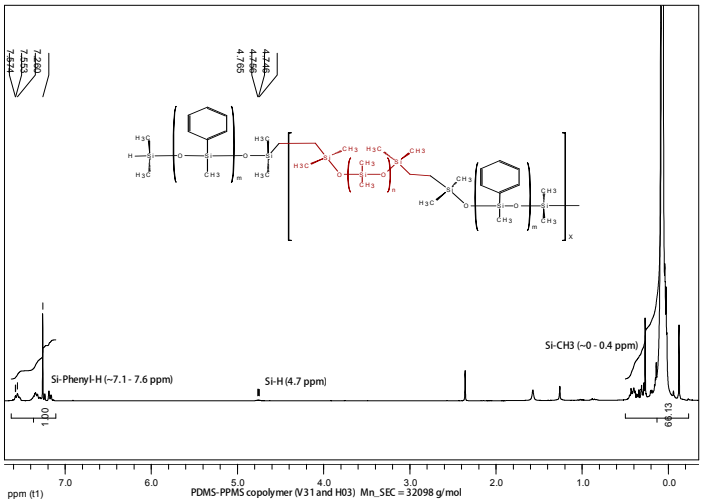

Figure S2 The NMR for 377DMS_2PMS.

b) PDMS-PPMS copolymer (**231DMS_2PMS**, $C_{C_6H_6}$ = 6.9 × 10^{-4} mol g^{-1})

^{1}H-NMR ($CDCl_3$, 300 MHz): δ -0.02 - δ 0.6 (m, 6 H's, -SiO(C**H$_3$**)$_2$-), δ 4.70 (m, 1 H, -Si**H**-), δ 7.10 - δ 7.60 (m, 5 H's, -SiC$_6$**H$_5$**-).

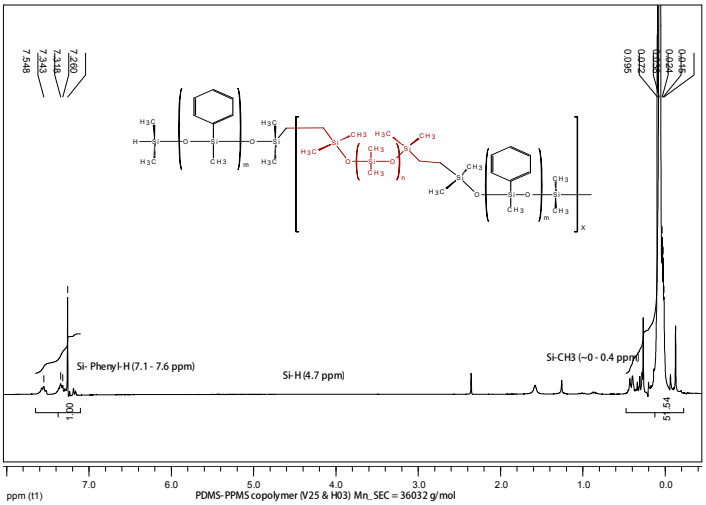

Figure S3 The NMR for 231DMS_2PMS.

c) PDMS-PPMS copolymer (**126DMS_2PMS**, $C_{C_6H_6}$ = 7.8 × 10^{-4} mol g^{-1})

^{1}H-NMR ($CDCl_3$, 300 MHz): δ -0.02 - δ 0.6 (m, 6 H's, -SiO(C**H$_3$**)$_2$-), δ 4.70 (m, 1 H, -Si**H**-), δ 7.10 - δ 7.60 (m, 5 H's, -SiC$_6$**H$_5$**-).

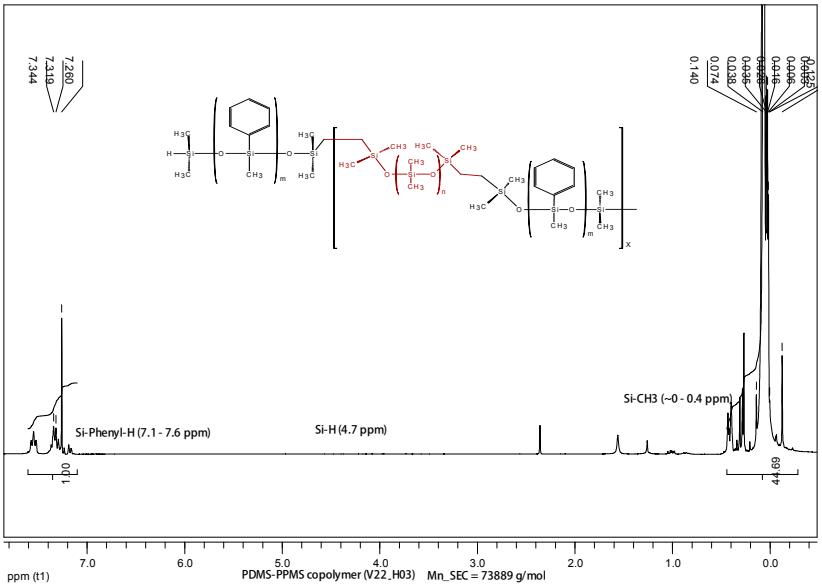

Figure S4 The NMR for 126DMS_2PMS.

d) PDMS-PPMS copolymer (**80DMS_2PMS**, $C_{C_6H_6}$ = 8.4 × 10^{-4} mol g^{-1})

^{1}H-NMR ($CDCl_3$, 300 MHz): δ -0.02 - δ 0.6 (m, 6 H's, -SiO(C**H$_3$**)$_2$-), δ 4.70 (m, 1 H, -Si**H**-), δ 7.10 - δ 7.60 (m, 5 H's, -SiC$_6$**H$_5$**-).

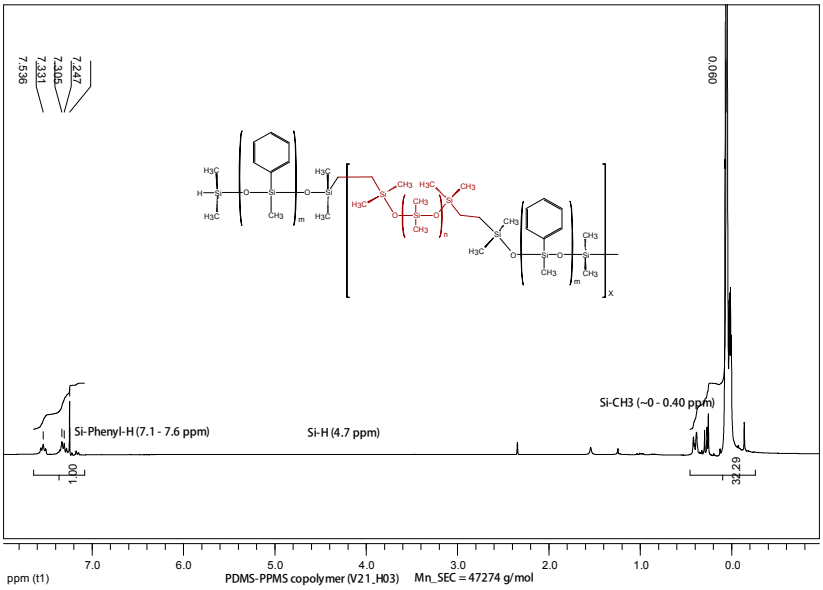

Figure S5 The NMR for 80DMS_2PMS.

e) PDMS-PPMS copolymer (**377DMS_6PMS**, $C_{C_6H_6}$ = 8.7 × 10^{-4} mol g^{-1})

^{1}H-NMR ($CDCl_3$, 300 MHz): δ -0.02 - δ 0.6 (m, 6 H's, -SiO(C**H$_3$**)$_2$-), δ 4.70 (m, 1 H, -Si**H**-), δ 7.10 – δ 7.60 (m, 5 H's, -SiC$_6$**H$_5$**-).

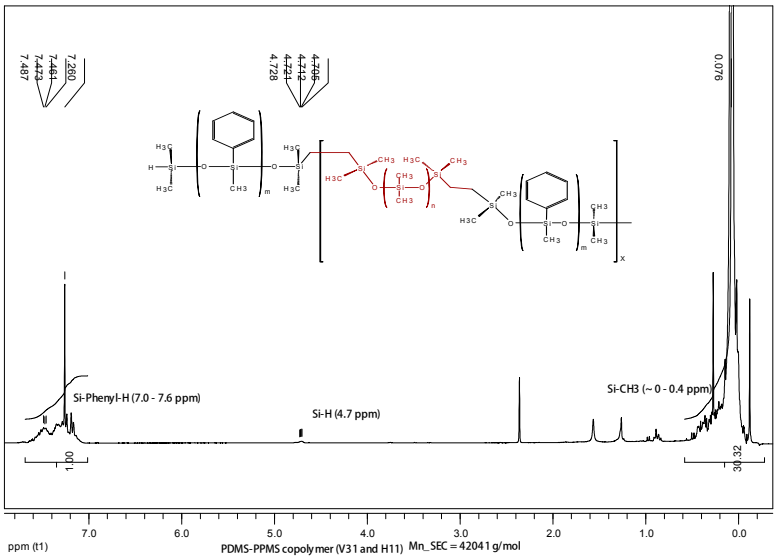

Figure S6 The NMR for 377DMS_6PMS.

f) PDMS-PPMS copolymer (**231DMS_6PMS**, $C_{C_6H_6}$ = 9.8 × 10^{-4} mol g^{-1})

^{1}H-NMR ($CDCl_3$, 300 MHz): δ -0.02 - δ 0.6 (m, 6 H's, -SiO(C**H$_3$**)$_2$-), δ 4.70 (m, 1 H, -Si**H**-), δ 7.10 - δ 7.60 (m, 5 H's, -SiC$_6$**H$_5$**-).

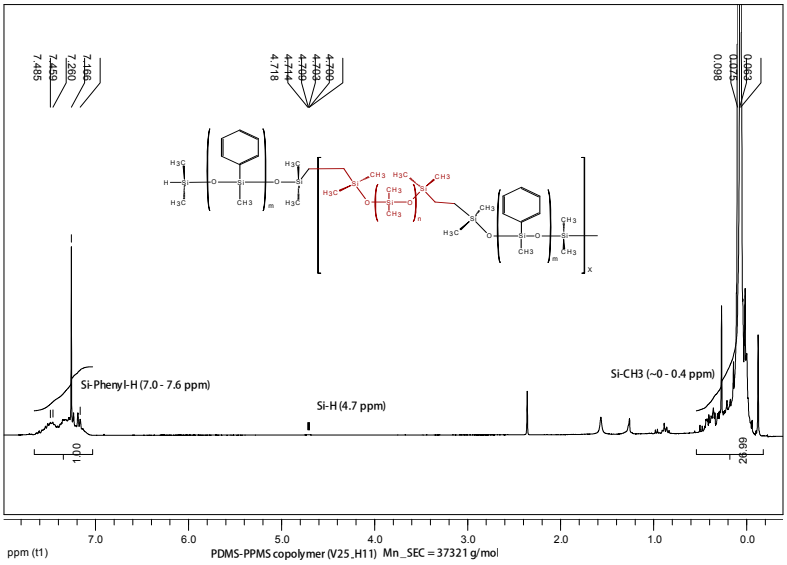

Figure S7 The NMR for 231DMS_6PMS.

g) PDMS-PPMS copolymer (**126DMS_6PMS**, $C_{C_6H_6}$ = 1.5 × 10^{-3} mol g^{-1})

^{1}H-NMR ($CDCl_3$, 300 MHz): δ -0.02 - δ 0.6 (m, 6 H's, -SiO(C**H$_3$**)$_2$-), δ 4.70 (m, 1 H, -Si**H**-), δ 7.10 - δ 7.60 (m, 5 H's, -SiC$_6$**H$_5$**-).

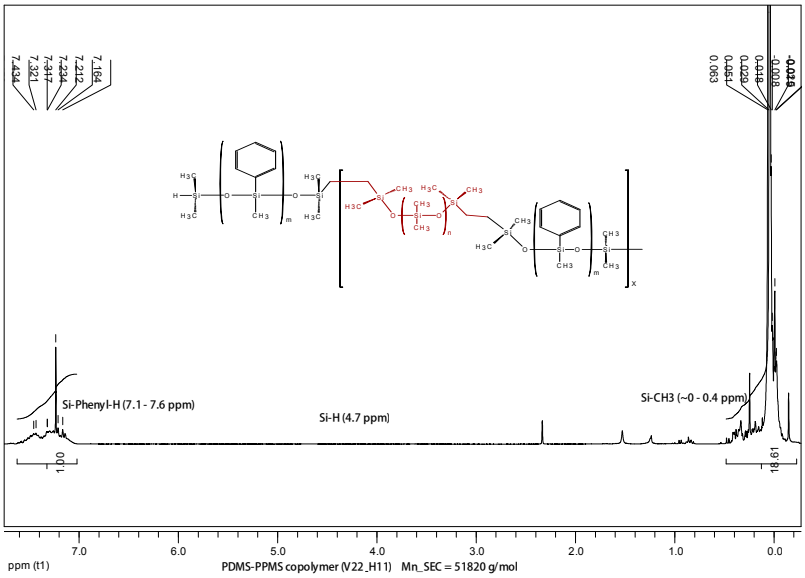

Figure S8 The NMR for 126DMS_6PMS.

h) PDMS-PPMS copolymer (**80DMS_6PMS**, $C_{C_6H_6}$ = 2.0 × 10^{-3} mol g^{-1})

^{1}H-NMR ($CDCl_3$, 300 MHz): δ -0.02 - δ 0.6 (m, 6 H's, -SiO(C**H$_3$**)$_2$-), δ 4.70 (m, 1 H, -Si**H**-), δ 7.10 - δ 7.60 (m, 5 H's, -SiC$_6$**H$_5$**-).

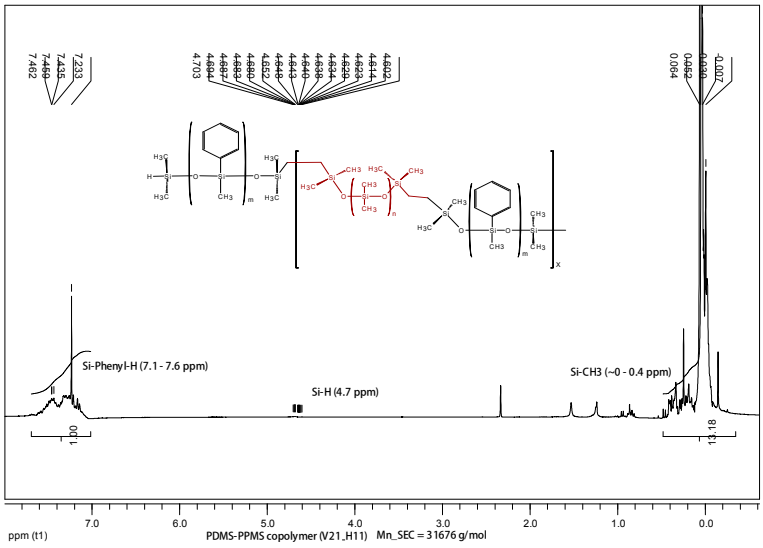

Figure S9 The NMR for 80DMS_6PMS.

6) Scanning electron microscopy (SEM) images for the cross-linked copolymers and the reference

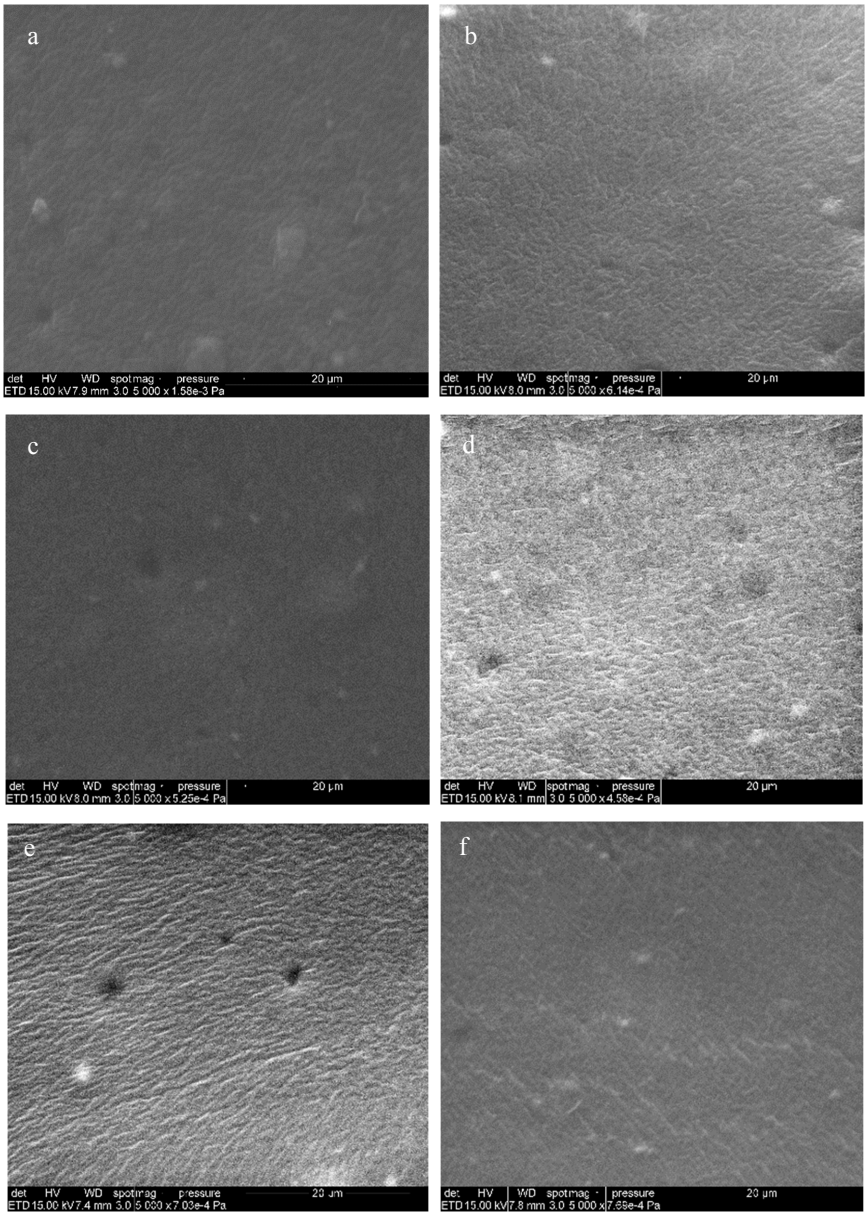

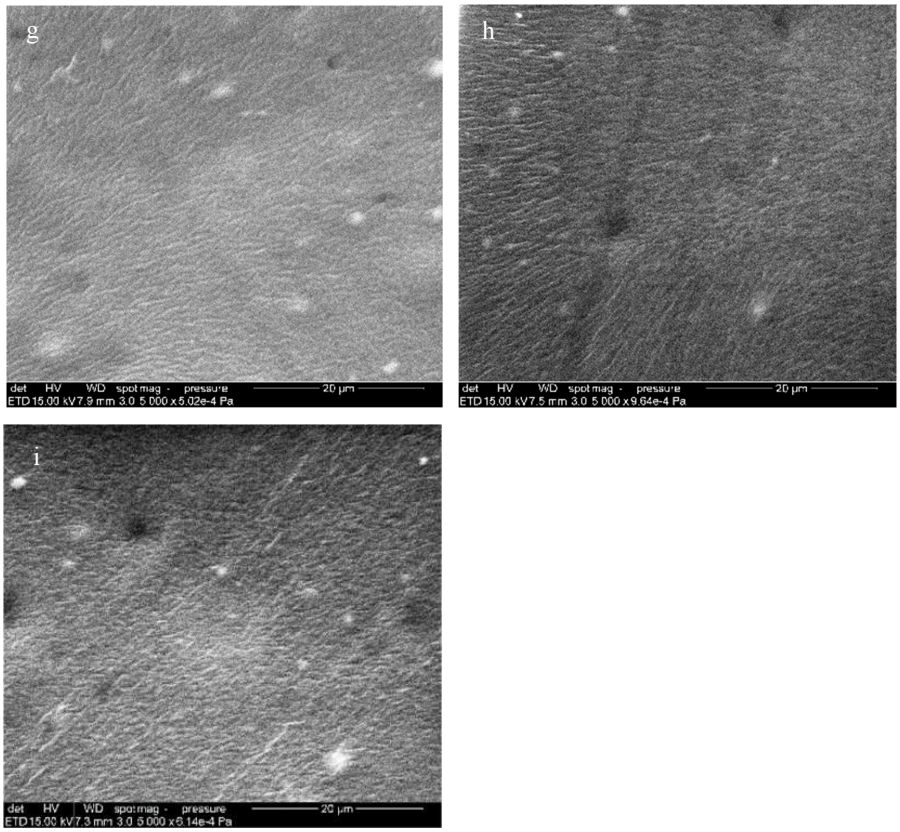

Figure S10 SEM images of: **a**) DMS-H31 (*C*=0), **b**) 377DMS_2PMS (*C*=5.0), **c**) 231DMS_2PMS (*C*=6.9), **d**) 126DMS_2PMS (*C*=7.8), **e**) 80DMS_2PMS (*C*=8.4), **f**) 377DMS_6PMS (*C*=8.7), **g**) 231DMS_6PMS (*C*=9.8), **h**) 126DMS_6PMS (*C*=15), and **i**) 80DMS_6PMS (*C*=20), *C* is in 10^{-4} g/mol.

7) Electrical breakdown strengths as function of Young's moduli for the cross-linked PDMS-PPMS copolymers and the reference elastomer

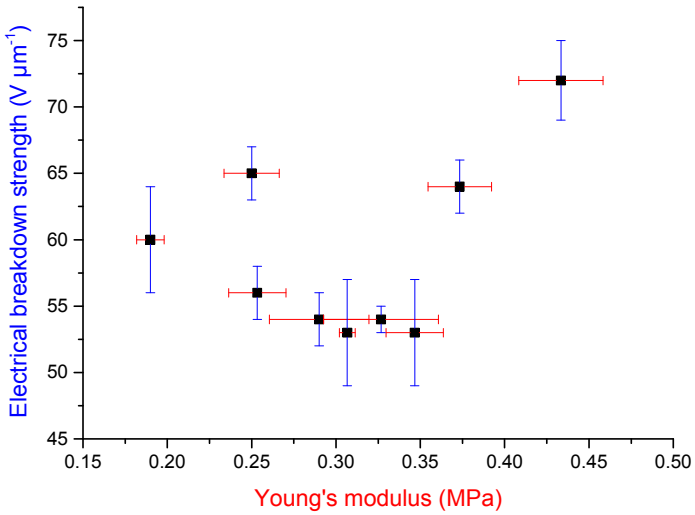

Figure S11 A plot of electrical breakdown strengths versus Young's moduli.

8) Weibull parameters *η* and *β* as function of Young's moduli for the cross-linked PDMS-PPMS copolymers and the reference elastomer

The curves of Weibull parameters *η* and *β* versus determined Young's moduli for the cross-linked copolymers and the reference are shown in Figure S12. Figure S12 (a) shows an optimum of *β*-parameter (60) occurring at Young's modulus of 0.33 MPa. For *η*-parameter, the optimum occurs at the highest Young's modulus of 0.43 MPa (see Figure S12 (b)).

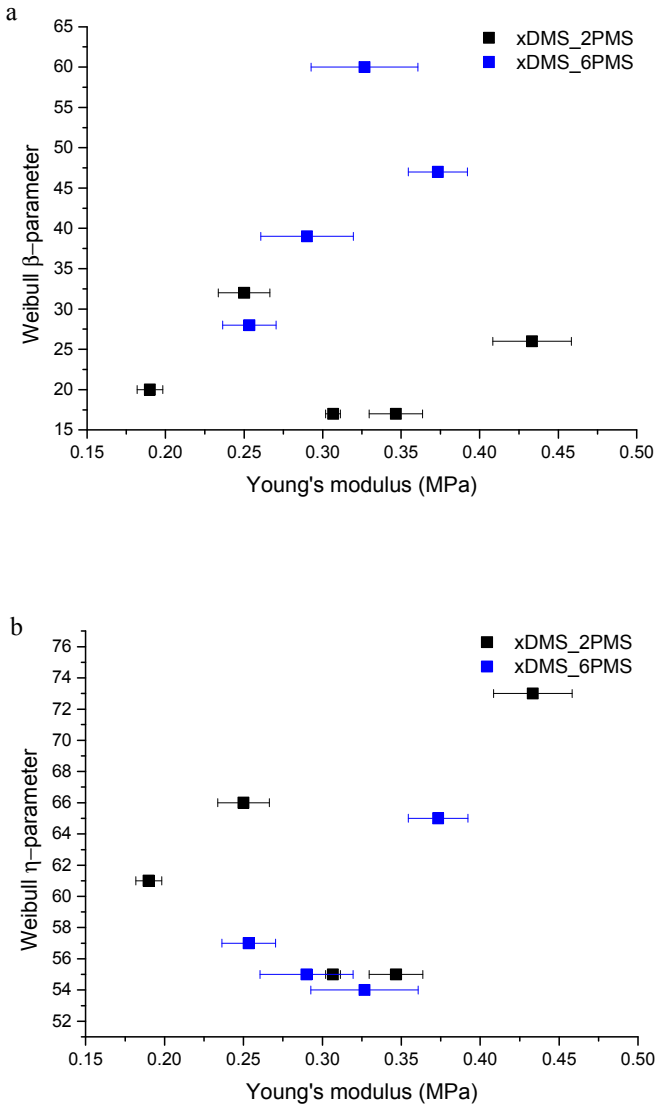

Figure S12 Weibull parameters versus Young's moduli: a) *β*-parameter, b) *η*-parameter.

9) Theoretical molar concentration of phenyl group

The numbers of phenyl groups in PPMS with $M_{n,PPMS}$ of 400 and 1000 g mol^{-1}, respectively, are given by:

$$m^* = \frac{M_{n,PPMS} - 2M_{end}}{M_{PMS}}$$

Equation 13

where M_{PMS} and M_{end} are molecular weights of phenylmethylsiloxane unit (M_{PMS} = 136 g mol^{-1}) and telechelic hydride groups, Si(CH$_3$)$_2$-H, (M_{end} = 56 g mol^{-1}), respectively. Thus a cross-linked PDMS-PPMS copolymer containing short- and long-chain PPMS are defined as m* = 2 and 6, respectively.

The theoretical molar concentration of phenyl groups in cross-linked PDMS-PPMS copolymers C_{t,C_6H_6} in mol g^{-1} was determined as:

$$C_{t,C_6H_6} = \frac{m^* \cdot n_{PPMS}}{m_{PPMS} + m_{PDMS}} = \frac{m^* \cdot n_{PPMS}}{n_{PPMS} \cdot M_{n,PPMS} + n_{PDMS} \cdot M_{n,PDMS}}$$

Equation 14

where m_{PPMS} and m_{PDMS} are masses of PPMS and PDMS, respectively, while n_{PPMS} and n_{PDMS} are molar amounts.

The molar amount of PPMS is expressed as $n_{PPMS} = (X + 1)n_{PDMS}$ and Equation 14 can be simplified as follows:

$$C_{t,C_6H_6} = \frac{m^* \cdot (X + 1)}{(X + 1)M_{n,PPMS} + M_{n,PDMS}}$$

Equation 15

The simplified theoretical molar concentrations of phenyl group in PDMS-PPMS can be calculated below:

$$C_{t,C_6H_6} = \frac{m^*}{M_{n,PPMS} + (X + 1)^{-1}M_{n,PDMS}}$$

Equation 16

Samples with different theoretical molar concentrations of phenyl groups in PDMS-PPMS copolymer are listed in Table S1:

Table S1 Theoretical phenyl concentrations of cross-linked PDMS-PPMS copolymers.

PDMS-PPMS copolymer (*n*DMS_*m*PMS)	Theoretical molar concentration of phenyl groups C_{t,C_6H_6} [10^{-4} mol g^{-1}]
377DMS_2PMS	1.3
231DMS_2PMS	1.6
126DMS_2PMS	2.3
80DMS_2PMS	3.5
377DMS_6PMS	3.7
231DMS_6PMS	5.6
126DMS_6PMS	7.3
80DMS_6PMS	11

10) UV/Vis spectra of the cross-linked copolymers and the reference elastomer

The absorption spectra of energy from UV/Vis light absorbed by different concentrations of phenyl group are shown in Figure S13. The phenyl group of the cross-linked copolymers absorbs UV/Vis light in the energy band of 4.5 – 5.5 eV as seen from the absorbance peaks.

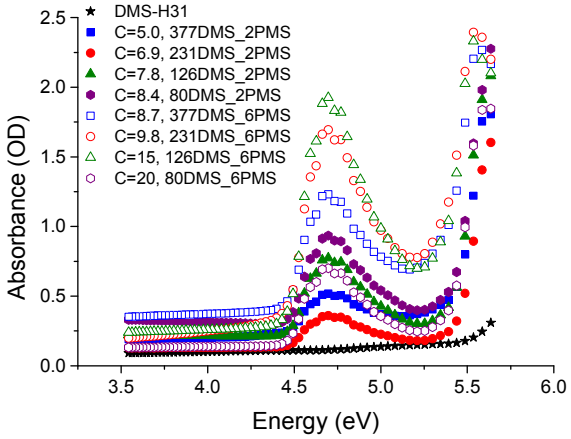

Figure S13 Spectra of UV/Vis absorption of PDMS elastomer and cross-linked PDMS-PPMS copolymers; *C* is in 10^{-4} mol g^{-1}.

Appendix III

A Razak AH, Yu L, Skov AL (2017) 'Voltage-stabilised elasotmers with increased relative permittivity and high electrical breakdown strength by means of phase separating binary copolymer blends in silicone elastomers' RSC Adv. (submitted)

RSC Advances

PAPER

View Article Online
View Journal | View Issue

Cite this: *RSC Adv.*, 2017, **7**, 17848

Voltage-stabilised elastomers with increased relative permittivity and high electrical breakdown strength by means of phase separating binary copolymer blends of silicone elastomers†

Aliff Hisyam A Razak,[ab] Liyun Yu[a] and Anne Ladegaard Skov*[a]

Received 3rd March 2017
Accepted 17th March 2017

DOI: 10.1039/c7ra02620j

rsc.li/rsc-advances

Increased electrical breakdown strength and increased dielectric permittivity of silicone-based dielectric elastomers are achieved by means of the addition of so-called voltage-stabilisers prepared from PDMS–PPMS copolymers as well as PDMS–PEG copolymers in order to compensate for the negative effect of softness on electrical stability of silicone elastomers. The voltage-stabilised elastomer, incorporating a high-permittivity PDMS–PEG copolymer, possesses increased relative permittivity, high electrical breakdown strength, excellent network integrity and low dielectric loss and paves the way towards specialised silicone elastomers for dielectric elastomer transducer products with inherent softness and electrical stability, and thus increased actuation at a given voltage.

1 Introduction

Silicone-based dielectric elastomers (DEs) possess a low Young's modulus, *i.e.* they are inherently soft and excellent for utilisation as dielectric actuators.[1,2] In order to achieve larger actuation strains at any given voltage, silicone DEs must possess increased relative permittivity combined with increased softness. However, the combination of softness and increased permittivity is not always simple.[3] For instance, a silicone elastomer incorporating metal oxide fillers has increased dielectric permittivity, but this results in a stiff elastomer due to strong particle–particle interactions.[4] Thus the electro-mechanical response is not improved. Furthermore the electrical breakdown strength depends on the Young's modulus, such that increased softness will decrease the electrical breakdown strength as well as the electromechanical stability being negatively influenced.[1,5]

Increased relative permittivity is often sought as the primary source for improved actuation, with approaches including integrating highly polarisable fillers,[4,6–9] covalent grafting of dipoles to the silicone backbone[10–13] and phase-separating systems containing high-permittivity liquids or copolymers.[14–16] Besides enhancing relative permittivity, the optimisation of silicone DEs with respect to largest achievable actuation strains can be done by enhancing electrical breakdown strength. For an improvement in this regard, approaches include elastomers incorporating either metal oxide fillers[17] or additives with a voltage-stabilising effect.[18–20] Furthermore, silicone elastomers containing phenyl groups have been shown to possess increased electrical breakdown strength *via* voltage stabilisation due to an electron trapping effect.[21] The voltage-stabilised silicone elastomer is prepared from a polydimethylsiloxane–polyphenylmethylsiloxane (PDMS–PPMS) copolymer, which is subsequently cross-linked. The cross-linked PDMS–PPMS copolymer phase separates microscopically, due to immiscibility between PPMS and PDMS. This microscopic phase separation in cross-linked PDMS–PPMS copolymers has been proven favourable with respect to electrical properties.[21]

Phase separation is commonly known to occur in polymer blends and block copolymers. Polymer blends phase separate due to the immiscibility of the polymers as a result of minimising free energy when the polymers separate.[22,23] Thermoplastic polymer blends possess different types of well-defined structures, such as bi-continuous structures,[23–25] islands[23] and holes,[23] and these phase-separated structures depend strongly on the volume fraction of the constituents in the polymer blends. A silicone elastomer prepared from a binary polymer blend consisting of a conducting PDMS–PEG copolymer and non-conducting PDMS was shown to result in the creation of a continuous phase of PDMS and a discontinuous phase of PEG.[16] Favourable phase morphologies in cross-linked blends can be achieved *via* proper blending and preparation methods.

Previous work on incorporating PDMS–PEG copolymers in commercial silicone elastomer[16] has resulted in elastomers with increased dielectric relative permittivity without compromising the inherent softness of the silicone elastomer. However, the electrical breakdown strength of such elastomers is comparable

[a]*Danish Polymer Center, Department of Chemical and Biochemical Engineering, Technical University of Denmark, Building 227, 2800 Kgs. Lyngby, Denmark. E-mail: al@kt.dtu.dk; Web: http://www.dpc.kt.dtu.dk/; Fax: +45 45882258; Tel: +45 45252825*

[b]*Faculty of Engineering Technology, University of Tun Hussein Onn Malaysia, 86400 Parit Raja, Batu Pahat, Johor, Malaysia*

† Electronic supplementary information (ESI) available. See DOI: 10.1039/c7ra02620j

to that of the commercial elastomer or slightly less. Voltage stabilization resulting in increased breakdown strength has been achieved by formulation of silicone elastomers with PDMS–PPMS and thus paves the way towards specially designed elastomers with high electrical stability.[21] Hence incorporating a relative permittivity enhancer such as PDMS–PEG copolymer in a voltage-stabilised silicone elastomer may show the favourable combination of high dielectric permittivity and high electrical breakdown strength.

In this work, phase separation as a means of optimising silicone elastomers is explored further by combining two recently synthesised copolymers (PDMS–PEG and PDMS–PPMS copolymers), which have been shown to enhance relative permittivity and electrical breakdown strength, respectively.

2 Experimental

2.1 Materials and methods

Telechelic vinyl-terminated polydimethylsiloxanes and telechelic hydride-terminated polyphenylmethylsiloxanes (used in the synthesis of a PDMS–PPMS copolymer) were DMS-V21 and PMS-H03, with an average molecular weight (M_n) of 6000 and 400 g mol^{-1}, respectively. In the synthesis of the PDMS–PEG copolymer, telechelic hydride-terminated polydimethylsiloxanes (H-PDMS) were DMS-H21, DMS-H11, DMS-H03 and SIH6117.0, with M_n of 6000, 1050, 550 and 208 g mol^{-1}, respectively. All of the abovementioned PDMS copolymers were purchased from Gelest Inc. The catalyst was platinum-divinyl-tetramethyl disiloxane complex [SIP6830.3], containing 3.25% of platinum in xylene, and the cross-linkers were vinyl-functional (4–5% vinylmethylsiloxane)-dimethylsiloxane copolymers [VDT-431] (M_n = 28 kg mol^{-1}, 15-functional) and hydride-functional (45–55% methylhydrosiloxane)-dimethylsiloxane copolymers [HMS-501] (M_n = 1050 g mol^{-1}, 9-functional). Both the catalyst and the cross-linkers were purchased from Gelest Inc. Telechelic vinyl-terminated polyethyleneglycol (V-PEG) was acquired from Sigma Aldrich. Fumed silica (SIS6962.0) and volatile methylsiloxane (VMS) [OS-20] were purchased from Fluorochem and Dow Corning, respectively.

The synthesised copolymers were synthesized from telechelic hydride-functional PDMS–PPMS copolymers and telechelic vinyl-functional PDMS–PEG copolymers. The degrees of conversion for the vinyl and hydride PDMS groups from the hydrosilylation reactions of the hydride-terminated PPMS and vinyl-terminated PDMS, and the hydride-terminated PDMS and vinyl-terminated PEG, respectively, were determined through proton nuclear magnetic resonance spectroscopy (^{1}H-NMR), which was performed on a Bruker 300 MHz NMR. The full conversion of hydride and vinyl groups during hydrosilylation reactions was monitored by observing the disappearance of hydride and vinyl peaks. The number of scannings per sample was 128, and sample concentration was 100 mg mL^{-1} in deuterated chloroform ($CDCl_3$).

The numbers of average molecular weights (M_n) of the copolymers were determined *via* size-exclusive chromatography (SEC), which was performed on a Viscotek GPCmax VE-2001 instrument equipped with a Viscotek TriSEC Model 302 triple detector, using two PLgel mixed-D columns from Polymer Laboratories. Solutions for SEC containing copolymers dissolved in toluene were prepared in a concentration of 2–3 mg mL^{-1} and were run at 35 °C at an elution rate of 1 mL min^{-1}. The software for molecular weight distributions was WinGPC Unity 7.4.0 and linear PDMS standards acquired from Polymer Standards Service GmbH.

Measurement of the electrical breakdown strength of thin films with a thickness of less than 135 μm was performed on an in-house-built device based on international standards (IEC 60243-1 (1998) and IEC 60243-2 (2001)). The film was placed on a plastic frame containing 12 holes and subsequently was slid between two metal electrodes which were hemi-spherical and 20 mm in diameter. For each sample, the electrical breakdown strength was measured and repeated 12 times, with a stepwise increasing voltage of 50–100 V per step applied at a rate of 0.5–1 steps s^{-1}. The average electrical breakdown strength from 12 measurements was then quantified as the electrical breakdown strength.

Dielectric properties were measured by dielectric spectroscopy, which was performed on a Novocontrol Alpha-A high-performance frequency analyser (Novo-control Technologies GmbH & Co. KG, Germany). Prior to dielectric measurement, the sample, approximately 1 mm thick, was sandwiched between two gold-coated plates. Dielectric measurement was operated in the frequency range 10^{-1} to 10^6 Hz at 23 °C, using an electrode diameter of 20 mm.

For linear viscoelasticity (LVE) properties, prepared films with a 25 mm in diameter were characterised at 23 °C, using an advanced rotational rheometer from TA Instruments (ARES-G2) by means of a parallel plate with a diameter of 25 mm. The axial force ranged from 5 to 12 N for sufficient contact between the plate and the sample. LVE properties were measured in the linear regime at a strain and a frequency of 2% and 10^{-2} to 10^2 Hz, respectively.

For stress–strain relationships, ultimate strengths and ultimate strains, as well as the Young's moduli at 5% strain, were measured in extensional rheological tests performed on an ARES-G2 rheometer using a SER2 universal testing platform consisting of two rotating drums 10.3 mm in diameter. The lateral offset of the centre axis of the two rotating drums was 12.7 mm. The sample was prepared in the following dimensions: 6 mm (width), 30 mm (length) and 1 mm (thickness). The ends of the sample were secured by means of strong glue to the surfaces of the rotating drums and then elongated within a confined length by winding up the sample with two rotary drums. Engineering strain and stress were used in the stress–strain relationship and were calculated from the measured Hencky strains and from the measured torque over the cross-sectional area of the sample, respectively (refer to ESI 1, eqn (1)–(5)† for details on engineering stress and strain).

The morphologies of prepared elastomers and the reference elastomer were inspected *via* scanning electron microscopy (SEM) images, which were performed on an FEI Quanta 200 ESEM FEG. Cross-sectional SEM samples were coated in 2 nm-thick gold by means of a sputter coater (Cressington, model 208HR) under vacuum conditions and a current of 10 mA. A

field emission gun with an accelerating voltage between 500 V and 30 kV was applied to detect the element distribution profile on the surface of the samples.

2.2 PDMS–PPMS copolymer synthesis

The procedure used to synthesise the PDMS–PPMS copolymer was taken from A Razak and Skov.[21] PDMS–PPMS copolymers were prepared through the hydrosilylation of hydride-terminated PPMS and vinyl-terminated PDMS, as illustrated in Scheme 1. The synthesised copolymer was telechelic hydride-functional. The theoretical number of PDMS–PPMS repeating units in the copolymer (X_1) was calculated from the targeted M_n of 30 kg mol^{-1}. The mixture containing DMS-V21, PMS-H03 and a 30 ppm Pt catalyst was speed-mixed at 3000 rpm for 5 min. The stoichiometric ratio for preparing the PDMS–PPMS copolymer (r_1) was calculated from the ratio (X_1 + 1) to X_1.[21]

2.3 Synthesis of PDMS–PEG copolymers

PDMS–PEG copolymers were synthesised as described by A Razak *et al.*[16] The theoretical number of PDMS–PEG repeating units in the copolymer (X_2) was calculated from M_n of 30 kg mol^{-1}. The stoichiometric ratio for preparing the PDMS–PEG copolymers (r_2) was calculated from the ratio (X_2 + 1) to X_2.[16] The synthesis of the PDMS–PEG copolymer was based on the hydrosilylation of hydride-terminated PDMS and vinyl-terminated PEG, as shown in Scheme 2. The synthesised PDMS–PEG copolymers were telechelic vinyl-functional.

Various volume fractions of PDMS in the PDMS–PEG copolymer were obtained by varying PDMS chain lengths, *i.e.* repeating PDMS units (m_2) were varied such that m_2 = 3, 7, 14, 81, while the number of repeating PEG units remained constant (n_2 = 4). The synthesised copolymers were named PDMS3–PEG, PDMS7–PEG, PDMS14–PEG and PDMS81–PEG, respectively.

2.4 Binary copolymer blends and sample preparations

PDMS–PEG copolymers were incorporated into a PDMS–PPMS copolymer in concentrations of 10 and 20 phr before being speed-mixed at 3500 rpm for 2 minutes. The loadings of 10 and 20 phr are considered low and high loadings, respectively. One possible network is illustrated in Fig. 1, such that hydride-functional PDMS–PPMS copolymers may bond covalently to vinyl-functional PDMS–PEG copolymers to form double copolymers, while some of them may cross-link with vinyl-functional cross-linkers (VDT-431) and vinyl-functional PDMS–PEG copolymers cross-link with hydride-functional cross-linkers (HMS-501). The stoichiometric ratio for both cross-linking reactions between PDMS–PPMS and VDT-431, and between PDMS–PEG and HMS-501 were 1.5.[16,21] Blends containing copolymers, cross-linkers, 30 ppm of Pt catalyst, 25 parts per hundred rubber (phr) of silica and 25 phr of VMS solvent (OS-20 from Dow Corning) were speed-mixed at 3000 rpm for 4 minutes.

The final mixtures were cast on Teflon substrates for easy release, and the films were prepared at thicknesses of

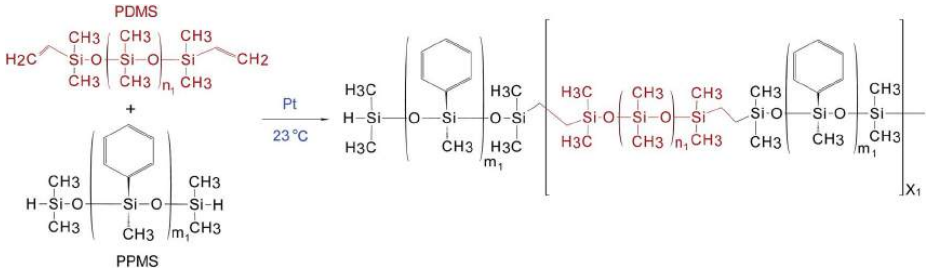

Scheme 1 The hydrosilylation reaction of a PDMS–PPMS copolymer, where m_1 is the number of repeating phenylmethylsiloxane (PMS) units in PPMS (m_1 = 2), and n_1 is the number of repeating dimethylsiloxane (DMS) units in PDMS (n_1 = 80).

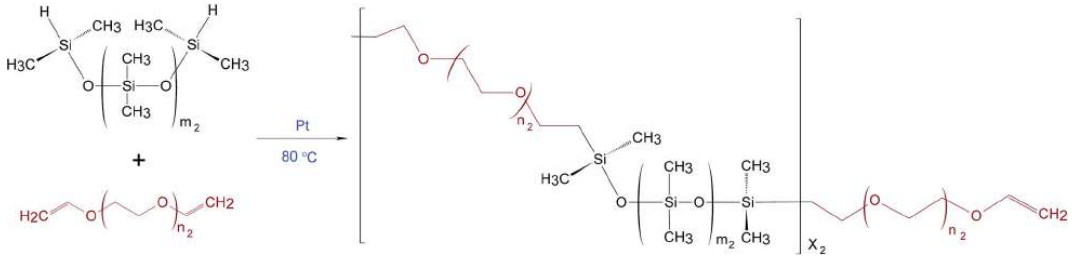

Scheme 2 Hydrosilylation reaction when synthesising a PDMS–PEG copolymer, where m_2 is the number of repeating DMS units in PDMS, n_2 = 4 is the constant number of repeating ethyleneglycol (EG) units in PEG.

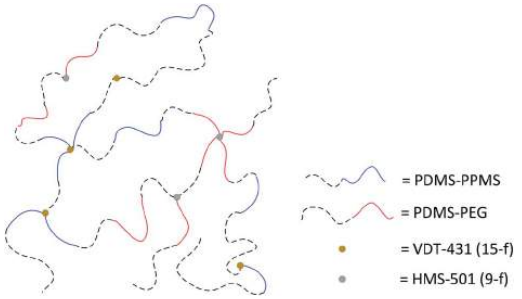

Fig. 1 Simplified illustration of the random network structure of PDMS–PPMS and PDMS–PEG copolymers, hydride-functional 9-functional and vinyl-functional 15-functional cross-linkers (HMS-501 and VDT-431, respectively). The cross-linkers are illustrated with fewer cross-linking sites than in the true network.

approximately 1 ± 0.5 mm and 100 ± 35 μm, as thick and thin films, respectively. Thin films were used for the measurement of electrical breakdown strength and thick films were used for measurements of linear viscoelasticity (LVE), the stress–strain relationship and dielectric properties. All films were placed in a vacuum oven at 23 °C for 2 hours and were subsequently cured at 40 °C for 12 hours for proper film formation. The samples were placed in the oven at 150 °C for 5–8 hours and subsequently post-cured at 200 °C for 2 hours.

The cross-linked PDMS–PPMS copolymer containing 80 repeating DMS units and two repeating PMS units, referred to as 80DMS_2PMS. 80DMS_2PMS, was used as the reference elastomer and was prepared without incorporating the PDMS–PEG copolymer. Due to its proven versatility as a voltage-stabilised silicone elastomer, 80DMS_2PMS was utilised in all prepared binary copolymer blends (BCBs). Furthermore, 80DMS_2PMS has been proven to possess the most increased electrical breakdown strength compared to other PDMS–PPMS elastomers.[21] Details of the cross-linked BCBs containing 80DMS_2PMS and PDMS–PEG copolymers, and the reference elastomer, are shown in Table 1.

Table 1 Sample details of cross-linked BCBs containing PDMS–PPMS and PDMS–PEG copolymers

	PDMS–PEG copolymer		
No.	Concentration (phr)	PDMS*xx*–PEG[a]	Samples
1	—	—	80DMS_2PMS (reference)
2	10	PDMS81–PEG	10 phr PDMS81–PEG BCB
3	20		20 phr PDMS81–PEG BCB
4	10	PDMS14–PEG	10 phr PDMS14–PEG BCB
5	20		20 phr PDMS14–PEG BCB
6	10	PDMS7–PEG	10 phr PDMS7–PEG BCB
7	20		20 phr PDMS7–PEG BCB
8	10	PDMS3–PEG	10 phr PDMS3–PEG BCB
9	20		20 phr PDMS3–PEG BCB

[a] *xx* is the PDMS chain length.

3 Results and discussion

A cross-linked binary copolymer blend consisting of PDMS–PPMS and PDMS–PEG copolymers can potentially assemble into several distinct morphologies or combinations thereof. The targeted morphology of the binary system of copolymer blends containing PDMS–PEG and PDMS–PPMS copolymers is a well-defined structure forming a continuous PDMS-rich phase and discontinuous phases of PEG and PPMS, as illustrated in Fig. 2. Alternatively no microscopic phase separation is desirable. However, with silicone polymers (and thus elastomers) this is very difficult – if not unrealistic – to achieve a completely homogeneous blend which is crosslinked into a likewise homogeneous network.

3.1 Synthesised PDMS–PPMS copolymer (80DMS_2PMS)

It has been shown previously that PDMS–PPMS copolymers possess excellent mechanical properties when they are cross-linked with a vinyl-functional cross-linker.[21] All vinyl groups of PDMS were consumed during the hydrosilylation of vinyl-terminated PDMS and hydride-terminated PPMS, which was confirmed by the disappearance of the Si–CH_2═CH_2 bond signal at 5.8–6.2 ppm in the ^{1}H-NMR spectra (refer to ESI 2 for NMR spectra in Fig. S1†). The synthesised PDMS–PPMS copolymer was telechelic hydride-functional. The determined molecular weight of 80DMS_2PMS was 32 kg mol^{-1}, while the molar concentration of phenyl groups of 80DMS_2PMS was 8.8 × 10^{-4} g mol^{-1}, determined from NMR integration areas.[21] A PDMS–PPMS copolymer containing a PDMS chain length of m_1 = 80 and a PPMS chain length of n_1 = 2 (80DMS_2PMS) was used in all cross-linked binary copolymer blends (BCBs), due to the highest electrical breakdown strength (E_{BD} = 72 V μm^{-1}) of the tested elastomers.

3.2 Synthesised PDMS–PEG copolymers

The disappearance of the Si–H bond signal at 4.70 ppm was checked by ^{1}H-NMR for a complete conversion of hydride PDMS groups in the hydrosilylation of hydride-terminated PDMS and vinyl-terminated PEG; refer to ESI 2 for NMR spectra in Fig. S2–S5.† Determined molecular weights from the SEC of PDMS–PEG copolymers PDMS81–PEG, PDMS14–PEG, PDMS7–PEG and PDMS3–PEG were 49, 29, 3 and 5 kg mol^{-1}, respectively.

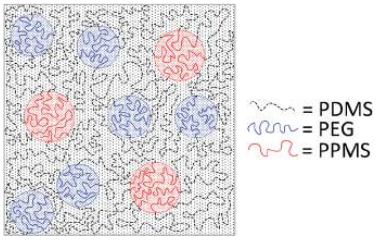

Fig. 2 Illustration of silicone copolymers prepared by phase-separation of PDMS–PEG copolymer in a PDMS–PPMS matrix by means of a binary system of copolymer blends.

3.3 Linear viscoelasticity

To evaluate the effect of loading different types of PDMS–PEG copolymers on viscoelastic properties, the prepared elastomers were characterised rheologically, as shown in Fig. 3. They are well cross-linked and behave elastically, *i.e.* the incorporation of PDMS–PEG copolymer into the BCB does not destabilise the PDMS–PPMS elastomers. The resulting storage moduli (G') for all prepared cross-linked BCBs and the reference are between 10^4 and 10^6 Pa. The cross-linked BCBs with 10 and 20 phr of PDMS81–PEG are the most rigid elastomers compared to other prepared elastomers and the reference elastomer, revealing that the elastomers have PEG-like properties, due to the semi-crystalline PEG acting as a reinforcing domain in the matrix. All prepared cross-linked BCBs and reference elastomer possess close-to-identical viscoelastic relaxations. Relative losses [tan(δ)] for all elastomers are low and are comparable to that of Elastosil RT625 (a commercial silicone elastomer from Wacker Chemie)[1] as well as that of the reference elastomer. It is obvious from Fig. 3 that all of the prepared elastomers maintain their network integrity in the small deformation regime.

3.4 Stress–strain relationship

Stress–strain curves and the Young's moduli of prepared samples are shown in Fig. 4 and Table 2, respectively. It is evident from Fig. 4 that all prepared samples and the reference elastomer have reduced their strain-hardening behaviour compared to the reference. The cross-linked BCBs with 10 and 20 phr of PDMS81–PEG show the most increased ultimate strain together with a stress-softening behaviour, indicating the irreversibility of the stress-behaviour of the thermoplastic part of the elastomer arising from the crystallinity of the PEG-rich domains (refer to Fig. 4). Furthermore, most elastomers mentioned herein possess higher or comparable ultimate strains than that of the VHB 4910 elastomer from 3 M, where VHB 4910 possesses an ultimate strain of 800%, as reported by Tugui *et al.*[26] On the other hand, the cross-linked BCB with 20 phr of PDMS14–PEG shows very low ultimate strain, indicating that the high loading of the PDMS14–PEG copolymer deteriorates network integrity, due to the macroscopic phase separation of PEG domains in the copolymer blend matrix.

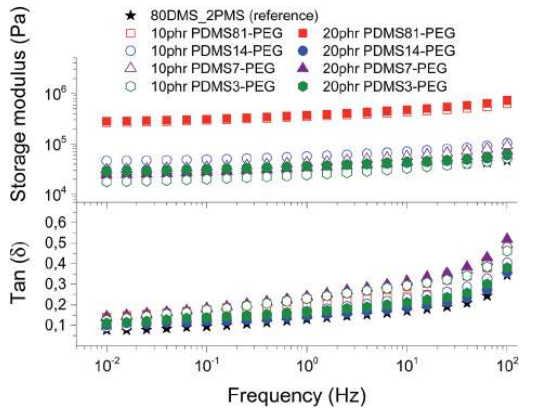

Fig. 3 The storage modulus and tan(δ) of prepared voltage-stabilised elastomers with different types and concentrations of PDMS–PEG copolymers at 23 °C.

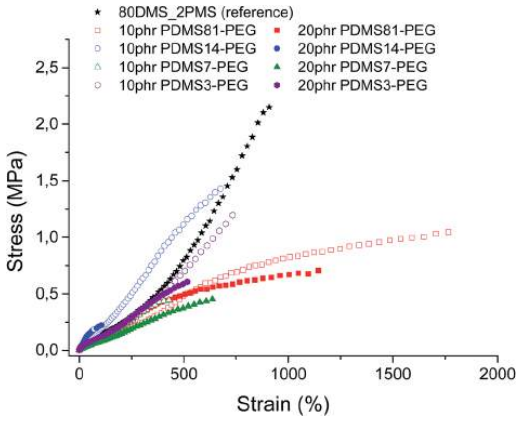

Fig. 4 Stress–strain curves for prepared cross-linked BCBs and the reference elastomer at 23 °C (standard deviations of ultimate strains and ultimate strengths were of order ±1–19% and ±3–16%, respectively).

All cross-linked BCBs show decreased ultimate strength compared to the reference elastomer. Cross-linking with 10 phr of PDMS14–PEG results in the most increased ultimate stress compared to other cross-linked BCBs, due to semi-crystalline PEGs acting as reinforcing domains.

Obviously, the resulting Young's moduli of all cross-linked BCBs are low, as well as that of the reference elastomer, as shown in Table 2. In comparison to the commercial silicone elastomer (RT625 from Wacker Chemie, $Y = 1$ MPa), all cross-linked BCBs and the reference elastomer are softer.

3.5 Dielectric properties

The conductivity and dielectric properties of the prepared elastomers are shown in Fig. 5 and 6, respectively. The resulting

Table 2 Young's moduli for cross-linked BCBs and reference elastomer

Sample	Young's modulus, Y (MPa)
0 phr PDMS–PEG (reference)	0.41 ± 0.05
10 phr PDMS81–PEG BCB	0.45 ± 0.08
20 phr PDMS81–PEG BCB	0.25 ± 0.05
10 phr PDMS14–PEG BCB	0.43 ± 0.05
20 phr PDMS14–PEG BCB	0.58 ± 0.13
10 phr PDMS7–PEG BCB	0.30 ± 0.10
20 phr PDMS7–PEG BCB	0.21 ± 0.03
10 phr PDMS3–PEG BCB	0.34 ± 0.06
20 phr PDMS3–PEG BCB	0.36 ± 0.05

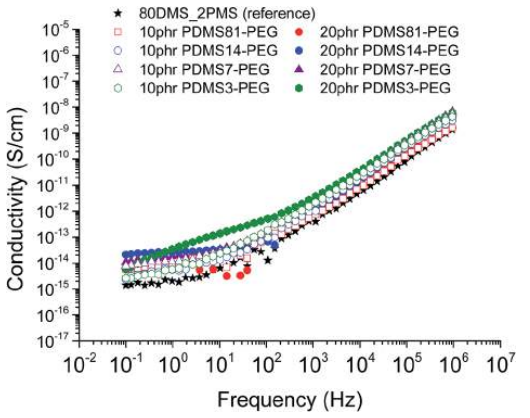

Fig. 5 The conductivity of 80DMS_2PMS elastomers with different concentrations of PDMS–PEG copolymers at 23 °C.

conductivities indicate that none of elastomers is conductive. The resulting conductivity of the cross-linked BCB with 20 phr of PDMS3–PEG indicates increased relaxation occurring at the frequencies 10^0 to 10^2 Hz, compared to other cross-linked BCBs and the reference elastomer, which may indicate a local phase separation of PEG-rich domains.

The resulting relative permittivity for the prepared elastomers with a low loading (10 phr) of PDMS–PEG copolymers is lower than the reference elastomer, except the cross-linked BCBs with 10 phr of PDMS7–PEG, which shows increased relative permittivity, improving by 27%. For the prepared elastomers with a high loading (20 phr) of PDMS–PEG copolymers, the relative permittivities are almost higher than the reference elastomer, whereby the cross-linked copolymer with 20 phr of PDMS7–PEG has the highest relative permittivity. Fig. 6 clearly shows that the cross-linked copolymers with low and high loadings of PDMS7–PEG possess increased relative permittivity, compared to the other elastomers and the reference. The phase separation of PDMS–PEG copolymers in the PDMS–PPMS matrix seems to occur on the micro- or nanoscopic scale, since the elastomers are macroscopically homogenous, as observed from light microscopy.

Dielectric losses, here represented by tan(δ), are relatively low for all cross-linked copolymers as well as the reference elastomer (see Fig. 6). Similar to the relaxation in Fig. 5, the cross-linked BCB with 20 phr of PDMS3–PEG shows increased relaxation occurring at the same frequency.

SEM imaging shows obviously different morphologies for prepared elastomers, as illustrated in Fig. 7. The SEM image of the cross-linked BCB with 20 phr of PDMS7–PEG shows clearly distinct PEG rich domains (white circles), which are well-distributed in the PDMS matrix, thereby indicating that a homogeneous elastomer on the macroscopic scale has been obtained (see Fig. 7b). On the other hand, SEM imaging of the reference elastomer shows the presence of PDMS and PPMS rich domains in the matrix (see Fig. 7a). Furthermore, the reference elastomer has a triangular pattern (PDMS rich domain) and that of a bent rectangle (PPMS rich domain), which is agrees with the SEM image of the cross-linked PDMS–PPMS copolymer[21] (see Fig. 7a). Other SEM images of prepared elastomers, which show different morphologies, can be seen in ESI 3, Fig. S6.†

For the reference elastomer, the PDMS-rich domains enhance elastomer softness, whilst PPMS domains which act as rigid zones reinforce the network, thus resulting in an elastomer with increased ultimate stress and increased ultimate strain, as shown in Table 3.

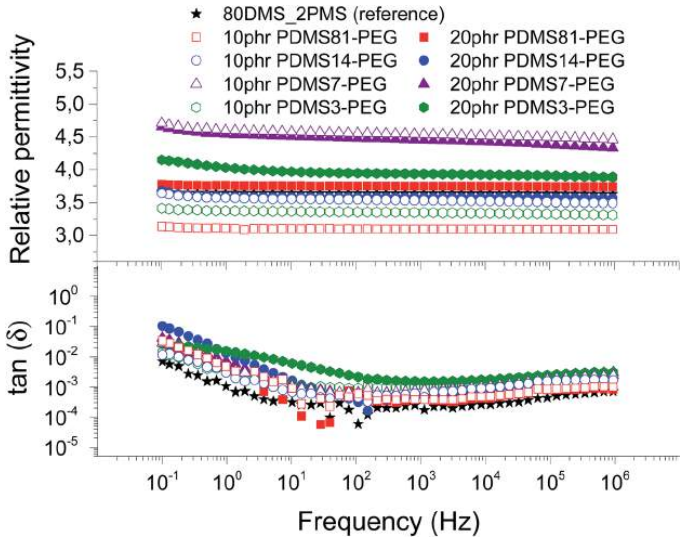

Fig. 6 The dielectric properties of 80DMS_2PMS elastomers with different concentrations of PDMS–PEG copolymers at 23 °C.

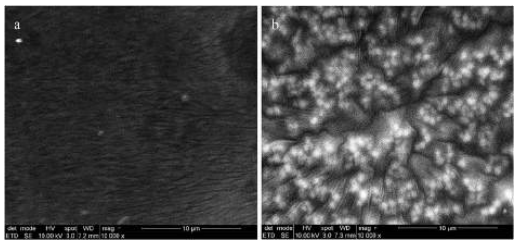

Fig. 7 SEM pictures of two representative samples, namely (a) 80DMS_2PMS (reference elastomer) and (b) binary copolymer blends with 20 phr of PDMS7–PEG.

3.6 Electrical breakdown and Weibull analysis

The influence of the different PDMS–PEG copolymer and their concentrations in cross-linked BCBs on electrical breakdown strength was investigated. The thicknesses of the prepared samples were in the range of 81 to 135 μm. The resulting electrical breakdown strengths of prepared elastomers incorporating PDMS–PEG copolymers are shown in Table 4. The cross-linked BCBs with 10 and 20 phr of PDMS14–PEG possess the highest electrical breakdown strength, namely 80 ± 5 and 81 ± 18 V μm^{-1}, respectively, improving by approximately 10% compared to the reference elastomer. Increased electrical breakdown is most likely due to the synergistic effect of the favourable phase separation of PEG and voltage stabilisation. Moreover, the cross-linked BCBs with PDMS7–PEG and PDMS3–PEG with a loading of 20 phr possess increased electrical breakdown strength compared to the reference elastomer. Clearly, the incorporation of PDMS81–PEG in the BCB decreases electrical breakdown strength (see Table 4), which indicates that PDMS81–PEG may destabilise voltage stabilisation and hence deteriorate the charge trapping effect caused by the π-electrons of phenyl groups.

The electrical reliability of the prepared elastomers was investigated *via* Weibull analysis. The β-parameter, the Weibull shape parameter, was determined from the slope of the Weibull plot of failure probability *versus* electrical breakdown strength. The η-parameter, the Weibull scale parameter, was determined at the point at which failure probability, $\ln[-\ln(1 - F)]$, was 63.2%.[16] Due to different film thicknesses, the determined electrical breakdown strengths were normalised, based on a reference thickness for better comparison. Normalised dielectric breakdown strengths were calculated using the equation of normalised electrical breakdown strength verified by Zakaria *et al.*[27] The reference thickness for normalisation was 100 μm. The results for the Weibull η- and β-parameters, R^2 of the linear fits for cross-linked copolymers and normalised electrical breakdown strength are presented in Table 4. The values of the coefficient of determination (R^2) for all investigated elastomers are above 0.80, excluding elastomers with 10 phr of PDMS7–PEG and 20 phr of PDMS3–PEG. A coefficient of determination above 0.85 indicates that the measured electrical breakdown strength correlates well with the fitted regression lines.[21] Cross-linked BCBs with 20 phr of PDMS81–PEG, 10 and 20 phr of PDMS7–PEG, 20 phr of PDMS3–PEG and the reference elastomer possess a high β-parameter, thereby indicating that electrical breakdown occurrences are narrowly dispersed and hence homogenous elastomers are obtained. The β-parameters of elastomers with the most increased electrical breakdown strength (10 and 20 phr of PDMS14–PEG BCBs) are lower than the β-parameter of the reference elastomer.

Thus far, combining the results for relative permittivity, electrical breakdown strength and Young's modulus, the cross-linked BCB with 20 phr of PDMS7–PEG possesses the most enhanced electrical properties ($\varepsilon_r = 4.66$, $E_{BD} = 76 \pm 3$ V μm^{-1}) as well as inherent softness ($Y = 0.21 \pm 0.03$ MPa). This elastomer is also the only investigated elastomer formulation which shows overall excellent properties and it gives a very clear indication of the complicated interplay of nano-scopic phase separation and electro-mechanical properties.

Increased electrical breakdown strength may have been established as the result of either an increased Young's modulus[17] or voltage stabilisation.[21] Further investigation into electrical breakdown was performed to evaluate whether increased electrical breakdown strength is the effect of changes in other properties, *e.g.* increased stiffness, increased relative permittivity or increased stretchability. The influences of the Young's modulus and relative permittivity on electrical breakdown strength are shown in Fig. 8, and 9. No obvious trend can been seen in Fig. 8 for increased electrical breakdown strength as a function of elastic modulus, indicating strongly that the increased electrical breakdown strength of all prepared elastomers is due to the synergistic effect of voltage stabilisation and/

Table 3 Relative permittivity and mechanical properties of prepared cross-linked BCBs and the reference elastomer

Sample	Young's modulus (MPa)	Relative permittivity	Ultimate stress (MPa)	Ultimate strain (%)
80DMS_2PMS (reference)	0.41 ± 0.05	3.71	1.86 ± 0.31	967 ± 33
10 phr PDMS81–PEG BCB	0.45 ± 0.08	3.14	1.10 ± 0.10	1748 ± 40
20 phr PDMS81–PEG BCB	0.25 ± 0.05	3.78	0.74 ± 0.02	1164 ± 17
10 phr PDMS14–PEG BCB	0.43 ± 0.05	3.64	1.57 ± 0.12	635 ± 52
20 phr PDMS14–PEG BCB	0.58 ± 0.13	3.67	0.25 ± 0.03	104 ± 1
10 phr PDMS7–PEG BCB	0.30 ± 0.10	4.71	0.40 ± 0.03	431 ± 19
20 phr PDMS7–PEG BCB	0.21 ± 0.03	4.66	0.42 ± 0.04	552 ± 103
10 phr PDMS3–PEG BCB	0.34 ± 0.06	3.41	1.14 ± 0.10	724 ± 40
20 phr PDMS3–PEG BCB	0.36 ± 0.05	4.15	0.56 ± 0.03	491 ± 43

Table 4 Electrical breakdown strength at 23 °C, Weibull parameters η and β and R^2 of the linear fit for all prepared cross-linked copolymers and the reference

Cross-linked PDMS–PPMS copolymer (80DMS_2PMS)	Electrical breakdown strength (V μm^{-1})	Weibull β-parameter	Weibull η-parameter	R^2	Normalised electrical breakdown strength
0 phr PDMS–PEG (reference)	72 ± 3	26	73	0.93	71.9 ± 3.1
10 phr PDMS81–PEG	61 ± 8	9	64	0.89	61.1 ± 7.8
20 phr PDMS81–PEG	54 ± 2	36	55	0.96	54.3 ± 1.7
10 phr PDMS14–PEG	80 ± 5	19	82	0.84	80.5 ± 5.2
20 phr PDMS14–PEG	81 ± 18	5	88	0.93	82.9 ± 18.8
10 phr PDMS7–PEG	64 ± 2	38	65	0.70	64.3 ± 2.3
20 phr PDMS7–PEG	76 ± 3	34	77	0.89	76.4 ± 2.6
10 phr PDMS3–PEG	63 ± 9	7	67	0.94	60.6 ± 8.7
20 phr PDMS3–PEG	74 ± 3	30	75	0.76	73.7 ± 3.0

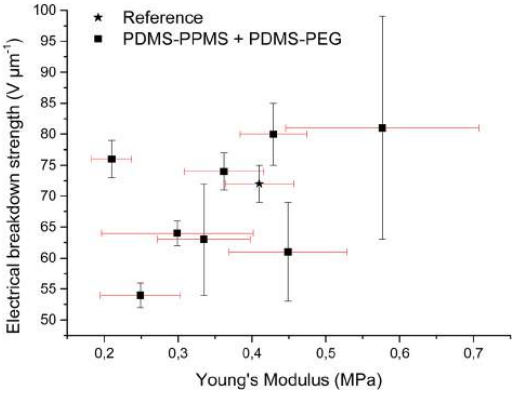

Fig. 8 Electrical breakdown strength *versus* Young's modulus. Existing theories predict a linear[4] or even an exponential increase[28] of the electrical breakdown strength with the Young's modulus. This is obviously not valid for the investigated phase-separating system.

or the favourable phase separation of PEGs rather than due to increased stiffness and thus resistance towards actuation. No clear trend can be observed for electrical breakdown strength *versus* relative permittivity, indicating that the increased electrical breakdown strength is not due to increased relative permittivity (see Fig. 9). Likewise the effect of film thickness on electrical breakdown strength was investigated in order to eliminate all possible experimental artefacts. Again, there is no obvious correlation as observed from Fig. 10 which again confirms that the voltage stabilization is an electrical effect.

The theoretical actuation strains were calculated from the actuation equation,[30] by assuming the maximum applicable electrical field, *i.e.* electrical breakdown strength can be realized and the elastomer does not break down mechanically or electromechanically before electrically.[21] Theoretical actuation strains and measured ultimate strains are shown in Table 5. The elastomer with 10 phr of PDMS81–PEG, which is highly extensible, shows the lowest theoretical actuation strain compared to the other elastomers. No correlation can be made from Table 5 about the dependence of theoretical actuation strain on ultimate strain. Previous theory predicts that the maximum actuation strain may

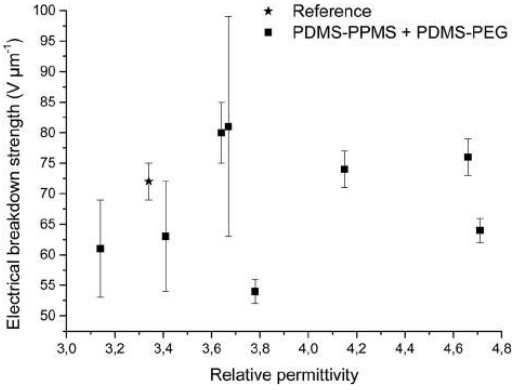

Fig. 9 Electrical breakdown strength *versus* relative permittivity. Existing theories predict that the electrical breakdown strength scales with the square root of dielectric permittivity.[29]

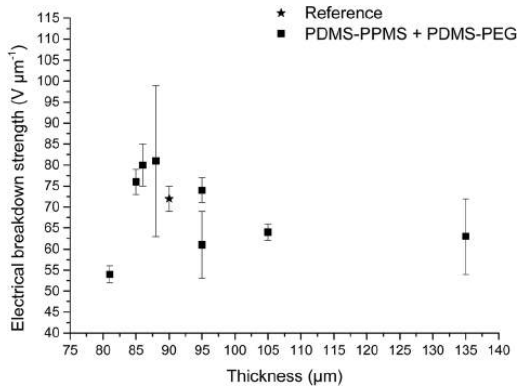

Fig. 10 Electrical breakdown strength as function of film thickness. Usually a strong increase in the electrical breakdown strength is observed with decreased thickness of elastomer film due to the reduction of volume and thus number of defects.

Table 5 Theoretical actuation strain and measured ultimate strain for prepared elastomers

Sample	Theoretical actuation strain (%)	Ultimate strain (%)
80DMS_2PMS (reference)	600	967 ± 33
10 phr PDMS81–PEG BCB	366	1748 ± 40
20 phr PDMS81–PEG BCB	629	1164 ± 17
10 phr PDMS14–PEG BCB	769	635 ± 52
20 phr PDMS14–PEG BCB	590	104 ± 1
10 phr PDMS7–PEG BCB	928	431 ± 19
20 phr PDMS7–PEG BCB	1821	552 ± 103
10 phr PDMS3–PEG BCB	578	724 ± 40
20 phr PDMS3–PEG BCB	881	491 ± 43

be achieved for the elastomer which is highly extensible.[21] However, a large actuation strain is also influenced by other parameters such as increased electrical breakdown strength and increased relative permittivity. Obviously, elastomers with decreased ultimate strain, such as the example with 20 phr of PDMS14–PEG, may break down mechanically before they break down electrically (see Table 5). However, it is obvious that this type of silicone elastomer is in general more stretchable than the maximum actuation demands.

4 Conclusions

A soft elastomer with high extensibility was prepared from phase-separating a PDMS–PEG copolymer in a binary copolymer blend consisting of a PDMS–PPMS copolymer as the primary copolymer. The elastomer possessed simultaneously increased relative permittivity and electrical breakdown. The increased electrical breakdown strength is due to voltage stabilisation arising from the phenyl groups of PPMS, while increased relative permittivity without achieving conductivity is due to the favourable phase separation of PEG constituents in the binary copolymer blend matrix. Thereby a facile method towards soft, reliable elastomers with good electrical properties allowing for large-strain actuation has been shown.

Acknowledgements

The Malaysian Ministry of Education (MoE) and Universiti Tun Hussein Onn Malaysia (UTHM) are gratefully acknowledged for their funding.

References

1 F. B. Madsen, A. E. Daugaard, S. Hvilsted and A. L. Skov, *Macromol. Rapid Commun.*, 2016, **37**, 378–413.
2 P. Brochu and Q. Pei, *Macromol. Rapid Commun.*, 2010, **31**, 10–36.
3 A. L. Larsen, P. Sommer-Larsen and O. Hassager, *Proc. SPIE*, 2004, **5385**, 108–117.
4 L. Yu and A. L. Skov, *Int. J. Smart Nano Mater.*, 2015, **6**, 268–289.
5 Z. Suo, *Acta Mech. Solida Sin.*, 2010, **23**, 549–577.
6 S. Vudayagiri, Large scale processing of dielectric electroactive polymers, Ph.D. thesis, Technical University of Denmark, Lyngby Denmark, 2014.
7 Z. Zhang, L. Liu, J. Fan, K. Yu, Y. Liu, L. Shi and J. Leng, *Proc. SPIE*, 2008, **6926**, 692610.
8 L. J. Romasanta, P. Leret, L. Casaban, M. Hernández, M. A. de la Rubia, J. F. Fernández, J. M. Kenny, M. A. Lopez-Manchado and R. Verdejo, *J. Mater. Chem.*, 2012, **22**, 24705–24712.
9 A. Bele, M. Dascalu, C. Tugui, M. Iacob, C. Racles, L. Sacarescu and M. Cazacu, *Mater. Des.*, 2016, **106**, 454–462.
10 H. Böse, D. Uhl and R. Rabindranath, *Proc. SPIE*, 2012, **8340**, 83402E.
11 B. Kussmaul, S. Risse, G. Kofod, R. Waché, M. Wegener, D. N. McCarthy, H. Krüger and R. Gerhard, *Adv. Funct. Mater.*, 2011, **21**, 4589–4594.
12 F. B. Madsen, A. E. Daugaard, S. Hvilsted, M. Y. Benslimane and A. L. Skov, *Smart Mater. Struct.*, 2013, **22**, 1–11.
13 F. B. Madsen, I. Javakhishvili, R. E. Jensen, A. E. Daugaard, S. Hvilsted and A. L. Skov, *Polym. Chem.*, 2014, **5**, 7054–7061.
14 P. Mazurek, S. Hvilsted and A. L. Skov, *Polymer*, 2016, **87**, 1–7.
15 P. Mazurek, L. Yu, R. Gerhard, W. Wirges and A. L. Skov, *J. Appl. Polym. Sci.*, 2016, **133**, 44153.
16 A. H. A Razak, P. Szabo and A. L. Skov, *RSC Adv.*, 2015, **5**, 53054–53062.
17 S. Vudayagiri, S. Zakaria, L. Yu, S. S. Hassouneh, M. Benslimane and A. L. Skov, *Smart Mater. Struct.*, 2014, **23**, 105017.
18 V. Englund, R. Huuva, S. M. Gubanski and T. Hjertberg, *Polym. Degrad. Stab.*, 2009, **94**, 823–833.
19 Y. Yamano, *IEEE Trans. Dielectr. Electr. Insul.*, 2006, **13**, 773–781.
20 Y. Yamano and H. Endoh, *IEEE Trans. Dielectr. Electr. Insul.*, 1998, **5**, 270–275.
21 A. H. A. Razak and A. L. Skov, *RSC Adv.*, 2017, **7**, 468–477.
22 Y. Li, K. Hu, X. Han, Q. Yang, Y. Xiong, Y. Bai, X. Guo, Y. Cui, C. Yuan, H. Ge and Y. Chen, *Langmuir*, 2016, **32**, 3670–3678.
23 J. Raczkowska, A. Bernasik, A. Budkowski, K. Sajewicz, B. Penc, J. Lekki, M. Lekka, J. Rysz, K. Kowalski and P. Czuba, *Macromolecules*, 2004, **37**, 7308–7315.
24 H. Jinnai, Y. Nishikawa, T. Koga and T. Hashimoto, *Macromolecules*, 1995, **28**, 4782–4784.
25 S. Walheim, M. Ramstein and U. Steiner, *Langmuir*, 1999, **15**, 4828–4836.
26 C. Tugui, S. Vlad, M. Iacob, C. D. Varganici, L. Pricop and M. Cazacu, *Polym. Chem.*, 2016, **7**, 2709–2719.
27 S. Zakaria, P. H. F. Morshuis, M. Y. Benslimane, L. Yu and A. L. Skov, *Smart Mater. Struct.*, 2015, **24**, 55009.
28 G. Kofod, P. Sommer-Larsen, R. Kornbluh and R. Pelrine, *J. Intell. Mater. Syst. Struct.*, 2003, **14**, 787–793.
29 K. H. Stark and C. G. Garton, *Nature*, 1955, **176**, 1225–1226.
30 R. Pelrine, R. Kornbluh, Q. Pei and J. Joseph, *Science*, 2000, **287**, 836–839.

Electronic Supplementary information

Voltage-stabilised elastomers with increased relative permittivity and high electrical breakdown strength by means of phase separating binary copolymer blends of silicone elastomers

Aliff Hisyam A Razak[1,2], Liyun Yu[1] and Anne Ladegaard Skov[1*]

[1] *Danish Polymer Center, Department of Chemical and Biochemical Engineering, Technical University of Denmark, Building 227, 2800 Kgs. Lyngby, Denmark.*
[2] *Faculty of Engineering Technology, University of Tun Hussein Onn Malaysia, 86400 Parit Raja, Batu Pahat, Johor, Malaysia.*
* al@kt.dtu.dk; phone +45 45252825; fax +45 45882258; http://www.dpc.kt.dtu.dk/

1) Calculation of engineering stress and strain

The engineering stress (σ_E) was calculated from the force (F) and the cross-sectional area of the strip (A):

$$\sigma_E = \frac{F}{A} = \frac{F}{t \times w} = \frac{\tau \cdot d}{t \cdot w}$$ Equation 1

where A = film thickness (t) · constant width (w = 6 mm) and F = torque (τ) · drum diameter (d = 10.3 mm).

The engineering strain (ϵ_E) was calculated as a ratio of a stretched strain ($L - L_0$) to an initial strain (L_0) as:

$$\epsilon_E = \frac{L - L_0}{L_0}$$ Equation 2

where a final strain after stretching (L) was determined from Hencky strain (ϵ_H) as follows:

$$\epsilon_H = ln\frac{L}{L_0}$$ Equation 3

$$L = L_0 e^{\epsilon_H} = L_0 e^{(r_H \cdot t_s)}$$ Equation 4

where ϵ_H is a product of Hencky rate (r_H = 1×10^{-3} rotation/s) and step time (t_s).

By putting equation (4) in (2), the final expression of engineering strain (ϵ_E) was obtained as below:

$$\epsilon_E = e^{\epsilon_H} - 1$$ Equation 5

Young's moduli were determined from slopes in the linear regime of stress-strain plots at 5 % strain.

2) NMR spectra of synthesised copolymers

The NMR spectra for synthesised PDMS-PPMS and PDMS-PEG copolymers are shown in Figures S1– S5.

a) PDMS-PPMS copolymer (**80DMS_2PMS**, $^{C_{C_6H_6}}$ = 8.4 · 10^{-4} mol g^{-1})

^{1}H-NMR ($CDCl_3$, 300 MHz): δ -0.02 - δ 0.6 (m, 6 H's, -SiO(C**H$_3$**)$_2$-), δ 4.70 (m, 1 H, -Si**H**-), δ 7.10 - δ 7.60 (m, 5 H's, -SiC$_6$**H$_5$**-).

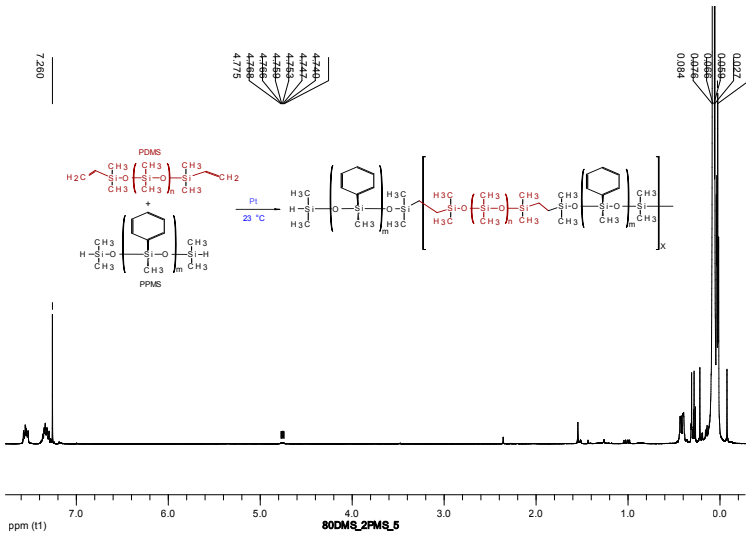

Figure S1 The NMR for 80DMS_2PMS.

b) PDMS-PEG copolymer (**PDMS81-PEG**)

^{1}H-NMR ($CDCl_3$, 300 MHz): δ 0.05 - δ 0.09 (m, 6 H's, -Si(C**H$_3$**)$_2$O-), δ 3.50 - δ 3.70 (m, 4 H's, -C$_2$**H$_4$**O-), δ 0.98 - δ 1.03 (t, 2 H's, -SiC**H$_2$**-), δ 3.53 - δ 3.57 (m, 2 H's, -CC**H$_2$**O-).

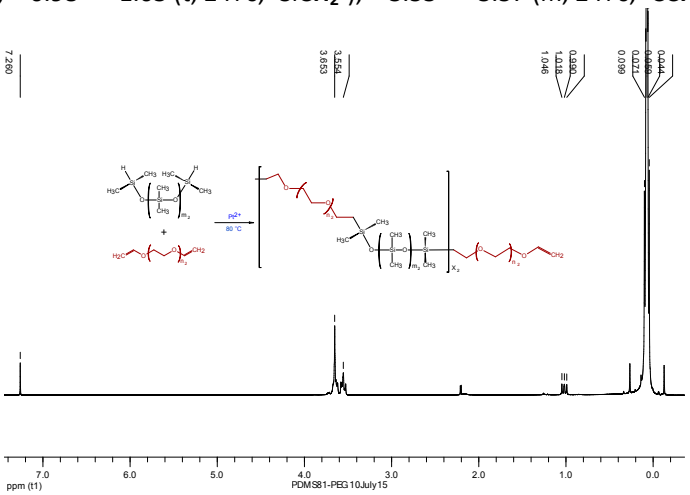

Figure S2 The NMR for PDMS81-PEG.

c) PDMS-PEG copolymer (**PDMS14-PEG**)

^{1}H-NMR ($CDCl_3$, 300 MHz): δ 0.05 - δ 0.09 (m, 6 H's, -Si(C**H$_3$**)$_2$O-), δ 3.50 - δ 3.70 (m, 4 H's, -C$_2$**H$_4$**O-), δ 0.98 - δ 1.03 (t, 2 H's, -SiC**H$_2$**-), δ 3.53 - δ 3.57 (m, 2 H's, -CC**H$_2$**O-).

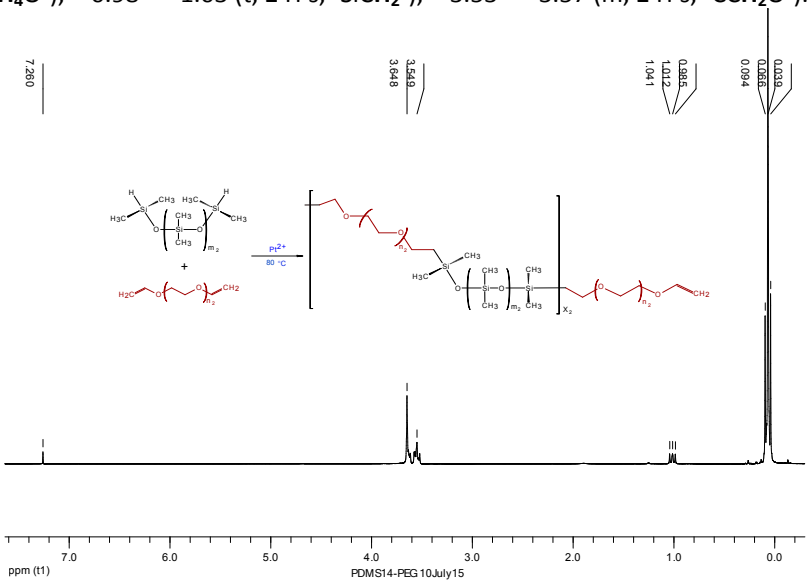

Figure S3 The NMR for PDMS14-PEG.

d) PDMS-PEG copolymer (**PDMS7-PEG**)

^{1}H-NMR ($CDCl_3$, 300 MHz): δ 0.05 - δ 0.09 (m, 6 H's, -Si(C**H$_3$**)$_2$O-), δ 3.50 - δ 3.70 (m, 4 H's, -C$_2$**H$_4$**O-), δ 0.98 - δ 1.03 (t, 2 H's, -SiC**H$_2$**-), δ 3.53 - δ 3.57 (m, 2 H's, -CC**H$_2$**O-).

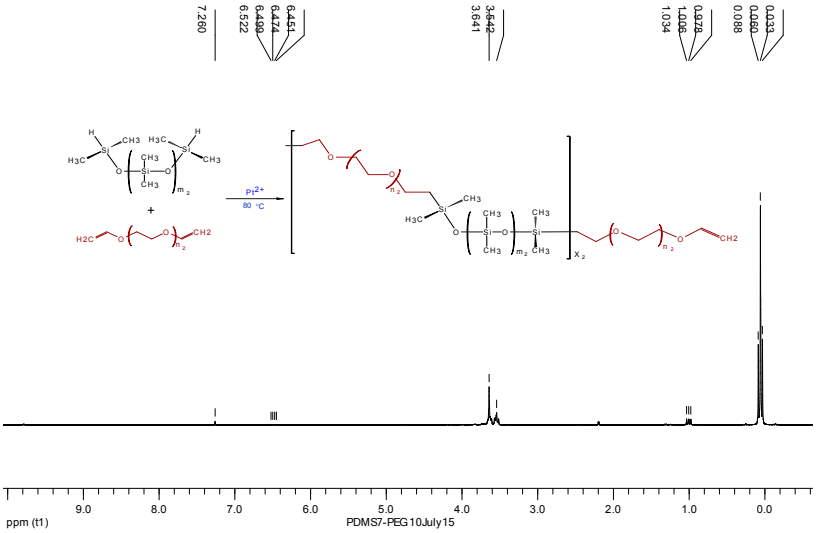

Figure S4 The NMR for PDMS7-PEG.

e) PDMS-PEG copolymer (**PDMS3-PEG**)

^{1}H-NMR ($CDCl_3$, 300 MHz): δ 0.05 - δ 0.09 (m, 6 H's, -Si(CH_3)$_2$O-), δ 3.50 - δ 3.70 (m, 4 H's, -C_2H_4O-), δ 0.98 - δ 1.03 (t, 2 H's, -SiCH_2-), δ 3.53 - δ 3.57 (m, 2 H's, -CCH_2O-).

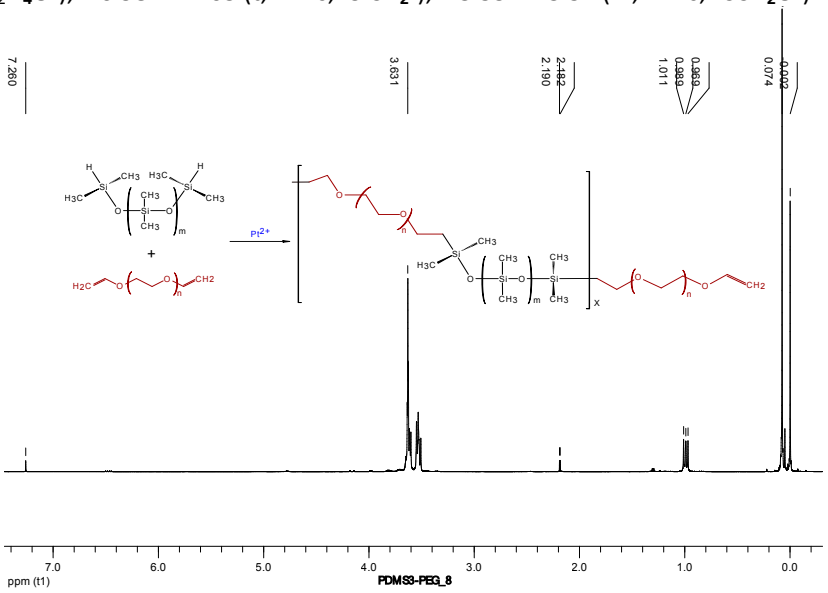

Figure S5 The NMR for PDMS3-PEG.

3) SEM images

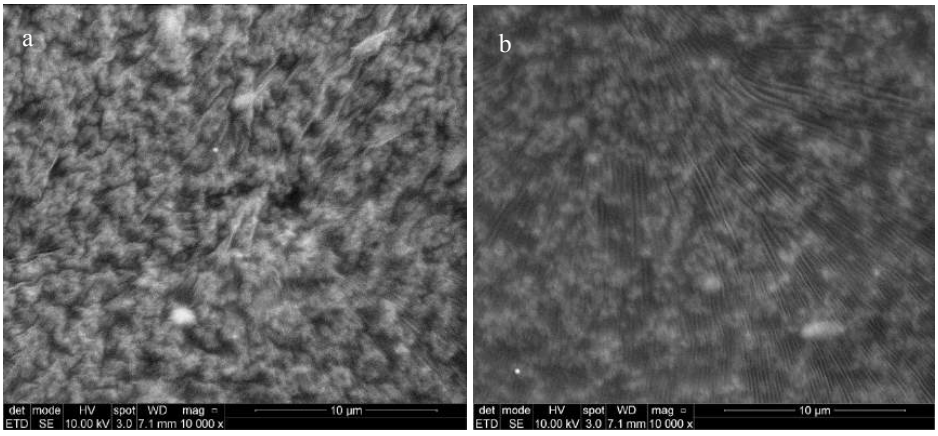

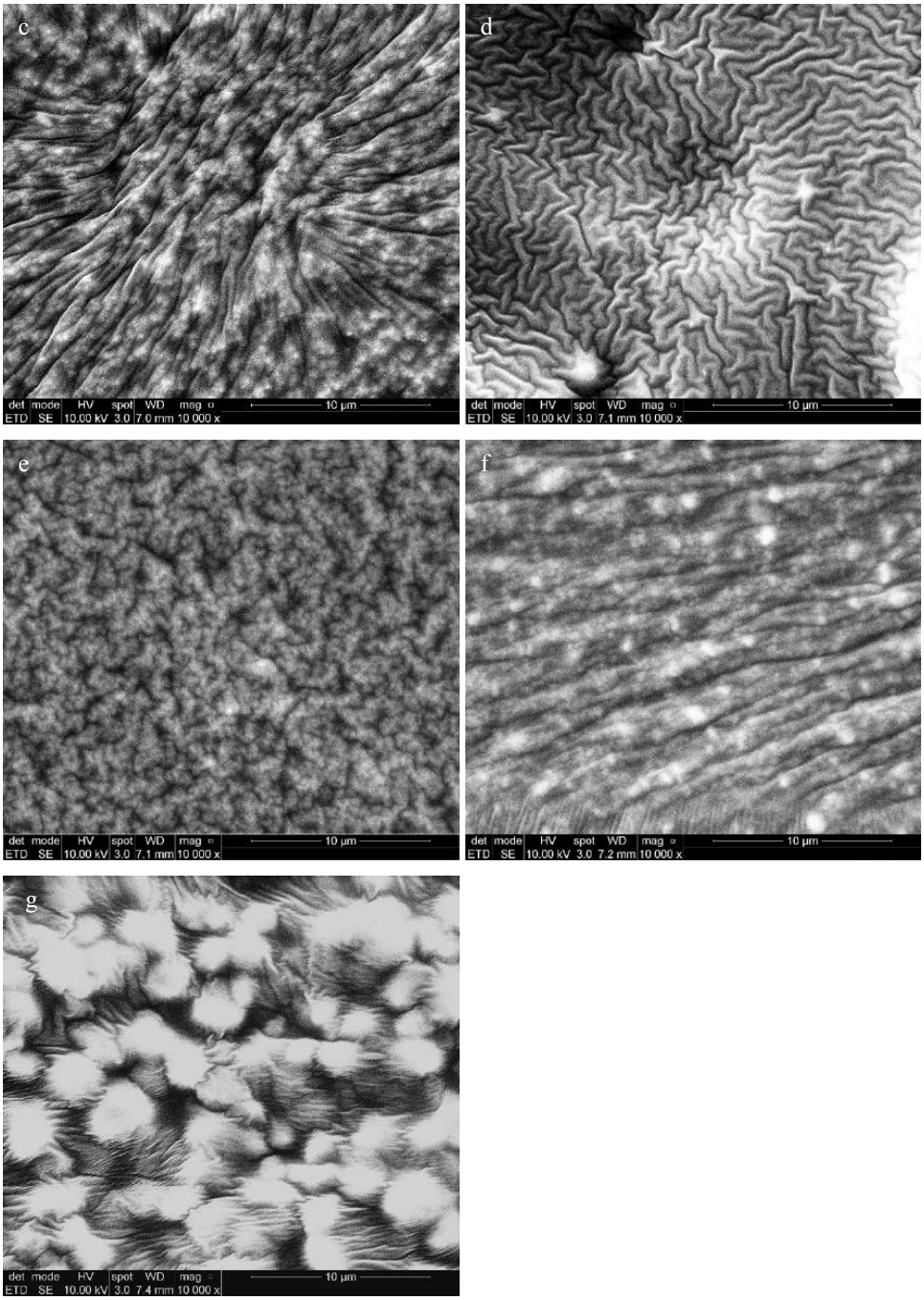

Figure S6 SEM images cross-linked BCBs with: **a**) 10 phr PDMS81-PEG, **b**) 20 phr PDMS81-PEG, **c**) 10 phr PDMS14-PEG, **d**) 20 phr PDMS14-PEG, **e**) 10 phr PDMS7-PEG, **f**) 10 phr PDMS3-PEG, and **g**) 20 phr PDMS3-PEG.

Appendix IV

A Razak AH, Madsen FB, Skov AL (2016) 'Mechanically compliant electrodes and dielectric elastomers from PEG-PDMS copolymers' MRS Adv. 1:3497-3508.

Mechanically Compliant Electrodes and Dielectric Elastomers from PEG-PDMS Copolymers

Aliff Hisyam A Razak, Frederikke Bahrt Madsen and Anne Ladegaard Skov

MRS Advances / *FirstView* Article / May 2016, pp 1 - 12
DOI: 10.1557/adv.2016.404, Published online: 24 May 2016

MRS Advances © 2016 Materials Research Society
DOI: 10.1557/adv.2016.404

Mechanically Compliant Electrodes and Dielectric Elastomers from PEG-PDMS Copolymers

Aliff Hisyam A Razak[1,2], Frederikke Bahrt Madsen[1] and Anne Ladegaard Skov[1]
[1] Danish Polymer Center, Department of Chemical and Biochemical Engineering, Technical University of Denmark, Building 227, 2800 Kgs. Lyngby, Denmark.
[2] Faculty of Engineering Technology, University of Tun Hussein Onn Malaysia, 86400 Parit Raja, Batu Pahat, Johor, Malaysia.

ABSTRACT

Soft conducting elastomers have been prepared from polydimethylsiloxane-polyethyleneglycol (PDMS-PEG) copolymer and surfactant-stabilized multi-walled carbon nanotubes (MWCNTs). The copolymer was chain-extended with PDMS of molecular weight 17.2 kg mol^{-1} in order to obtain a crosslinkable PDMS with molecular weight around 20 – 30 kg mol^{-1}. MWCNTs were treated with surfactant and sonicated for better dispersion in the polymer matrix. The conductivity and mechanical properties of conducting elastomers were thoroughly investigated including stress and strain at break. The developed conducting elastomers showed high conductivity combined with inherent softness. The high conductivity and softness, PDMS-PEG copolymers with incorporated MWCNTs hold great promises as compliant and highly stretchable electrodes for stretchable devices such as electro-mechanical transducers.

INTRODUCTION

Stretchable, conductive materials have been extensively studied for many applications such as biomedical devices [1], electro-mechanical transduction [2] and solar power [3]. For the dielectric elastomer (DE) technology, an inherently soft and highly conductive compliant electrode material is required for optimum performance in electro-mechanical transduction. Conventional compliant electrodes, such as carbon black in the form of powder and carbon grease, can be easily applied on surfaces, but they lack adhesion to the elastomer. Other investigated electrode materials for DEs include silver nanowires, ionic hydrogels, single-walled carbon nanotubes (SWCNTs) and polymer-carbon conductive composites [2]. These materials however suffer from poor stretchability which renders them unattractive as flexible electrodes [2]. On the other hand, commercial conductive elastomers such as LR3162 from Wacker Chemie have high conductivity, but they contribute with a stiffening effect due to their high Young's modulus.

As an alternative to the above mentioned materials polydimethylsiloxane-polyethyleneglycol (PDMS-PEG) copolymers, which are somewhat conductive with conductivities around 10^{-8} S cm^{-1} [4], have great adhesion to silicone surfaces and great flexibility and compliance due to their partly silicone nature. Furthermore, their moderate conductivities can be easily enhanced by incorporating highly conductive nano-fillers such as multi-walled carbon nanotubes (MWCNTs). The high interaction energies of MWCNTs due to strong van der Waals forces, however, often result in poor dispersibility and weak interfacial interactions with the matrix[5]. Well-dispersed MWCNTs are important in order to avoid agglomeration which would give uneven conductive and mechanical properties throughout the matrix.

High levels of dispersion of MWCNTs in polymer matrices can be obtained using probe sonicators and ball milling prior to mixing with the matrix [6], [7]. Chemical modification of MWCNTs can also lead to a higher degree of dispersion due to higher compatibilities with the matrix. Methods such as oxidation by nitric acid [8] and solutions of hydrogen peroxide/ammonium hydroxide [9], however, worsen the intrinsic properties of MWCNTs such as a decrease in the tube length and conductivity. On the other hand, treatment of MWCNT surfaces using non-ionic surfactants such as Triton X-100 and sodium dodecyl sulfate (SDS), does not change the intrinsic properties of MWCNTs significantly since each MWCNT is coated with surfactant molecules through their hydrophilic head and hydrophobic tails obtaining surfactant-stabilized MWCNTs [10].

In this paper we demonstrate how synthesized PDMS-PEG copolymer matrices with different concentrations of surface-modified MWCNT nano-fillers show promising properties for high conductivity, stretchable electrodes. The conductivities and mechanical properties of prepared samples of PDMS-PEG copolymers with different concentration of MWCNTs were investigated as well as the dispersion of MWCNT in the polymer matrix by SEM and TEM analysis.

EXPERIMENTAL PROCEDURES

Materials

Vinyl-terminated polydimethylsiloxane-polyethyleneglycol block co-oligomers (PDMS-PEG) were synthesized according to a previously published procedure [4]. The number average molecular weight (M_n) of the resulting PDMS-PEG copolymer was $M_n = 3900$ g mol^{-1}. Vinyl-functional PDMS cross-linker (15-functional, VDT-431), telechelic hydride-functional PDMS (DMS-H25, $M_n = 17.2$ kg mol^{-1}) and platinum-divinyltetramethyl disiloxane complex with 3.25% of platinum in xylene (SIP6830.3) were purchased from Gelest Inc. Pristine multi-walled carbon nanotubes (MWCNTs) (NANOCYL™ NC7000) with average diameter, length and surface area of 9.5 nm, 1.5 μm and 250-300 m^2/g, respectively, were obtained from Nanocyl S.A., Belgium. N-methyl pyrrolidinone (NMP) and polyoxyethylene octyl phenyl ether (Triton X-100) were obtained from Sigma-Aldrich.

Synthesis of PDMS-PEG copolymers

The previously synthesized PDMS-PEG co-oligomer ($M_n = 3900$ g mol^{-1}) was chain-extended by hydrosilylation with telechelic hydride functional PDMS, PDMS232, ($M_n = 17{,}200$ g mol^{-1}) in the presence of a Pt catalyst according to Scheme 1. PDMS-PEG co-oligomer, PDMS232 and Pt catalyst were speedmixed at 3000 rpm for 4 min. The transparent reaction mixture turned into milky yellow. The resulting copolymer of CE-(PDMS-PEG) was characterized and verified by size-exclusive chromatography (SEC) to observe the shift of molecular weight from the low molecular weight of PDMS-PEG copolymer to high molecular weight of CE-(PDMS-PEG) copolymer ($M_n = 24$ kg mol^{-1} / $M_w = 52$ kg mol^{-1}). ^{1}H-NMR spectroscopy was used to confirm the completion of the reaction by the absence of vinyl-protons from PDMS-PEG co-oligomer between $\delta_H = 5.8 - 6.2$ ppm.

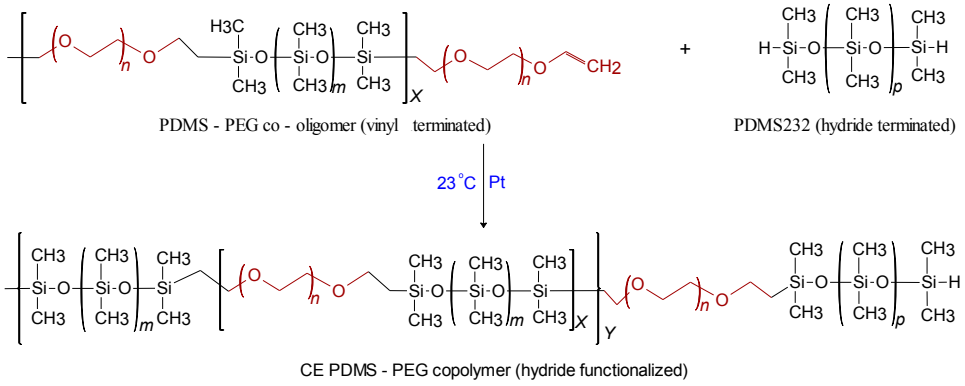

Scheme 1 The hydrosilylation reaction utilized for chain-extended CE-(PDMS-PEG) copolymer in the presence of 30 ppm Pt catalyst at 23 °C, where $m = 3$ and $p = 232$, respectively, are the number of repeating dimethylsiloxane units in the two PDMS parts. $n = 4$ is the constant number of repeating ethyleneglycol units, and X and Y are the number of repeating PDMS-PEG units and the number of CE-(PDMS-PEG) blocks, respectively.

Dispersion of MWCNTs

Dispersion of MWCNTs in 96 wt% NMP and 1 wt% Triton X-100 was achieved by ultrasonication in water bath (1510E-DTH, BRANSONIC–Ultrasound Cleaner, USA, Input: 155 W & 50-60 kHz, Output: 70 W & 42 kHz).

Preparation of CE-(PDMS-PEG) elastomers with surface-modified MWCNT

CE-(PDMS-PEG) copolymer was cross-linked using 15-functional vinyl cross-linker (VDT-431) with addition of surface-treated MWCNTs in NMP and Triton X-100 (1, 2 and 3 phr MWCNT) by speedmixing using SpeedMixer™ (DAC 150 FVZ, Flack Tek. Inc.) at 3000 rpm for 3 - 6 min. The final mixtures were cast on hollow metal plates placed on Teflon substrates. Films with ~ 1 mm thickness were cured initially at a temperature of 70 °C which was gradually increased to 150 °C over a period of 7 days to ensure gradual removal of NMP solvent and proper film formation.

Methods

Linear viscoelasticity properties (LVE) were measured by a strain-controlled rheometer (ARES G2, TA Instruments, USA) at 23 °C using 25 mm parallel plate geometry with axial force, strain and frequency ranges of 7 N, 2% and 100–0.01 Hz, respectively. Young's moduli (determined as the slope of the stress-strain curve at 5% strain) and stress-strain behaviour of samples with 20 mm length and 6 mm width were determined by the ARES G2 using the SER2 geometry with extensional rate of 0.001 s^{-1}. The measurements of conductivity, relative permittivity and dielectric loss were measured by a Novocontrol Broadband Dielectric Spectrometer BDS-40 (Novocontrol Technologies GmbH & Co. KG, Germany) with diameter of electrode of 20 cm in the frequency range of 10^{-1} to 10^{6} Hz at 23 °C. The SEM model, FEI

Inspect S, performed energy-dispersive X-ray and wave-length dispersive measurements to characterize micro-scale images of dispersion of MWCNTs in the polymer. Accelerating voltage and resolution were 200 V to 30 kV and 50 nm at 30 kV, respectively, while the imaging modes used high vacuum. SEM images were taken from cross-sections prepared by a sharp razor. The TEM model, FEI Tecnai T20 G^2 was used to characterize micro and nano-scale images using transmitted electrons from the electron source of Thermionic LaB_6/CeB_6. TEM samples were prepared using grinding tool and were placed on a grid coated by Copper Naphthenate (Coppernate). Thermal analysis of crystallization was performed by differential scanning calorimetry (DSC) from TA Instrument (Discovery series) in a nitrogen atmosphere with a heating rate of 10 °C min^{-1} from -190 °C to 50 °C.

RESULTS AND DISCUSSION

Stretchable and high-conductivity electrode materials for dielectric elastomers were prepared by the synthesis of PDMS-PEG copolymers according Scheme 1. The copolymers were prepared by the chain extension of a previously synthesized[4] PDMS-PEG co-oligomer with commercially available telechelic hydride-functional PDMS of M_n = 17,200 g mol^{-1} resulting in a telechelic hydride-functional CE-(PDMS-PEG) copolymer of M_n = 24 kg mol^{-1}. Well-dispersed surface-modified MWCNTs were prepared by ultra-sonication using 1 wt% of non-ionic surfactant (Triton X-100) in an organic solvent (NMP). The CE-(PDMS-PEG) copolymer was then cross-linked using a vinyl-functional cross-linker containing on average 15 vinyl-groups in the presence of a Pt catalyst and surface-modified MWCNTs in various concentrations (1, 2 and 3 parts per hundred rubber (phr)).

Dispersion MWCNTs in CE-(PEG-PDMS)

It has been previously shown that conductivities of conductive materials depend greatly on how well MWCNTs (or other nano-fillers) are dispersed in the polymer matrix [7], [10]. Therefore, in order to obtain high-conductivity elastomer electrodes a high level of dispersion of MWVNTs is required. As previously mentioned, strong van der Waals forces exist between single MWCNT strands which are therefore agglomerated and intertwined in their natural and pure state as shown in Figure 1. This behavior makes direct dispersion of pure MWCNTs in polymer matrices extremely difficult. Pre-dispersal in solvent and surface-modifications of the MWCNTs using surfactants can, however, result in well-dispersed fillers [7], [10].

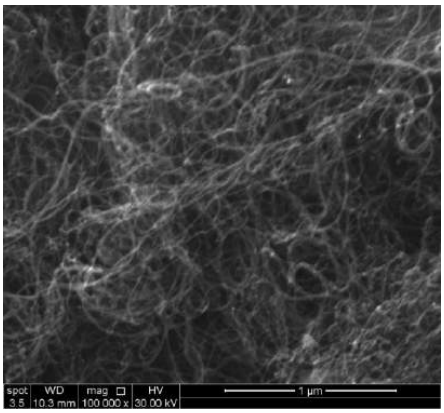

Figure 1 SEM image of pure MWCNTs showing their agglomerated and intertwined nature.

Based on the studies by Geng et al. [7] and Rastogi et al. [10] who tested the dispersion of MWCNT in organic solvents using different surfactants a polyoxyethylene octyl phenyl ether type surfactant (Triton X-100) was chosen as the ideal surfactant for well-dispersed MWCNTs. This surfactant was also found to have a high tolerance to various organic solvents in which the MWCNTs were dispersed in. The optimal solvent for a high level of dispersion was chosen based on the study by Goswami et al. [11] who used *N*-methyl pyrrolidinone (NMP) as a compatible organic solvent to disperse low concentrations of MWCNTs in a PDMS matrix. The chosen system in our study was therefore based on a solution containing of MWCNTs in 1 wt% Triton X-100 in NMP solvent which was ultra-sonicated for several hours before the resulting dispersed MWCNTs were mixed into the CE-(PDMS-PEG) matrix.

In order to investigate the effectiveness of dispersion of MWCNT-treated by Triton X-100, the settling of MWCNTs in the organic solution after the sonication was monitored over time. The dispersion method used in this work was compared to a reference method using the same surface treatment method of 1 wt% Triton X-100 and NMP, but with a mechanical shaker instead of ultra-sonication. Theoretically, no settlement of MWCNTs in the solution of Triton X-100 and NMP should be observed when the surface of MWCNT is well treated by Triton X-100. In Figure 2 (top) the settlement of MWCNTs dispersed by means of the reference method (mechanical shaking) is seen. It can be seen that over time, the MWCNTs have settled on the bottom of the white-capped flask. This indicates that each MWCNT strand is not well covered by surfactant when mechanical shaking has been used as the mixing method. The MWCNTs are therefore able to agglomerate and the dispersion will not be stable over time.

On the other hand, the same system of MWCNTs in 1 wt% of Triton X-100 in NMP which were mixed with ultra-sonication for 6 hours at 23 °C creates a stable dispersion of MWCNTs over time. This is shown in Figure 2 (bottom). No settling/agglomeration of MWCNTs was observed over the investigated time frame. This indicates that ultra-sonication gives MWCNTs that are well-covered in Triton X-100 surfactant.

Figure 2 Top: Settlement of MWCNTs over time for the reference method (MWCNT/NMP/Triton X-100) dispersed by a mechanical shaker at 23 °C after standing for: a) 0 min b) 5 min c) 30 min d) 60 min. Bottom: MWCNT/NMP/Triton X-100 mixed by ultra-sonication at 23 °C

After the initial successful dispersion of MWCNTs in NMP solvent, the obtained MWCNT mixture was blended with CE-(PDMS-PEG) copolymer, cross-linker and catalyst where after the NMP solvent was allowed to evaporate slowly during the elastomer cross-linking process creating MWCNT/CE-(PDMS-PEG) nanocomposites. In order to verify the effectiveness of dispersion of MWCNTs in the CE-(PDMS-PEG) elastomer matrix, microscale and nanoscale images were obtained by SEM and TEM, respectively. SEM images revealed details on overall dispersion of MWCNTs in the copolymer matrix whereas TEM images revealed details on the morphology of MWCNTs in CE-(PDMS-PEG) matrix.

In Figure 3 (top) the obtained SEM images, displaying random micros-structures of MWCNTs in the CE-(PDMS-PEG) matrix, are shown. The attained images are similar to those observed in literature for well-dispersed MWCNTs in polymer matrices [11]. Figure 3 (bottom) shows a single strand of MWCNT illustrating that the MWCNTs are well-dispersed as single strands in the matrix. The dimension of the single strand of MWCNT observed in TEM matches data specifications provided by the supplier; diameter and length are 6 – 9 nm and 1.5 µm, respectively. SEM and TEM thus corroborates that the used dispersion method creates nanocomposites with well-dispersed MWCNTs.

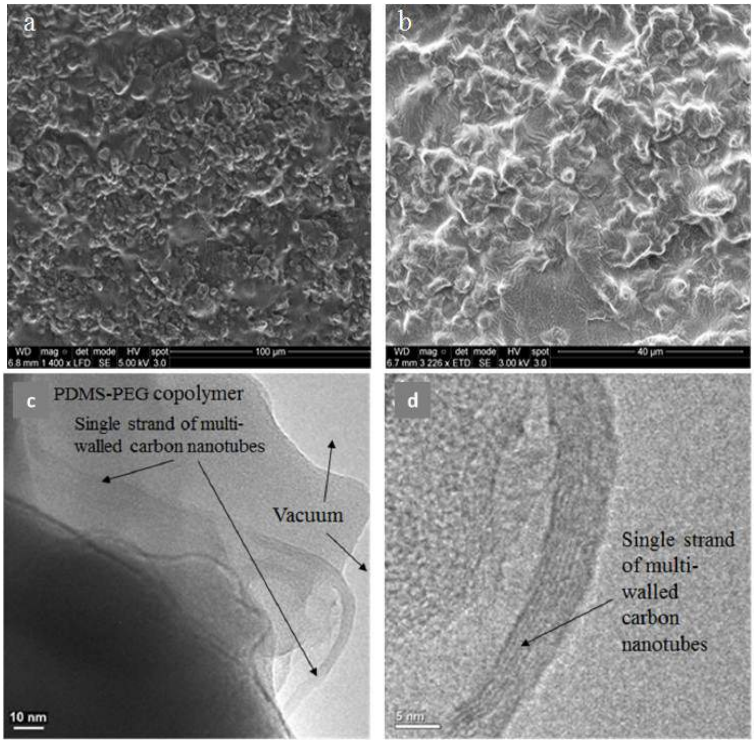

Figure 3 Images of CE-(PDMS-PEG) nanocomposites with 3 phr MWCNTs. a) and b) SEM images, and c) and d) microscope pictures.

Mechanical properties of CE-(PDMS-PEG)/MWCNTs nanocomposites

Mechanical properties of the obtained CE-(PDMS-PEG)/MWCNTs nanocomposites were tested by shear rheology. Rheological properties of the cross-linked CE-(PDMS-PEG) copolymers with 0 – 3 phr of MWCNT were compared to a commercial conductive elastomer reference material, LR3162, as shown in Figure 4. The rheological properties of the nanocomposites were furthermore compared to a CE-PDMS-PEG elastomer prepared without MWCNTs. The reference elastomer (CE-PDMS-PEG copolymer with 0 wt% MWCNTs) is seen to be stiffer than CE-(PDMS-PEG)/MWCNT nanocomposites with 1 to 3 phr of MWCNT. Compared to LR3162, CE-(PDMS-PEG)/MWCNTs nanocomposites are also softer. This implies that incorporating MWCNT in a CE-(PDMS-PEG) copolymer matrix results in soft, stretchable elastomers which therefore hold great promise as stretchable electrode materials for dielectric elastomers. Modulus loss factors (tan (δ)) for CE-(PDMS-PEG)/MWCNT nanocomposites with 1 – 3 phr MWCNTs are low (< 0.5) at various frequencies.

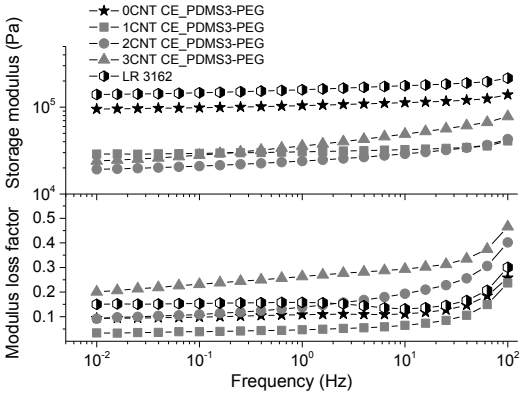

Figure 4 The storage modulus and modulus loss factor for CE-(PDMS-PEG)/MWCNT nanocomposites as well as a CE-(PDMS-PEG) reference elastomer and commercial elastomer LR3162.

Table 1 shows the maximum elongation and stress at break of the commercial conductive elastomer and CE-(PDMS-PEG) elastomers with different concentrations of MWCNTs. The benchmark conductive elastomer, LR3162, has higher elongation at break (168 %) than CE-(PDMS-PEG) elastomer nanocomposites with 1-3 phr MWCNTs. LR3162 however shows strain-hardening behavior with high stress at break. The strain-hardening behavior of LR3162 is coherent with high Young's modulus at 5% strain ($Y = 4.11$ MPa). On the other hand, CE-(PDMS-PEG) elastomers with and without MWCNTs demonstrate increased strain-softening behavior as the concentration of MWCNT increases. Thus, these behaviors of strain-hardening and strain-softening show that CE-(PDMS-PEG) elastomers with MWCNTs become softer with strain compared to LR3162. Another significant finding from Table 1 is that CE-(PDMS-PEG) elastomers with 0 – 3 phr of MWCNT show more than 100% strain meaning that the addition of MWCNT does not destroy the properties of the elastomers at the micro-scale. This can also be a further indication of the well-dispersed nature of the MWCNTs.

Table 1 Elongation and stress at break of PDMS-PEG/MWCNTs elastomers and LR3162

Sample	Elongation at break (%)	Stress at break (MPa)	Young's modulus (MPa)
LR3162	168	1.8	4.11
CE_PDMS-PEG + 0CNT	120	0.67	0.92
CE_PDMS-PEG + 1CNT	116	0.58	1.28
CE_PDMS-PEG + 2CNT	112	0.19	0.32
CE_PDMS-PEG + 3CNT	118	0.19	0.31

Conductivity of CE-(PDMS-PEG)/MWCNTs nanocomposites

The measured conductivities as functions of frequency of the CE-(PDMS-PEG)/MWCNTs nanocomposites as well as the CE-(PDMS-PEG) reference elastomer and

commercial elastomer LR162 are shown in Figure 5. The CE-(PDMS-PEG copolymer shows increased conductivities as the concentration of MWCNT in polymer matrix increases. CE PDMS-PEG) elastomer without addition of MWCNT is non-conductive, (~10^{-13} S cm^{-1} at low frequencies). For CE-(PDMS-PEG) with 1 phr of MWCNT, the conductivity increases substantially to 10^{-7}. The addition of 2 and 3 phr of MWCNT in PDMS-PEG copolymer causes conductivities of 10^{-4} and 10^{-3} S cm^{-1}, respectively, comparable to that of the commercial conductive elastomer from Wacker Chemie (LR3162). Another interesting finding from the conductivity is that plateau regions are observed in Figure 5 for samples with 2 and 3 phr of MWCNT indicating the materials are highly conductive.

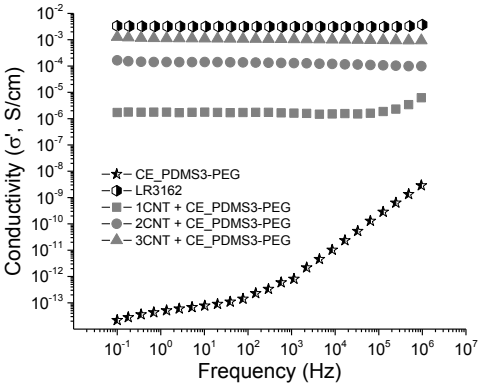

Figure 5 Conductivity of PDMS-PEG/MWCNTs elastomers at room temperature compared to the conductivity of the commercial benchmark elastomer (LR3162).

The high observed conductivities together with the soft and stretchable nature of the prepared CE-(PDMS-PEG)/MWCNTs nanocomposites makes them ideal candidates for flexible dielectric elastomer electrodes.

Interpenetrating network of PDMS-PEG copolymer and ionic network

In an attempt to increase the conductivities of the prepared CE-(PDMS-PEG)/MWCNTs nanocomposite elastomers even further, ionic silicone based networks were included as an extra additive creating interpenetrating networks. The ionic network was prepared by mixing stoichiometric amounts (r = 1) of amine-functional PDMS (4-amine groups on average, AMS-162) and telechelic carboxylic acid-functional PDMS (DMS-B12). Upon mixing the two components a network is formed due to protonation of the functional groups. The preparation procedure of the ionic networks was amended from Yu et al.[12]. The interpenetrating networks consist of the CE-(PDMS-PEG) copolymer and the silicone-based ionic network. Preliminary studies on interpenetrating network from ionic network and CE-(PDMS-PEG) copolymer was investigated to determine the optimum conditions of conductivity and morphology of the system before incorporating MWCNTs. Interpenetrating network samples without MWCNT were prepared at 10, 20, 30, 40 and 50 wt% of the ionic network. The dielectric and conductive properties of the interpenetrating networks with 10 – 50 wt% of ionic network were investigated and are shown in Figure 6. Conductivities of interpenetrating network samples gradually increase

with increased concentration of ionic network. Interpenetrating networks with 10 – 50 wt% of ionic network have conductivities of the order of 10 to 10^3 higher than pure CE-(PDMS-PEG) copolymer as seen in Figure 6a. Relative permittivities and dielectric loss (tan (δ)) of the interpenetrating networks also increase with increasing concentration of ionic network, see Figure 6b. The dynamic dipole orientation of polymer molecules resulting from polarization are observed for interpenetrating network of 30 and 40 wt% of ionic network, as Debye-relaxation peaks occur at frequencies of 10^0 to 10^2 Hz.

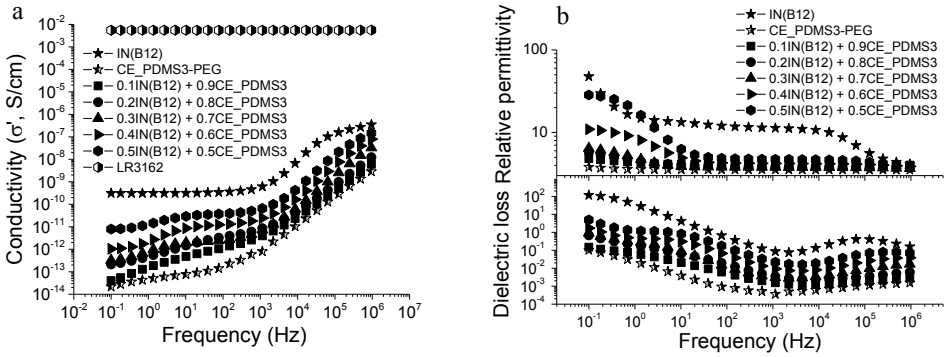

Figure 6 Dielectric properties of interpenetrating network of PDMS-PEG copolymer and ionic network: a) conductivities b) relative permittivity and dielectric loss factor.

SEM analysis shows the presence of visible spheres in interpenetrating network with 30 – 50 wt% of ionic network as seen in Figure 7. These spheres are ionic network formed by phase separation in CE-(PDMS-PEG) copolymer matrix. The size of the spheres increases as the amount of ionic network increases in from 30 to 50 wt%. Interpenetrating networks of 40 and 50 wt% of ionic network contain large sizes of spheres (>50 μm) which may destabilize the elastomers (see Figure 7b and c). Therefore, the further work where MWCNT is incorporated into the interpenetrating network used 30 wt% of ionic network due to the resulting smaller spheres (10 – 20 μm) as shown in Figure 7a.

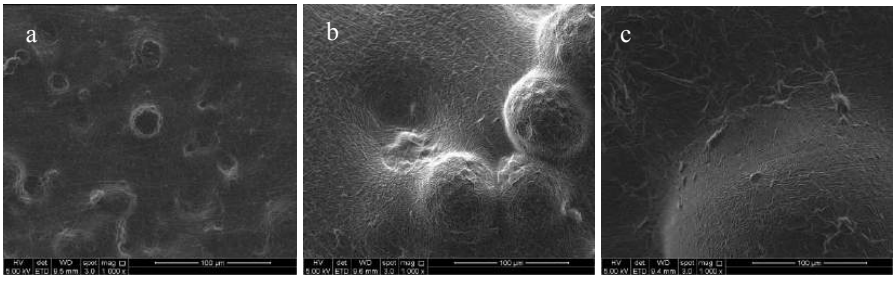

Figure 7 SEM images of interpenetrating networks of CE-(PDMS-PEG) copolymer and ionic network: a) 30 wt% b) 40 wt % c) 50 wt% of ionic network.

Samples from interpenetrating networks with 30 wt% of ionic network were added 1 – 3 phr of MWCNTs. Conductivities of interpenetrating networks (30 wt% ionic network) with MWCNTs were compared with reference elastomers which are based on pure ionic network, pure CE-(PDMS-PEG) copolymer and LR3162 as shown in Figure 8. Conductivities of interpenetrating networks with 1 – 3 phr of MWCNTs are lower than CE-PDMS-PEG copolymer with the same amount of MWCNTs and the addition of MWCNT to interpenetrating network may destabilize the resulting elastomers causing less conductivity than CE-(PDMS-PEG) copolymer with MWCNTs. One major advantage of elastomers with ionic networks may however be that they are able to show self-healing properties [12], [13].

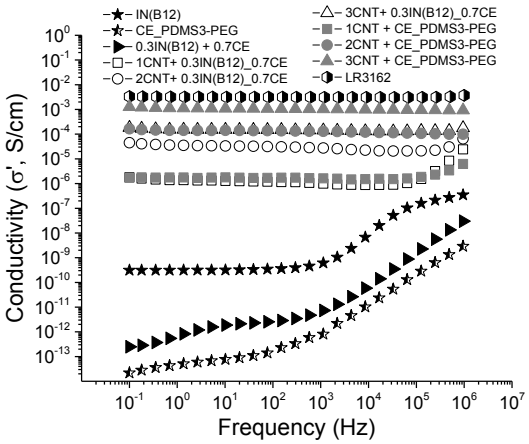

Figure 8 Conductivities of interpenetrating networks of CE-(PDMS-PEG) copolymers and ionic networks with MWCNTs compared to LR3162.

CONCLUSIONS

A new stretchable elastomer with high conductivity was successfully created from PDMS-PEG copolymers and MWCNT. PDMS-PEG copolymer based elastomers with 3 phr of MWCNT is not only soft, but also has conductivity close to a commercial conducting polymer benchmark which possesses limited softness. A high level of dispersion of MWCNTs within the PDMS-PEG matrix was obtained using a combination of surfactant and ultra-sonication. Higher loadings of MWCNT (> 3phr) in PDMS-PEG copolymer may increase the conductivity further, but excessive amounts of MWCNT may on the other hand deteriorate the elastomer with resulting poor mechanical properties. Furthermore, the elongation strain of PDMS-PEG/3 phr MWCNT nanocomposite elastomer is more than 100%. Interpenetrating networks of PDMS-PEG copolymer and a silicone-based ionic network with MWCNTs may have self-healing properties, but the conductivity is lower than PDMS-PEG copolymer with MWCNTs.

ACKNOWLEDGMENTS

The Malaysian Ministry of Education (MoE), Universiti Tun Hussein Onn Malaysia (UTHM), the Danish Council for Independent Research and Innovationsfonden Danmark are gratefully acknowledged for their funding.

REFERENCES

[1] D. Kim, N. Lu, R. Ma, Y.-S. Kim, R.-H. Kim, S. Wang, J. Wu, S. M. Won, H. Tao, A. Islam, K. J. Yu, T. Kim, R. Chowdhury, M. Ying, L. Xu, M. Li, H.-J. Chung, H. Keum, M. McCormick, P. Liu, Y. Zhang, F. G. Omenetto, Y. Huang, T. Coleman, and J. A. Rogers, "Epidermal electronics," *Science*, vol. 333, pp. 838–843, 2011.

[2] S. Rosset and H. R. Shea, "Flexible and stretchable electrodes for dielectric elastomer actuators," *Appl. Phys. A Mater. Sci. Process.*, vol. 110, pp. 281–307, 2013.

[3] D. J. Lipomi and Z. Bao, "Stretchable, elastic materials and devices for solar energy conversion," *Energy Environ. Sci.*, vol. 4, no. 9, pp. 3314–3328, 2011.

[4] A. H. A Razak, P. Szabo, and A. L. Skov, "Enhancement of dielectric permittivity by incorporating PDMS-PEG multiblock copolymers in silicone elastomers," *RSC Adv.*, vol. 5, pp. 53054–53062, 2015.

[5] A. Thess, R. Lee, P. Nikolaev, H. Dai, P. Petit, C. Xu, Y. H. Lee, S. G. Kim, A. G. Rinzler, D. T. Colbert, G. E. Scuseria, D. Tománek, J. E. Fischer, R. E. Smalley, J. Robert, and D. Tomanek, "All use subject to JSTOR Terms and Conditions Crystalline Ropes of Metallic Carbon Nanotubes," *Science*, vol. 273, pp. 483–487, 2014.

[6] P. C. Ma, S. Q. Wang, J.-K. Kim, and B. Z. Tang, "In-Situ amino functionalization of carbon nanotubes using ball milling," *J. Nanosci. Nanotechnol.*, vol. 9, pp. 749–753, 2009.

[7] Y. Geng, M. Y. Liu, J. Li, X. M. Shi, and J. K. Kim, "Effects of surfactant treatment on mechanical and electrical properties of CNT/epoxy nanocomposites," *Compos. Part A Appl. Sci. Manuf.*, vol. 39, no. 12, pp. 1876–1883, 2008.

[8] K. C. Park, T. Hayashi, H. Tomiyasu, M. Endo, and M. S. Dresselhaus, "Progressive and invasive functionalization of carbon nanotube sidewalls by diluted nitric acid under supercritical conditions," *J. Mater. Chem.*, vol. 15, no. 3, pp. 407–411, 2005.

[9] Y. J. Kim, T. S. Shin, H. Do Choi, J. H. Kwon, Y.-C. Chung, and H. G. Yoon, "Electrical conductivity of chemically modified multiwalled carbon nanotube/epoxy composites," *Carbon N. Y.*, vol. 43, pp. 23–30, 2005.

[10] R. Rastogi, R. Kaushal, S. K. Tripathi, A. L. Sharma, I. Kaur, and L. M. Bharadwaj, "Comparative study of carbon nanotube dispersion using surfactants," *J. Colloid Interface Sci.*, vol. 328, no. 2, pp. 421–428, 2008.

[11] A. E. Vladár, "Strategies for scanning electron microscopy sample preparation and characterization of multiwall carbon nanotube polymer composites," *NIST Spec. Publ. 1200-17*, vol. 1, pp. 1–16, 2015.

[12] L. Yu, F. B. Madsen, S. Hvilsted, and A. L. Skov, "High energy density interpenetrating networks from ionic networks and silicone," *Proc. SPIE*, vol. 9430, pp. 94300T–1–94300T–11, 2015.

[13] D. Y. Wu, S. Meure, and D. Solomon, "Self-healing polymeric materials: A review of recent developments," *Prog. Polym. Sci.*, vol. 33, no. 5, pp. 479–522, 2008.

Joint author statement

If a thesis contains articles* made in collaboration with other researchers, a joint author statement about the PhD-student's part of the article shall be made by each of the co-authors, cf. article 12, section 4 of the Ministerial Order No. 18 February 2008 about the PhD degree. We refer to the Vancouver protocol's definition of authorship.

Titel of the article:	Enhancement of dielectric permittivity by incorporating PDMS-PEG multiblock copolymers in silicone elastomers		
Author(s):	A Razak A. H., Szabo P., Skov A. L.		
Journal/conference (if applicable):	RSC Advances		
Name of PhD student:	Aliff Hisyam A Razak	Date of birth:	20/12/1982

* by article is meant: published journal and conference articles, unpublished manuscripts, chapters etc.

Description of the PhD students contribution to the above-mentioned article:

1) PDMS-PEG copolymers with different PDMS chain lengths were synthesised.
2) The elastomers were prepared by incorporating synthesised PDMS-PEG copolymers in a commercial silicone elastomer (MJK 4/13 from Wacker Chemie).
3) The abovementioned PhD student, who is the 1st author, prepared the article under supervision by Anne L. Skov (main supervisor and corresponding author) and Peter Szabo (co-supervisor).

Signature of the PhD-student: Date: 24 January 2017

As a co-author I state that the description given above to the best of my knowledge corresponds to the process and I have no further comments.

Signatures of co-authors:

Date (dd/mm/yy)	Name	Signature
25/1-2017	Anne Ladegaard Skov	ALSkov
24/1-2017	Peter Szabo	P.Szabo

Joint author statements shall be delivered to the **PhD administration** together with the PhD thesis.

Joint author statement

If a thesis contains articles* made in collaboration with other researchers, a joint author statement about the PhD-student's part of the article shall be made by each of the co-authors, cf. article 12, section 4 of the Ministerial Order No. 18 February 2008 about the PhD degree. We refer to the Vancouver protocol's definition of authorship.

Titel of the article:	Silicone elastomers with covalently incorporated aromatic voltage stabilisers		
Author(s):	A Razak A. H. and Skov A. L.		
Journal/conference (if applicable):	RSC Advances		
Name of PhD student:	Aliff Hisyam A Razak	Date of birth:	20/12/1982

* by article is meant: published journal and conference articles, unpublished manuscripts, chapters etc.

Description of the PhD students contribution to the above-mentioned article:

1) The elastomers were prepared from synthesised PDMS-PPMS copolymers, which contained different concentrations of phenyl groups acting as voltage stabilisers.
2) The synthesised PDMS-PPMS copolymers were subsequently cross-linked in order to obtain silicone elastomers with voltage stabilisation effect.
3) The abovementioned PhD student, who was the 1st author, prepared the manuscript under supervision of Anne L. Skov as the main supervisor and the corresponding author.

Signature of the PhD-student:  Date: 24 January 2017

As a co-author I state that the description given above to the best of my knowledge corresponds to the process and I have no further comments.

Signatures of co-authors:

Date (dd/mm/yy)	Name	Signature
25/01/2017	Anne Ladegaard Skov	

Joint author statements shall be delivered to the **PhD administration** together with the PhD thesis.

Joint author statement

If a thesis contains articles* made in collaboration with other researchers, a joint author statement about the PhD-student's part of the article shall be made by each of the co-authors, cf. article 12, section 4 of the Ministerial Order No. 18 February 2008 about the PhD degree. We refer to the Vancouver protocol's definition of authorship.

Titel of the article:	Voltage-stabilised elastomers with increased relative permittivity and high electrical breakdown strength by means of phase separating binary copolymer blends of silicone elastomers.
Author(s):	A Razak A. H., Yu L., Skov A. L.
Journal/conference (if applicable):	RSC Advances (unpublished)
Name of PhD student:	Aliff Hisyam A Razak
Date of birth:	20/12/1982

* by article is meant: published journal and conference articles, unpublished manuscripts, chapters etc.

Description of the PhD students contribution to the above-mentioned article:

1) The abovementioned PhD student performed experimental works of silicone elastomers prepared from binary copolymer blends consisting of a PDMS-PEG and a PDMS-PPMS copolymers.
2) The abovementioned PhD student, who was the 1st author, prepared the unpublished manuscript under supervision of Anne L. Skov.

Signature of the PhD-student: Date: 24 January 2017

As a co-author I state that the description given above to the best of my knowledge corresponds to the process and I have no further comments.

Signatures of co-authors:

Date (dd/mm/yy)	Name	Signature
25/01/2017	Anne Ladegaard Skov	A Skov
25/01/2017	Liyun Yu	Liyun Yu

Joint author statements shall be delivered to the **PhD administration** together with the PhD thesis.

Joint author statement

If a thesis contains articles* made in collaboration with other researchers, a joint author statement about the PhD-student's part of the article shall be made by each of the co-authors, cf. article 12, section 4 of the Ministerial Order No. 18 February 2008 about the PhD degree. We refer to the Vancouver protocol's definition of authorship.

Titel of the article:	Mechanically compliant electrodes and dielectric elastomers from PEG-PDMS copolymers
Author(s):	A Razak A. H., Madsen F. B., Skov A. L.
Journal/conference (if applicable):	MRS Advances
Name of PhD student:	Aliff Hisyam A Razak
Date of birth:	20/12/1982

* by article is meant: published journal and conference articles, unpublished manuscripts, chapters etc.

Description of the PhD students contribution to the above-mentioned article:

1) First, pristine multi-walled carbon nanotubes (MWCNTs) were dispersed by means of surface treatment using an organic solvent (N-methyl pyrrolidinone-NMP) and a surfactant (Triton-X-100), and the mixture was subsequently sonicated for 4 to 6 hours.
2) The synthesised PDMS-PEG copolymer was chain-extended by hydrosilylation of telechelic vinyl-functional PDMS-PEG copolymer and telechelic hydride-functional PDMS (M_n=17200 g mol^{-1}).
3) The samples were prepared by incorporating different concentrations of dispersed MWCNT (1 to 5 phr) in the chain-extended PDMS-PEG copolymer.
4) The electrical and mechanical properties of PDMS-PEG/MWCNT composites were compared with the properties of conductive elastomers prepared from interpenetrating network containing ionic network, chain-extendend PDMS-PEG copolymer and MWCNTs.
5) The abovementioned PhD student, who was the 1st author, prepared the article under supervision of Anne L. Skov (main supervisor and corresponding author) and Frederikke B. Madsen (post-doc).

Signature of the PhD-student: Aliff Date: 23 January 2017

As a co-author I state that the description given above to the best of my knowledge corresponds to the process and I have no further comments.

Signatures of co-authors:

Date (dd/mm/yy)	Name	Signature
25/1-2017	Anne Ladegaard Skov	A Skov
24/1 -17	Frederikke Bahrt Madsen	F. Bahrt Madsen

Joint author statements shall be delivered to the **PhD administration** together with the PhD thesis.

Danish polymer Centre
Department of Chemical and Biochemical Engineering
Technical University of Denmark
Søltofts Plads, Building 227
2800 Kgs. Lyngby
Denmark

Phone: +45 45 25 28 00
Web: www.kt.dtu.dk/